USING THE MODIFIED HIRSCH MODEL AND THE SLIVER TEST TO FORWARD CALCULATE ASPHALT MIXTURE COMPLEX MODULUS AND BACKWARD CALCULATE ASPHALT BINDER COMPLEX MODULUS

by

MOHAMED MONIR HAGGAG

A Dissertation submitted to the

Graduate School-New Brunswick

Rutgers, The State University of New Jersey

In partial fulfilment of the requirements

For the degree of

Doctor of Philosophy

Graduate Program in Civil and Environmental Engineering

Written under the direction of

Ali Maher, Ph.D.

And approved by

____

____

____

____

New Brunswick, New Jersey

May 2018

ABSTRACT OF THE DISSERTATION

USING THE MODIFIED HIRSCH MODEL AND THE SLIVER TEST TO FORWARD CALCULATE ASPHALT MIXTURE COMPLEX MODULUS AND BACKWARD CALCULATE ASPHALT BINDER COMPLEX MODULUS

By Mohamed Monir Haggag

Dissertation Advisor:

Ali Maher, Ph.D.

Protecting our asphalt pavements structures from possible distresses such as pavement cracking and pavement rutting require good understanding of materials used to construct pavement structures.

When conducting QA/QC or a forensic analysis to characterize asphalt materials that were used on existing roads and highways requires extensive number of cores to be taken per section. The coring process will initiate cracks in the coring location, which will propagate later on and may lead to the formation of alligator cracks and potholes. Many of the currently utilized test apparatus utilize a minimum of a 6-inches core to provide a sample large enough to test. Sample preparation after coring is limited further by lift thickness; to not test a composite material one must cut the field core sample to ensure only one pavement lift is being tested. If the pavement design specifies a lift that is less than the minimum size for current test apparatus, no testing can be completed on that sample.

Incorporating recycled asphalt materials and shingles in mixture designs makes it even more challenging to characterize combined asphalt mixture properties. The combination of virgin and recycled asphalt requires the development and implementation of material testing methods that can test asphalt mixtures in the solid form. Labs that are interested in studying the impact of aging, time, and temperature on the commingling of RAP and/or shingle asphalt on the stiffness modulus of bituminous mixtures find it difficult to use current asphalt mixture performance tests. This is due to different reasons such as time-consuming performance testing process, samples size, and test/analysis complexity.

In this research, a new methodology was developed to simplify and expedite forensic testing. The developed methodology addressed previously mentioned asphalt mixture performance testing issues. The developed methodology consists of two main tools. A new test procedure using the Sliver Test ASTM D7552. A forward and backward models based on the modified Hirsch model developed by, Christensen et al, currently being used in the pavement design guide. The developed methodology successfully analyzed asphalt mixture and asphalt binder response parameters from the sliver test output. Developed methodology successfully helped forward calculate asphalt mixture complex modulus and backward calculate asphalt binder complex modulus avoiding asphalt binder chemical extraction process.

The methodology was developed using 700 data points then verified using a total 1050 data points. Statistical goodness of fit parameters and coefficient of variance was performed. Results showed promise and the methodology was able to forward calculate asphalt mixture ($R^2 > 95.5\%$) and asphalt binder complex modulus ($R^2 > 87\%$).

Acknowledgement and/or Dedication

I would like to express my sincere appreciation to Dr. Ali Maher and Dr. Thomas Bennert for allowing me to work with them and the staff at the Center for Advanced Infrastructure and Transportation (CAIT) over the past eight years. Their guidance and support throughout the course of my research and studies is very much appreciated.

I would like to thank my committee members of Dr. Nenad Gucunski, Dr.Trefor Williams, and Walaa Mogawer for their advice and encouragement during this research project and for providing many engineering tools for which I had gathered from their classes and discussions.

I would like to thank the staff of the Rutgers Asphalt Pavement Laboratory for assisting in some of the material testing. The assistance of Chris Ericson, Ed Wass Jr., John Henken, Ed Haas, Darius Pezeshki, Rustislav Shamborovskyy, Brett DiFrancesco is much appreciated. I would also like to thank Ed Wass Sr., laboratory technician for the Department of Civil Engineering. His time and effort in helping maintaining and fixing equipment, as well as his general encouragement, is greatly appreciated.

I am tremendously grateful for the love and support of my parents and family during this whole process. They were supportive from the start of this whole process, even when I gave them reasons not to be. Special thanks to my uncle Mokhtar Haggag and Aunt Mona Haggag for hosting me for over 10 years! Thank you.

Most importantly, I am so grateful and fortunate to have such great friends. I thank them for their continuous support and putting up with me throughout this entire experience.

I would like to dedicate this work to my grandfather, Monir Haggag, who passed away before I was able to graduate high school. His advice and memory provided me with all the strength needed to get the job done. His memory put a smile on my face no matter how stressed I could be. This work is also dedicated to my grandmother, Fatma Amer, who passed away before I was able to graduate from my graduate studies. Her love, support, and lessons of life are memories that will never be forgotten and hopefully I can pass them to my children to be.

Table of Contents

List of Tables

List of Figures

List of Equations

Chapter 1 – Problem definition

Test procedures and Equipment that are currently being used to determine asphalt binder and mixture properties is expensive, complex, and some of these procedures use chemicals that might be of health risk to research workers (binder extraction process). Moreover, there is no test procedure that is able to study asphalt mixtures properties throughout the thickness of the constructed pavement and field cores.

Pavement cracking and pavement rutting are the most common forms of pavement distresses. Current distress models that are being used in asphalt pavements mechanistic empirical design software MEPDG require asphalt mixture complex modulus as a key input.

State DOTs and asphalt pavement industry are now using recycled asphalt and shingles in their mix design and highways construction to preserve our natural and environmental recourse, in addition to reduce material cost and overall job cost. Using such materials might affect pavement performance requiring a better understanding of how recycled asphalt and shingles are commingling with virgin asphalt mixtures.

This dissertation presents a new developed methodology that is able to forward calculate asphalt mixtures complex modulus and backward calculate asphalt binder complex modulus. The developed methodology allows backward calculation of asphalt binder complex modulus without the need to go through the expensive, time consuming chemical extraction process.

Chapter 2 – Objectives

The goal is to provide pavement engineers and researchers a toll the allow them to obtain a reliable asphalt mixture and binder modulus within a practical time span. This goal was achieved through two objectives.

The first objective was to develop a methodology that is able to calculate asphalt mixture complex modulus. This methodology was named as the “Forward calculation Methodology”.

The second objective was to develop a methodology that is able to calculate asphalt binder complex shear modulus without using any time-consuming asphalt binder extraction techniques and performance tests. This methodology is referred to as the “backward calculation methodology”.

Chapter 3 – Literature review

3.1 Introduction

There are about 4 million miles of roads in the United States. Approximately 70 percent of the United States roads are flexible pavements. Research shows that there is an urgent need to dedicate funding towards asphalt pavement rehabilitation. These projects will have a direct impact on the quality of transportation networks which will impact the United States economy. Asphalt pavements are considered to be durable and recyclable. Asphalt pavements are used for airport runways as well as highway and urban roadways. Asphalt pavements are also resistant to winter road safety maintenance such as de-icing salts. It produces less noise compared to other conventional paving methods. It can also be used to reduce water splash during rainy seasons. There are two types of pavements; flexible pavements, and rigid pavements. The proposed research will discuss flexible pavements.

Figure 1 : Asphalt mixture type can reduce water splash during rainy season [1]

There are different types of flexible pavements. The most common characteristic between all different types is that the whole pavement structure deflects. That is why they are called flexible pavements. Figure 2 shows the main three components of Flexible pavement structure. Flexible pavement consists of three main structural elements; surface course, base course, and sub-base course.

Figure 2 : Flexible pavements structural elements

3.2 Common pavement distresses

Pavement distress can be defined in different ways. In the 1950s, Western Association of State Highway officials (WASHO) recognized the need to have a quantifiable measure of pavement performance [2]. The WASHO failed to come up with definitions for failure conditions for their tests. In the 1960s, Carey and Irick [3] stated that “performance is defined as the area under a serviceability-time curve from the time of construction to the time performance is being evaluated” [4]. Distress can be defined as physical condition of pavement material which affects pavement structure, performance, and/or serviceability [5]. There are different types of distresses that can affect asphalt pavement structures. Some of these distresses are load associated distresses (e.g. fatigue cracking, rutting) and others are non-load associated distresses (e.g. thermal cracking). According to previous studies, seven distress models were selected to be used in various asphalt pavement design methods [6] . These models include the following:

1. Load-associated cracking
2. Non-load associated cracking
3. Reflective cracking
4. Distortion (shoving, rutting, and slippage)
5. Disintegration
6. Reduced skid resistance
7. Roughness

Many of these models were used in the design charts developed by Hveem [7]. Figure 3 shows two of the most common load associated pavement distresses; fatigue cracking and rutting.

Figure 3 : Common pavement distress fatigue cracking and rutting

3.3 Hot mix asphalt test types

Asphalt mixtures tests can be classified in to 3 classifications [8] [9] [10]:

1. Fundamental tests
2. Empirical tests
3. Simulative tests

Fundamental tests are performance based tests that are able to measure true (intrinsic) properties of the material independent of its testing conditions. Material response for different testing conditions is measured and recorded. Asphalt mixtures performance evaluation can be completed using the recorded material response. Asphalt mixtures dynamic modulus test and shear modulus are good examples of fundamental tests.

Empirical tests are tests with no direct relation with intrinsic material properties. Fundamental material properties cannot be calculated from empirical tests results. Hveem and Marshall Stability tests are good examples of asphalt mixtures empirical tests. Tests procedures and details will be discussed in later sections.

Simulative tests are physical test that try to replicate certain conditions. Asphalt mixture production at the plant, laydown, and service conditions are common conditions that researchers and industry engineers interested in. AASHTO and ASTM standards provide simulative tests such as Asphalt Pavement Analyzer APA, and Hamburg Wheel tests. More details regarding empirical tests will be discussed in later sections [9] [10].

3.4 Mixture design methods

Mixture design methods can be classified in different ways. One of the common classifications is listed in this section by luminari and Fidato in 1998. Luminari and Fidato classified asphalt mixtures design methods in to 6 categories, which are:

1. Recipe mix design method
2. Empirical mix design method
3. Analytical mix design method
4. Volumetric mix design method
5. Performance-related mix design method
6. Performance-based mix design method

The following section is to list examples of various mixture design classifications as well as discuss common mixture design procedures that are being used in the United States.

The recipe mix design method is based totally on designer experience with local mixtures. The designer's decision is based on good performance history records of the mixture. There is no testing/samples required for this mix design method.

The empirical mix design method is based on empirical tests and optimization of different variables that are usually chosen based on previous experience. The designer will select binder content and aggregate gradation based on required empirical test. As mentioned in earlier section, empirical tests cannot be used to directly measure mixture performance.

The analytical mix design method is based totally on analytical calculations of mixture properties. There are no tests or samples required by this design procedure.

The volumetric mix design procedure is based on volumetric properties computations of asphalt mixture samples. Volumetric properties are calculated based on lab fabricated samples, which are meant to replicate field laydown and compaction conditions. In this method asphalt mixture binder content and aggregate skeleton are selected based on volumetric parameters such as mixture percent air voids (% AV), voids in mineral aggregates (VMA), voids filled with asphalt (VFA).

The performance-related mix design methods are based on volumetric criteria as well as performance related tests. In this mix design method lab compacted samples that simulated the production and laydown of the mixture in the field are used for volumetric computation and analysis. Mixtures that pass the volumetric criteria are used to make more samples for performance- related tests. Final qualified mixture will be chosen based on the volumetric and performance-related criteria.

The performance-based mix design methods are based on volumetric criteria as well as performance-based tests. Lab compacted samples are fabricated simulating mixture production and laydown conditions. Volumetric analysis is performed using lab compacted specimens. Qualified mixture is then used to make more samples that are used for mixture performance based tests. Performance based tests can be used to directly measure asphalt mixture performance.

European countries follow various mix design procedures.

Table **1** shows compiled luminari and Fidato in 1998 to compare different procedures used in European countries such as Australia, Belgium, Finland, France, Germany, Italy, Switzerland, Netherlands, United Kingdom.

Table **1** also contains data related to mix design procedures used in the United States of America.

Mix Design Method	Specimens Fabricated & Compacted	Specimens Compact./ in-situ Comp. Process	Empirical Tests	Simulation Tests	Fundamental Tests	Fundamental Properties-Proven Relation To Performance	Mix Design Category
Australia-NARC guide '96 Level I	Yes	Yes	no	Yes	no	no	Recipe/Volumetric
Australia-NARC guide '96 Level II/III	Yes	Yes	no	Yes	no	no	Recipe/Volumetric/Performance Related
Belgium-CRR R61/87	no (^)	no	yes (^)	no	no (*)	no	Analytical Empirical
Belgium CRR 1996 (draft)	no (^)	no (§)	yes (^)	yes (^)	no (*)	no	Analytical/Empirical/Performance Related
Finland ASTO/ Pank 95	Yes	Yes	no	Yes	Yes	no	Recipe/Volumetric/Performance Related
France AFNOR	Yes	Yes	Yes	Yes	Yes (#)	no	Recipe/Volumetric/Performance Related
Germany—DIN	Yes	no	Yes	no (*)	no (*)	no	Recipe\Empirical
Italy—CNR, ANAS & AUTOST RADE	Yes	no (*)	Yes	no	no (*)	no	Recipe\Empirical
Switzerland-SN640431a la	Yes	no	Yes	no	no	no	Recipe\Empirical
The Netherlands RAW	Yes	no	Yes	no	no	no	Recipe\Empirical

Mix Design Method	Specimens Fabricated & Compacted	Specimens Compact./ in-situ Comp. Process	Empirical Tests	Simulation Tests	Fundamental Tests	Fundamental Properties-Proven Relation To Performance	Mix Design Category
Standards							
The Netherlands CROW (draft)	Yes	Yes	Yes	Yes	Yes	no	Volumetric\Performance Related
United Kingdom BS 594/BS 4987	no	no	no	no	no	no	Recipe
UK-BS 598	Yes	no	Yes	no	no	no	Recipe\Empirical
UK Nottinhgam Univ.	Yes	Yes	no	Yes	Yes	no	Volumetric/Performance Related
USA—Asph. Inst.'84 /'91	Yes	no	Yes	no	no	no	Volumetric
USA SHRP Superpave Level II	Yes	Yes (=)	no	Yes	Yes	Yes (+)	Volumetric\Performance Based
USA SHRP Superpave Level III	Yes	Yes (=)	no	Yes	Yes	Yes	Volumetric\Performance Based
USA SHRPA-698	Yes	Yes	no	no	Yes	Yes	Performance Based

Table 1 : Mix design methods, criteria, and categories

Where:

(°) Yes, only for some criteria used.

(^) Yes, only for the verification of the base composition.

(§) Yes, only for simulation and fundamental tests.

(*) Compaction and/or Test procedure used only for special design studies, and not for routine mix design.

(#) Test carried out only for study of a completely new formula with nontraditional materials or materials of unknown performance.

(+) No reference was found with a comparison between actual in situ performance and predicted laboratory performance.

(−) Only volumetric analysis.

(/) It should only be noted that at the expected in-situ volumetric characteristics, the mix still has the desired performance.

(=) Some researchers agree that the gyratory compactor may not produce specimens suitable for performance-based analysis.

3.5 Mixture design practices in the United States of America

Campbell Crawford has been gathering and documenting mix design practices information in the United States of America since the 1960s. This information was published in a research paper under the name of “The Rocky Road of Mix Design” [11]. Marshalls and Hveem mix design method were used starting in 1940s to the 1990s. State DOTs and industry researchers were not satisfied with the results that they are getting using the mix design methods. In 1984, a survey was performed showing that 75% of state DOTs require using Marshall Mix design and 25% of state DOTs requires using Hveem mix design. Some other states were using a combination of both mix design procedures (Marshalls and Hveem) to get better understanding of asphalt mixture behavior [12]. The following section will discuss various design procedures being used in the United States of America.

3.5.1 Marshall mix design method

Bruce Marshall at Mississippi Department of Transportation developed Marshall Mix design method. Marshall Mix Design method was then modified by the Army Corps of Engineers and put in to ASTM D1559 and AASHTO T245. Marshall Mix design method is a performance- related mix design procedure. Like any other performance related procedure, it starts with material acceptance testing phase. Once materials pass the acceptance-testing requirement, the designer then performs volumetric analysis for the fabricated samples. Based on the results from the volumetric analysis the designer will proceed to the performance related testing stage. Marshall Mix design requires performing two tests, which are Marshall Stability and Marshall Flow. All data and results are tabulated and plotted to help identify the mix that will provide optimum performance. Finally, the designer can choose the mix based on the plots, the desired mix are those providing optimum asphalt content. Marshall Mix design method can be found in in asphalt institute publication "Mix Design Method for Asphalt Concrete and Other Hot Mix Types", Manual Series No. 2 (MS-2). In summary, here is a review of the main steps for Marshall Mix design method according to Asphalt Institute publication [13] [14]:

a. Aggregate evaluation
b. Asphalt cement evaluation
c. Preparation of Marshall specimens
d. Density and voids analysis
e. Marshall stability and flow test
f. Tabulating and Plotting test results
g. Optimum asphalt content determination

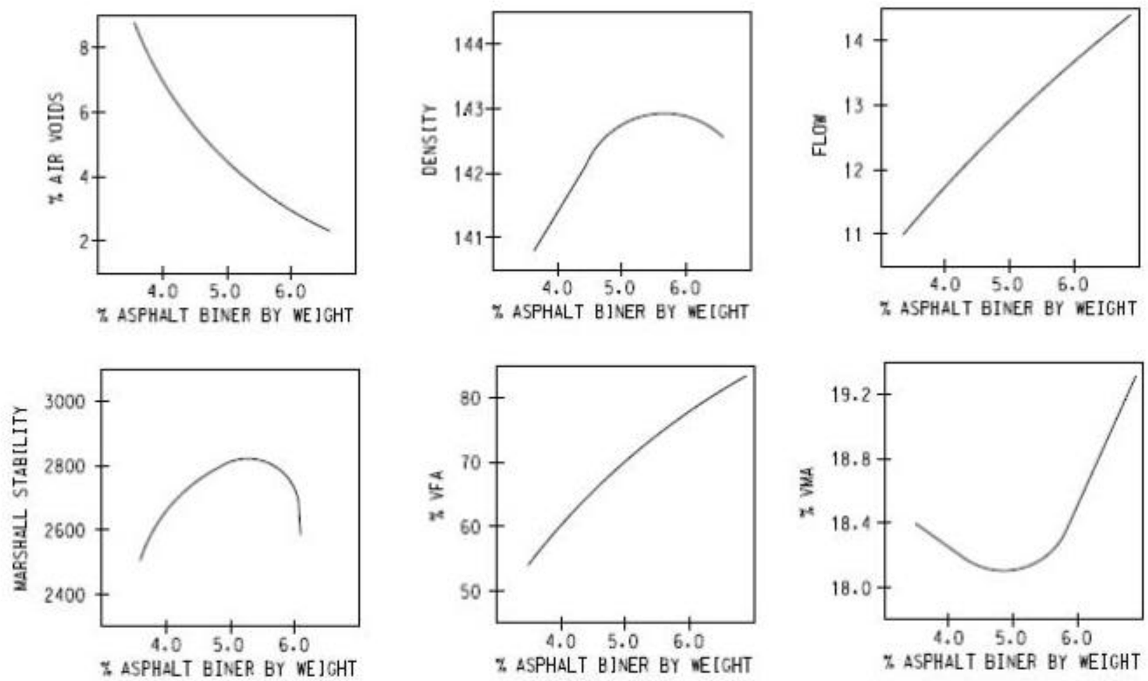

Figure 4 : Marshall mix design results, mixture properties vs asphalt content [15]

Traffic Category	Light		Medium		Heavy	
Compaction, No. of blows/side	35		50		75	
	Min.	Max.	Min.	Max.	Min.	Max.
Stability, lb (N)	750 (3333)	-	1200 (5333)	-	1800 (8000)	-
Flow, 001 in. (0.25 mm)	8	18	8	16	8	14
Air Voids, %	3	5	3	5	3	5
VFA, %	65	75	65	78	70	80

Table 2 : Marshall mix design criteria [16]

Overall, Marshall Mix design method has multiple advantages. The most important is it is a simple method that can be performed by most of asphalt materials laboratories (including field labs) as it doesn’t require expensive equipment or setup. Marshall Mix design method is believed to be better than other volumetric or empirical mix design method as it uses Marshall Stability and Flow to predict the mixture resistance to permanent deformation. However, researchers and materials engineers expressed many doubts on Marshall’s tests permanent deformation prediction accuracy. Some researchers believe that it is not reliable enough to use Marshall Tests to calculate mixtures shear strength. They have also considered it “out of date” and initiated studies towards developing relatively reliable mix design procedures.

3.5.2 Hveem mix design method

Hveem Mix design method was developed by Francis N. Hveem a formerly materials and research engineer with California Division of Highways (CALTRANS).

CALTRANS studied the ability of presenting Hveem new approach to the industry in the 1940s. CALTRAN's objective was to present a practical and reliable mix design method to DOTs and asphalt mixtures industrial labs.

Hveem Mix design method can be applied to mixtures with maximum aggregate size of 25 mm (1 in.) or less. Hveem Mix design method is a performance-related procedure. In other words, materials need to be accepted by designated material acceptance testing first. Volumetric analysis is then performed on laboratory compacted samples. Approximate asphalt binder content is determined using centrifuging Kerosene equivalent test and then lab compacted samples are made using the approximate asphalt contents. (High asphalt content, Target asphalt content, Low asphalt content). Qualified samples are then tested using Hveem stability test. Hveem stability test is a direct measurement of the internal friction component of mixture shear strength.

The following list is Hveem Mix design method steps:

a. Aggregate evaluation
b. Asphalt cement evaluation
c. Preparation of asphalt mixture test specimens
d. Hveem mixture testing
e. Analyzing Hveem mixture test results

Unlike Marshal Mix design method, asphalt materials engineers believe that the kneading method used in Hveem test provides better correlation with actual densification of asphalt mixtures in pavement structures. Hveem test is also used to investigate asphalt mixture resistance to swell in the presence of water as well as the ability of asphalt mixture sample ability to resist lateral displacement from application of vertical load.

On the other hand, Hveem is found to use relatively expensive equipment. Another disadvantage is that volumetric related to durability are not required to be determined on routinely basis which can risk mixture overall durability. Some researchers believe that Hveem mix design will produce asphalt mixtures with low asphalt binder content.

More details regarding Hveem mix design procedure can be found in Vallegra and Lovering report [10]. Vallegra and Lovering combined all critical design elements and summarized them in the following quote “Use a dense, well-graded aggregate with high internal friction without an excess of fines and add as much asphalt binder as the mixture will tolerate without losing stability. At least 3 percent air voids are desired in the Hveem Mix design method”.

3.5.3 Superpave mixture design method

The word SUPERPAVE stands for “Superior Performing Asphalt Pavement. Superpave was initiated under the Strategic Highway Research Program (SHRP) in 1988 to overcome mix design challenges at the time of its development. SHRP completed the project in 1993 providing a volumetric mix design procedure called Superpave mix design procedure to the pavement industry [17] [18] [19]. The SHRP program published their efforts in the following three reports [20] [21] [22]

1. SHRP-A-357 “Development and validation of Performance Prediction Models and Specifications for Asphalt Binder and Paving Mixes”.
2. SHRP-A-407 “The SuperPave Mix Design Manual for New Construction and Overlays”.
3. SHRP-A-379 “The SuperPave Mix Design, Test Methods, and Practices”.

Bituminous materials are highly affected by traffic level and climatic conditions. Taking in to considerations these two factors, SHRP team decided to incorporate traffic level and climatic conditions in the material selection step of the SuperPave design procedure. For rough climatic conditions and high traffic levels (ESAL’s), extra caution is needed by adding higher factor of safety and more testing. Although there are no materials fundamental properties, currently being used; Researchers and engineers still believe that incorporating material fundamental properties in the design process will add confidence and accuracy to the final design. Materials fundamental properties can be used to predict asphalt pavements service life by developing performance models.

The Superpave mix design method introduced new asphalt materials compaction machine called the Superpave Gyratory Compactor (SGC). The SGC is used to compact asphalt mixtures samples to a specific height and diameter. The SGC possess some similarities as well as differences compared to other compactors. One of the advantages of the SGC is the ability to provide information that can be related to mixtures workability (number of generations needed for the sample to reach a certain height). One more advantage over other compactors (e.g. Marshalls compactor) is the ability to compact stiff mixtures that require more compaction energy and usually they fail to compact. The following are the Superpave mixture design procedure steps:

1. Material selection
2. Asphalt Binder selection
3. Determine weather and traffic conditions
4. Select reliability
5. Determine design temperature
6. Verify asphalt binder grade
7. Temperature-viscosity relationship for lab mixing and compaction

3.5.4 Flexible pavement design methods

- **Asphalt institute method**

The Asphalt Institute was created in 1919 to connect asphalt manufacturers/suppliers. Asphalt institute represents 90% of the liquid asphalt produced in North America and a good percentage in the international market. The institute is focus is to promote, educate, and resolve issues related the asphalt industry. Starting 1954, The Asphalt Institute published multiple editions of the manual series no.1 (MS-1) for the thickness design of asphalt pavements. AI manuals (from 1 to 6) were all based on empirical procedures. The seventh and eighth edition were based on tests performed at the AASHO road test, WASHO road test, number of British road tests, comparison with the design procedure of the U.S. Army Corps of Engineers, and some other state agencies. The industry realized the importance of incorporating mechanistic properties in their design procedures. As a result, Asphalt Institute's ninth edition was developed using a mechanistic empirical approach in parallel to the mechanistic multi-layer theory and empirical failure criteria to find pavement thicknesses. Design charts for three different temperatures were used in the AI ninth edition.

a. Asphalt institute design criteria

The Asphalt Institute method relies on two critical strains, the horizontal critical strain at the bottom of the asphalt layer and vertical critical strain at the top of the subgrade. The horizontal strain at the bottom of the asphalt layer is used to control fatigue cracking. The vertical strain at the top of the subgrade layer is used to control permanent deformation.

For standard asphalt mixtures, Asphalt Institute uses Equation 1 to predict number of cycles to failure for standard asphalt mixtures.

$$\mathrm{N_f} = \mathrm{CK_1}\left(\frac{1}{\varepsilon_t}\right)^{k_2}\left(\frac{1}{\mathrm{E}}\right)^{k_3}$$

$$N_f = 0.0796(\varepsilon_t)^{-3.291}|E^*|^{-0.854}$$

Equation 1 : Fatigue equation flexible pavement design method

Where:

$\mathrm{N_f}$ = Number fo Cycles to failur

ε_t = Tensile strain @ bottom of AC layer

k_1 = Field Correlation shift factor

k_2 & k_3 = Laboratory determined values

C = Laboratory to field adjustment factor

$\mathrm{N_f}$ Is the number of cycles to failure and E^* is the asphalt mixture dynamic modulus. The preceding equation applies only to standard asphalt mixtures (11%, 5% air voids). If the asphalt mixture is different from the standard mixes, a correction factor C must be applied. According to published reports on fatigue cracks of the selected section of AASHO road test, the Asphalt Institute fatigue model will result in fatigue cracking of 20% of the total area [23].

Permanent deformation is the second criteria governing the AI design method. AI uses Equation 2 to determine the allowable number of load repetitions to control permanent deformation:

$$N_d = 1.365 \times 10^{-9}(\varepsilon_c)^{-4.477}$$

Equation 2 : Allowable number of load repetitions to control permanent deformation

Where:

$\mathrm{N_d}$ = Number fo Cycles to failur

ε_c = Vertical Compressive strain @ the top of the subgrade

f_4 = Field Correlation shift factor

The model was used to develop design charts for permanent deformation predictions. Design charts only works for pavements that are designed and compacted properly. If all permanent deformation design condition is followed, the pavement should not show more than 0.5 inches (12.7 mm) of rutting for the design traffic.

b. Asphalt institute material characterization

Asphalt institute pavement design method requires various testing to be performed on material. Such properties can be resilient moduli and Poisson ratios of subgrade, granular base, and asphalt layer. A Poisson ratio of 0.45 for subgrade soils and 0.35 for all other materials can be reasonably assumed.

c. Asphalt institute environmental effects

Researchers and engineers acknowledged the effect of environment on asphalt mixture design by providing design charts that takes in to consideration the effect of change in the stiffness of HMA and emulsified asphalt mixtures as well as the effect of freeze and thaw on the subgrade and granular materials resilient modulus. This effect was established by increasing the modulus values during the freezing seasons and reduced modulus during the thaw seasons.

- **AASHTO design method**

The American Association of State Highway and Transportation Officials (AASHTO) initiated the work on developing a new pavement design method to overcome challenges at the time in the late 1950s and early 1960s. The initial version of the AASHTO design method was based on results from the AASHO road test conducted in Ottawa, Illinois. The AASHO design committee published an interim design guide in 1961. In 1972 and 1981, the design procedure was revised. In 1984-1985, the design procedure was reviewed and expanded by the AASHO subcommittee under NCHRP project 20-7/24. The design guide was further revised in 1986 and1993 before being approved and published in 1993. All the models used in the design procedure was then modified and calibrated to work with changes in other regions in the nation. It should be kept in mind that the original equations were developed under a given climate setting with a specific set of pavement materials and subgrade soils. The climate at the site is with an average annual precipitation of about 34 in. (864mm). The average depth of frost penetration is about 28 in. (711 mm). The subgrade soils consist of A-6 and A-7-6 that are poorly drained, with CBR values ranging from two to four.

This section will provide an overview on the different input parameters and design considerations used in the AASHTO 1993 design procedure.

a. AASHTO design method design variables

Different design variables were included in the AASHTO design method. These variables are mainly related to flexible and rigid pavements properties. However, some other variables might apply such as effective roadbed, soil resilient modulus, and structural number.

The design committee realized the effect of these variables on the pavement structure performance. Therefore, the design procedure encourages the use of a longer analysis period than the performance period.

The AASHTO design method defines the performance period as the time the pavement structure is expected to perform before it requires rehabilitation. The AASHTO also defines the analysis period as the time covered by the design methodology. Another definition for pavement performance period is time taken for the pavement structure to drop from its initial serviceability to its terminal serviceability. As mentioned earlier in this section, the performance period of the pavement structure can be affected by engineering consideration such as material properties, functional classification of the pavement, level of maintenance applied and other factors as well.

In the AASHTO design method, traffic is taken in to account by converting all traffic loads in to cumulative expected 18-Kip (80KN) equivalent single-axle load (ESAL). If the pavement is expected to perform for a certain period, the ESAL can be uniformly distributed on analysis period. Another important consideration is using a measure for pavement serviceability. The AASHTO design method uses a serviceability index to measure pavement quality. Once a pavement reaches a certain PSI value (usually Terminal serviceability index), pavement maintenance/rehabilitation is required.

AASHTO design methods uses "structural number" to determine pavement layer thickness. Structural Number (SN) is function of pavement layer thickness and drainage coefficients. a_i Is a layer coefficient used by the SN to calculate pavement layer thickness. a_i can be function of material properties or results from road sections. It is preferred to use more fundamental properties to calculatea_i. For the higher stiffness materials, such as HMA and stabilized bases, that may be tested by the repeated load indirect tensile test (ASTM D-4123), All materials should be tested by the resilient modulus test methods (AASHTO T274).

3.6 Asphalt binder rheology historical review

Rheology can be defined as the science of deformation and flow of all kinds of matter. The science of rheology and viscoelasticity was not introduced as early as the other industries because rheologists were mostly interested in other industrial materials that poses properties between ideal liquids and ideal solids. In the engineering world, rheological properties can be expressed as mathematical equations "constitutive equations".

Rheological constitutive equations are usually function of stress and strain history. The science of rheology was introduced formally in 1929. Table 3 summarizes some of the references regarding rheology discussions before the formal creation in 1929. [24], [25] , [26], [27], [28], [29]

FLUIDS/MODELS CLASS		KEY TIME	REPRESENTATIVE WORKS
Ideal Materials	a) Perfect rigid bodies	Antiquity	Archimedes (~250 BCE). Newton (1687)
	b) Ideal elastic solids	1600s	Boyle (1660), Hooke (1678), Young (1807), Cauchy (1827)
	c) Inviscid fluids	1700s	Pascal (1663), Bernoulli (1738), Euler (1755)
	d) Newtonian liquids	Early 1800	Newton (1687), Navir (1823), Stokes (1845), Hagen (1839), Poiseuille (1841), Weidemann (1856)
Linear viscoelasticity		Mid 1800s	Weber (1835), Kohlrausch (1863), Wiechert (1893), Maxwell (1867), Boltzman (1878), Poynting & Thomson (1902)
Genaralized Newtonian (viscous) liquids		Late 1800s-Early 1900s	Schwedoff (1890), Trouton & Andrews (1904), Hatchek (1913) Bingham (1922), Ostwald (1925) de Waele (1923), Herschele & Bulkley (1926)
Non-linear viscoelasticity		Early 1900s	Poynting (1913), Zaremba (1903), Jaumann (1905), Hencky (1929)
Key material description	a) Suspensions	Early 1900s	Archimedes (~250 BCE). Newton (1687)
	b)Polymers		Boyle (1660), Hooke (1678), Young (1807), Cauchy (1827)
	c) Extensional viscosity		Pascal (1663), Bernoulli (1738), Euler (1755)
The genesis of rheology		1929	Bingham, Reiner and Others

Table 3 : Significant rheological works prior to the formal inception of rheology 1929 [30]

Table 4 summarizes some of the efforts that were done since the rheology inception 1929. [30] The report showed that from this brief review of rheological history, it is apparent that it took over a century before contributions by scientists from widely varied fields turned in to the formal field of rheology. Since approximately 1600 BCE, rheology has primarily been concerned with solving practical problems. However, rheology attracted the finest scientific minds from different fields due to the complexity of material rheology (mathematical and physical in nature). As a result, rheological materials are modeled using mechanistic-empirical concepts that we know today.

Area of Activity		Representative Works
Constitutive Equation	a) Differential model	Oldroyd (1950), Truesdell (1952), Rivlin and Ericksen (1955), Giesekus (1962), White-Metzner (1963)
	b) Integral models	Green & Rivlin (1957), Coleman & Noll (1961)
	c) Network models	Gren & Tobolsky (1946), Lodge (1956), Yamamoto (1956), Kaye (1962) - Bernstein et al. (1963)
	d) Reptation models	Edwards (1967), De Gennes (1971), Doi & Edwards (1978, 1986)
	e) Molectular models	Kuhn (1934), Rouse (1953), Zimm (1956), Kirkwood (1967), Bird et al. (1987)
Constitutive Equation	a) Shear flows and the non slip boundry condition	Eisenschitz et al.. (1929), Mooney (1931, 1936), Schofield & Blair (1930), Pearson & Petrie (1968) Grassley (1977), Ramamurthy (1986)
	b) Normal streses and rod-climbing effects	Lander (1945), Weissenberg (1947), Markowitz (1957), Philipoff (1957), Ginn & Metzner (1969), Binnington & Boger (1985)
	C) Dynamic Studies	Eisenchitz & Philippoff (1933), Schofield & Scott Blair (1932)m Leaderman (1943), Cox-Merz (1958), Doraiswamy et al. (1991)
	d) Thixotropy	Freundlich & Bircumshaw (1926), Cheng & Evans (1965), Mewis (1979), (Barnes (1997)
	e) Flow instabilities	Nason (1945), Tordella (1958), Petrie & Denn (1976), Bousfield et al. (1986)
	f) Turbulent drag reduction	Toms (1949), Agoston et al. (1954), Hershey & Zakin (1967), Seyer & Metzner (1967)
	g) Optical studies/ Birefringence	Adams et al. (1965), Carothers & Hill (1932), Hermans & Platzek (1939), Janeschitz-Kriegl (1983), fuller (1985)
	h) Time Temperature Superposition	Williams et al. (1955), Ferry (1970)
	i) Extensional behavior	Merrington (1943), Treolar (1944), Ballman (1965), Cogswell (1969), Metzner (1968), Meissner (1969), Dealy et al. (1976), Spearot & Metzner (1972), Laun & Munstedt (1978), Srihar & Gupta (1985)
Advanced Materials	a) LCPs	Leslie (1968)-Erocksen 1961), Doi (1981), Wissbrun (1985), Doraiswamy & Metzner (1986), Marrucci & Greco (1992)
	b) Composites and two phase systems	Taylor (1934), Krieger-Dougherty (1959), Rumscheidt & Mason (1961), Leal (1975), Batchelor (1977), Folgar & Tucker (1984), Heller & Kuntamukkula (1987), Khan
	c) ER/MR fluids	Winslow (1949), Parthasarthy & Klingenberg (1996)
Computatio nal Rheology	a) Continuum Simulations	Turner et al. (1956), Gottlieb & Orzag (1977), Cruse & Risso (1968), Yoo & joseph (1985), Beris et al. (1987), walters & Tanner (1992), Crochet & walters (1993)
	b) Molecular Dynamic Simulations	Adler & Wainright (1957), Ashurst & Hoover (1975), Evans & Morriss (1988), Davis & Todd (1998)

Table 4 : Rheology since its inception in 1929

3.7 Bituminous materials models

Asphalt concrete mixtures reacts differently based on the surrounding environment and loading conditions. Engineers and researchers faced a lot of difficulties to record and analyze asphalt concrete pavement strains due to the applied stresses. Recording and analyzing data is not as complex process as before due to the great advancements in technologies the past 20 years. State DOTs and researchers are developing mathematical models to help predict asphalt mixtures and asphalt pavement performance with limited amount of testing. The section will discuss various asphalt mixtures and asphalt pavement models used to predict different properties of asphalt mixtures and performance of asphalt pavements.

3.8 Modeling of viscoelastic properties of asphalt binders

Various models can be used to express asphalt mixture viscoelastic properties. Asphalt pavements scientists and researchers used mechanical analogs models (e.g. generalized Burger model and Prony series), and phenomenological models (curve fitting of experimental data) [31]. The ability to measure and record asphalt pavement response using advanced computer systems put Phenomenological model approach in favor of other modeling approaches. In 1969, Jongepier and Kuilman log Gaussian distribution of relaxation times were used to predict asphalt binder rheological properties [32]. In this approach, asphalt binder rheological properties were introduced as a simple liquid while a width parameter and equiviscous temperature were used in order to account for the effect of loading time and temperature on the rheological behavior of asphalt binders [32].

In 1974, Dickenson and Witt introduced a new mathematical function that accounts for loading time dependency of rheological parameters. According to [31] authors who followed the same mathematical functions developed by Dobson for the temperature dependency in 1969.

All previously mentioned mathematical models were evaluated in several following work and the accuracy of the model have been tested using many types of aged and unaged asphalt binders [33] [34] [35].

All previously mentioned asphalt pavements researchers do agree that asphalt can realistically be represented as a linear viscoelastic material that is thermorheologically simple [31]. They also specified two main asphalt behaviors needed in order to characterize such materials, these two behaviors are:

1. The dependency of rheology on loading time
2. The dependency of rheology on temperature

In 1992, Christensen and Anderson introduce a function that was based on Weibel distribution to represent asphalt rheology. This work was done for the Strategic Highway Research Program SHRP. Marasteanu and Anderson introduced a modified version of the original function proposed by Christensen and Anderson. This model was called the CAM model [36]. According to [31], The “CAM” was used and evaluated in asphalt related various studies. It was found to be an effective phenomenological model for unmodified asphalt binders whose properties are within the linear viscoelastic range.

Because of all previously mentioned efforts, Zeng et al. 2001 proposed a generalized model that can relate the complex behavior of asphalt binder and mixtures. This model allowed for a shift for the nonlinearity (Strain dependency) and the plateau region at high temperatures or very long loading times [37]. The model reduces dynamic test data, measured at multiple temperatures and strains, by developing single complex modulus and phase angle curves. The model was considered universal because it is used to reduce the test data for the binder and the mixtures with four formulations for complex modulus master curve, phase angle master curve, temperature shift factor, and strain shift factor. Details of the development of the model can be found in [37].

3.9 Asphalt binder viscoelastic properties selected in the SHRP

Viscoelastic properties of asphalt bituminous materials can be characterized using various methods. One of the main outcomes from the SHRP, researches preferred the dynamic (oscillatory) testing as the best technique to represent the behavior of bituminous materials. In the shear loading, the dynamic modulus (G*) and phase angle (δ) are measured. The dynamic shear modulus (G*) represents the total resistance of the material to deformation under the applied load while the phase angle (δ) represents the relative distribution of this total response between the elastic (in phase component) and the viscous (out of phase) component.

SHRP asphalt pavement researchers realized the importance of understanding asphalt materials failure behavior. Earlier researches showed that asphalt pavement failure behavior is also highly dependent on temperature and time loading [38]. One of the main outcomes was that new testing protocols are needed in order to better understand bituminous mixtures failure behavior.

3.10 Asphalt superpave binder system and assumptions

The Superpave binder specifications contains criteria based on assumptions that were made to simplify the testing required and evaluate characteristics that are most critical to pavement performance. These assumptions were validated for neat asphalts; this might not be valid for asphalts modified with different additives. This was Based on detailed review of the SHRP Project A-002A report [39], and other recent published literature [40] [41] The most important assumptions that are related to the behavior of modified binders [31] are listed as follows:

1. No strain/stress dependency of rheological response (wide linear viscoelastic range)
2. No shear rate dependency of viscosity (wide Newtonian range)
3. Testing at loading rate is sufficient (similar loading rate dependency
4. Binders are homogeneous and isotropic (no sample geometry or particulate additives effects)
5. Similar time-temperature equivalency for all binders (one shift is used)
6. Binders are not thixotropic (no effect of mechanical working)
7. Stability of asphalt is affected mainly by oxidation

The essence of the above assumptions is that asphalt is a simple material that can be characterized using linear viscoelasticity and simple geometry within which stress and strain fields are simple to calculate.

Some of the important behaviors that will need to be characterized were, however, not addressed due to the need of simplification. Of particular importance are the possible thixotropic effect and the dissimilarity of the effect of the repeated loading. Some modified binders can show significant reduction in G* due to mechanical working (repeated loading).

Two main conclusions can be made through the review mentioned above [31]:

1. The existing protocols cannot be used fully to characterize all asphalt binders modified with different additive. The main reason is that they are based on simplifying assumptions that cannot be reliably extended to modified binders.
2. Some additives can result in binders that are too complex to be evaluated by any binder only protocols. Such additives will result in anisotropy or interference with testing geometry such that only actual replication of films that will exist in mixtures will allow reliable estimation of their role in pavement performance.

SHRP and the NCHRP 9-10 project discussed in details behavior of modified asphalt binder. Moreover, they provided a detailed review on asphalt binder resistance parameters. The following is a summary of the points that were concluded based on the results and analysis of the binder rutting and fatigue studies [31]:

1. $G^*/\sin(\delta)$ was derived from testing that does not provide good representation of traffic loading in the field. The parameter could not be found useful in describing the accumulation of permanent flow, which is important in rutting evaluation.
2. Binder Repeated creep test is a better method for estimating binder resistance to permanent deformation.
3. A new test is needed to determine the relation between mixture fatigue life and binder rheological properties.

3.11 Asphalt concrete modeling

Asphalt concrete modeling is a growing subject. The great advancement in computational power and test protocols will help asphalt pavement researchers and pavement engineers to use more realistic, advanced, and powerful model to predict the performance of asphalt materials and pavements.

3.12 Pavement response model versus performance model

The most common approach towards predicting asphalt pavement performance consists of two main steps:

1. Pavement response prediction
2. Pavement performance prediction

In this approach, responses of undamaged pavement (e.g. tensile strain at the bottom of the asphalt layer) are estimated from a structural model (e.g., multilayered elastic theory) using, initial undamaged properties of the layer materials. Asphalt concrete models are developed using laboratory test results and relate the initial response of the asphalt concrete to the life of those specimens. The responses estimated from the structural model are then input in to the performance model to determine the life of the pavement. The previously mentioned approach is the state-of-the-practice method that is adopted in most recent mechanistic-empirical pavement design methods, including the Mechanistic-Empirical Pavement Design Guide (MEPDG) developed under the NCHRP project 1-37A (2004).

3.13 Pavement response model versus performance model

Asphalt materials and pavement researchers and engineers showed great interest in developing asphalt pavement models to help predict asphalt pavement performance. Performance models are used in the new Mechanistic Empirical design guide to design pavement layers using the lowest cost.

In this approach asphalt pavement structure responses (e.g. tensile strain at the bottom of the asphalt layer) before applying any loads are estimated using a structural model (e.g. multilayer elastic theory). Asphalt mixtures test responses recorded in the laboratory are then related using mathematical models to the responses estimated by the structural model. The responses predicted by the structural models are then used as an input in to the performance model to determine the life of the pavement. The previously discussed approach is the state of the practice method that is currently being used in the most recent mechanistic-empirical pavement design methods, including the current Mechanistic-Empirical Design Guide (MEPDG) developed under the NCHRP project 1-37A (2004).

One of the most famous asphalt mixture properties is the dynamic modulus. This section will discuss different models that predicts the asphalt mixture dynamic modulus.

Asphalt pavement researchers and engineers recommend the use of asphalt mixtures fundamental properties as an input to pavement performance models. The dynamic modulus is a fundamental property that can be used as a measure of the asphalt mixture stiffness. The dynamic modulus can be in different forms such as compression modulus and shear modulus. In the 1980s, the significance of the dynamic modulus was not known yet due to the limitation in testing data collection abilities. For these reasons, the dynamic modulus was not included in the US-LTPP material characterization plans. In 2011, the federal Highway Administration FHWA adopted a study in order to back calculate asphalt mixture dynamic modulus from asphalt binder properties (Asphalt binder data was available and recorded for older material). As a result, the primary objective of the 2011 FHWA study was to "develop estimates of the dynamic modulus of HMA layers on the LTPP test sections following the models used in the MEPDG" [42]. This was determined to be feasible; since the existing LTPP database contains HMA mixtures and binder laboratory test data that could be used as input in the models [43].

Currently the dynamic compression modulus is being used in the ME design and Darwin ME software. The Mechanistic Empirical design guide software and the Darwin ME was completed under NCHRP project 1-37A and 1-40D. This section will discuss different dynamic modulus prediction models that are currently in use.

3.13.1 Original Witczak equation (NCHRP 1-37A)

The Original Witczak model was developed in 1972. The model was developed using nonlinear regression techniques of laboratory dynamic compression modulus E* values. Witczak research team relied on values from 29 Hot Mix Asphalt mixtures with a total of 87 points in building their analysis database.

In 1999, Witczak and his team modified the 1972 original dynamic modulus prediction model. 205 laboratory mixtures with a total of 2750 points were used in the modification procedure. Witczak and his team included 171 unmodified asphalt binders and 34 modified binders. As mentioned earlier, the Mechanistic-Empirical Design Guide MEPDG is currently adopting Witczak 1999 modified equation to predict asphalt mixtures dynamic modulus at different speeds and temperatures.

In 2006, Witczak and his research team further modified the model in 2006. The 2006 Witczak model incorporated 346 HMA mixtures with 7400 data points [44]. Although Witczak modified the ability of the 1999 version in the 2006 version, the 1999 model is the most famous since it is currently being used in the MEPDG design software.

Equation 3 describes Witczak 1999 dynamic modulus predictive model.

$$
\begin{aligned}
&log|E^*| \\
&= 3.750063 + 0.02932\rho_{200} - 0.001767(\rho_{200})^2 - 0.002841\rho_4 - 0.05809V_a \\
&- 0.802208\left(\frac{V_{beff}}{V_{beff} + V_a}\right) \\
&+ \frac{3.871977 - 0.0021\rho_4 + 0.003958\rho_{38} - 0.000017(\rho_{38})^2 + 0.00547\rho_{34}}{1 + e^{(-0.603313 - 0.31335\,log(f) - 0.393532\,log(\eta))}}
\end{aligned}
$$

Equation 3 : Witczak dynamic modulus E* predictive model

Where,

$|E^*|$= dynamic modulus (psi).

η= bitumen viscosity (10^6Poise)

F= loading frequency (Hz)

V_a=air void content (%)

V_{beff}=effective bitumen content (% by volume)

ρ_{34}= Cumulative % retained on the 19-mm (3/4inch) sieve

ρ_{38}=cumulative % retained on the 9.5-mm (3/8inch) sieve,

ρ_{4}= cumulative % retained on the 4.75-mm (No.4) sieve, and

ρ_{200}= % passing the 0.075-mm (No.200) sieve.

3.13.2 Modified Witczak dynamic shear (|G*|) equation (NCHRP 1-40D)

In 2006, Witczak modified the 1999 model to incorporate asphalt binder results from the Dynamic Shear Rheometer (DSR). The dynamic shear rheometer is the main tool of studying asphalt binder modulus at different frequencies and temperatures. Despite the great effect of loading frequency on the asphalt binder rheological properties, Witczak 1999 model dealt with the loading frequency of the asphalt binder as an independent variable. In 2006, Witczak incorporated the asphalt binder shear modulus results produced by the DSR at different frequencies and temperatures instead of the binder viscosity. Dynamic modulus values are then used to develop master curves (Dynamic modulus values at different frequencies for specific reference temperature). Witczak modified Equation 4

$$log_{10} E^* = -0.349 + 0.754(|G_b^*|^{-0.0052}) \times \Bigg(6.65 - 0.032\rho_{200} + 0.0027{\rho_{200}}^2 + 0.011\rho_4 - 0.0001{\rho_4}^2 + 0.006\rho_{38} - 0.00014{\rho_{38}}^2 - 0.08V_a - 1.06\left(\frac{V_{beff}}{V_a+V_{beff}}\right)\Bigg) + \frac{2.56+0.03V_a+0.71\left(\frac{V_{beff}}{V_a+V_{beff}}\right)+0.012\rho_{38}-0.0001{\rho_{38}}^2-0.01\rho_{34}}{1+e^{(-0.7814-0.5785\,log|G^*|+0.8834\,log\,\delta_b)}}$$

can be expressed as follows [45]

Equation 4: Modified Witczak equation based on |G*| (NCHRP 1-40D) Witczak dynamic modulus E* predictive model

Where,

$|E^*|$= dynamic modulus (psi).

V_a=air void content (%)

V_{beff}=effective bitumen content (% by volume)

ρ_{34}= Cumulative % retained on the 19-mm (3/4inch) sieve

ρ_{38}=cumulative % retained on the 9.5-mm (3/8inch) sieve,

ρ_4= cumulative % retained on the 4.75-mm (No.4) sieve, and

ρ_{200}= % passing the 0.075-mm (No.200) sieve.

$|G^*|$=dynamic shear modulus of binder (psi), and

3.13.3 Artificial neural network model-ANN model

According to Federal Highway Administration (FHWA) [42], Artificial Neural Network (ANN) can be defined as “a mathematical or computational model that tries to simulate the structure and functional aspects of biological neural networks as shown in Figure 5. It consists of an interconnected group of artificial neurons and processes information using a connectionist approach to computation” [46] [43]. Artificial Neural Network (ANN) is a nonlinear statistical modeling tool that is used to model complex relationships between inputs and outputs as well as finding relationships between data. The ability to learn new patterns and adapt during the learning phase is a unique property for Artificial Neural Networks (ANN) [46] [47].

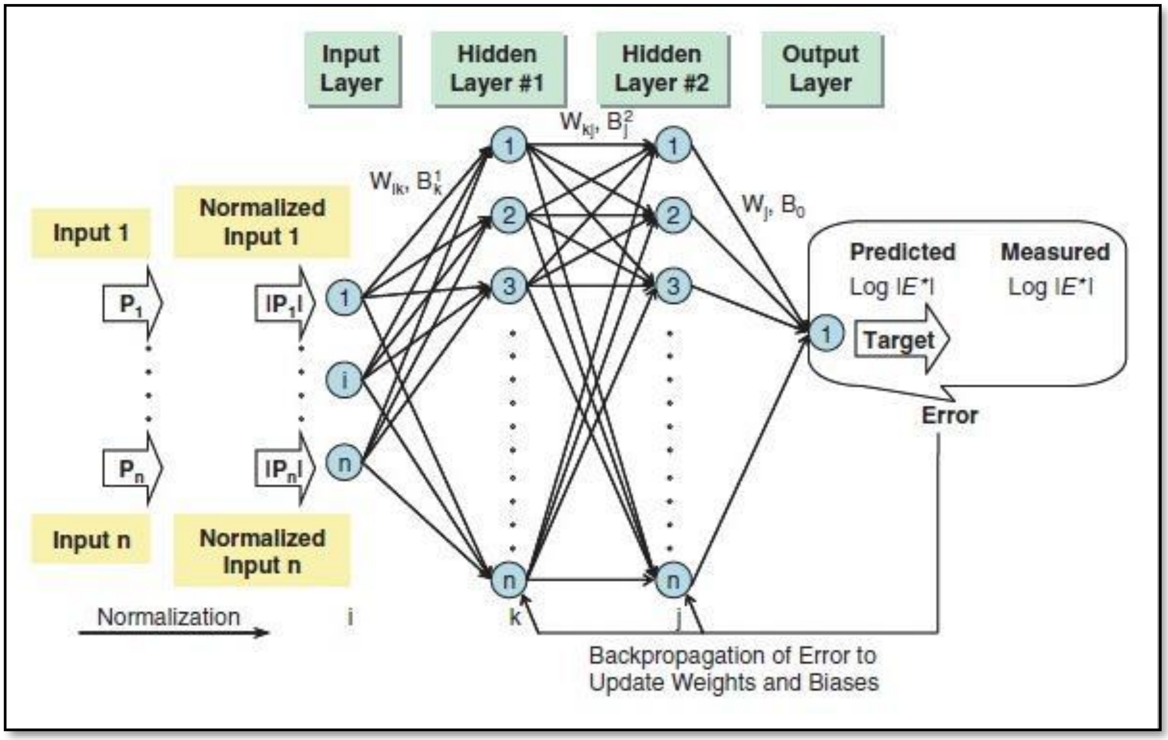

Figure 5 : ANN schematic structure [42]

The FHWA study produced three models to predict asphalt materials properties. The ANN used three main inputs in their models resilient modulus MR, binder viscosity VV, binder shear modulus |G*|. The FHWA ANN models primary inputs were chosen for multiple reasons; first the resilient modulus was selected as it is part of the US-LTPP program as a mixture stiffness indicator. Second, the shear modulus was selected after evaluation of the Hirsch model showed more promising statistical predictions than both of the Witczak model [42]

3.13.4 Hirsch model

Hirsch model is the focus of this research. In this section Hirsch model will be discussed in details as well as a summary of the state of the art of using this model in predicting asphalt mixtures modulus.

Hirsch model was first developed in 1960 by Y.J. Hirsch. Y.J. Hirsch based his model on number of various forms of the law of the mixtures. The Hirsch model is a semi-empirical equation that predicts asphalt mixture dynamic modulus E* values. The rule of mixture or as it is called "Law of Mixtures" takes advantage of the following assumptions [48]:

1. Fibers are uniformly distributed throughout the matrix
2. Perfect bonding between fibers and matrix
3. Matrix is free of voids
4. Applied loads are either parallel or perpendicular on the fiber direction
5. Lamina is initially in a stress free state (no residual stresses)
6. Fiber and matrix behave as linearly elastic materials

There are two different forms of the law of mixtures. The first form can be used when the applied stresses and representative volume element is in the parallel direction. The second form is used when the applied stresses and representative volume element is in the transverse direction (in series). Both orientations can be expressed using Equation 5:

$$E_c = v_1 E_1 + v_2 E_2$$

$$\frac{1}{E_c} = \frac{v_1}{E_1} + \frac{v_2}{E_2}$$

Equation 5 : Mathematical equations of two different versions of the law of mixture

Where:

E_c = composite material property

v_1 & v_2 = volume fraction of component phase 1 & 2

E_1 & E_2 = material properties of component phase 1 & 2

In this case, E_c is the composite material modulus, which is the asphalt mixture dynamic modulus. v_1 & v_2 Are the volume fraction of material one (aggregates) and material two (asphalt binder). E_1 & E_2 Are the modulus of the aggregates and asphalt binder consecutively. The Hirsch Model is based on the concept that any composite material property is a combination of its constituent material property and its effect is directly proportional with its constituent material property as well. Composite material components can be arranged in parallel or in series or a combination of both. The Hirsch model uses a combination of both arrangements to achieve relatively accurate modulus predictions. Figure 6 is a Schematic Representation of Hirsch Model and Four Modified Versions [49].

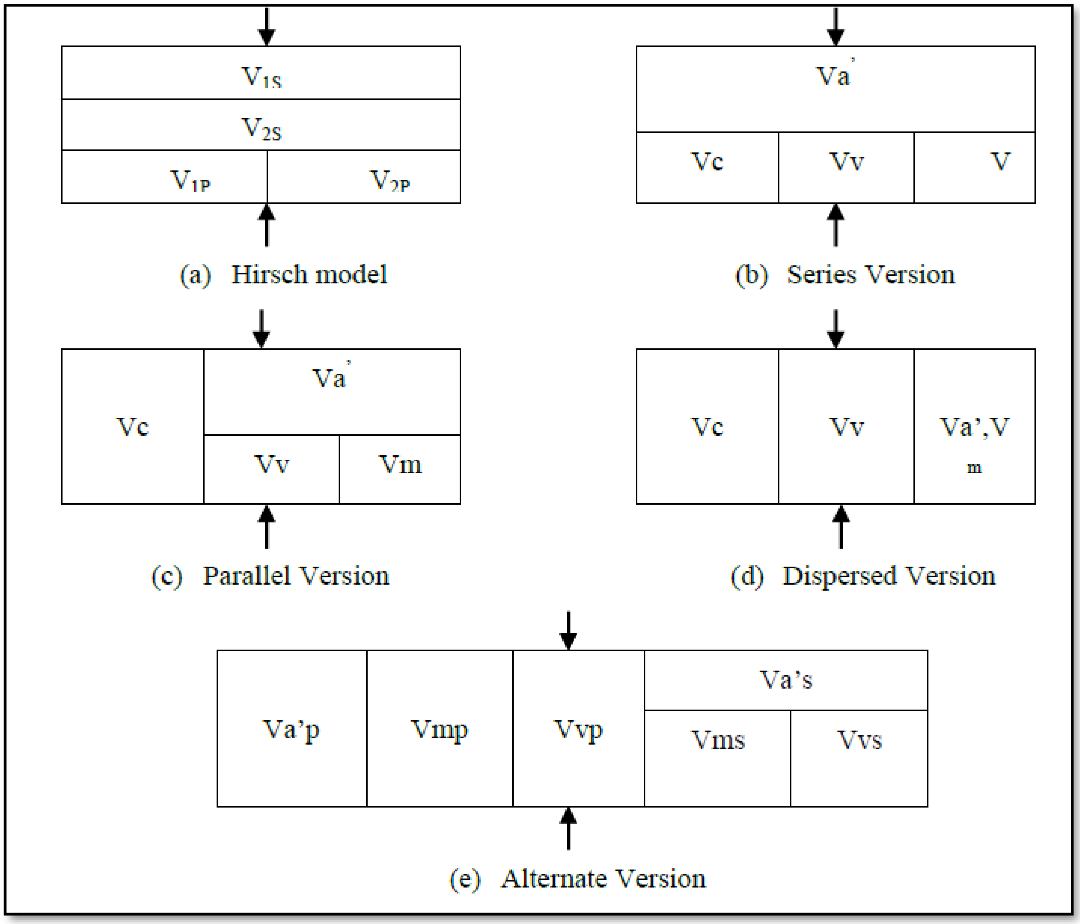

Figure 6 : Schematic representation of Hirsch model and four modified versions [49]

Va' is the volume fraction of aggregate excluding the contact volume and mineral filler, Vc is the aggregate contact volume, Vv is the volume fraction of air voids, and Vm is the mastic volume. The subscripts "p" and "s" refer to the arrangement type "parallel" and "series", respectively Hirsch model was evaluated and calibrated earlier 2002 in order to predict asphalt mixture dynamic modulus using uniaxial compression test.

Hirsch model consists of three main components, which are air voids, aggregates, and asphalt binder. As mentioned earlier Hirsch model was evaluated and calibrated in 2002.

Christensen and his research team published the work they did comparing different parallel and series combinations of the three phases aggregate, binder, and air. In 2003, Christensen, Pellenin and Bonaquist evaluated different versions of the Hirsch model including a version with mastic as the asphalt binder, a version with the effect of film thickness on the asphalt binder modulus. Christensen and his research team found that the alternate version shown in Equation 3 in its simplest form (no mastic effect & no film thickness effect) is the most effective and accurate version of the Hirsch model [42] [43].

Hirsch model alternate version predicts asphalt mixture dynamic modulus as a function of asphalt binder modulus$|G_b^*|$, asphalt mixture Voids in Mineral Aggregates (VMA), and Voids Filled with Asphalt (VFA). Christensen and his research team used Hirsch model alternate version to produce two equations. The first equation is to help predict asphalt mixtures dynamic modulus $|E^*|$ using a uniaxial cyclic compression test. The second equation is to predict asphalt mixture dynamic shear modulus $|G_{mix}^*|$ using the Superpave Shear Test (SST).

The alternate version of Hirsch model can be mathematically represented as Equation 6 shows [49]:

$$E_c = P_c\left(V_a\ \ E_a + V_b E_b\right) + (1 - P_c)\left[\frac{V_a}{E_a} + \frac{(V_b + V_v)^2}{V_b E_b}\right]^{-1}$$

Equation 6: **Alternate version of Hirsch model**

Where,

E_c = modulus of asphalt mixture,

E_a = aggregate modulus,

E_m = mastic modulus, and

P_c = aggregate contact volume fraction.

Other parameters are as defined before. The aggregate contact volume can be calculated as Equation 7 shows [49]:

$$P_c = \frac{\left(P_0 + \frac{VFA \times E_b}{VMA}\right)^{P_1}}{P_2 + \left(\frac{VFA \times E_b}{VMA}\right)^{P_1}}$$

Equation 7 : Aggregate contact volume

Where,

VMA’= voids in the mineral aggregate,

VFM = voids filled with mastic, and

P0, P1, and P2= empirically determined constants

Several Hirsch model equations were constructed and evaluated by Christensen and his team. The final model for predicting mixture dynamic modulus is presented as Equation 8 shows. [49]

$$E_{mix}^{*} = Pc\left[4{,}200{,}000\left(1-\frac{VMA}{100}\right)+3G_{binder}^{*}\frac{VFA\times VMA}{10{,}000}\right] + (1-Pc)\left[\frac{1-\frac{VMA}{100}}{4{,}200{,}000}+\frac{VMA}{3VFA\times G_{binder}^{*}}\right]^{-1}$$

$$Pc = \frac{\left[20+\frac{VFA\times 3G_{binder}^{*}}{VMA}\right]^{0.58}}{650+\left[\frac{VFA\times 3G_{binder}^{*}}{VMA}\right]^{0.58}}$$

Equation 8 : Final 2003 Hirsch model developed by Christensen et al. to predict asphalt mixture dynamic modulus $\mathbf{E_{mix}^{*}}$

Where,

$\mathrm{G_{binder}^{*}}$ = complex shear modulus for ashalt binder, psi;

VMA = voids in mineral aggregate;

VFA = voids filled with asphalt;

Pc = contact factor;

$\mathrm{E_{mix}^{*}}$ = complex modulus for ashalt mixture, psi;

The dynamic modulus of asphalt binder is considered approximately 3 times the binder dynamic shear modulus $|G_b^*|$ recorded using dynamic shear rheometer. Christensen estimated the aggregate modulus as 4,200,000 psi with standard error 6.5%. The predicted dynamic modulus of the asphalt mixture units is in pounds per square inch.

The previously discussed version of Hirsch model showed relatively accurate dynamic modulus predictions. However, some independent researches that used Hirsch model showed model's poor accuracy in some cases. As a result, Ramon Bonaquist and Christensen performed further modifications to the Hirsch model in 2014. These modifications were in the following areas [50]:

a. Simplification of the Hirsch Model
b. Possible changes in modulus with time
c. Variation in the aggregate modulus (steric hardening)
d. Changes in modulus with stress (or strain) level

Asphalt pavement researchers were able to show that the HMA parallel arrangement portion in the Hirsch model alternate version had negligible effect on the final value of the calculated Hot Mix Asphalt dynamic modulus [50]. Because of, Bonaquist et al. simplified the Hirsch model alternate version to reflect the effect of the series portion and neglect the effect of the HMA parallel portion. The 2014 Hirsch model most up to date version can be expressed mathematically using the following equation presented in Equation 9:

$$|E^*|_{mix} = Pc\left[E_{agg}\ (1 - VMA/100) + 3\,|G^*|_{binder}\left(\frac{VFA \times VMA}{10{,}000}\right)\right]$$

$$Pc = \frac{\left(H_1 + \dfrac{VFA \times 3|G^*|_{binder}}{VMA}\right)^{H_3}}{H_2 + \left(\dfrac{VFA \times 3|G^*|_{binder}}{VMA}\right)^{H_3}}$$

Equation 9 : Simplified Hirsch model equation

Where $|E^*|_{mix}$, VMA and VFA are as defined above in Equation 9- Simplified Hirsch model equation; E_{agg} is the aggregate modulus (4,200,000 lb/in^2 in Equation 5) and H_1, H_2 and H_3 are calibration constants determined statistically.

3.14 Asphalt materials performance testing

One of the objectives of the NCHRP project 9-19 was to recommend a simple performance test to complement the SuperPave volumetric mixture design procedure. The need for a simple performance test arose from the concern that the SuperPave mixture design procedure was based entirely upon volumetric proportioning of the asphalt mixture and did not include any direct test method to evaluate permanent deformation resistance of the mix. Asphalt mixture laboratory testing can be divided into three general categories: empirical, performance related, and performance based. Empirical test like Marshall Stability are often limited usefulness because the property measured in the test does not relate directly to performance. Performance related tests like compressive strength, on the other hand, measure engineering properties that have found to be roughly correlate to mixture performance; however, these properties by themselves usually insufficient too as the basis of a fundamental performance prediction models over wide variety of mixture types. Performance based tests measure material properties that can be used in models to predict mixture response to a wide range of load and environmental conditions. Performance-based tests are clearly the best candidates for a simple performance test.

Performance-based test methods can be categorized by the type of the test, type of load application, and type of load pulse as summarized in Table 5. In order to provide accurate and realistic relationships between laboratory measured strains in asphalt mixtures and pavement deformation in the field, it is important to conduct the laboratory tests under stress and environmental conditions similar to those in the field. Any simple performance test must be sensitive to these fundamental factors.

Three fundamental factors are very important to consider:

1. Climatic conditions (e.g., pavement temperature) at the given geographic site.
2. Traffic level (i.e., number of repetitions) expected during the pavement service life, including the rate of loading.
3. Stress levels expected within the asphalt layer for a given pavement structure.

Type of Test or Test Geometry	**Type of Load Application**	**Type of Load Pulse**
Uniaxial or Traxial Compressive	Static Creep Test	None
Indirect Tension	Constant Deformation Rate	Square
Direct Tension	Repeated Load or Cyclic	Haversine
Simple Shear	Dynamic Loading	Sinusoidal
Direct Shear	Constant deformation	Triangular

Table 5 : Categories of performance-based test methods

A successful way to evaluate the permanent deformation characteristics of paving materials is to

apply a repeated load for several thousand repetitions and record the cumulative permanent deformation as a function of the number of cycles (e.g. Monismith et al. (1975) and Witczak and Kaloush (1998) for uniaxial loading: Brown and cooper (1984) for confined conditions). Typically, a haversine pulse load of 0.1 s and 0.9 s dwell (rest time) is applied over a test duration of approximately three hrs. This loading history results in approximately 10,000 load cycles applied to the specimen.

The plot of cumulative permanent strain deformation as a function of the number of load repetitions (in log-log space) is generally defined by three zones: primary, secondary, and tertiary. The load Cycle at the onset of tertiary flow is termed the flow numberF_N.

The flow number test uses a loading cycle of 1.0 second in duration, and applies a 0.1 second

Haversine load followed by 0.9-second rest period [9]. The specimen is tested for 10,000 cycles

Or until tertiary flow, whichever occurs first. Permanent axial strains are recorded throughout the

test. The test is conducted at an effective temperature and stress level of 54.0 ℃ (130 °F) and 207

KPa (30 psi), respectively. The "Flow Number" is defined as the starting point, or cycle number, at which tertiary flow occurs on a cumulative permanent strain curve obtained during the test.

Permanent deformation or rutting is a common problem in asphalt pavements, particularly in hot

regions [3]. Rutting is the result of a complex combination of densification and shear flow. The primary mechanism of rutting is shear deformation (flow), which is caused by large stresses in upper portions of asphalt concrete. Shear deformation is affected primarily by temperature. Studies have shown that rutting in asphalt pavement is proportional to the number of load cycles and the permanent deformation is limited to the upper 100 mm (4 in.) of the asphalt concrete layer [4]. While significant rutting may be interpreted as a major structural failure, it is also a serious safety issue for road users because there is a potential for hydroplaning when water accumulates in the ruts.

The SHRP program concluded with the introduction of the Superpave (Superior Performing Asphalt Pavements) mix design and analysis system. As part of Superpave, a series of mechanical testing procedures using the Superpave Shear Tester (SST) were developed for advanced mixture performance analysis [5]. Those mechanical testing procedures were adopted

by the American Association of State Highway and Transportation Officials (AASHTO) as

provisional standards AASHTO Designation TP7-94 [6]. However, since the original Superpave

Performance Models were determined to contain critical errors [5, 7]; AASHTO TP-7 was notWidely used in the Superpave analysis system. On the other hand, the mechanical property tests

In addition, associated analyses are still being used by at least 10 research and state agencies in the United States [5]. In the past few years, major research was conducted under the National

Cooperative Highway Research Program (NCHRP) Project 9-19 "Superpave Support and Performance Models Management" [8], which aimed to recommend a "Simple Performance Test (SPT)" to complement the Superpave volumetric mixture design method. The results from NCHRP Project 9-19 recommended three candidate SPTs (AMPT): flow time (FT), flow number (FN), and dynamic modulus |E*| tests. In addition, the dynamic modulus test was selected for the HMA materials characterization input utilized in the Mechanistic and Empirical (M-E) Guide for

Design of New and Rehabilitated Pavement Structures, developed under NCHRP Project 1-37A.

Recently, both NCHRP Projects 9-19 [8] and 9-29 [9] have reported the use of SPTs to complement the Superpave mix design method.

3.14.1 Asphalt mixture performance testing

- **Asphalt Mixture Performance Tester (AMPT)**

The AMPT shown in Figure 7 is designed to determine dynamic modulus of asphalt core samples. Dynamic modulus is the stiffness of the asphalt core under a variety of temperatures and loading scenarios. AMPT is a key component in evaluating the quality of asphalt performance samples. Currently, the Mechanistic-Empirical Pavement Design Guide (MEPDG) relies on dynamic modulus as a basis for design criteria. The AMPT is also calibrated to conduct repeated load testing and static creep testing, which determines permanent deformation properties.

Figure 7 : Asphalt Mixture Performance Tester

- **Asphalt Pavement Analyzer (APA)**

The APA shown in Figure 8 is designed to simulate traffic loading created by vehicle wheels. A moving wheel load atop a pressurized rubber hose replicates the repeated loads a pavement will see during its daily cycle. The rate and pressure of the loading is controlled by a dedicated computer, which also acquires data for the APA. The entire chamber also is environmentally controlled so rutting potential can be measured for an array of conditions. Engineers can determine the rutting potential of specific asphalt mixtures using the APA as a comparative tool.

Figure 8 : Asphalt Mixture Performance Tester

- **Dynamic Shear Rheometer (DSR) solid fixtures**

An older Dynamic Shear Rheometer (DSR) will be fitted with a solid fixture based on the sliver test specimen dimensions. Different materials with known material properties will be used to calibrate the DSR solid fixture equipment used. A detailed schematic diagram of Rutgers DSR solid fixtures is presented in Figure 9.

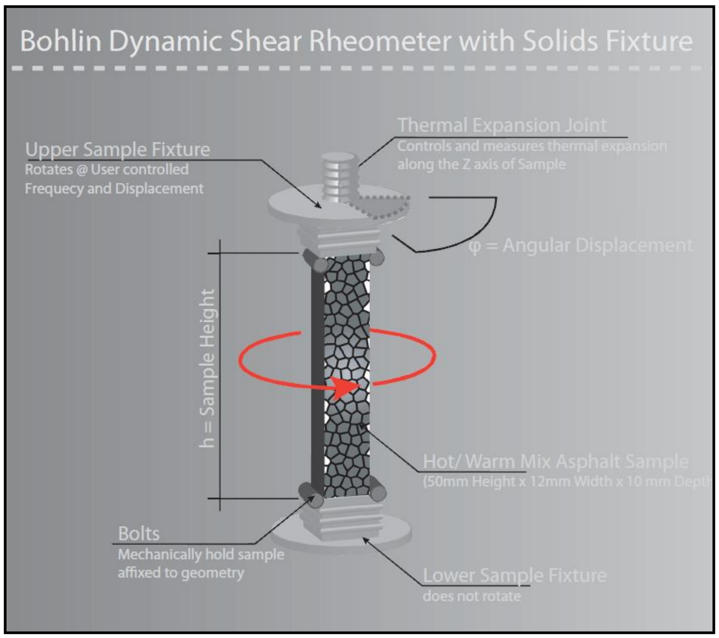

Figure 9 : Schematic diagram of the Dynamic Shear Rheometer

3.14.2 Asphalt binder performance testing

- **Bending Beam Rheometer (AASHTO T 313)**

As the name suggests, the BBR shown in Figure 10 bends beams/bars of asphalt samples to determine the properties of asphalt binder at low temperatures. These properties must be quantified to determine the low-temperature cracking threshold of the binder.

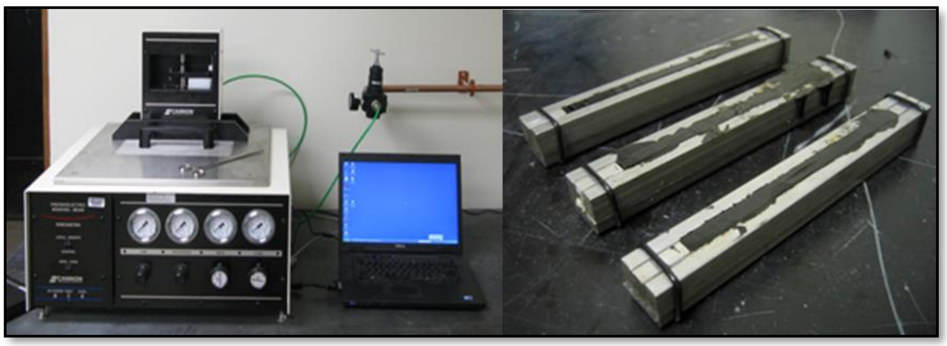

Figure 10 : Bending Beam Rheometer

- **Dynamic Shear Rheometer (AASHTO T 315)**

For many years, the asphalt and highways industry used empirical testing and professional judgment in order to characterize asphalt binder properties [51]. The low grade is selected based on a single low temperature occurrence [51]. For example, we expect PG70-22 binder to perform in a climate with a high average 7-day temperature being 70 °C and a low temperature being -22 °C. Depending on the speed and traffic volume, these grades can be altered by using „grade bumping‟. For a slow-moving traffic condition, the rutting potential is higher, and therefore, an engineer may choose to bump or increase the high temperature grade by one (i.e. 70 to 76). In the instance of standing traffic, an engineer may choose to bump up the high temperature grade by two levels over the standard climate base grade (i.e. 70 to 82) [51]. During these modifications, the low temperature grade may also be altered. This grade adjustment is solely based on experience and professional judgment as specified in AASHTO M 320.

The dynamic shear rheometer (DSR) is used to characterize the viscous and elastic behaviors of asphalt binders at medium and high temperatures [52]. It measures the rheological properties, including phase angle (δ) and complex shear modulus (G*) at a loading frequency of 10 rad/sec, over a specific temperature [52]. The temperature is chosen based on the yearly 7-day average high air temperature [51] [52]. Complex shear modulus (G*) is a measure of material to resist deformation, and phase angle (δ) is indicator of elastic and viscous component. When δ=zero the binder is purely elastic and when δ =90 it is purely viscous. In terms of rutting behavior, the binder should be stiff and elastic, therefore the rutting parameter G*/sinδ should be maximized. In terms of fatigue resistance, the binder should be elastic, but not too stiff therefore the fatigue parameter G*sinδ should be minimized [52].

The DSR shown in Figure 11 is used in the laboratory for high temperature performance-grade (PG) testing outlined in AASHTO T 315. It is also used to perform the Multiple Stress Creep Recovery (MSCR) test on asphalt binders (AASHTO TP-70).

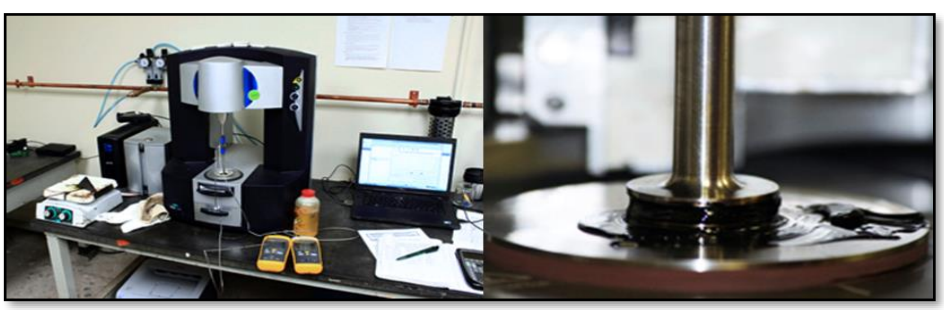

Figure 11 : Dynamic Shear Rheometer

- **Asphalt binder extraction and recovery**

Asphalt Binder Extraction and Recovery Solvent extraction, the oldest of the three test methods, uses a chemical solvent (trichloroethylene, trichloroethane or methylene chloride) to remove the asphalt binder from the aggregate. Typically, a loose HMA sample is weighed and then a solvent is added to disintegrate the sample. The asphalt binder/solvent and aggregate are then separated using a centrifuge and the aggregate is weighed. The initial and final weights are compared and the difference is assumed the asphalt binder weight. Using this weight and the weight of the original sample a percent asphalt binder by weight can be calculated. A gradation test can then be run on the aggregate to determine gradation. Today, the solvent extraction method is only sparingly used due to the hazardous nature of the specified solvents.

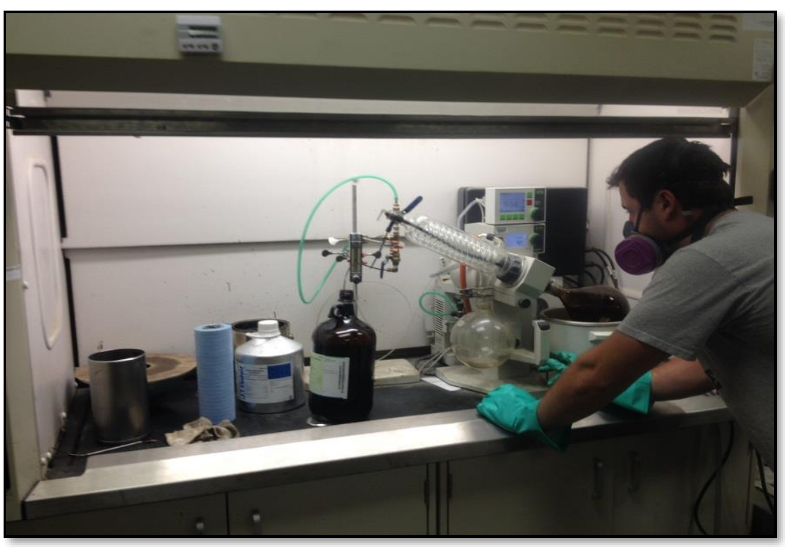

Figure 12 : Binder extraction and recovery

3.15 Literature review summary

This literature review examined the history of pavement design in the United States and explained the direction it is heading in the near future. The MEPDG will be required for pavement design practices for the near future. However, a huge level of effort is still required to calibrate and validate the existing MEPDG models to local conditions.

Research on the dynamic modulus, |E*|, of HMA mixtures were summarized and discussed as it is the most important material characterization property when running an MEPDG analysis on an asphalt pavement section. It is not economically feasible for provincial agencies to perform large-scale dynamic modulus testing on HMA mixtures.

As shown in the literature review, current design procedure as well as distress models requires asphalt mixture dynamic modulus and/or asphalt binder shear modulus as a key input. Also, the literature review indicated that there is a growing demand to understand the effect of aging on asphalt pavement layers as well as understand the effect of incorporating recycled asphalt pavement (RAP) and/or asphalt shingles in new asphalt mixture mix designs and pavement layers. Current asphalt pavements quality control and quality assurance procedures cannot ensure the quality of the produced asphalt mixtures.

The following four factors need to be considered in order to characterize asphalt pavement materials:

1. Conduct performance testing on laboratory prepared, plant prepared, and field cores in order to achieve best performance results.
2. Conduct performance test on the asphalt mixture in its solid form.

3. Ensure that required performance tests are not complex and/or time consuming.
4. Ensure that number of cores needed and sample size are within practical and realistic considerations.

Chapter 4 – Experimental methodology

4.1 Approach to forward calculate asphalt mixture properties and backward calculate asphalt binder properties

As shown in the literature review, current design procedure and distress models requires asphalt mixture dynamic modulus and/or asphalt binder shear modulus as a key input. Also, there is a growing demand to incorporate recycled asphalt pavement (RAP) and/or asphalt shingles in new asphalt mixture mix designs. The literature stated that current asphalt pavements quality control and quality assurance procedures could not ensure the quality of the produced asphalt mixtures. The literature did indicate that in order to predict asphalt mixtures and asphalt binder properties, characterize asphalt mixture that incorporates RAP and/or asphalt shingles, and provide practical QC/QA methodology; the following four factors need to be considered:

1. Conduct performance testing on laboratory prepared, plant prepared in order to achieve best performance results.
2. Conduct performance test on the asphalt mixture in its solid form.
3. Ensure that required performance tests are not complex and/or time consuming.
4. Ensure that number of cores needed and sample size are within practical and realistic considerations.

This section discusses the approach followed in this research to develop a practical methodology to forward predict asphalt mixture properties and backward predict asphalt binder properties. The developed methodology can be further utilized to predict pavement distress resistance for fatigue cracking and permanent deformation. The following flow chart illustrates the overall methodology that will be followed during the development of this thesis.

4.2 Developed methodology criteria

Based on the information generated from the Literature Review, the developed methodology forward calculates asphalt mixture complex modulus and backward calculate asphalt binder complex modulus of existing state highways and roads. Asphalt mixture properties methodology will rely on:

1. Developing a test protocol that uses small asphalt mixture rectangular slivers.
2. Simulating actual environmental and traffic loading conditions.
3. Develop a model to forward calculate asphalt mixture properties
4. Develop a model to backward calculate asphalt binder properties.
5. Verify the developed forward model
6. Verify the developed backward model

4.3 What is "Forward" calculation of asphalt mixture properties?

It is a methodology that is developed to predict asphalt mixture dynamic modulus E*binder using small geometry asphalt mixture samples (Sliver size asphalt mixtures specimen). A new model was developed that can be used to predict these properties.

4.4 What is "Backward" calculation of asphalt mixture properties?

It is a methodology that is developed predict asphalt binder shear modulus G*binder using small geometry asphalt mixture samples (Sliver size asphalt mixtures specimen). A new model was developed that can be used to predict these properties.

4.5 Develop methodology

Following the developed methodology, asphalt mixture lab specimens were fabricated and tested using AASHTO TP 79 "Standard Test Method for Determining the Dynamic Modulus and Flow Number for Asphalt Mixtures Using the Asphalt Mixture Performance Tester (AMPT)". Asphalt mixture complex modulus values were recorded. More test specimens were fabricated according to ASTM D7552 "Standard Test Method for Determining the Complex Shear Modulus (G*) of Bituminous Mixtures Using Dynamic Shear Rheometer. Asphalt mixture complex shear modulus G* was recorded. AMPT E* data was used in parallel with the sliver test G* data to develop the forward calculation model. **Figure 13** is flow chart that describe the forward model development experimental plan.

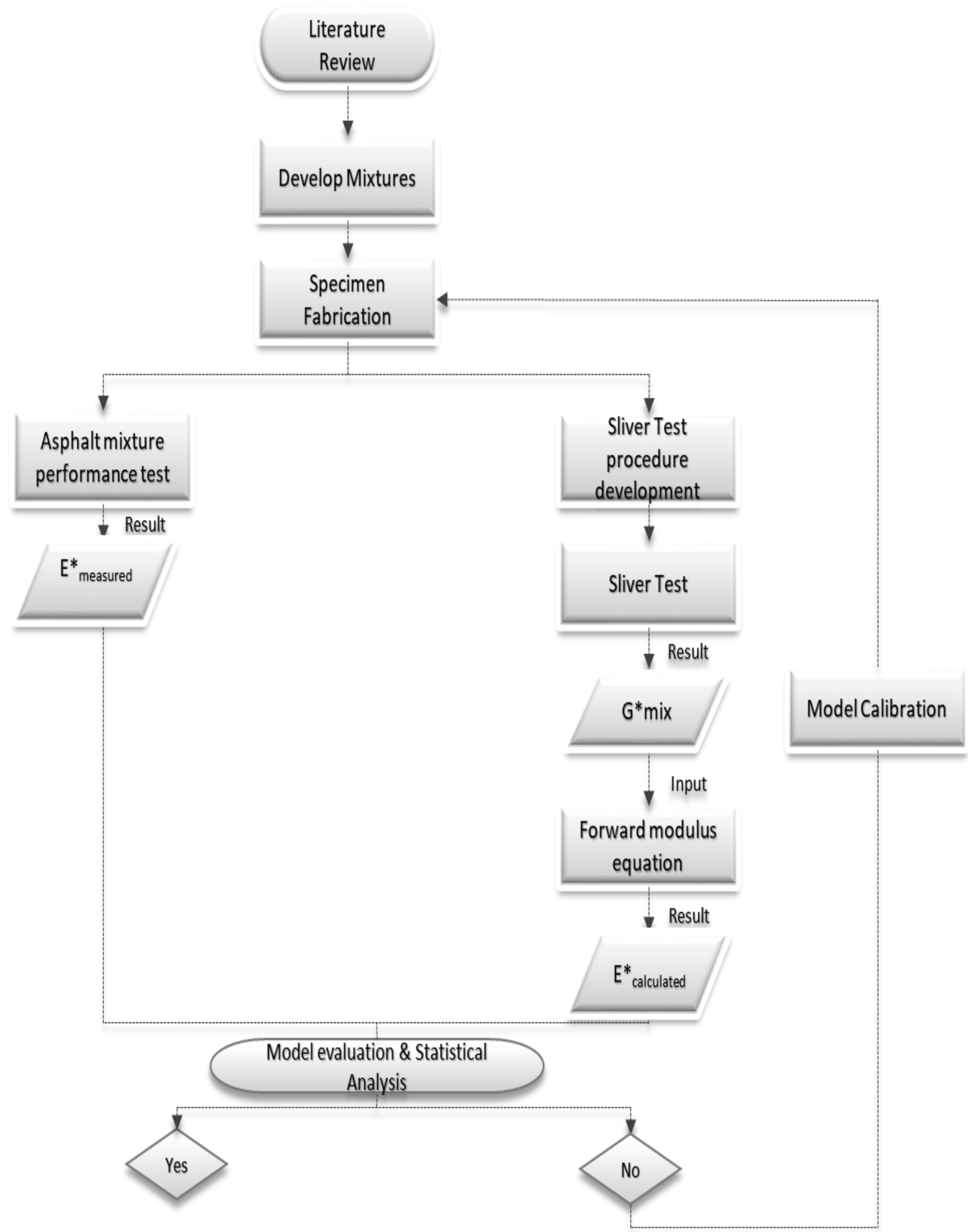

Figure 13 Asphalt mixture forward model development flow chart

In regards of the developed backward methodology, asphalt mixture sliver test specimen was used in the asphalt binder extraction and recovery process. The extraction and recovery process was performed on sliver test specimens according to AASHTO T164 “Standard Method of Test for Quantitative Extraction of Asphalt Binder from Hot Mix Asphalt (HMA)” and ASTM D5404 “Standard Practice for Recovery of Asphalt from Solution Using the Rotary Evaporator”. Asphalt binder specimen were fabricated and tested according to AASHTO T315 “Standard Method of Test for Determining the Rheological Properties of Asphalt Binder Using a Dynamic Shear Rheometer (DSR)”. Asphalt binder shear modulus G*binder was recorded using the Dynamic Shear Rheometer. The recorded data was used in parallel with the sliver test data to develop the backward calculation model. **Figure 14** is a flow chart describes the backward model development experimental plan.

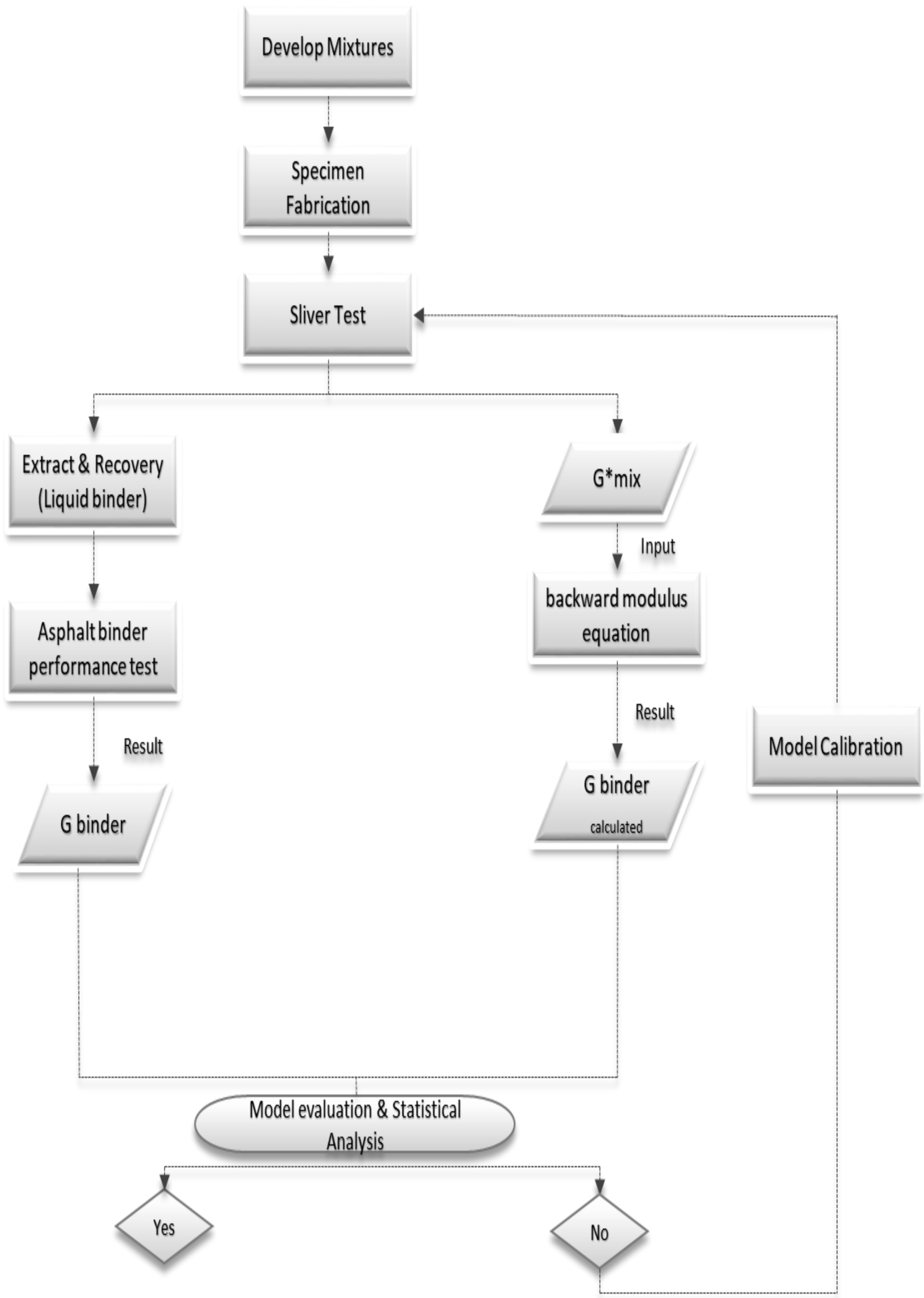

Figure 14 Asphalt binder backward model development

4.6 Verify methodology

Additional laboratory and plant samples were used from different state highways, airfields that corporate different types of binder and materials were tested according following the developed methodology. Data was processed and a full material characterization forensic analysis was performed.

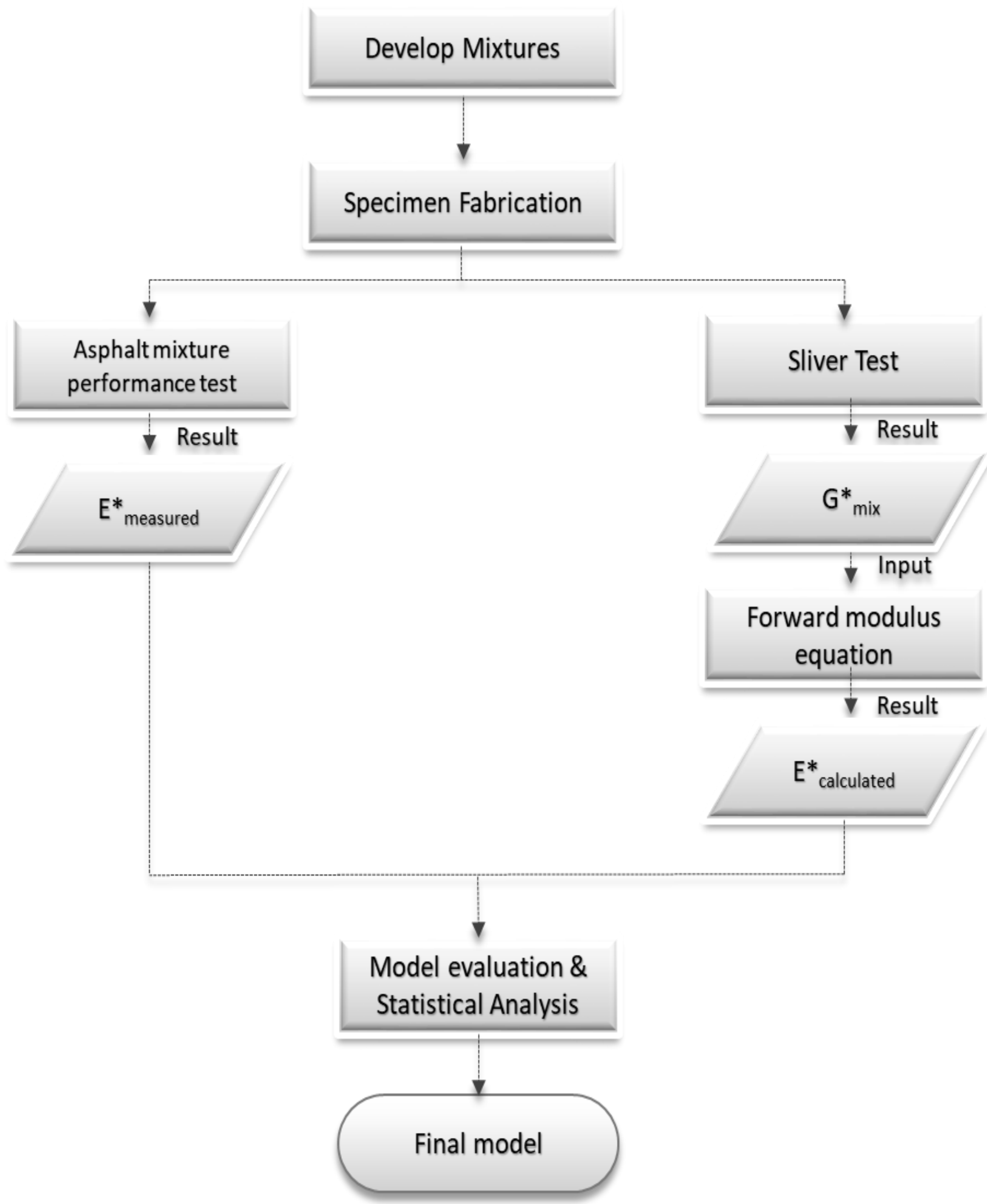

Figure 15 Asphalt mixture forward model verification

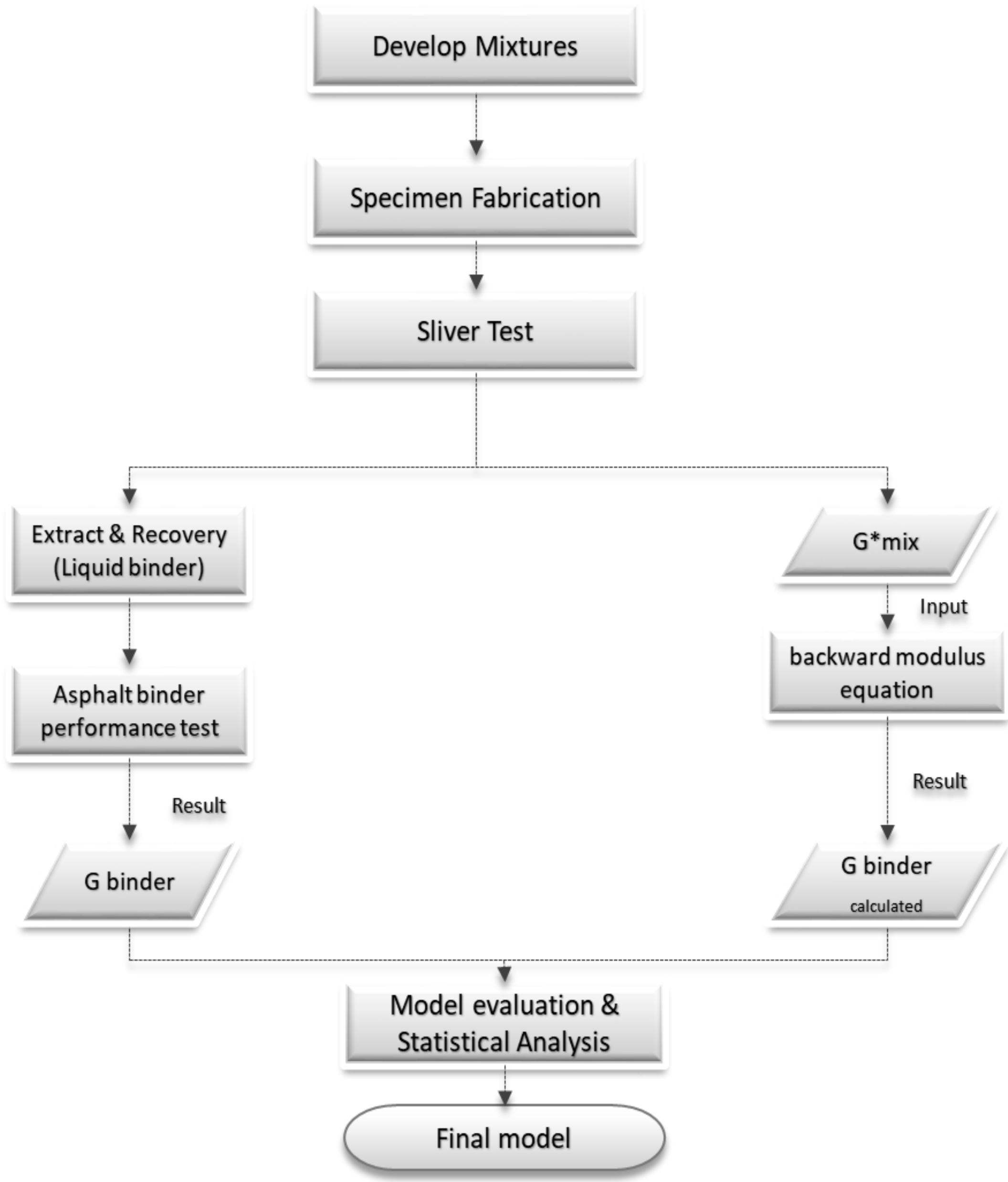

Figure 16 Asphalt binder backward model verification

Chapter 5 - Laboratory tests

5.1 Asphalt mixtures laboratory tests

5.1.1 Asphalt mixture dynamic modulus E* test using the asphalt mixture performance tester AMPT

The dynamic modulus test is the oldest and best documented of the triaxial compression tests. It was standardized in 1979 as ASTM D3497, "Standard Test Method for Dynamic Modulus of Asphalt Concrete Mixtures." The test consists of applying a uniaxial sinusoidal (i.e., haversine) compressive stress to an unconfined or confined HMA cylindrical test specimen. The stress-to-strain relationship under a continuous sinusoidal loading for linear viscoelastic materials is defined by a complex number called the "complex modulus" (E^*). The absolute value of the complex modulus, $|E^*|$, is defined as the dynamic modulus. The dynamic modulus is mathematically defined as the maximum (i.e., peak) dynamic stress (σo) divided by the peak recoverable axial strain (εo) The real and imaginary portions of the complex modulus (E^*) can be written as shown in Equation 10.

$$E^* = E' + iE''$$

It is an indicator of the viscous properties of the material being evaluated. Mathematically, this is expressed as

$$E^* = |E^*| \cos \varphi + i\,|E^*| \sin \varphi$$

Equation 10 : Dynamic modulus

Where E' is generally referred to as the storage or elastic modulus component of the complex modulus; E'' is referred to as the loss or viscous modulus. The phase angle, φ, is the angle by which εo lags behind σo.

Stiffness (dynamic modulus) is a key material property that determines strains and displacements in pavement structures. The 2002 Design Guide: Design of New and Rehabilitated Pavement Structures, developed under NCHRP Project 1-37A, uses the HMA dynamic modulus (E*) as the design stiffness parameter and the E* test for all three levels of hierarchical input for the HMA characterization. The 2002 Design Guide is referred as the new Mechanistic-Empirical Pavement Design Guide (M-E PDG).

The E* test is also a leading candidate for the SPT Simple Performance Test (Asphalt Mixture Performance Test), developed under NCHRP Project 9-19, for use in the Superpave Mix Design procedure.

Thus, the E* test will be playing a very dominant role in the material characterization behavior of all dense-graded HMA mixtures in the future technological methodologies.

For linear viscoelastic materials such as HMA mixes, the stress-to-strain relationship under a continuous sinusoidal loading is defined by its complex dynamic modulus (E*).

This complex number relates stress to strain for linear viscoelastic materials subjected to continuously apply sinusoidal loading in the frequency domain. The complex modulus is defined as the ratio of the amplitude of the sinusoidal stress (at any given time, t, and angular load frequency, (ω), $\sigma = \sigma 0 \sin(\omega t)$ and the amplitude of the sinusoidal strain $\varepsilon = \varepsilon 0 \sin(\omega t-\varphi)$, at the same time and frequency, that results in a steady state response The complex dynamic modulus (E*) can be mathematically expressed as shown in Equation 11.

$$E^{*} = \frac{\sigma}{\varepsilon} = \frac{\sigma_0 e^{i\omega t}}{\varepsilon_0 e^{i(\omega t - \emptyset)}} = \frac{\sigma_0 \sin \omega t}{\varepsilon_0 \sin(\omega t - \emptyset)}$$

Equation 11 : Complex dynamic modulus

Where,

σ0 = peak (maximum) stress

ε0 = peak (maximum) strain

φ = phase angle, degrees

ω = angular velocity

t = time, seconds

Mathematically, the "dynamic modulus" is defined as the absolute value of the complex modulus, i.e. |E*| = σ0/ε0. As a conventional practice, however, the dynamic modulus is denoted as E* (not |E*|) in this report. Stiffness data of an HMA mix as obtained from the E* test provide very important information about the linear viscoelastic behavior of that particular mix over a wide range of temperature and loading frequency.

5.1.2 Asphalt mixtures shear modulus G* using the Dynamic Shear Rheometer DSR

A Rheometer is an instrument that provides information about material viscosity, viscoelastic properties and transient response. Material viscosity usually depends on shear rate/stress, time and temperature dependence. Viscoelastic properties can be expressed in terms of the shear storage modulus, shear loss modulus, and phase angle between stress and strain.

Rheological properties of materials can be used as a “finger print of that material. An understanding of the rheology of “good” and “poor” performing materials can aid in formulation, quality control of different project types.

- **Background**

There are two major types of rheometers: a rotational (shear) rheometers and solids (tensile/bending) rheometers. The focus of this study is on the rotational shear rheometers. Three main dynamic shear rheometers properties will directly affect future research objectives: Torque range, frequency range, and temperature range. Fundamentally, a rotational rheometer will measure:

1. Torque (Force)
2. Angular Displacement
3. Angular Velocity

- **Torque**

Torque is a measure of how much force acting on an object will cause that object to rotate. Torque range is fixed and defined by instrument specifications.

Angular Displacement

Angular displacement is the angle (distance) that a rotating body goes through.

Angular Velocity

Angular velocity can be expressed as strain rate, or in other words, it can be expressed as the change of strain per unit time of measurement. Usually the angular speed is either directly controlled by the motor or measured under application of torque.

- **Rotational rheometer design**

Three main advantages are accompanied with using the torsion rectangular fixtures. The three advantages are:

1- The ability to test high modulus Samples

2- Small temperature gradient

3- Simple test procedure

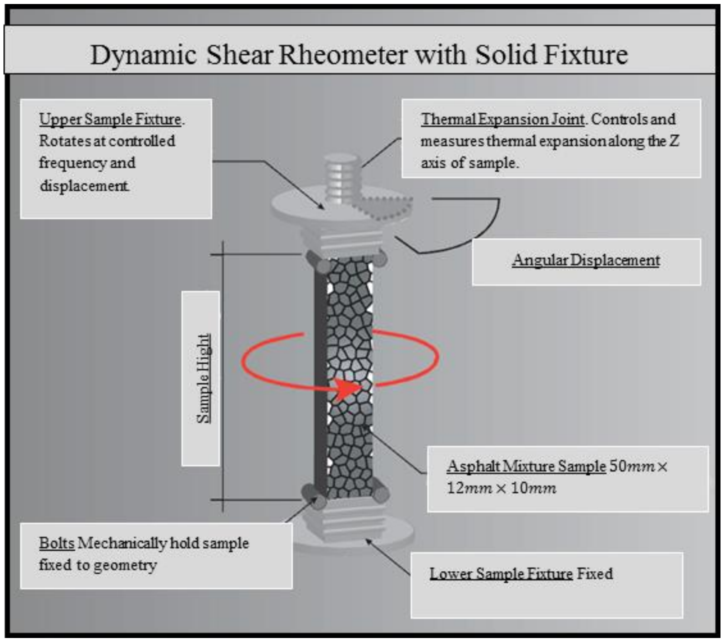

Figure 17 : Schematic Diagram of the dynamic shear rheometer

Strait line Motion	**Rotational Motion**
Force	Torque
Mass	Moment of Inertia
Acceleration	Angular Acceleration
Velocity	Angular Velocity
Displacement	Angular Displacement

Table 6 : Straight line and rotational analogs

- **Oscillation testing**

In order to be able to identify the shear modulus of rectangular solid sample, an oscillation test should take place. An oscillation test is applying a shear stress/strain on the specified sample using a sinusoidal load. Shear stress/strain, amplitude, and frequency are used as test inputs.

- **Frequency**

Frequency is defined as the inverse of the time needed to complete one full oscillation. Frequency is can be measured in radians/seconds or Hz.

- **Phase angle**

Phase angle is a very important parameter that measures the shift between the input wave and the output wave.

- **Viscoelastic parameters**

Stresses in a dynamic experiment can be expressed as complex stresses. There are two main complex stresses components: elastic stress and viscous stress. An elastic stress can be defined as the degree to which a material behaves like an elastic solid, while viscous stress can be defined as the degree to which the material behaves like an ideal liquid. The final viscosity measured in an oscillatory experiment can be referred as complex viscosity. Complex viscosity consists of an elastic component and a term similar to the steady state viscosity.

- **The “sliver test” testing procedure**

The ASTM D7552 can measure asphalt mixture complex shear modulus which is considered fundamental property of the material. The test was refined by Goodrich (Chevron) [53]and then Reinke [54]. The sliver test can be used to determine asphalt mixtures dynamic shear modulus and/or flow time at different temperatures. Rectangular torsion bars “slivers” are cut to 12 mm width, 10 mm thickness and 50 mm length. There is no current AASHTO specification that covers a testing procedure for the sliver test. However, the sliver test is currently described under ASTM D7552 “Standard test method for Determining the Complex Shear Modulus (G*) of Bituminous Mixtures Using the Dynamic Shear Rheometer”. ASTM D7552 recommends using this test standard for asphalt mixtures having complex shear modulus exceeding $1 \times 10^4 Pa$ when tested over temperatures for $10℃\ to\ 76℃$ at frequencies of 0.01 to 10 Hz and strains of 0.01% to 0.1%.

Specimen preparation can be conducted on either laboratory compacted or field compacted specimens. Figure 18 depicts the theoretical methodology utilized to prepare samples for the purposes of this study. By cutting the samples in this manner, oxidative aging from the exterior surface of the sample is reduced for the test specimens. An initial cut is made using a 500mm asphalt saw to remove the top surface of the core. A second cut is made at 12mm to select the plane from which the samples would be generated. From this point on, to cut the small sample size in a more controlled manner, a 230mm diamond bladed tile saw was utilized. Then the 50mm length is removed from the middle of the puck. Once this has occurred, the final slicing of the slivers is conducted at 10mm to create several samples from a single gyratory/field core. It outlines the procedure for cutting 150 mm diameter gyratory/field core samples in the laboratory to achieve the plan outlined. Figure 18 also shows the final preparation of the samples and an example of finalized samples that were ready to be tested.

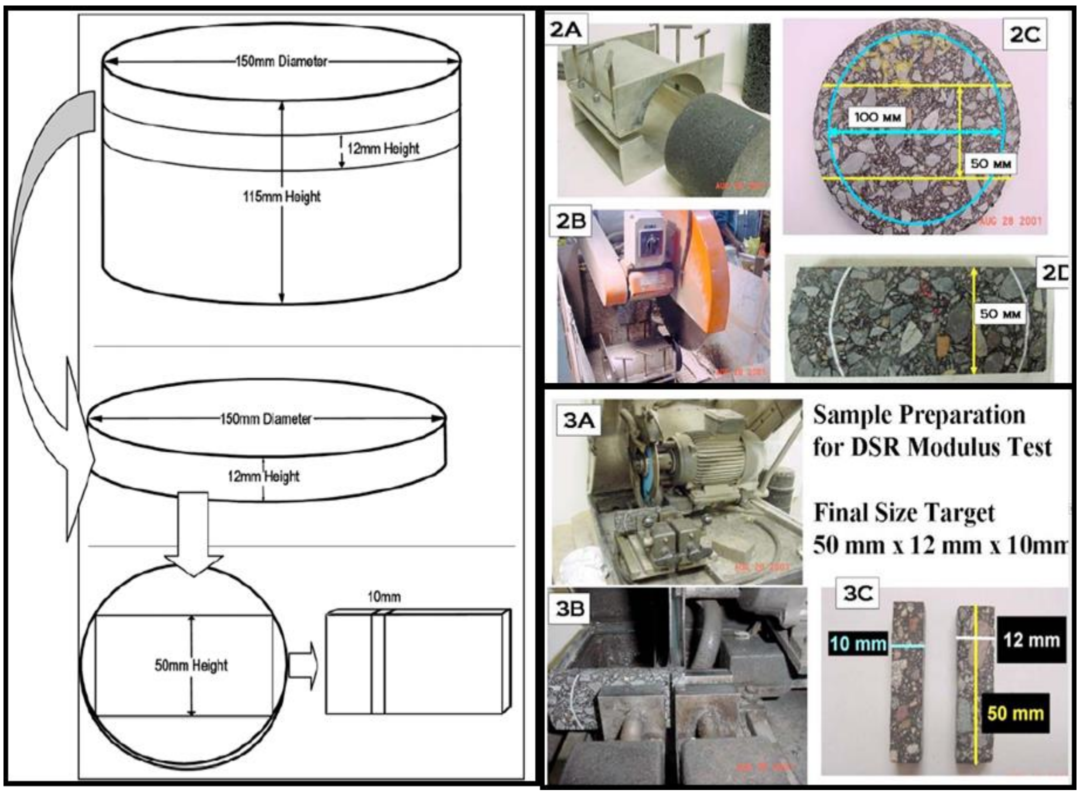

Figure 18 : Test sample preparation [55]

- **Dynamic Shear Rheometer for sliver testing verification**

Figure 19 describes the relation between the complex shear modulus and time. There is an inverse relation between the complex shear modulus and time. At a constant stress, as the temperature increase, the measured complex shear modulus decrease. In other words, the lower the temperature the stiffer the sample.

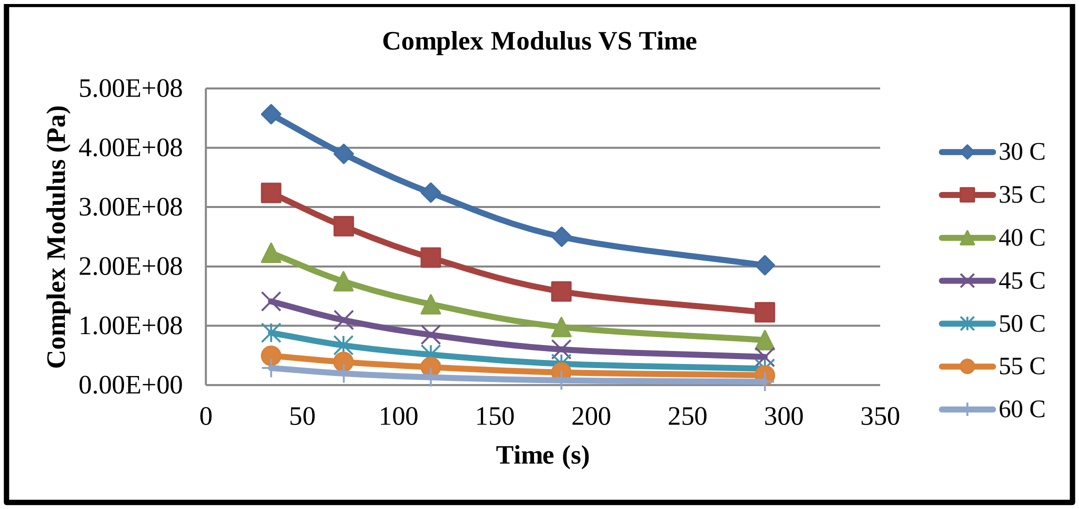

Figure 19 : Comparison of complex shear modulus at different temperatures

Figure 20 is a plot of strain as a function of time, as the time pass the more the measured strain. In this experiment, the sample was tested at 7 different temperature. The figure also shows that there is a direct relation between strain and temperature. There is a huge difference between the measured strain at 60˚C and other test temperatures. This difference might be related to the damage occuring in the sample due to overloading or being long time in the testing chamber.

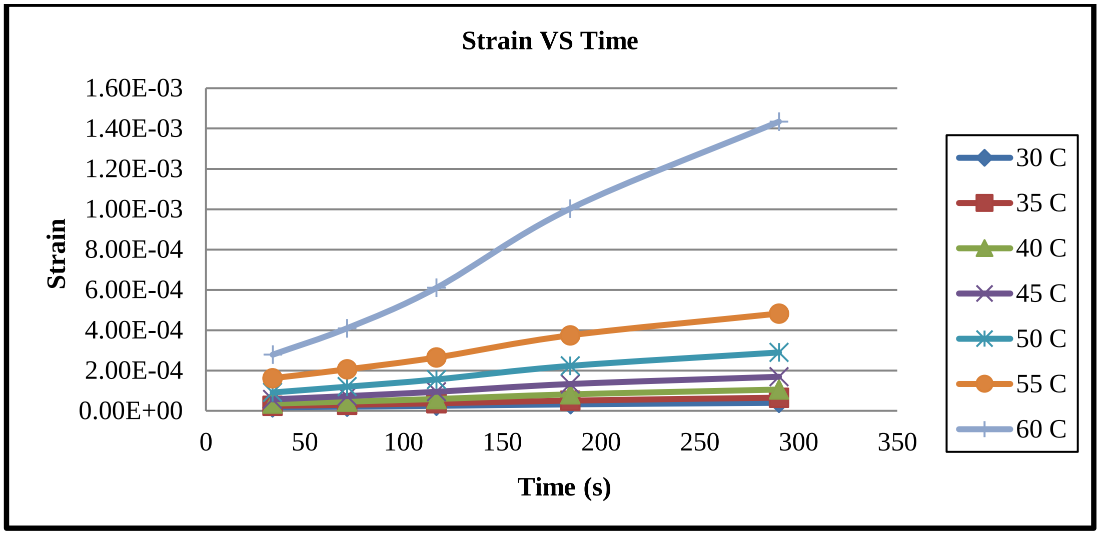

Figure 20 : Comparison of resulting shear strains at different temperatures

Using all the data generated from the frequency-temperature sweep test, the desired master curve at the specified reference temperature can be easily developed. Figure 21 shows an example of test data generated during the study and the resultant master stiffness curve. Asphalt mixture slivers were tested using two differrent dynamic shear rheometers and then three master curves were generated. For calibration purposes, the three master curves were ploted on the same graph to show a complete overlap of each curve.

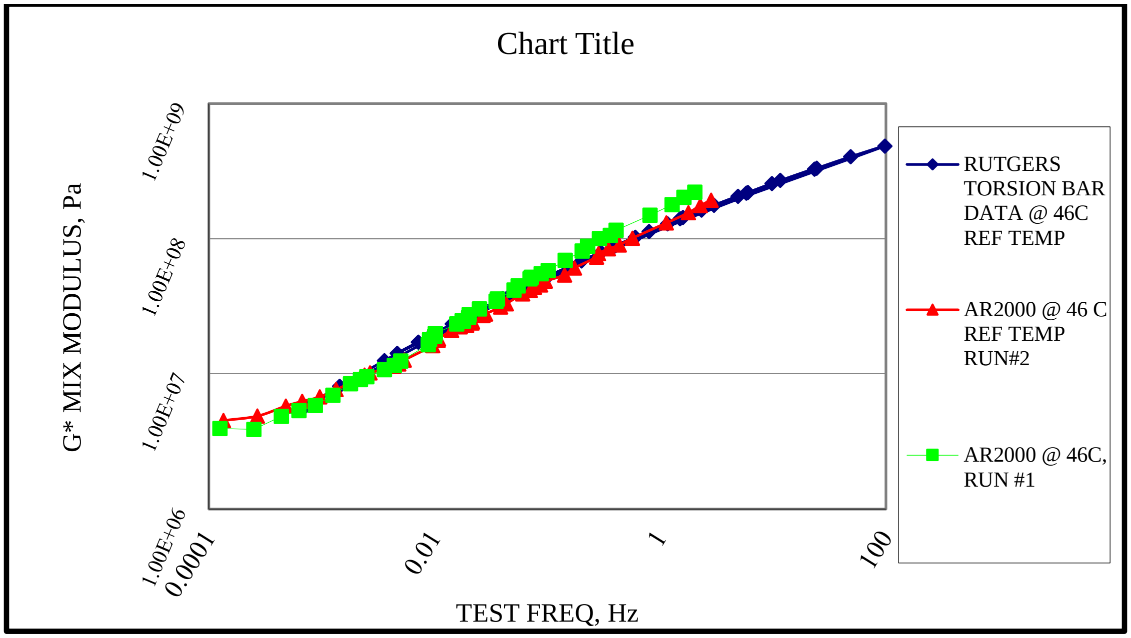

Figure 21 : Master curves developed for the round robbin mix samples

Mathematically, the "dynamic modulus" is defined as the absolute value of the complex modulus, i.e. $|E^*| = \sigma 0 / \varepsilon 0$. As a conventional practice, however, the dynamic modulus is denoted as E* (not |E*|) in this report. Stiffness data of an HMA mix as obtained from the E* test provide very important information about the linear viscoelastic behavior of that particular mix over a wide range of temperature and loading frequency.

Based on the literature review, current design procedure and models require asphalt mixture dynamic modulus and/or asphalt binder shear modulus as key input(s).

The literature review has also shown that asphalt mixture E* is primarily measured experimentally using AASHTO TP-79 and the asphalt mixture performance tester. Asphalt mixture performance tester is a servo hydraulic machine that is capable to test approximately 6-inch cylindrical asphalt mixture specimens (plant mix or lab mix) at different temperature/frequencies. AASHTO TP-79 requires at least two samples to produce a test report.

An approach to determine the applicability of the sliver test was based on experimental testing and the creation of a mathematical model was desired. The following factors were considered to determine the applicability of the sliver test for use as a performance test:

1. The ability to conduct ASTM D7552 testing on laboratory prepared, plant prepared, and field cores in order to achieve best range of performance results.
2. The ability to conduct ASTM D7552 on the asphalt mixture in its solid form.
3. ASTM D7552 was not complex and/or time consuming.
4. Ensure that number of cores needed and sample size required are within practical and realistic considerations.

A material testing program was followed to allow for the development of a new model that used the sliver test laboratory results and Hirsch model to predict asphalt mixture dynamic (compression) modulus E* (forward calculation) and predict asphalt binder shear modulus G* (backward calculation).

Asphalt mixture cylindrical samples were prepared According to AASHTO TP-79 to obtain individual asphalt mixture dynamic modulus E* at the lab. Similarly, Asphalt binder samples were prepared according to AASHTO T-315 to obtain asphalt binder shear modulus for different PG grades at the lab. Results were compared with the predicted values of the forward and backward calculation process. As an outcome of this project, a full analysis and a calibrated model was developed.

Developed methodological approach:

1. Obtain desired asphalt mixture sample
2. Perform volumetric analysis on the gyratory/core sample prior to cutting (Voids in Mineral Aggregates VMA, Voids Filled with Asphalt VFA, Air Voids AV%, etc.)
3. Cut prepared gyratory/core sample to desired sliver geometry with multiple samples for repeatability.
4. Obtain eight sliver specimens (use 3 slivers to define Linear Visco Elastic Region LVE, and 5 to perform the test).
5. Assign required stresses/temperature to the test sequence based on step 4
6. Input results in the developed analysis sheets to forward calculate the asphalt mixture dynamic modulus (E*) and backward calculate asphalt binder dynamic shear modulus (G*).

5.1.3 Asphalt binder laboratory test

- **Asphalt binder dynamic modulus G* using the Dynamic Shear Rheometer DSR**

The asphalt binder from the laboratory gyratory specimen were extracted and recovered in accordance with AASHTO T164, Procedure for Asphalt Extraction and Recovery Process using Tri-ChlorEthylene (TCE) as the solvent medium. The asphalt binder content was determined during the extraction process. The asphalt binder was recovered from the TCE solvent in accordance with ASTM D5404, Standard Practice for Recovery of Asphalt from Solution Using the Rotary Evaporator shown in Figure 22. After recovery, the asphalt binder was tested for its respective shear modulus properties using frequency sweep sequence at different temperatures.

Figure 22: Rotary evaporator

The four-stage process allows for the separation of asphalt binder from mineral aggregates. After the binder is recovered, it is utilized for asphalt binder testing to determine its physical and mechanical performance properties.

Figure 23: Extraction and recovery process

First, the asphalt mixture specimen was cut into lifts using a wet saw and then they were broken down in the oven at 110±5°C until the material was workable. After the sample was dried to constant mass, the initial weight (W1) was determined. The sample was then placed in the 3000-gram extraction bowl, submerged with tri-chloroethylene (TCE) solvent and covered with a filter and the lid for up to one hour. After soaking the asphalt mixture the centrifuge was started thus separating majority of the binder and TCE solvent from mineral aggregate. This process was repeated at least 3 times or until the solution coming out of the centrifuge was not darker than light straw color. The dried weight of the sample after this primary centrifuge was recorded as W_3. The TCE binder solution was then ran through the continuous 100-gram filler centrifuge, separating the very fine mineral (passing the No. 200 sieve) matter that was initially missed by the primary centrifuge. The dried mineral matter weight was then recorded as W_4. The three weights were then used in determining the asphalt binder content of the material, as shown in Equation 12. [56]

$$AC\% = \frac{(W1-W2)-(W3+W4)}{(W1-W2)} * 100$$

Equation 12: Determining the asphalt binder content of the material

Where:

W_{1}=initial mass of the sample,

W_2=mass of water in the sample (assumed to be 0),

W_3=mass of extracted mineral aggregate,

W_4=mass of th mineral mattter in the extract

The last step included the recovery of the asphalt binder from tri-chloroethylene (TCE) solvent following ASTM-D5404 specifications. Utilizing the Rotovap equipment as shown in figure.

Allowed us to separate the tri-chloroethylene (TCE) solvent from the binder through a distillation process. For repeatable results, the temperature and applied vacuum is controlled [56]. After the binder has been recovered, it is then used for classification/verification of the performance grade, and other innovative binder testing. In order to verify the extraction and recovery procedure, Rutgers Asphalt Pavement Laboratory participated in the sensitive study with 10 other AMRL accredited laboratories. The study consisted of performing an extraction and recovery, and further grading the binder for its continuous performance grade. The results show that, the grading for high, intermediate, and low temperatures all fall within the mean minimum error of testing [57] . This verifies the extraction and recovery process as well as the performance grading of the binder.

Chapter 6 – Forward and Backward Model Development

This chapter discusses the experimental test plan and materials used in the model development phase. The correlation of different asphalt mixtures and binder properties will be presented and discussed. Results and analysis of the developed forward and backward model is discussed.

Finally, a presentation of developed models to calculate asphalt mixture and asphalt binder phase angle using sliver test complex shear modulus data.

6.1 Materials

Asphalt mixture dynamic modulus is sensitive to asphalt binder stiffness. The compression complex modulus is currently used as the primary input for the Mechanistic Empirical Design Guide MEPDG. It is used to calculate stresses and strains in the Asphalt layers. Calculated stresses and strains are then used in asphalt pavement distresses predictions. Asphalt mixtures dynamic modulus is also used to evaluate asphalt mixtures additives such as Recycled Asphalt Pavement (RAP), Warm Mix Asphalt (WMA), asphalt rubber, etc.

A detailed experimental test plan was designed to develop an asphalt mixture modulus forward calculation model that is sensitive to a wide range of asphalt binder/mixture stiffness. Tests were performed at wide range of temperatures to cover cold, intermediate, and hot temperature conditions.

This data was helpful in the development of the proposed final model, which integrates the data from the Sliver test as well as other HMA mixtures and binder performance tests to estimate and verify the performance of the model with the inclusion of data from bituminous mixes with different stiffness.

Selected PG binder modulus ranged from unaged binder (soft) PG64-22 and PG76-22 to a long term aged (stiff) PG64-22 and long term aged 76-22 binder. Different PG binder grades and aging conditions were used within this study to show the sliver test's sensitivity to mixture stiffness. On top of different binder grades and age condition, three different binder contents were used with each binder grade 6.1%, 6.5%, 6.9% asphalt binder as shown in Table 7.

Mix Designation	Aging	Binder Grade	NMAS	Gsa Conmbined	Gsb Mixture	AC%
FPP 2017 EWR Axeon 6.1% 64-22 LTOA	Long Term	64-22	12.5	2.693	2.313	6.1
FPP 2017 EWR Axeon 6.1% 64-22 STOA	Short Term	64-22	12.5	2.693	2.282	6.1
FPP 2017 EWR Axeon 6.1% 76-22 LTOA	Long Term	76-22	12.5	2.693	2.309	6.1
FPP 2017 EWR Axeon 6.1% 76-22 STOA	Short Term	76-22	12.5	2.693	2.303	6.1
FPP 2017 EWR Axeon 6.5% 64-22 LTOA	Long Term	64-22	12.5	2.693	2.287	6.5
FPP 2017 EWR Axeon 6.5% 64-22 STOA	Short Term	64-22	12.5	2.693	2.292	6.5
FPP 2017 EWR Axeon 6.5% 76-22 LTOA	Long Term	76-22	12.5	2.693	2.296	6.5
FPP 2017 EWR Axeon 6.5% 76-22 STOA	Short Term	76-22	12.5	2.693	2.275	6.5
FPP 2017 EWR Axeon 6.9% 64-22 LTOA	Long Term	64-22	12.5	2.693	2.271	6.9
FPP 2017 EWR Axeon 6.9% 64-22 STOA	Short Term	64-22	12.5	2.693	2.251	6.9
FPP 2017 EWR Axeon 6.9% 76-22 LTOA	Long Term	76-22	12.5	2.693	2.271	6.9
FPP 2017 EWR Axeon 6.9% 76-22 STOA	Short Term	76-22	12.5	2.693	2.244	6.9

Table 7 : Model development material test matrix

The material test matrix shown above in Table 8 introduced the model to a wide range of asphalt mixture shear modulus (G*sliver) and asphalt mixture dynamic modulus (E*mix).

Test	Minimum Modulus, psi	Maximum Modulus, psi
G*Sliver	27	433568
E*Mix	950	2325531

Table 8 : Asphalt mixture shear modulus and dynamic modulus data range used in the forward prediction model

6.2 Mix design

The mix design procedure used for the samples tested in this study was developed using AASHTO M323 “Superpave Volumetric Mix Design” and related AASHTO standards. As an output of the mix design phase, a wide range of Hot Mix Asphalt modulus was created. The dense graded mix was used to make specimens using the SuperPave gyratory compactor. HMA mixtures were designed using PG64-22, and PG76-22. The aggregate blend bulk specific gravity was 2.693. The aggregate blend had 12.5 mm-nominal maximum aggregates size and 52.42 % fine aggregate passing sieve # 4 (4.75 mm) as shown in **Table 9.**

Seive Size	Blend
50.00	100.00
37.50	100.00
25.00	100.00
19.00	100.00
12.50	91.48
9.50	79.08
4.75	52.42
2.36	35.45
1.18	24.13
0.60	16.96
0.30	11.48
0.15	7.18
0.08	4.18
Gsb	2.69
Gsa	2.73
% Absorption	0.53

Table 9 : Model development job mix formula aggregate blend

Following the mix design phase, four asphalt mixture specimens with 170 mm (6 inches) in height and 150 mm (4 inches) in width were fabricated from each mix type. Three asphalt mixture specimens were used for performing AASHTO TP 79 “Standard Test Method for Determining the Dynamic Modulus and Flow Number for Asphalt Mixtures Using the Asphalt Mixture Performance Tester (AMPT)”. Out of the four test specimens, one test specimen was used for ASTM D 75552 “Standard Test Method for Determining the Complex Shear Modulus (G*) of Bituminous Mixtures Using Dynamic Shear Rheometer”. The asphalt mixture shear modulus specimen is the cut in to sliver size according to ASTM 7552. The specimen is further used for asphalt binder extraction and master curve test.

Table **11** shows a summary table for volumetrics average test results performed on asphalt mixture test specimens. Asphalt mixture specimen had average percent air voids of 6.5%. Table 10 is a summary for the range of volumetric properties used in developing the model.

Bulk Specific Gravity (g/cm^3)	Minimum	Maximum
Air Voids (%)	6.1	7.3
VMA (%)	19.3	22.2
VFA (%)	64.2	71.0
Effect. AC by Vol (%)	13.1	15.3

Table 10 : Model development asphalt mixture specimens volumetric range of results

Sample Type	Sample ID	Wt in Air (grams)	Wt in Water (grams)	SSD Water (grams)	Bulk Specific	Max. Specific	Air Voids (%)	VMA (%)	VFA (%)	Effect. AC by Vol (%)
170	FPP 2017 EWR Axeon 6.1% 64-22 LTOA	6688.3	3842.0	6733.4	2.313	2.462	6.1	19.3	68.7	13.3
170	FPP 2017 EWR Axeon 6.1% 64-22 STOA	6655.1	3770.3	6686.3	2.282	2.462	7.3	20.4	64.2	13.1
170	FPP 2017 EWR Axeon 6.1% 76-22 LTOA	6682.5	3862.9	6759.2	2.309	2.462	6.2	19.5	68.1	13.3
170	FPP 2017 EWR Axeon 6.1% 76-22 STOA	6683.5	3823.9	6725.9	2.303	2.462	6.4	19.7	67.3	13.2
170	FPP 2017 EWR Axeon 6.5% 64-22 LTOA	6632.9	3783.3	6683.3	2.287	2.447	6.5	20.6	68.3	14.1
170	FPP 2017 EWR Axeon 6.5% 64-22 STOA	6661.9	3779.7	6692.7	2.292	2.447	6.3	20.4	69.0	14.1
170	FPP 2017 EWR Axeon 6.5% 76-22 LTOA	6636.7	3821.6	6714.6	2.296	2.447	6.2	20.3	69.5	14.1
170	FPP 2017 EWR Axeon 6.5% 76-22 STOA	6636.5	3779.1	6697.1	2.275	2.447	7.0	21.0	66.5	14.0
170	FPP 2017 EWR Axeon 6.9% 64-22 LTOA	6535.6	3707.5	6585.5	2.271	2.422	6.2	21.5	71.0	15.3
170	FPP 2017 EWR Axeon 6.9% 64-22 STOA	6531.5	3685.3	6588.4	2.251	2.422	7.1	22.2	68.1	15.1
170	FPP 2017 EWR Axeon 6.9% 76-22 LTOA	6539.6	3741.3	6624.0	2.271	2.422	6.2	21.5	70.9	15.3

Table 11 : Asphalt mixture volumetric used in the forward model development phase

6.3 Forward asphalt mixture modulus calculation model results and analysis

6.3.1 Asphalt mixture E*mix (AMPT) and G*mix (Sliver Test) results and correlations

Test data showed that there is a strong correlation between asphalt mixture shear modulus G*sliver and asphalt mixture dynamic modulus E* mix. An example of such correlations will be discussed in this section.

Asphalt mixture dynamic modulus test and asphalt mixture shear modulus test were performed and analyzed at the same test conditions. Eight test temperatures were used (4℃, 10℃, 20℃, 30℃, 35℃, 40℃, 45℃, 50℃) to represent three test temperature conditions cold, intermediate, and hot weather climates. Eight frequencies were used for each temperature to simulate different asphalt pavement loading conditions. (25 Hz, 10 Hz, 5 Hz, 1 Hz, 0.5 Hz, 0.1 Hz, 0.05, 0.01). For each mix, a master excel sheet was created to include sheer modulus and dynamic modulus results. Table 12, Table 13 & Table 14 shows an example of the developed database master excel sheet. Each table shows the asphalt mixture shear modulus (orange highlight) section and its corresponding asphalt mixture dynamic modulus at a specific temperature and specific frequency. Test results units are usually exported in Pascal. However, the model input would need to be converted to psi.

Table 12 through Table 14 shows an example of the dynamic modulus test, shear modulus sliver test and their corresponding test temperatures and frequencies. A detailed database was used to store asphalt mixture properties used in this research.

Asphalt Mixture Shear Modulus G*sliver				Asphalt Mixture Dynamic Modulus E*		
Temperature	Frequency	Shear Modulus (pa)	Shear Modulus (psi)	Temperature, C	Frequency Hz	E* (psi)
4	25	2,337,521,248	339,029	4	25	2,322,321
4	10	2,073,204,559	300,693	4	10	2,059,221
4	5	1,893,176,827	274,582	4	5	1,876,890
4	1	1,537,944,320	223,060	4	1	1,523,823
4	0.5	1,406,306,558	203,968	4	0.5	1,383,037
4	0.1	1,143,880,179	165,906	4	0.1	1,121,907
4	0.05	1,046,667,893	151,806	4	0.05	1,021,604
4	0.01	852,732,506	123,678	4	0.01	828,784
10	25	1,733,549,555	251,430	10	25	1,782,733
10	10	1,482,182,267	214,972	10	10	1,533,861
10	5	1,316,473,116	190,938	10	5	1,366,614
10	1	1,002,289,284	145,370	10	1	1,051,841
10	0.5	891,283,077	129,270	10	0.5	934,599
10	0.1	678,701,510	98,437	10	0.1	718,499
10	0.05	603,428,141	87,520	10	0.05	640,244
10	0.01	459,365,370	66,625	10	0.01	492,217

Table 12 : Table of asphalt mixture shear modulus and dynamic modulus summary table for cold temperatures

Asphalt Mixture Shear Modulus G*sliver				Asphalt Mixture Dynamic Modulus E*		
Temperature	Frequency	Shear Modulus (pa)	Shear Modulus (psi)	Temperature, C	Frequency Hz	E* (psi)
20	25	1,053,345,271	152,775	20	25	1,147,341
20	10	847,228,798	122,880	20	10	938,838
20	5	718,532,946	104,214	20	5	805,362
20	1	490,998,929	71,213	20	1	567,078
20	0.5	416,781,492	60,449	20	0.5	486,345
20	0.1	284,343,049	41,240	20	0.1	341,882
20	0.05	240,983,138	34,952	20	0.05	293,844
20	0.01	163,832,720	23,762	20	0.01	206,545
30	25	640,037,233	92,830	30	25	738,412
30	10	484,283,648	70,239	30	10	574,640
30	5	392,176,329	56,880	30	5	474,609
30	1	240,529,308	34,886	30	1	305,728
30	0.5	194,895,221	28,267	30	0.5	253,083
30	0.1	119,125,961	17,278	30	0.1	162,677
30	0.05	96,238,257	13,958	30	0.05	134,862
30	0.01	58,430,961	8,475	30	0.01	86,671

Table 13 : Asphalt mixture shear modulus and dynamic modulus summary table for intermediate temperatures

Asphalt Mixture Shear Modulus G*sliver				Asphalt Mixture Dynamic Modulus E*		
Temperature	Frequency	Shear Modulus (pa)	Shear Modulus (psi)	Temperature, C	Frequency Hz	E* (psi)
35	25	498,910,316	72,361	35	25	592,383
35	10	366,141,835	53,104	35	10	449,571
35	5	289,733,507	42,022	35	5	364,341
35	1	168,349,461	24,417	35	1	224,482
35	0.5	133,274,656	19,330	35	0.5	182,567
35	0.1	77,106,025	11,183	35	0.1	112,215
35	0.05	60,817,463	8,821	35	0.05	91,364
35	0.01	34,895,082	5,061	35	0.01	56,144
40	25	388,901,598	56,405	40	25	475,232
40	10	276,820,916	40,149	40	10	351,723
40	5	214,050,412	31,045	40	5	279,693
40	1	117,829,887	17,090	40	1	164,827
40	0.5	91,136,837	13,218	40	0.5	131,699
40	0.1	49,908,006	7,239	40	0.1	77,406
40	0.05	38,433,403	5,574	40	0.05	61,896
40	0.01	20,839,410	3,023	40	0.01	36,369
45	25	303,149,581	43,968	45	25	381,249
45	10	209,289,987	30,355	45	10	275,171
45	5	158,136,970	22,936	45	5	214,711
45	1	82,470,607	11,961	45	1	121,025
45	0.5	62,321,850	9,039	45	0.5	95,004
45	0.1	32,303,689	4,685	45	0.1	53,395
45	0.05	24,287,868	3,523	45	0.05	41,932
45	0.01	12,445,336	1,805	45	0.01	23,559
50	25	236,305,711	34,273	50	25	305,852
50	10	158,233,341	22,950	50	10	215,281
50	5	116,829,027	16,945	50	5	164,826
50	1	57,722,206	8,372	50	1	88,863
50	0.5	42,617,377	6,181	50	0.5	68,533
50	0.1	20,909,036	3,033	50	0.1	36,832
50	0.05	15,348,641	2,226	50	0.05	28,407
50	0.01	7,432,378	1,078	50	0.01	15,261

Table 14 : Asphalt mixture shear modulus and dynamic modulus summary table for hot temperatures

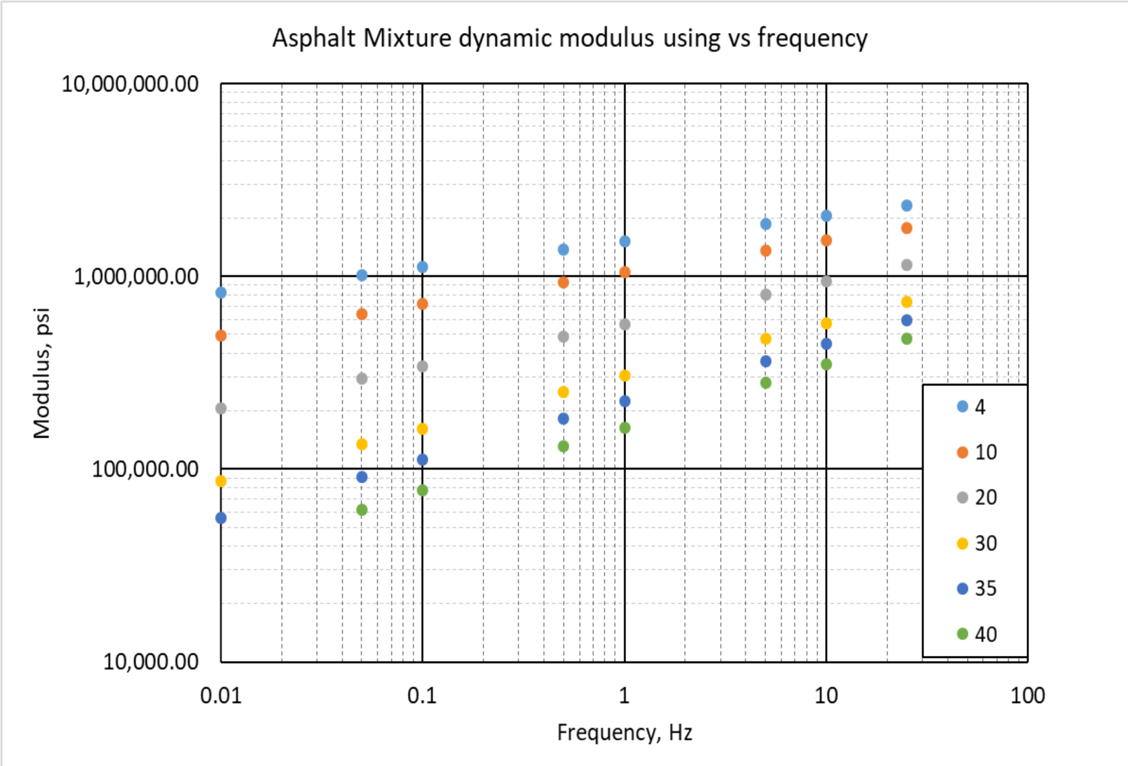

Figure 24 : Asphalt mixture dynamic modulus isotherm example

Figure 24 is an example of asphalt mixture dynamic modulus isotherm after testing one of the model development mixture. The figure shows that asphalt mixture modulus is inversely proportional with testing temperature. In other words, asphalt mixture modulus is highest at lower temperatures and vice versa. Results also showed that asphalt mixture stiffness is directly proportional with testing frequency. At lower test frequency, lower asphalt mixture stiffness was recorded.

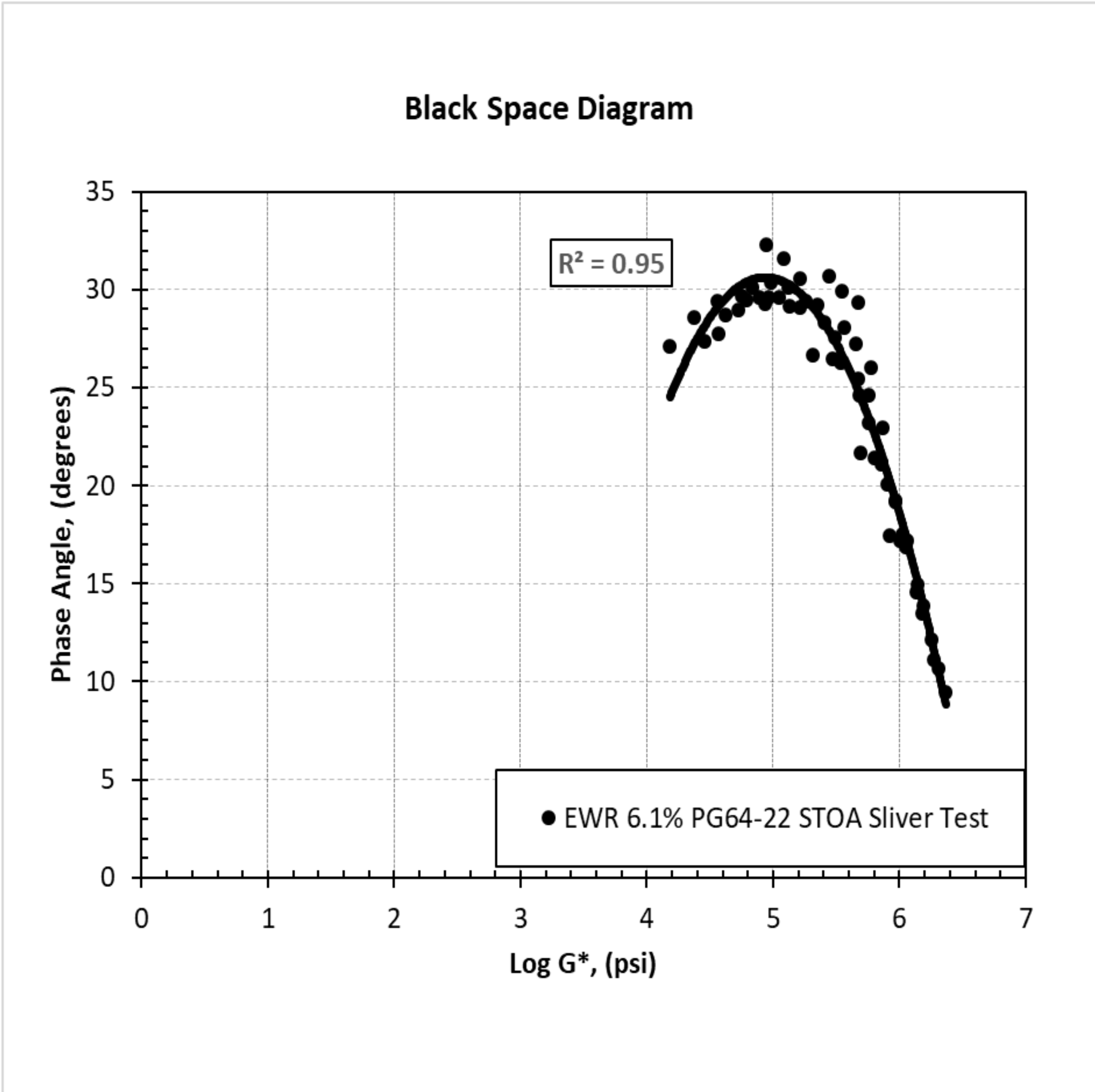

Figure 25 : Asphalt mixture dynamic modulus test black space plot example

Figure 25 is an example of asphalt mixture dynamic modulus test AASHTO TP 79 black space diagram for one of the materials used in the model development phase. Black space diagram is a plot of the asphalt mixture phase angle (y-axis) and the asphalt mixture modulus (x-axis). The phase angle is the time takes a material to respond to applied stress.

Different materials will respond differently to applied stresses. Black space plots are used to better understand viscoelastic material. It is also used to evaluate test data quality. Test specimens black space statistical analysis data had a minimum of 90% R^2 value.

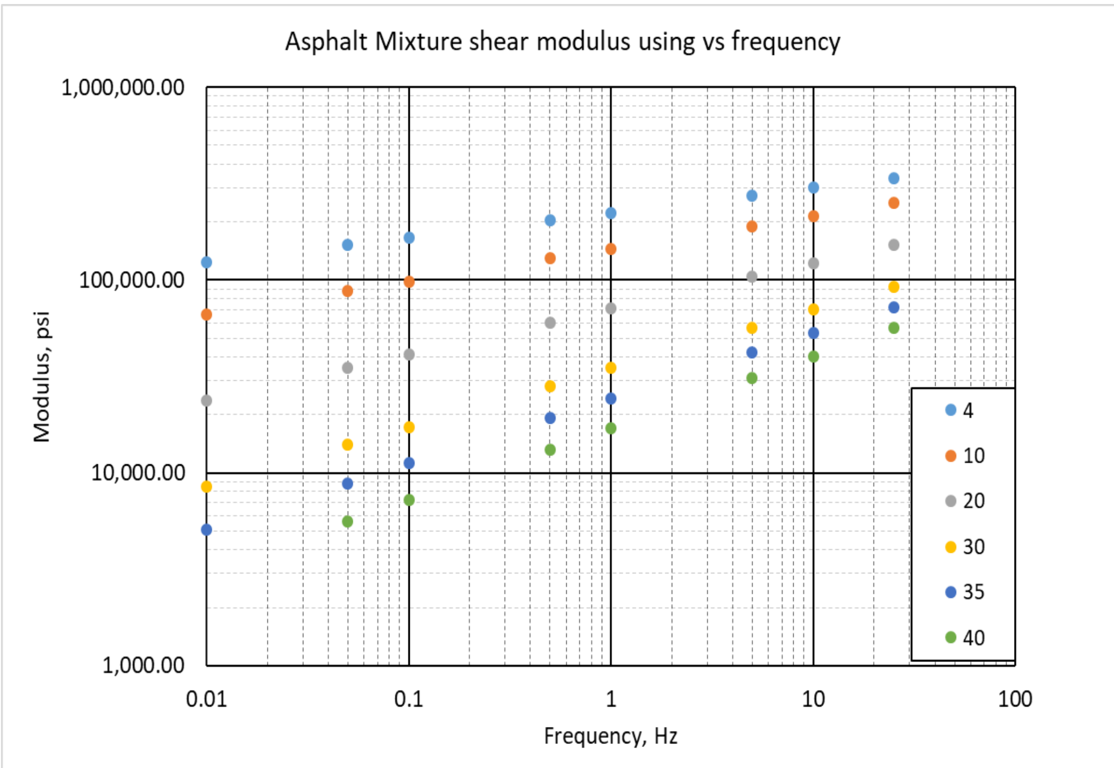

Figure 26 : Asphalt mixture shear modulus isotherm example

Figure 26 shows an example of asphalt mixture dynamic shear modulus isotherm ASTM D7552 after testing one of the model development mixtures listed in earlier sections. The figure shows that asphalt mixture modulus has an inverse proportional with testing temperature. Moreover, it shows that asphalt mixture stiffness is directly proportional with testing frequency.

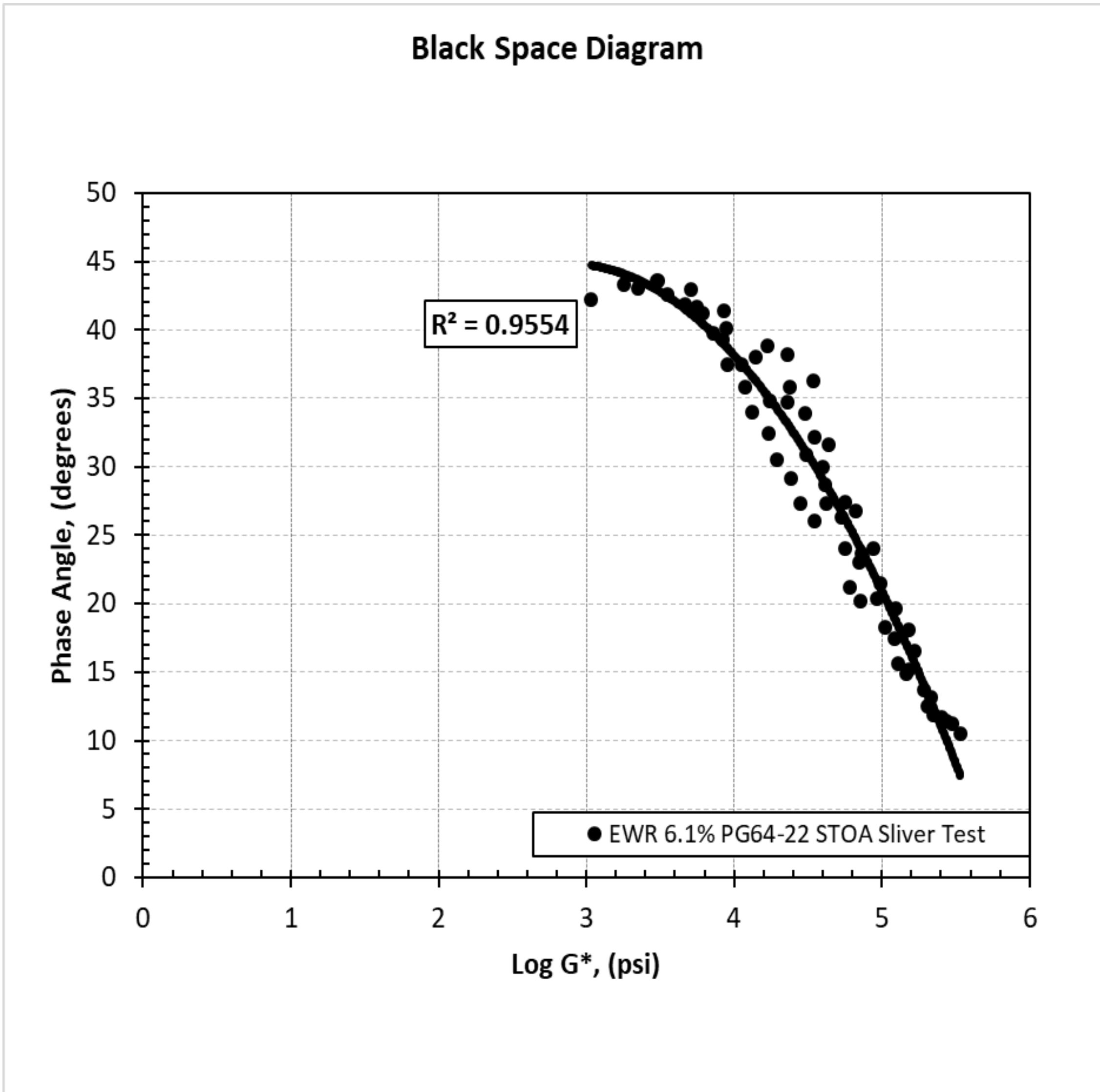

Figure 27 : Asphalt mixture shear modulus (sliver test) black space plot example

Figure 27 is an example of asphalt mixture dynamic shear modulus test ASTM D 7552 black space diagram for one of the materials used in the model development phase. Black space diagram was produced and analyzed. Similarly, Black space statistical analysis data had a minimum of 90% R^2 value.

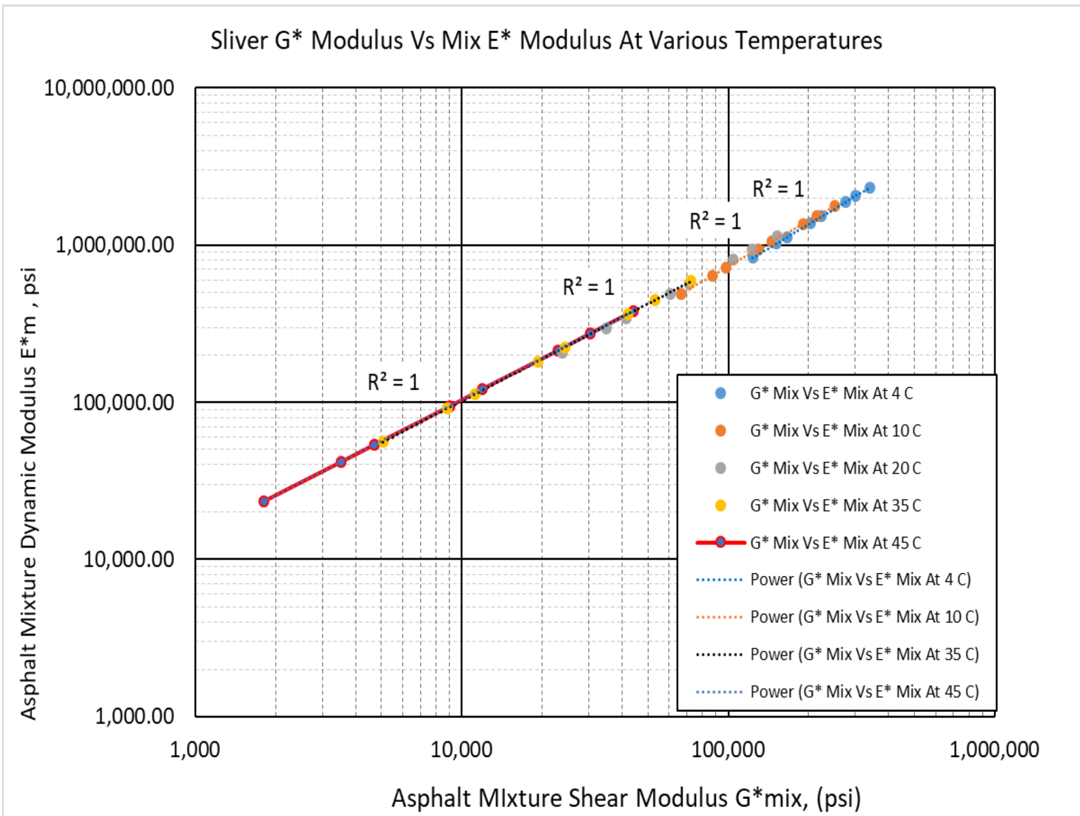

Figure 28 : Asphalt mixture shear modulus and dynamic modulus correlation example

Asphalt mixture dynamic modulus and shear modulus correlation was investigated for each mix and asphalt binder. Figure 28 shows an example of such correlation for one of the asphalt mixtures. The figure showed strong correlation at the cold, intermediate and hot temperature conditions.

6.3.2 Developed forward calculation model

The model inputs for the forward calculation process is the asphalt mixture shear modulus (ASTM D7552) for asphalt mixtures slivers, percent Voids in Mineral Aggregates VMA, percent Voids Filled with Asphalt VFA, and percent Air Voids.

Linear regression analysis and goodness of fit parameters were used to develop and evaluate the asphalt mixture prediction model. A MATLAB code was developed and used in the model development and data analysis. A total of approximately 700 data points were used to develop the model. A plot was developed for each mix to investigate asphalt mixture dynamic modulus and asphalt mixture shear modulus correlation. A model was developed for each mix. A final model was then developed and calibrated for the twelve mixes used in the model development phase.

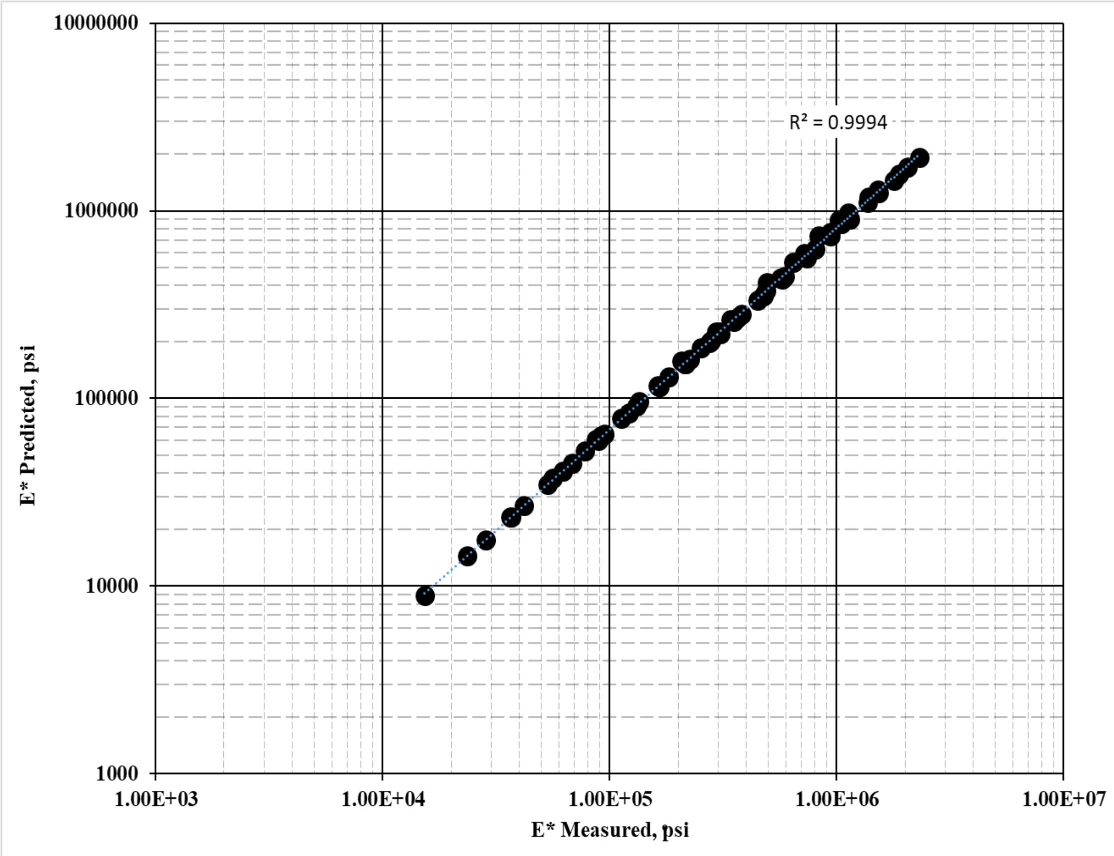

Figure 29 : Predicted dynamic modulus vs measured dynamic modulus correlation example for as specific mix

Figure 29 shows predicted dynamic modulus values using the developed uncalibrated model versus measured dynamic modulus values using the asphalt mixture performance tester. In this case, the model was specifically designed for this specific mix. The data showed promising correlation with a R^2 value 99.94 %.

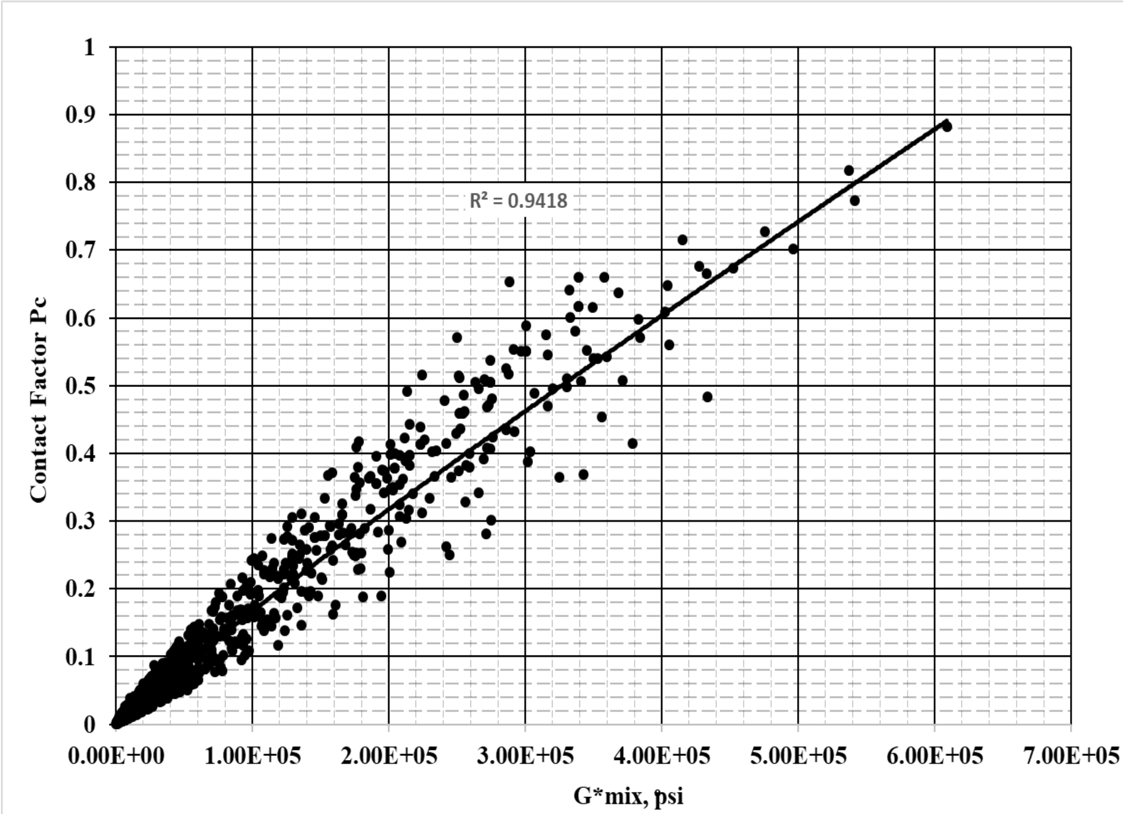

Figure 30 : Contact factor Pc and sliver test shear modulus correlation

Figure 30 shows a plot for the contact factor Pc (Y-axis) versus asphalt mixture shear modulus values (X-axis). A best-fit first order polynomial line was used. The figure shows a strong correlation with an $R^2 = 94.2\%$.

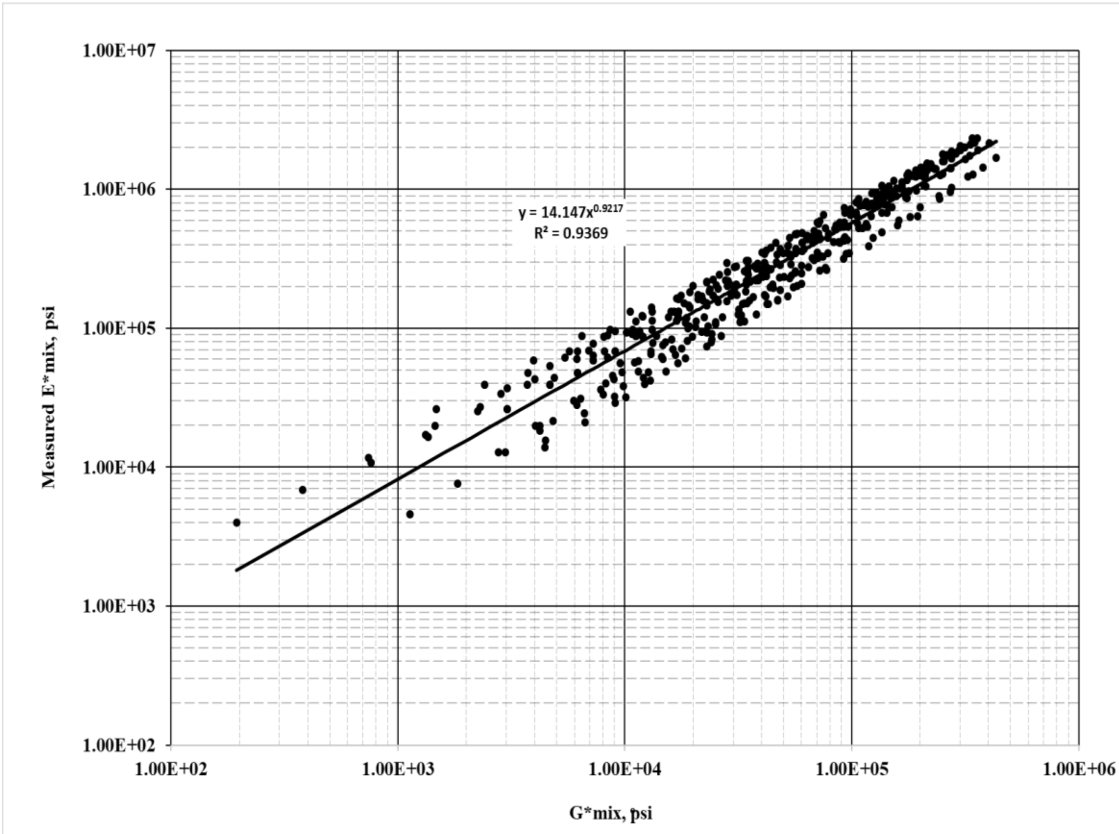

Figure 31 : Asphalt mixture dynamic modulus E* and the sliver test shear modulus corelation

The correlation between asphalt mixture dynamic modulus and asphalt mixture shear modulus G* sliver was investigated using linear regression model. The regression model showed promising results as the data plotted in Figure 31 using asphalt mixture shear modulus G* sliver on the x-axis and asphalt mixture dynamic modulus E* on the y-axis R^2 value of 93.69%. The forward model was developed using approximately 700 data points.

In the developed model below, The Pc parameter as function of shear modulus G* measured using the sliver test was used as an input. The final forward model shown was used to predict asphalt mixture dynamic modulus (forward calculation) as shown in

$$|E^*_{mix}| = P_C\left[E_{agg}\left(1 - \frac{VMA}{100}\right) + 3|G^*_{mix}|\left(\frac{VFA \times VMA}{10000}\right)\right]$$

$$|E^*_{mix}| = P_C\left[4200000\left(1 - \frac{VMA}{100}\right) + 3|G^*_{mix}|\left(\frac{VFA \times VMA}{10000}\right)\right]$$

$$P_C = a_1 {G^*_{mix}}^{b_1}$$

$$P_C = 4.08 G^{*(0.9273)}_{mix}$$

Equation 13:

Equation 13 : Forward model using the silver test

Where $|E^*_{mix}|$ is the asphalt mixture dynamic modulus (Psi), VMA is the Voids in Mineral Aggregates (%), VFA is the Voids Filled with Asphalt (%), $|G^*_{mix}|$ is the asphalt mixture dynamic shear modulus using the sliver test (Psi), a_1 and a_2 are model calibration factors.

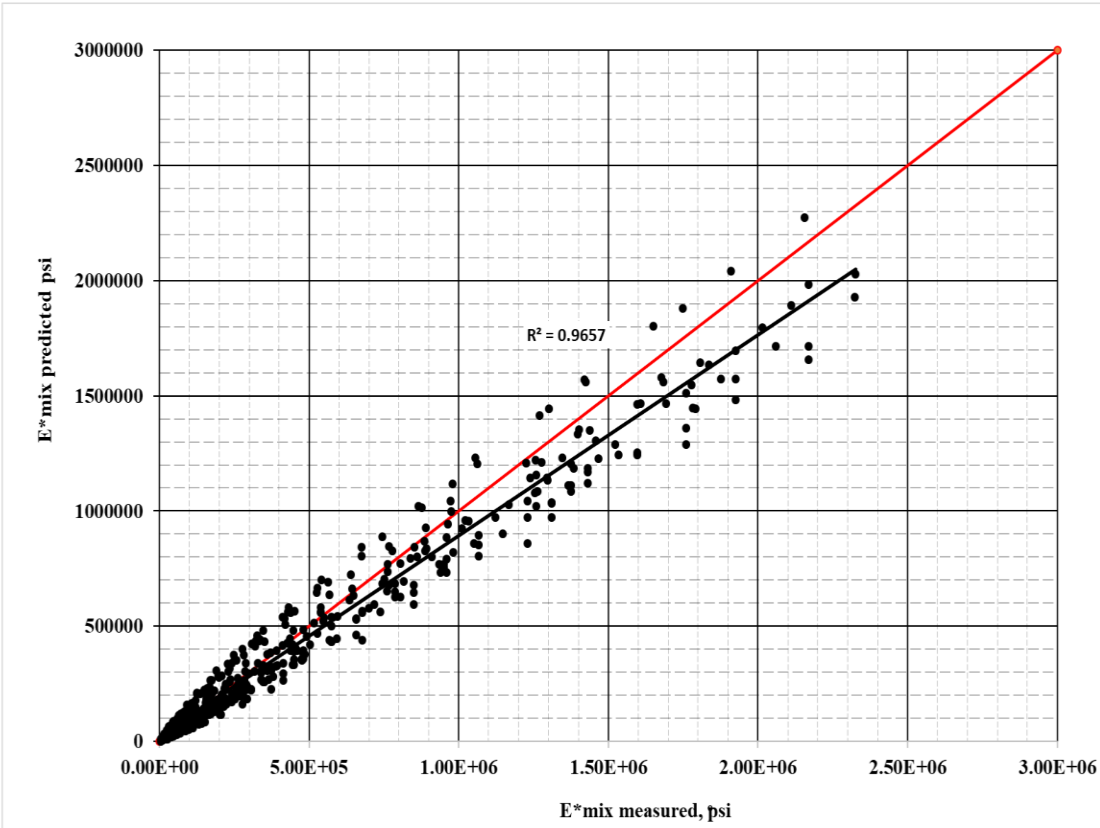

Figure 32 : Asphalt mixture predicted dynamic modulus and asphalt mixture measured dynamic modulus correlation

Asphalt mixture shear modulus values were obtained experimentally using ASTM D7552 at 4 ℃, 10 ℃, 20 ℃, 35 ℃ and frequencies of 25Hz, 10Hz, 5Hz, 5Hz, 1 Hz, 0.1Hz, as shown in Figure 32. Shear modulus values were used in conjunction with the calibrated modified Hirsch model to forward calculate asphalt mixture modulus E* for all 12 mixtures with different PG grades (PG 64-22, and PG 76-22) at different aging durations. Figure 32 shows the comparison of experimental vs forward calculated modulus results used to develop the proposed model. Data showed good correlation for forward calculation represented by$R^2 = 96.570\%$.

A separate statistical analysis was performed to study the correlation of asphalt mixture dynamic modulus with the sliver test shear modulus at specific test temperatures and test frequencies. The objective was to identify what test temperatures/frequencies provides strong correlation between asphalt mixture dynamic modulus and the sliver test shear modulus.

Table 15 through Figure 38 below show results and analysis for the data set described earlier at specific temperatures/frequencies.

Forward Model Goodness of Fit										
Field	Pc VGm	All	4 C	10 C	20 C	30 C	35 C	40 C	45 C	50 C
sse	3.09E-01	3.63E+12	1.84E+12	1.25E+12	7.49E+11	4.67E+11	3.33E+11	2.35E+11	2.35E+11	2.35E+11
rsquare	0.97	0.98	0.87	0.88	0.86	0.82	0.81	0.80	0.80	0.80
dfe	574.00	574.00	70.00	70.00	70.00	70.00	70.00	70.00	70.00	70.00
adjrsquare	0.97	0.98	0.87	0.88	0.86	0.82	0.81	0.80	0.80	0.80
rmse	0.02	7.95E+04	1.62E+05	1.33E+05	1.03E+05	8.17E+04	6.90E+04	5.80E+04	5.80E+04	5.80E+04

Table 15 : Forward modulus prediction model statistical analysis for individual temperatures

In Table 15 , the forward modulus prediction model showed strong correlation between E*mix calculated versus E*mix measured with a minimum R^2 of 80% at 40℃ and maximum R squared of 88% for the 10 ℃ degrees Celsius. Below is an example of MATLAB scatter plots. The plots at different temperatures. Data scatter plots with 95% confidence interval confirmed that calculated modulus falls within the 95% confidence bounds.

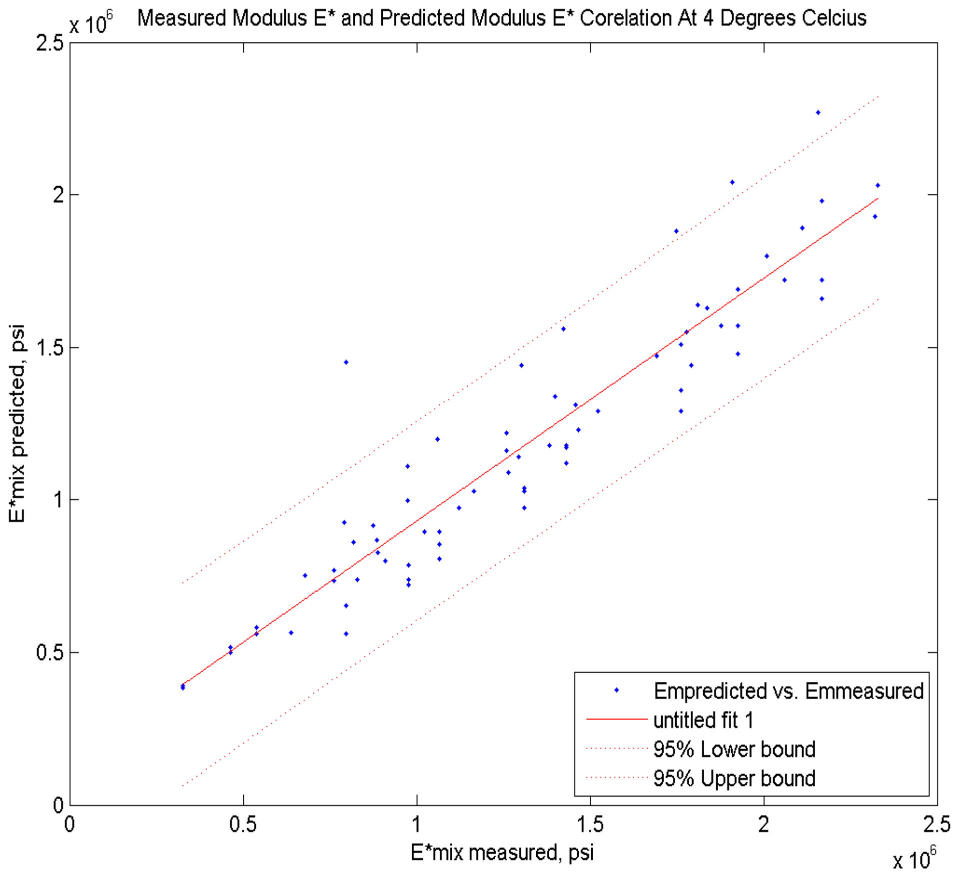

Figure 33 : Forward modulus prediction model correlation at 4 ℃

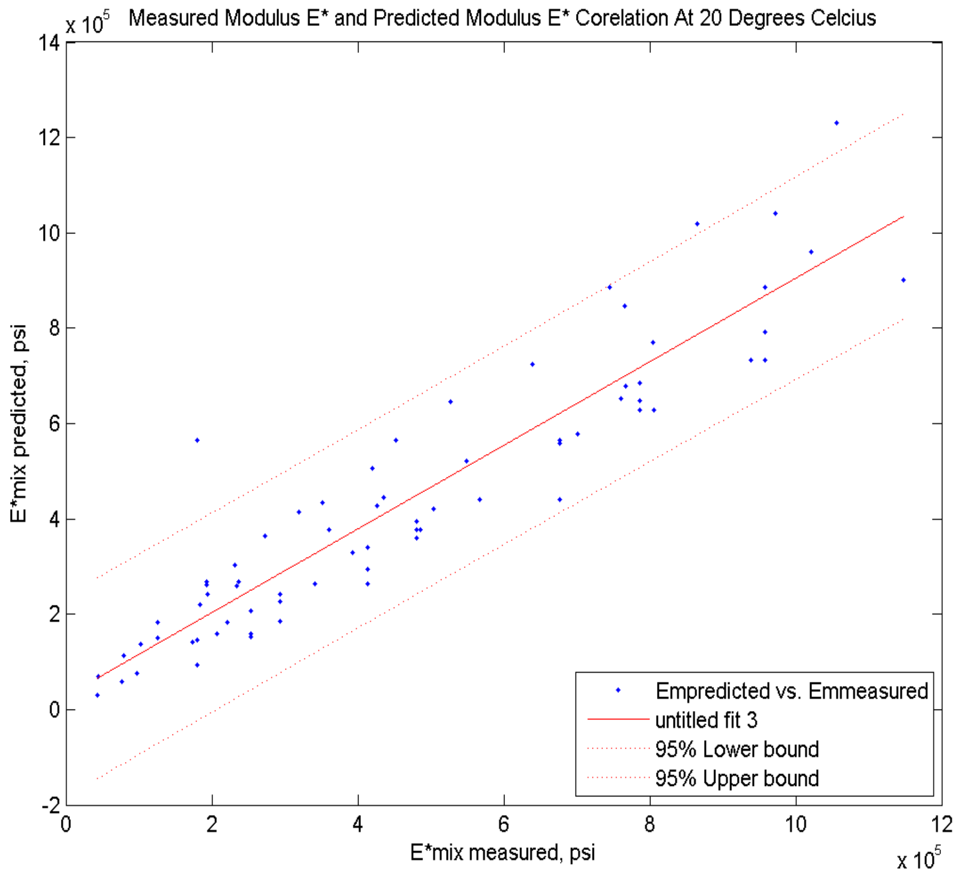

Figure 34 : Forward Modulus Prediction Model Correlation at 20 ℃

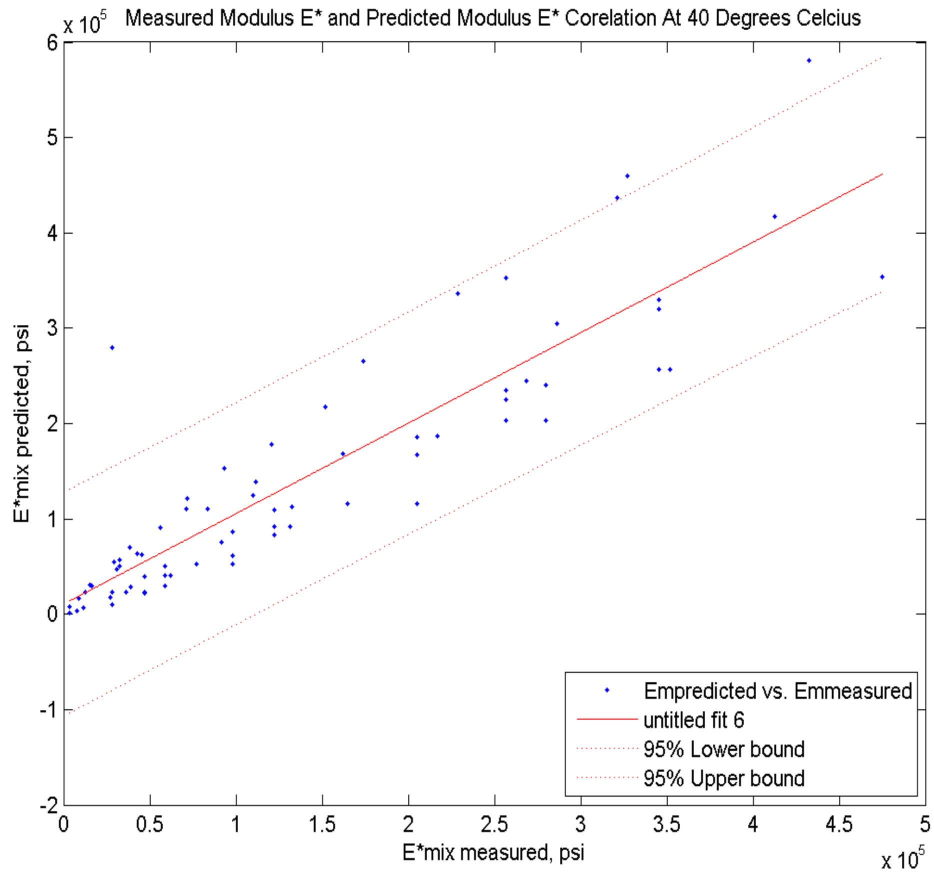

Figure 35 : Forward modulus prediction model correlation At 40 ℃

Similar goodness of fit statistical analysis was performed on asphalt mixture calculated modus at individual frequencies. Table 16 shows a summary of goodness of fit parameters, the forward modulus calculation model showed strong correlation between E*mix predicted versus E*mix for the 25 Hz, 10 Hz, 5 Hz, 1 Hz, 0.5 Hz, 0.1 Hz. Tests with a minimum R squared of 95% at the 0.1 Hz.

E* Predicted VS E* measured Goodness of Fit At						
Field	**25 Hz**	**10 Hz**	**5 Hz**	**1 Hz**	**0.5 Hz**	**0.1 Hz**
sse	9.79E+11	6.81E+11	7.16E+11	4.09E+11	4.36E+11	2.88E+11
rsquare	0.96	0.96	0.96	0.96	0.95	0.95
dfe	70.00	70.00	70.00	70.00	70.00	70.00
adjrsquare	0.96	0.96	0.95	0.96	0.95	0.95
rmse	1.18E+05	9.86E+04	1.01E+05	7.64E+04	7.89E+04	6.42E+04

Table 16 : Forward modulus prediction model statistical analysis for individual frequencies

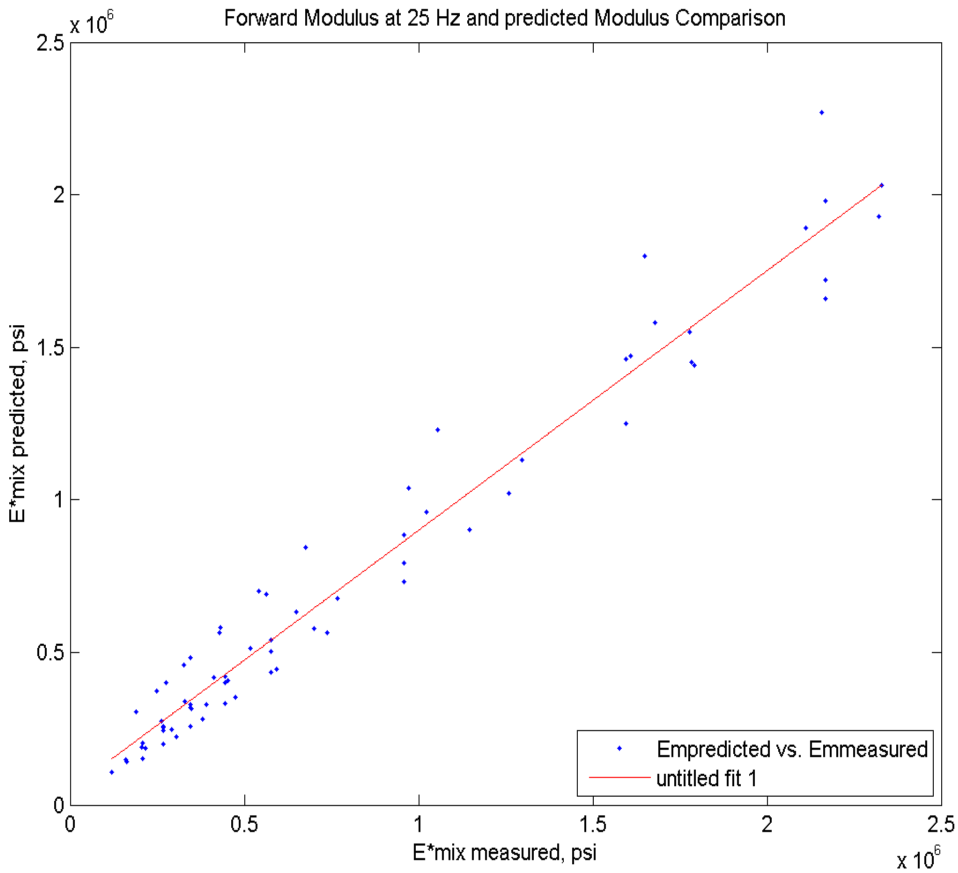

Figure 36 : Forward modulus prediction model correlation At 25 Hz

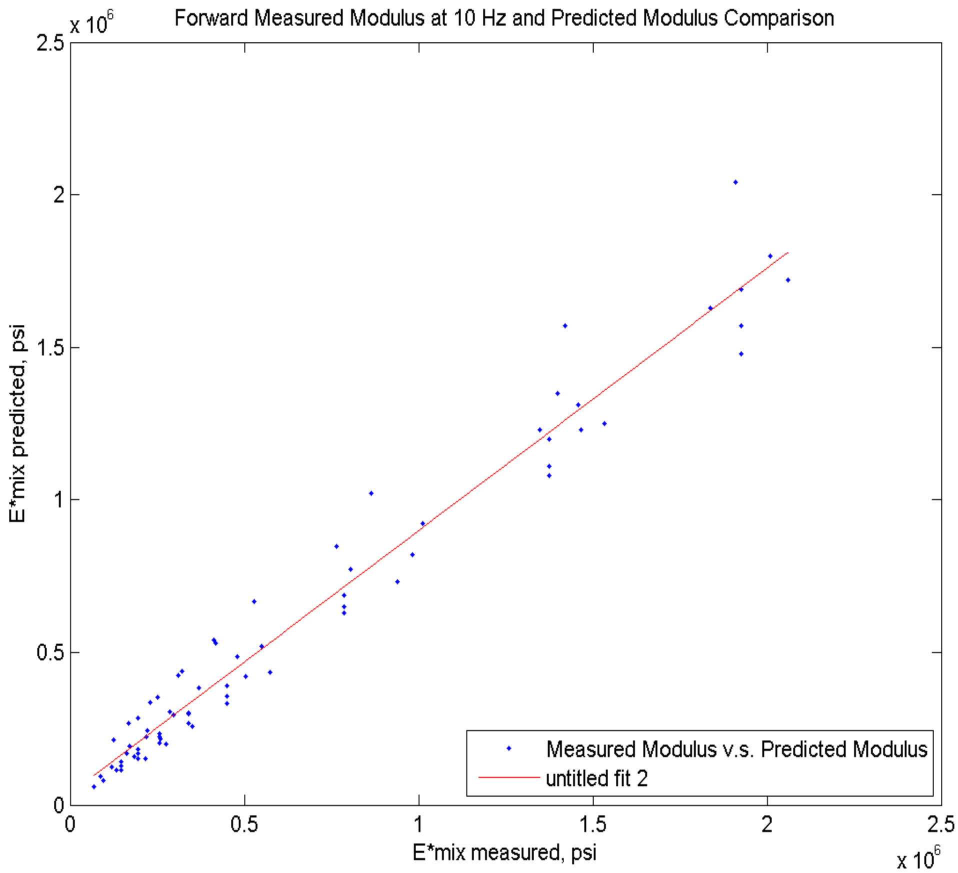

Figure 37 : Forward modulus prediction model correlation at 10 Hz

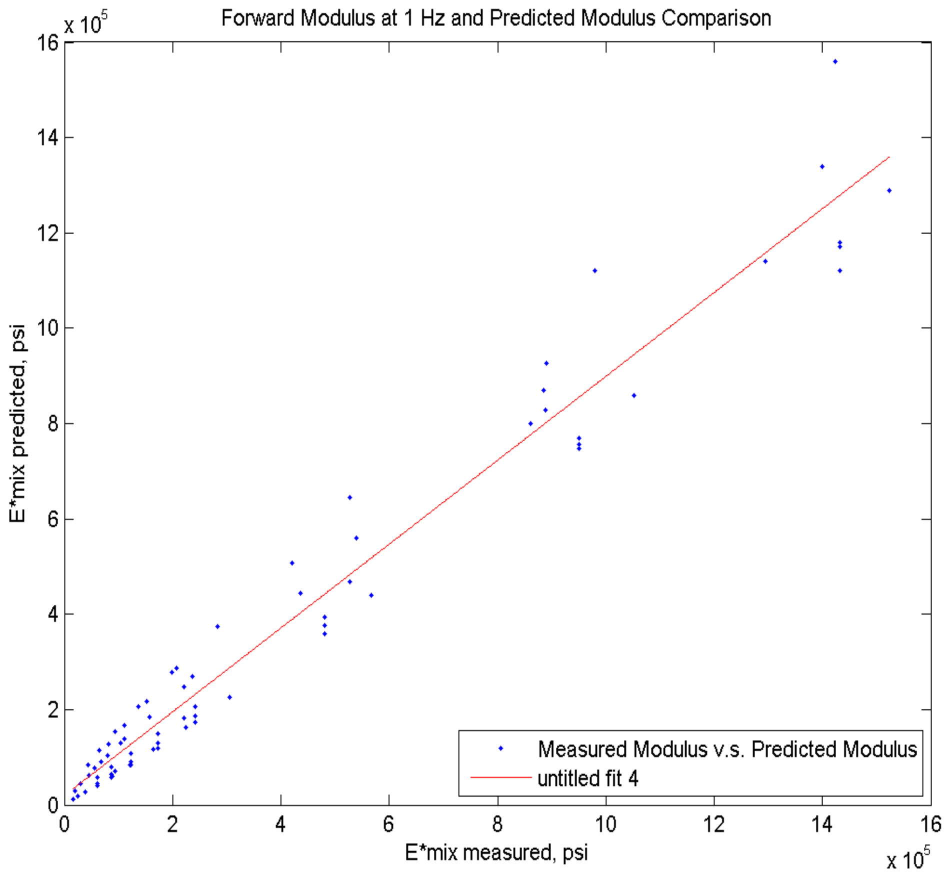

Figure 38 : Forward modulus prediction model correlation At 1 Hz

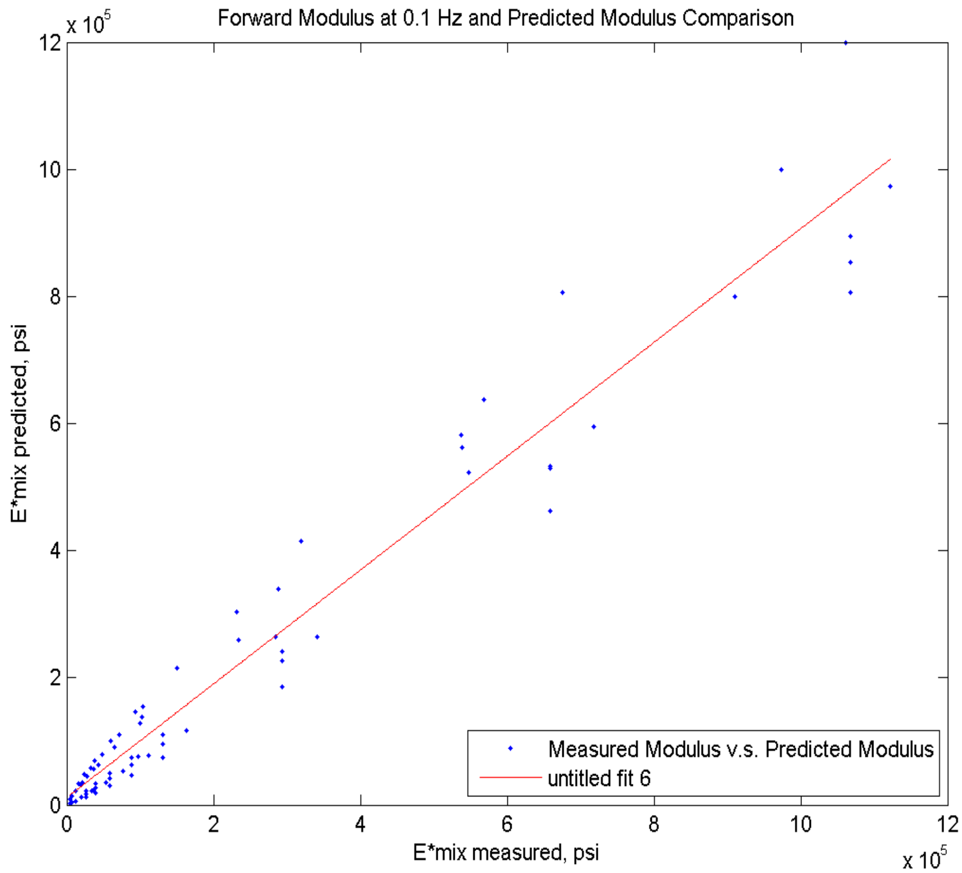

Figure 39 : Forward modulus prediction model correlation At 0.1 Hz

6.4 Forward asphalt mixture phase angle calculation model results and analysis

6.4.1 Materials results and analysis

Asphalt mixture phase angle in parallel with the modulus is currently used in number of models such as the Strategic Highway Research Program SHRP fatigue model. The complex modulus test calculates the asphalt mixture phase angle as one of its primary outputs. Asphalt mixture phase angle is calculated from the test outputs of the different frequency sweep tests performed. Phase angle is used to further understand the viscous and elastic properties of asphalt concrete.

The Phase angle obtained from the asphalt mixture dynamic complex modulus test and/or the sliver shear complex modulus test is usually calculated by locating the peak values of the strains for their corresponding time delays using the raw data.

Similar to the forward prediction model, the developed test plan was used to collect data needed to calculate specimen phase angle. The material test matrix showed in

Table **11** introduced the model to a wide range of asphalt mixture shear modulus/stiffness (G*sliver) and asphalt mixture dynamic modulus (E*mix). Some of the mixture were polymer modified (i.e. PG 76-22). Table 17 is a summary table for the minimum and maximum shear modulus used to develop the forward phase angle prediction model.

Test	Minimum Phase Angle, degrees	Maximum Phase Angle, degrees
G*Sliver	195	433568
Phase Angle	9	47

Table 17 : Maximum and minimum values for forward phase angle prediction model

6.4.2 Developed forward phase angle prediction model

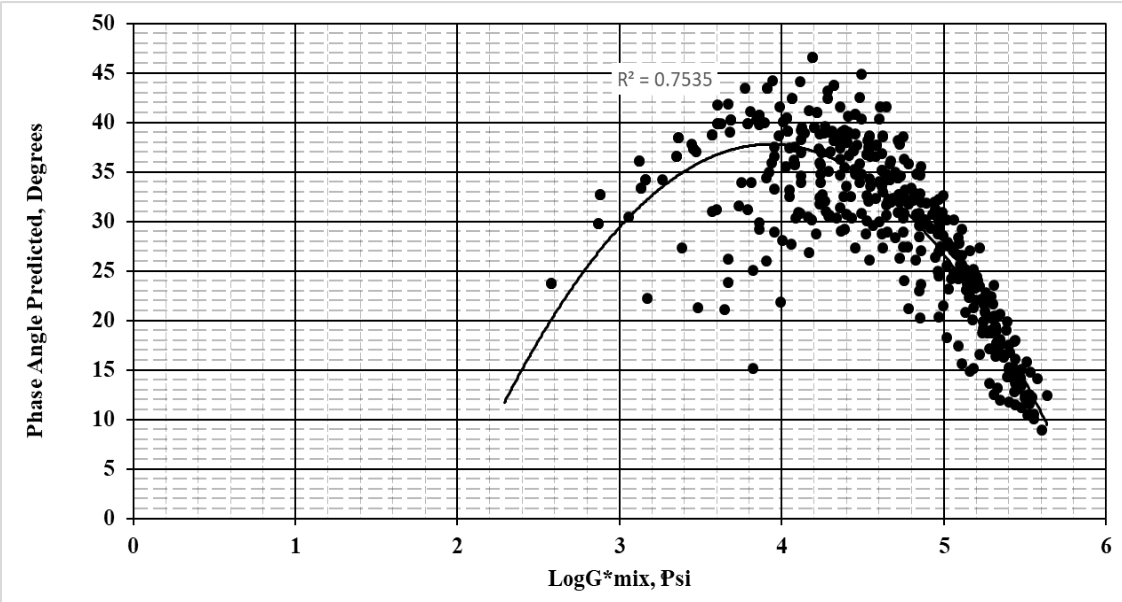

Figure 40 : Phase angle as a function of Log (G*Mix), sliver test

Figure 40 is a graphical plot for the phase angle calculated data (Y-axis) and the shear modulus values (X-axis). In this research, developing a forward phase angle calculation model was a secondary item. This model can be useful for future research to better characterize viscoelastic properties of asphalt mixtures. The model was able to predict asphalt mixture phase angle at cold and intermediate temperatures ($\log G^* > 4\,psi$). Calculated phase angle showed good correlation with asphalt mixture shear modulus with $R^2 = 75.35\ \%$.

Using the above correlation, a model was developed to forward predict the asphalt mixture phase angle. Equation 14 can describe the model:

$$\delta = -8.4911(\log \mathrm{G}^*)^2 + 67.393 \log \mathrm{G}^* - 98.668$$

Equation 14 : Asphalt mixture phase angle

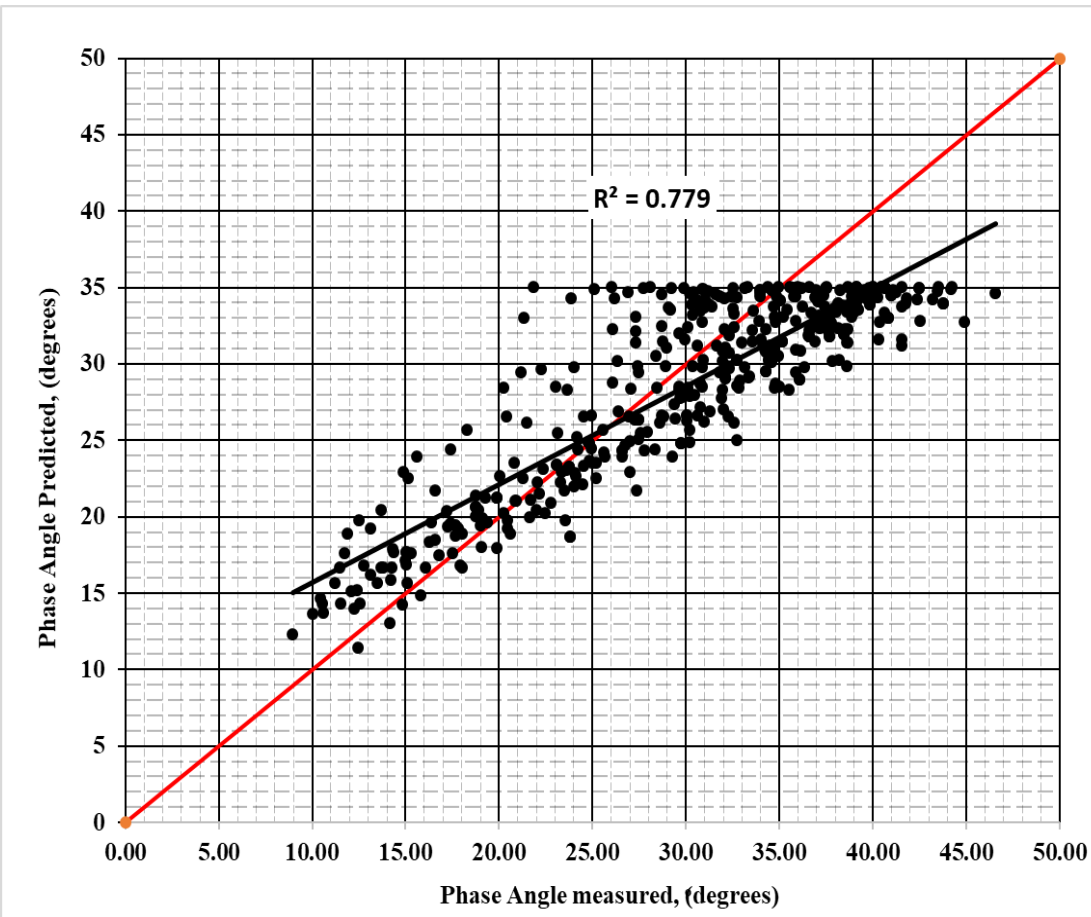

Figure 41 : Forward predicted phase angle and measured phase angle correlation

Figure 41 shows a plot of the forward predicted phase angle and measured phase angle. The above comparison showed a relatively strong correlation with $R^2 = 77.9$ %.Table 18 is the goodness of fit statistical analysis output.

To further understand the overall correlation between asphalt mixture phase angle and Log the asphalt mixture shear modulus, a separate analysis was performed on individual test frequency and temperature.

G* Predicted VS G* measured Goodness of Fit At								
Field	4 C	10 C	20 C	30 C	35 C	40 C	45 C	50 C
sse	136.43	180.82	242.45	292.79	268.59	296.95	296.95	296.95
rsquare	0.83	0.82	0.75	0.51	0.29	0.11	0.11	0.11
dfe	58.00	58.00	58.00	58.00	54.00	52.00	52.00	52.00
adjrsquar	0.82	0.81	0.74	0.50	0.28	0.09	0.09	0.09
rmse	1.53	1.77	2.04	2.25	2.23	2.39	2.39	2.39

Table 18 : Phase angle forward prediction model goodness of fit statistical analysis parameters at individual test temperatures

Table 18 is a table for the statistical analysis that performed the model development dataset. The data set was filtered based on test temperature. The table shows a relatively strong correlation ($R^2 > 71\%$) at 4 ℃, 10 ℃, 20 ℃. However, a noticeable drop in the R squared ($R^2 < 32\%$) value was noticed at higher temperatures 30 ℃, 35 ℃, 40 ℃, 45 ℃, 50 ℃.

G* Predicted VS G* measured Goodness of Fit At						
Field	25 Hz	10 Hz	5 Hz	1 Hz	0.5 Hz	0.1 Hz
sse	260.33	234.17	235.29	477.39	659.00	1172.27
rsquare	0.91	0.92	0.92	0.78	0.67	0.32
dfe	68.00	68.00	69.00	70.00	73.00	71.00
adjrsquare	0.91	0.92	0.92	0.78	0.67	0.31
rmse	1.96	1.86	1.85	2.61	3.00	4.06

Table 19 : Phase angle forward prediction model goodness of fit statistical analysis parameters at individual test frequencies

Similarly, Table 19 is a table for the statistical analysis performed on the same dataset used to develop the phase angle forward prediction model. The goodness of fit analysis showed relatively high R squared values ($R^2 > 60\%$) for tests at 25 Hz, 10 Hz, 5 Hz, 1 Hz, 0.5 Hz. a significant drop in the R squared value was noticed at the 0.1 Hz.

6.5 Backward asphalt binder modulus calculation model results and analysis

6.5.1 G*binder and G*sliver results and correlations

Test data showed that there is a strong correlation between extracted asphalt binder shear modulus G*binder and asphalt mixture sliver test shear modulus. An example of such correlations will be discussed in this section.

Asphalt binder master curve test and asphalt mixture shear modulus sliver test were performed and analyzed at the same test conditions. Eight test temperatures were used ($4℃$, $10℃, 20℃, 30℃, 35℃, 40℃, 45℃, 50℃$) to represent three test temperature conditions cold, intermediate, and hot weather climates. Eight frequencies (25 Hz, 10 Hz, 5 Hz, 1 Hz, 0.5 Hz, 0.1 Hz) were used for each temperature. For each mix type, a master excel sheet was created to include asphalt mixture shear modulus and asphalt binder shear modulus results.

Table 20, Table 21, & Table 22 shows an example of the developed asphalt binder properties database. Each table shows the asphalt mixture shear modulus (orange highlight) section and its corresponding asphalt binder shear modulus at a specific temperature and specific frequency. Test results units are usually exported in Pascal. However, the model input would be converted to psi.

Asphalt Binder Shear Modulus G*binder				Asphalt Mixture Shear Modulus G*sliver			
Temperature, C	Frequency Hz	Shear Modulus (pa)	Shear Modulus (psi)	**Temperature**	**Frequency**	**Shear Modulus (pa)**	**Shear Modulus (psi)**
4	25	141,989,377	20,594	4	25	2,337,521,248	339,029
4	10	110,697,643	16,055	4	10	2,073,204,559	300,693
4	5	92,004,713	13,344	4	5	1,893,176,827	274,582
4	1	59,597,274	8,644	4	1	1,537,944,320	223,060
4	0.5	49,368,773	7,160	4	0.5	1,406,306,558	203,968
4	0.1	31,942,872	4,633	4	0.1	1,143,880,179	165,906
4	0.05	26,499,019	3,843	4	0.05	1,046,667,893	151,806
4	0.01	17,150,342	2,487	4	0.01	852,732,506	123,678
10	25	88,156,377	12,786	10	25	1,733,549,555	251,430
10	10	65,475,927	9,496	10	10	1,482,182,267	214,972
10	5	52,344,130	7,592	10	5	1,316,473,116	190,938
10	1	31,118,728	4,513	10	1	1,002,289,284	145,370
10	0.5	24,806,807	3,598	10	0.5	891,283,077	129,270
10	0.1	14,695,614	2,131	10	0.1	678,701,510	98,437
10	0.05	11,738,895	1,703	10	0.05	603,428,141	87,520
10	0.01	6,956,094	1,009	10	0.01	459,365,370	66,625

Table 20 : Asphalt mixture shear modulus and asphalt binder shear modulus summary table for cold temperatures

Asphalt Binder Shear Modulus G*binder				Asphalt Mixture Shear Modulus G*sliver			
Temperature, C	Frequency Hz	Shear Modulus (pa)	Shear Modulus (psi)	**Temperature**	**Frequency**	**Shear Modulus (pa)**	**Shear Modulus (psi)**
20	25	39,833,659	5,777	20	25	1,053,345,271	152,775
20	10	27,288,969	3,958	20	10	847,228,798	122,880
20	5	20,447,074	2,966	20	5	718,532,946	104,214
20	1	10,536,125	1,528	20	1	490,998,929	71,213
20	0.5	7,878,347	1,143	20	0.5	416,781,492	60,449
20	0.1	4,029,124	584	20	0.1	284,343,049	41,240
20	0.05	3,021,966	438	20	0.05	240,983,138	34,952
20	0.01	1,545,918	224	20	0.01	163,832,720	23,762
30	25	17,998,929	2,611	30	25	640,037,233	92,830
30	10	11,373,460	1,650	30	10	484,283,648	70,239
30	5	7,987,196	1,158	30	5	392,176,329	56,880
30	1	3,567,303	517	30	1	240,529,308	34,886
30	0.5	2,502,069	363	30	0.5	194,895,221	28,267
30	0.1	1,104,673	160	30	0.1	119,125,961	17,278
30	0.05	777,951	113	30	0.05	96,238,257	13,958
30	0.01	343,564	50	30	0.01	58,430,961	8,475

Table 21 : Asphalt mixture shear modulus and asphalt binder shear modulus summary table for intermediate temperatures

Asphalt Binder Shear Modulus G*binder				Asphalt Mixture Shear Modulus G*sliver			
Temperature, C	Frequency Hz	Shear Modulus (pa)	Shear Modulus (psi)	Temperature	Frequency	Shear Modulus (pa)	Shear Modulus (psi)
35	25	12,098,872	1,755	35	25	498,910,316	72,361
35	10	7,342,523	1,065	35	10	366,141,835	53,104
35	5	4,992,016	724	35	5	289,733,507	42,022
35	1	2,075,724	301	35	1	168,349,461	24,417
35	0.5	1,410,040	205	35	0.5	133,274,656	19,330
35	0.1	578,422	84	35	0.1	77,106,025	11,183
35	0.05	394,715	57	35	0.05	60,817,463	8,821
35	0.01	161,964	23	35	0.01	34,895,082	5,061
40	25	8,132,857	1,180	40	25	388,901,598	56,405
40	10	4,740,215	688	40	10	276,820,916	40,149
40	5	3,120,021	453	40	5	214,050,412	31,045
40	1	1,207,811	175	40	1	117,829,887	17,090
40	0.5	794,627	115	40	0.5	91,136,837	13,218
40	0.1	302,870	44	40	0.1	49,908,006	7,239
40	0.05	200,269	29	40	0.05	38,433,403	5,574
40	0.01	76,353	11	40	0.01	20,839,410	3,023
45	25	5,466,903	793	45	25	303,149,581	43,968
45	10	3,060,207	444	45	10	209,289,987	30,355
45	5	1,950,020	283	45	5	158,136,970	22,936
45	1	702,795	102	45	1	82,470,607	11,961
45	0.5	447,812	65	45	0.5	62,321,850	9,039
45	0.1	158,587	23	45	0.1	32,303,689	4,685
45	0.05	101,612	15	45	0.05	24,287,868	3,523
45	0.01	35,995	5	45	0.01	12,445,336	1,805
50	25	3,674,850	533	50	25	236,305,711	34,273
50	10	1,975,621	287	50	10	158,233,341	22,950
50	5	1,218,767	177	50	5	116,829,027	16,945
50	1	408,939	59	50	1	57,722,206	8,372
50	0.5	252,364	37	50	0.5	42,617,377	6,181
50	0.1	83,038	12	50	0.1	20,909,036	3,033
50	0.05	51,556	7	50	0.05	15,348,641	2,226
50	0.01	16,969	2	50	0.01	7,432,378	1,078

Table 22 : Asphalt mixture shear modulus and asphalt binder shear modulus summary table for hot temperatures

Figure 42 through Figure 46 shows an example of the binder shear modulus test, asphalt mixture sliver test and their corresponding backspace diagram. Test results showed similar trends for target test temperatures and frequencies.

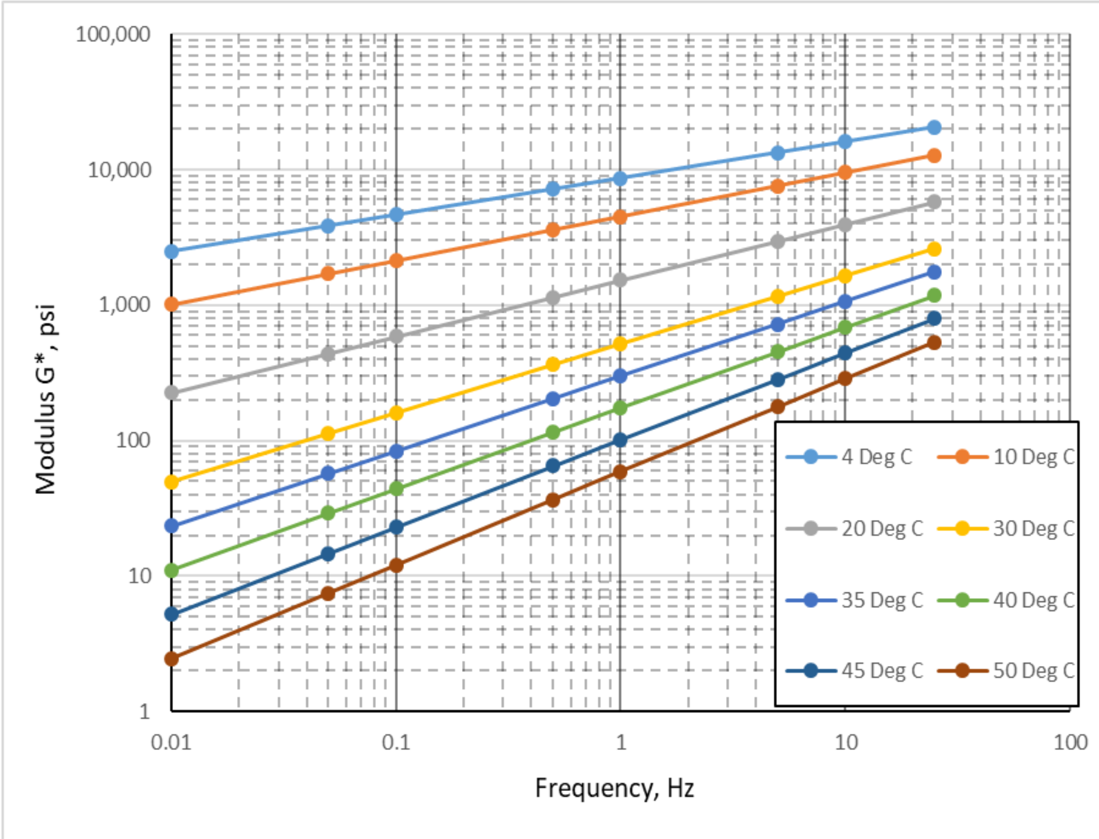

Figure 42 : Asphalt binder shear modulus isotherm example

Figure 42 is an example of asphalt binder shear modulus isotherm after testing one of the model development mixtures extracted binders listed in earlier sections. The figure shows that asphalt binder modulus is inversely proportional with testing temperature. In other words, asphalt binder shear modulus is highest at lower temperatures and vice versa. Results also showed that asphalt mixture stiffness is directly proportional with testing frequency. At lower test frequency, lower asphalt binder stiffness was recorded.

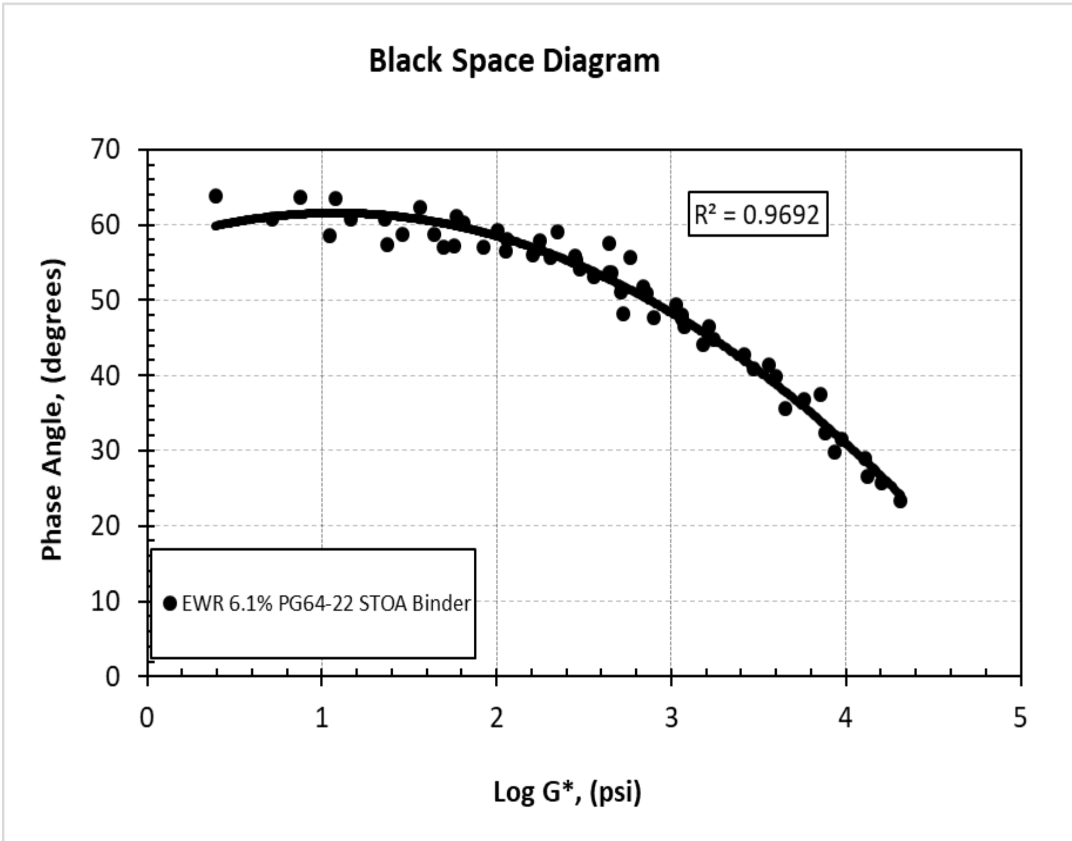

Figure 43 : Asphalt binder shear modulus sliver test black space plot example

Figure 43 is an example of extracted asphalt binder shear modulus master curve test black space diagram for one of the materials used in the model development phase. Black space diagram was produced and analyzed. Black space statistical analysis data had a minimum of 90% R squared value.

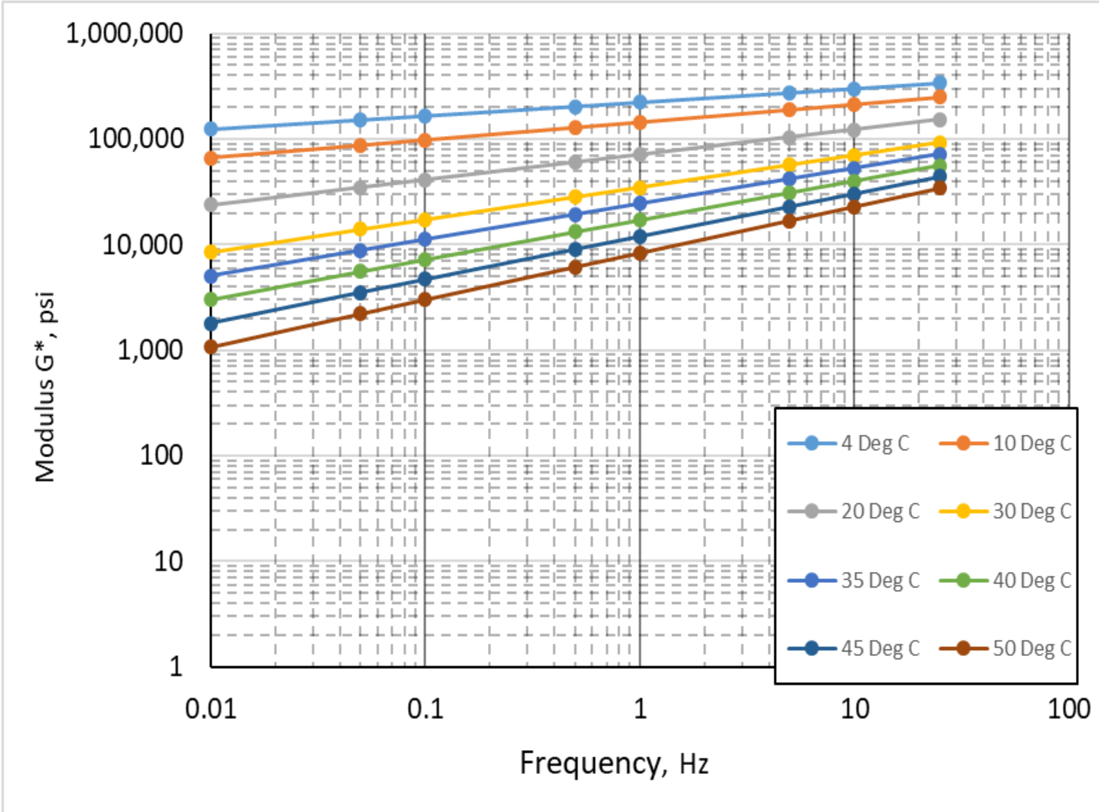

Figure 44 : Asphalt mixture shear modulus isotherm example

Figure 44 shows an example of asphalt mixture dynamic shear modulus isotherm ASTM D7552 after testing one of the model development mixtures listed in earlier sections. The figure shows that asphalt mixture modulus has an inverse proportional with testing temperature. The above figure shows that asphalt mixture stiffness is directly proportional with testing frequency.

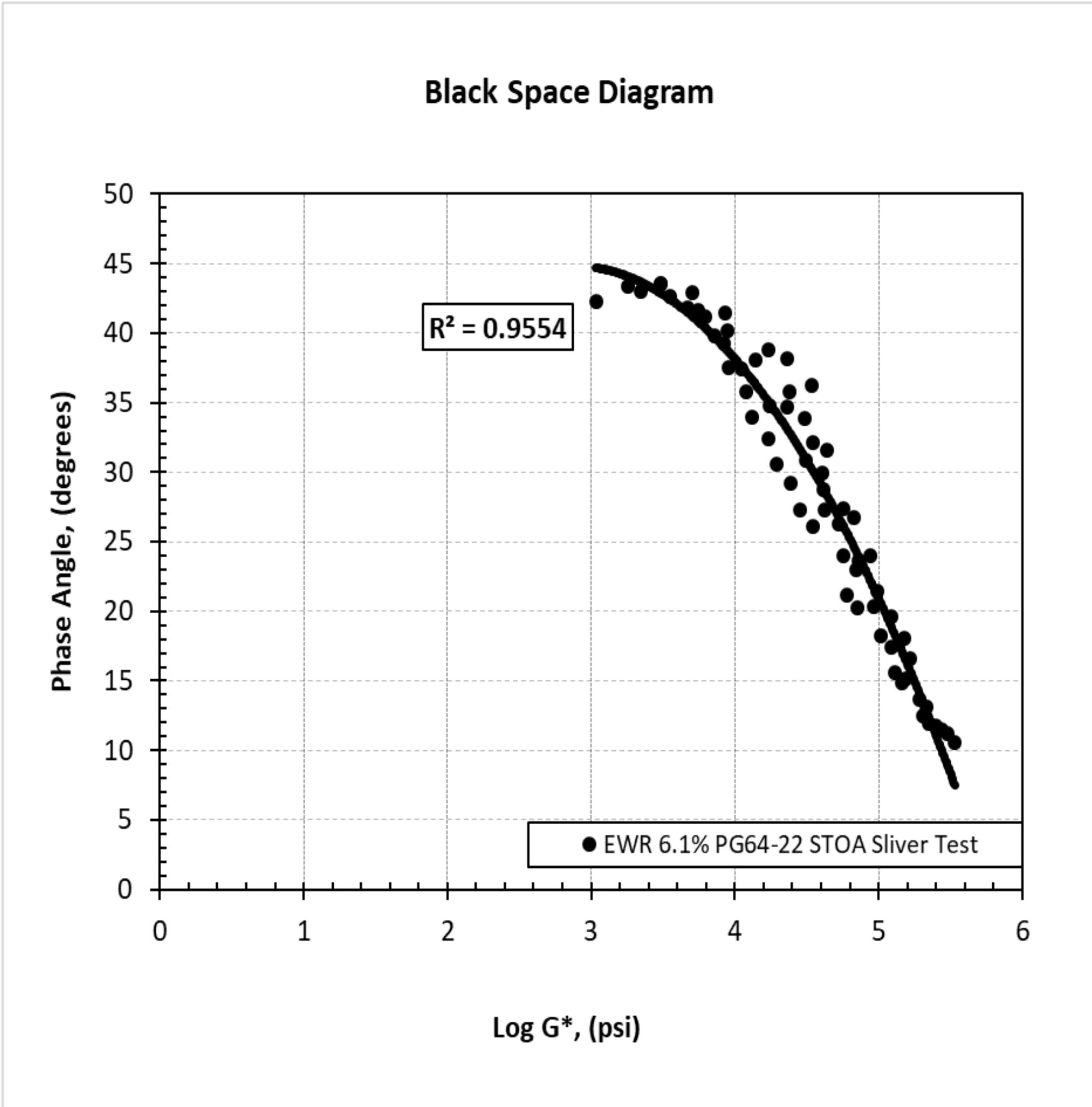

Figure 45 : Asphalt mixture shear modulus (sliver test) black space plot example

Figure 45 is an example of asphalt mixture dynamic shear modulus test ASTM D 7552 black space diagram for one of the materials used in the model development phase. Black space diagram was produced and analyzed. Similarly, Black space statistical analysis data had a minimum of 90% R squared value.

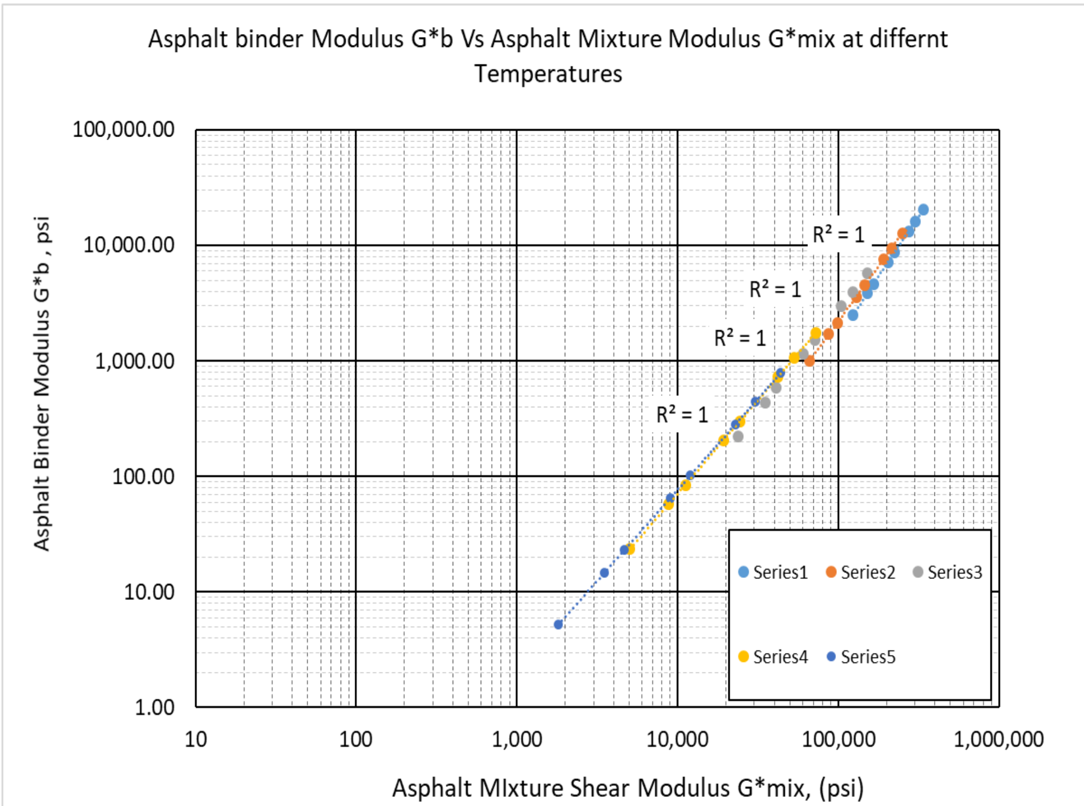

Figure 46 : Asphalt Binder Shear Modulus and Asphalt Mixture Sliver Test Modulus Correlation at Different Test Temperature

Extracted asphalt binder modulus and asphalt mixture shear modulus correlation was investigated. Figure 46 shows an example of such correlation for one of the asphalt mixtures. The figure showed strong correlation at the cold, intermediate and hot temperature conditions.

6.5.2 Developed backward asphalt binder prediction model

Backward calculation is the process of predicting asphalt binder modulus using the sliver test and the developed model. The developed backward model uses the same input as the forward model, which are as follows:

a. Voids in mineral aggregates (% VMA)
b. Voids filled with asphalt (%VFA)
c. Asphalt mixture shear modulus using the sliver test (psi)

Linear regression analysis and goodness of fit parameters were used to develop and evaluate the asphalt mixture prediction model. A MATLAB code was developed and used in the model development and data analysis. Approximately 700 data points were used to develop the model. A plot was developed for each mix to investigate extracted asphalt binder shear modulus and asphalt mixture shear modulus using the sliver test correlation.

A model was developed for each mix. A final model was then developed and calibrated for the twelve mixes used in the model development phase.

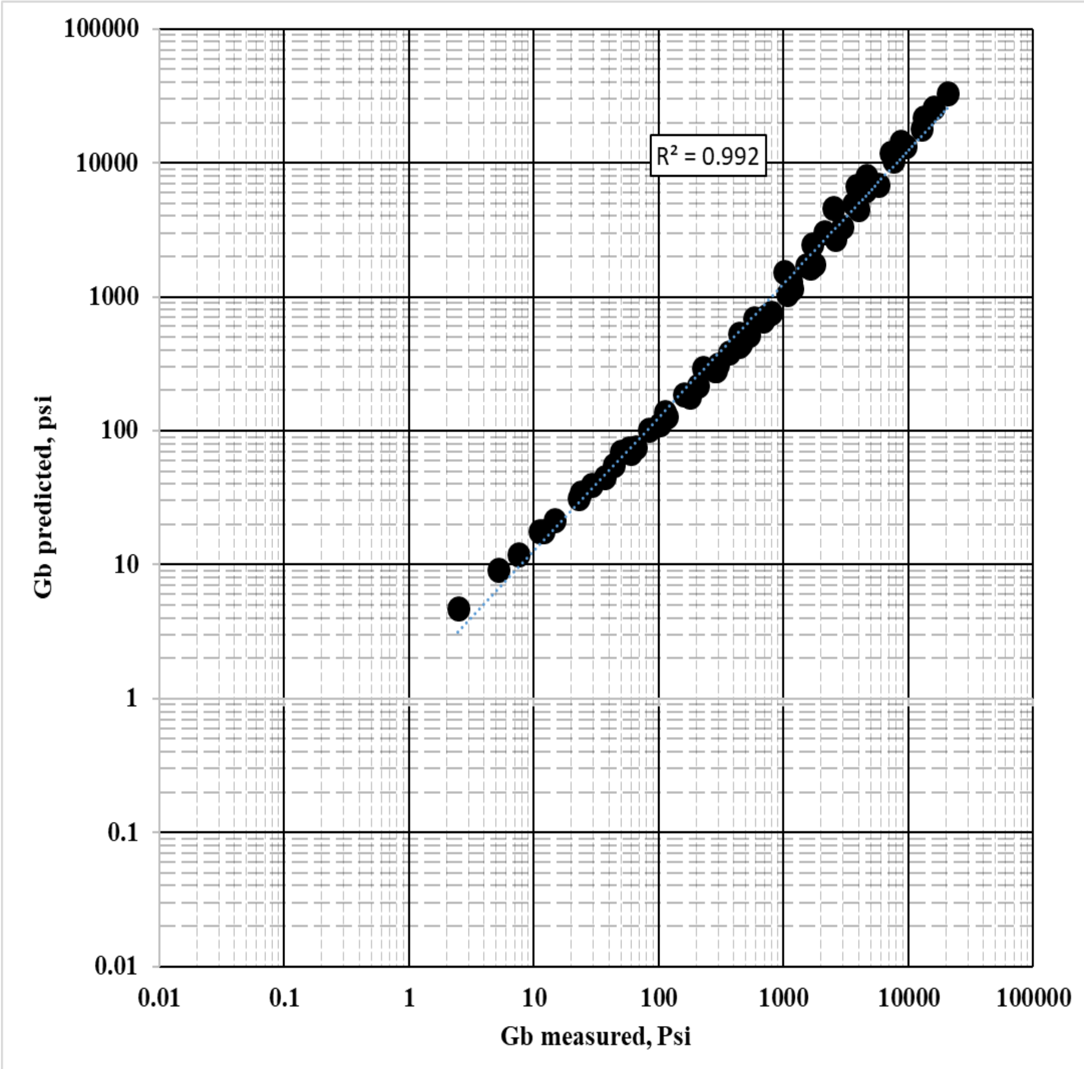

Figure 47 : Predicted asphalt binder shear modulus vs measured asphalt binder modulus correlation example for as specific mix

Figure 47 shows predicted asphalt binder shear modulus values using the developed model versus measured asphalt binder actual modulus values using the dynamic shear rheometer. In this case, the model was specifically designed for this specific mix. The data showed promising correlation with an R^2 value 99.92 %.

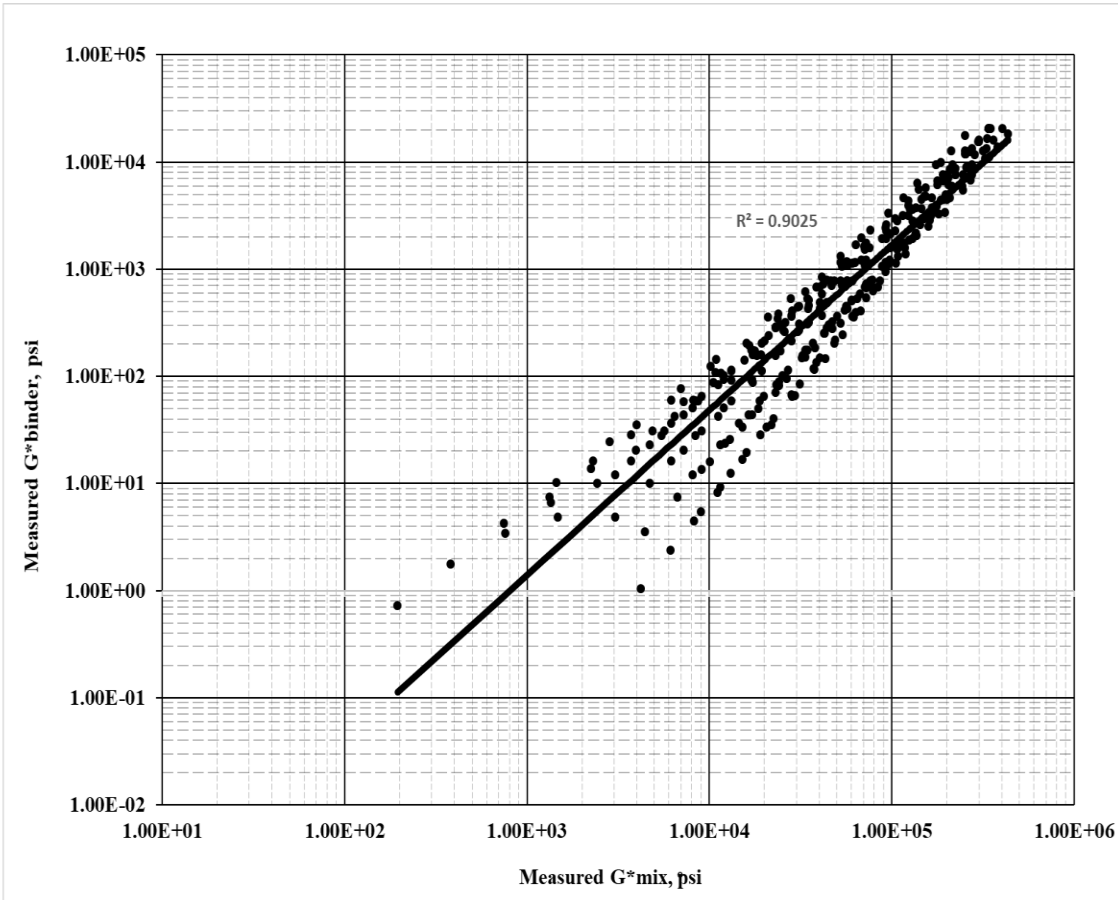

Figure 48 : Asphalt binder G*binder and asphalt mixture G*mix correlation

Asphalt mixture and asphalt binder shear modulus values were obtained experimentally using ASTM D7552 at 4 ℃, 10 ℃, 20 ℃, 35 ℃ and frequencies of 25Hz, 10Hz, 5Hz, 5Hz, 1 Hz, 0.1Hz. Figure 48 shows the comparison of measured asphalt binder complex shear modulus and measured asphalt binder complex shear modulus. Data showed good correlation with $R^2 = 90.25$ %.

The developed asphalt binder calculation model was developed using the same input parameters as the forward model.

The model is represented using **Equation 15**:

$$|G^*_{binder}| = P_C\left[E_{agg}\left(1 - \frac{VMA}{100}\right) + 3|G^*_{mix}|\left(\frac{VFA \times VMA}{100}\right)\right]$$

$$|G^*_{binder}| = P_C\left[4200000\left(1 - \frac{VMA}{100}\right) + 3|G^*_{mix}|\left(\frac{VFA \times VMA}{100}\right)\right]$$

$$P_C = a_1 G^{*\,b_1}_{mix}$$

$$P_C = 3.00 G^{*(1.1815)}_{mix}$$

Equation 15: Backward model equation

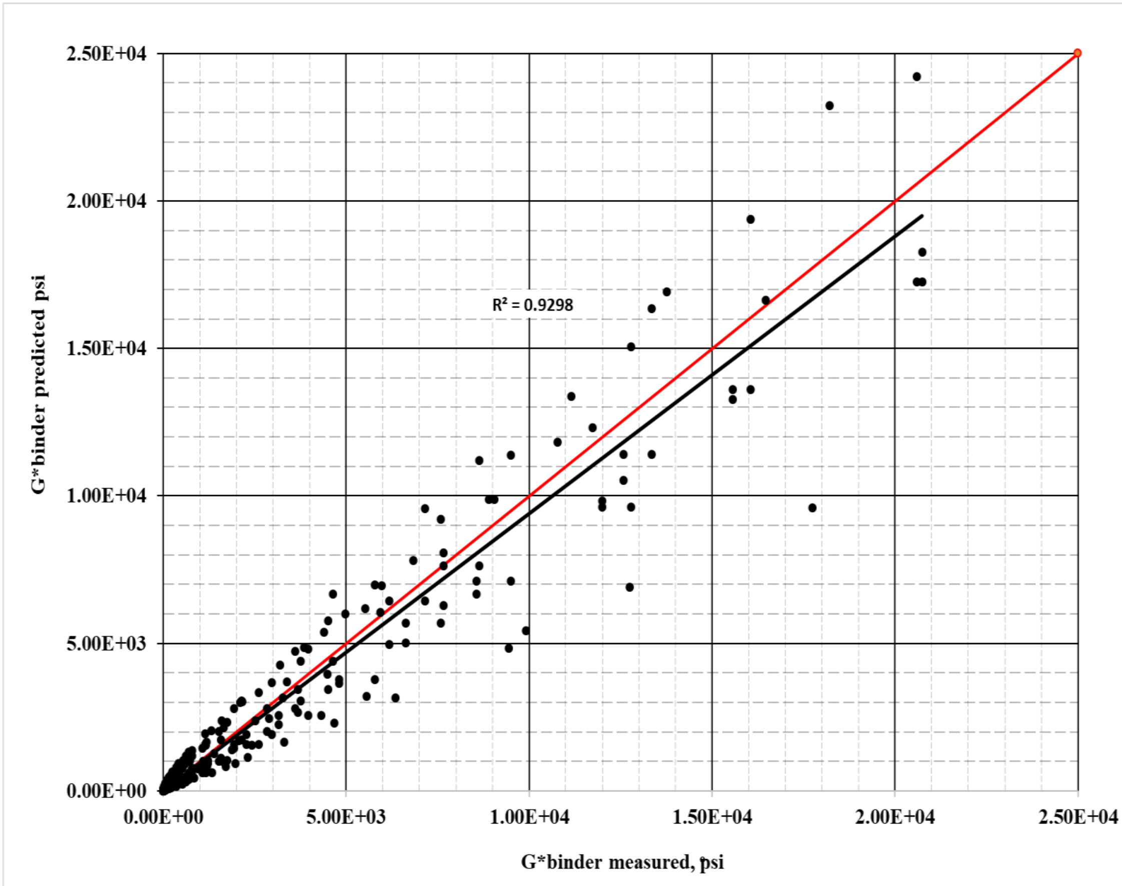

Figure 49 : Predicted asphalt binder modulus and DSR measured modulus correlation

6.5.3 Developed backward asphalt binder phase angle prediction model results and analysis

- **Materials Results and Analysis**

The developed experimental plan introduced the model to a wide range of asphalt mixture shear modulus/stiffness (G*sliver) and asphalt binder shear modulus (G*binder). Some of the mixture where polymer modified (i.e. PG 76-22).

Table 23 is a summary table for the minimum and maximum shear modulus used to develop the forward phase angle prediction model.

Test	Minimum Phase Angle, degrees	Maximum Phase Angle, degrees
G*Sliver	195	433568
Asphalt Binder Phase Angle	21	81

Table 23: Asphalt mixture shear modulus and asphalt binder phase angle data range used in the backward phase angle prediction model

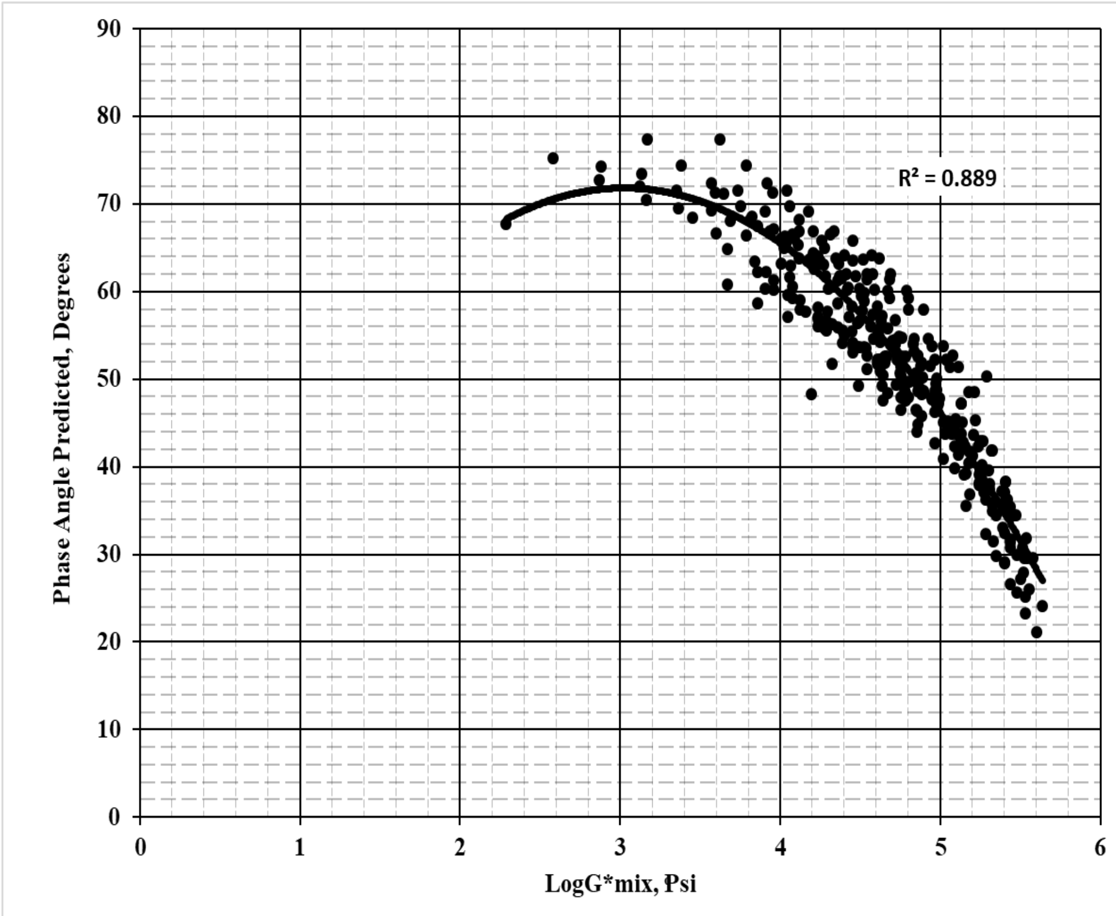

Figure 50: Model to backward predict the asphalt mixture phase angle

In addition to the need of forward predicting the asphalt binder shear modulus G*, the team was able to develop a model to backward predict the asphalt mixture phase angle. The model can be described in Equation 16:

$$\delta = -4.9828(\log G^*)^2 + 26.07 \log G^* + 39.435$$

Equation 16: Backward prediction of the asphalt mixture angle

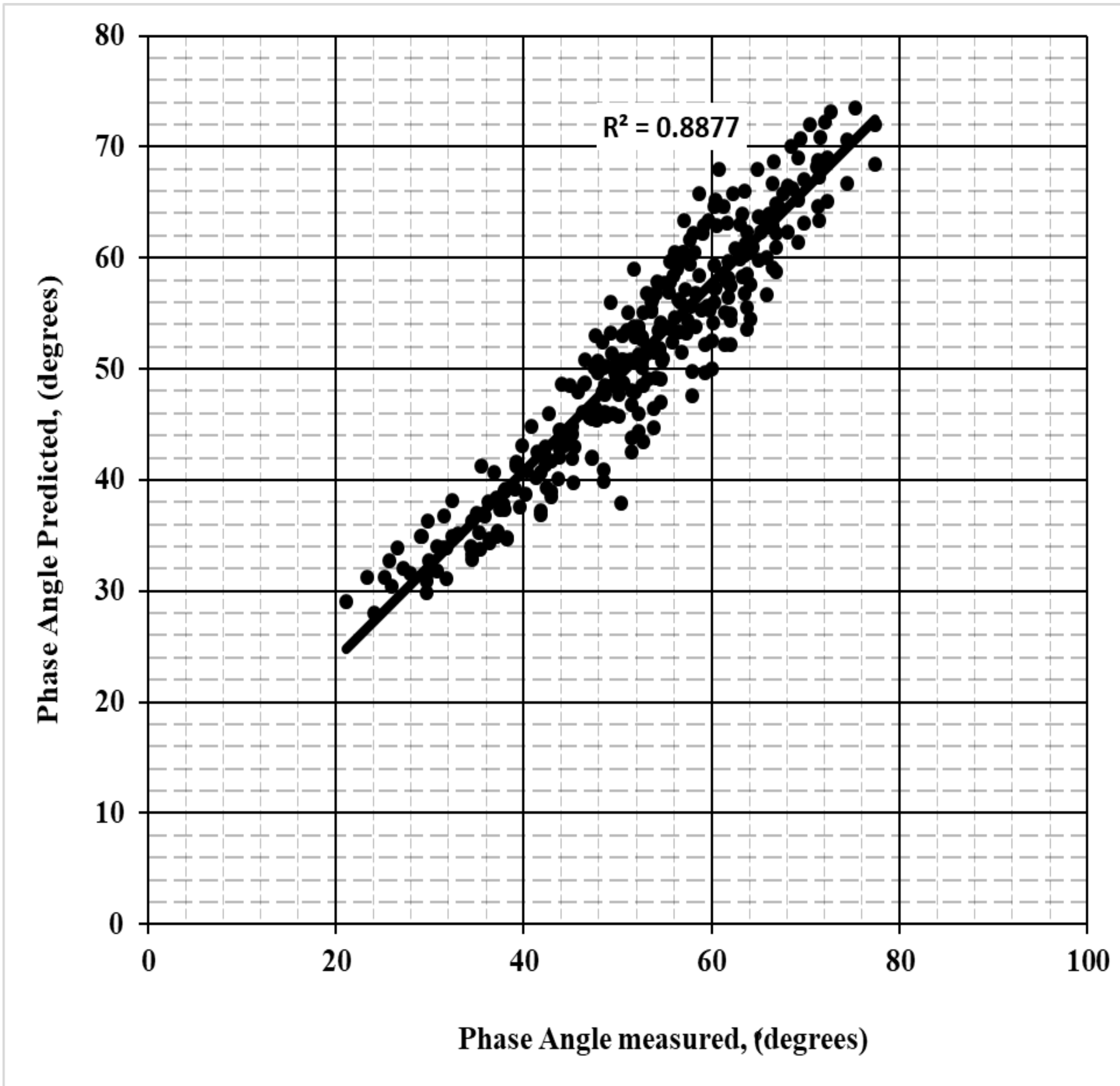

Figure 51 :Predicted and measured phase angle correlation

Figure 51 shows a plot of the forward predicted phase angle and measured phase angle. The above comparison showed a relatively strong correlation with $R^2 = 88.7\%$.

Chapter 7 – Forward and Backward Model Verification

7.1 Verification Forward Modulus Calculation Model

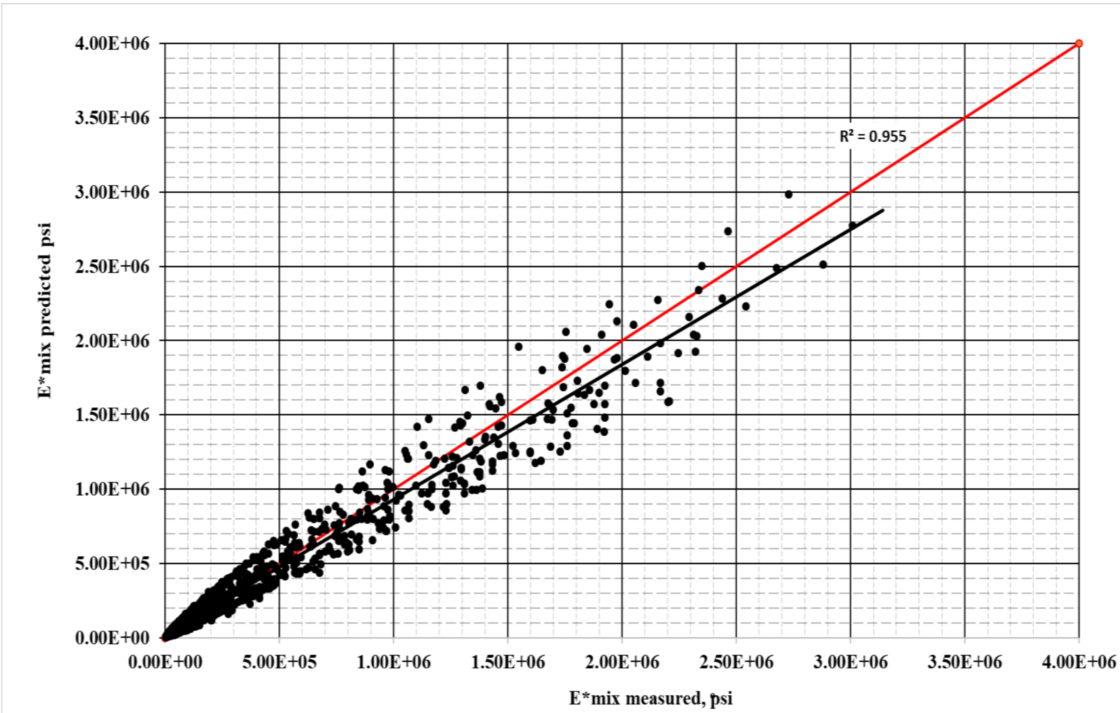

Figure 52: Predicted VS measured modulus results correlation for verification mixtures

Asphalt mixture shear modulus values were obtained experimentally using ASTM D7552 at 4 ℃, 10 ℃, 20 ℃, 35 ℃ and frequencies of 25Hz, 10Hz, 5Hz, 5Hz, 1 Hz, 0.1Hz. Shear modulus values were used in conjunction with the calibrated modified Hirsch model to forward calculate asphalt mixture modulus E* for 18 asphalt mixtures with different PG grades at different aging durations, HPTO, Recycled asphalt mixtures. Figure 52 shows the comparison of experimental vs forward calculated modulus results used to verify the forward model. Data showed good correlation for forward calculation represented by $R^2 = 95.50\%$.

7.2 Verification of Forward Phase Angle Calculation Model

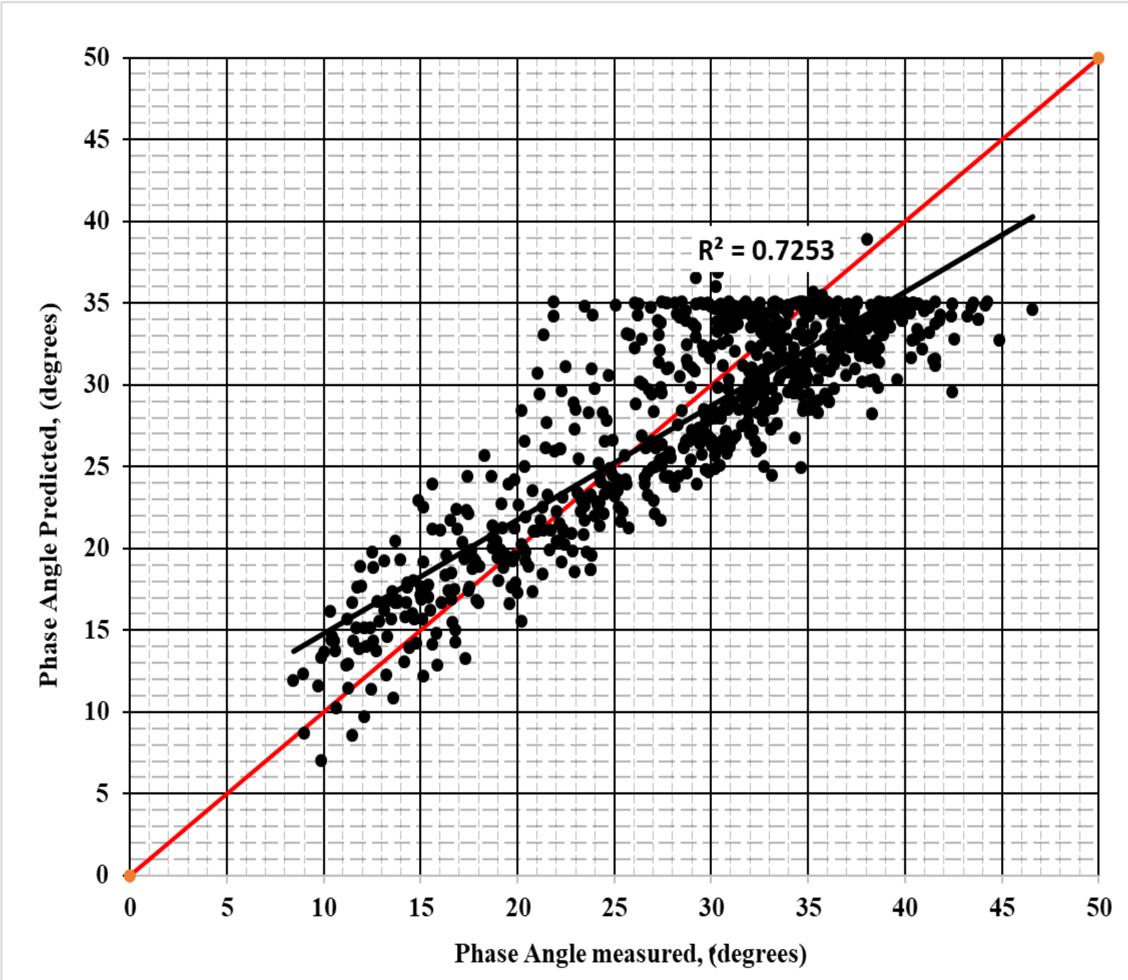

Figure 53: Predicted VS measured for verification asphalt mixture phase angle

Figure 53 shows a plot of the forward predicted phase angle and measured phase angle. The above comparison showed a relatively strong correlation with $R^2 = 72.53\%$.

7.3 Verification Backward Modulus Calculation Model

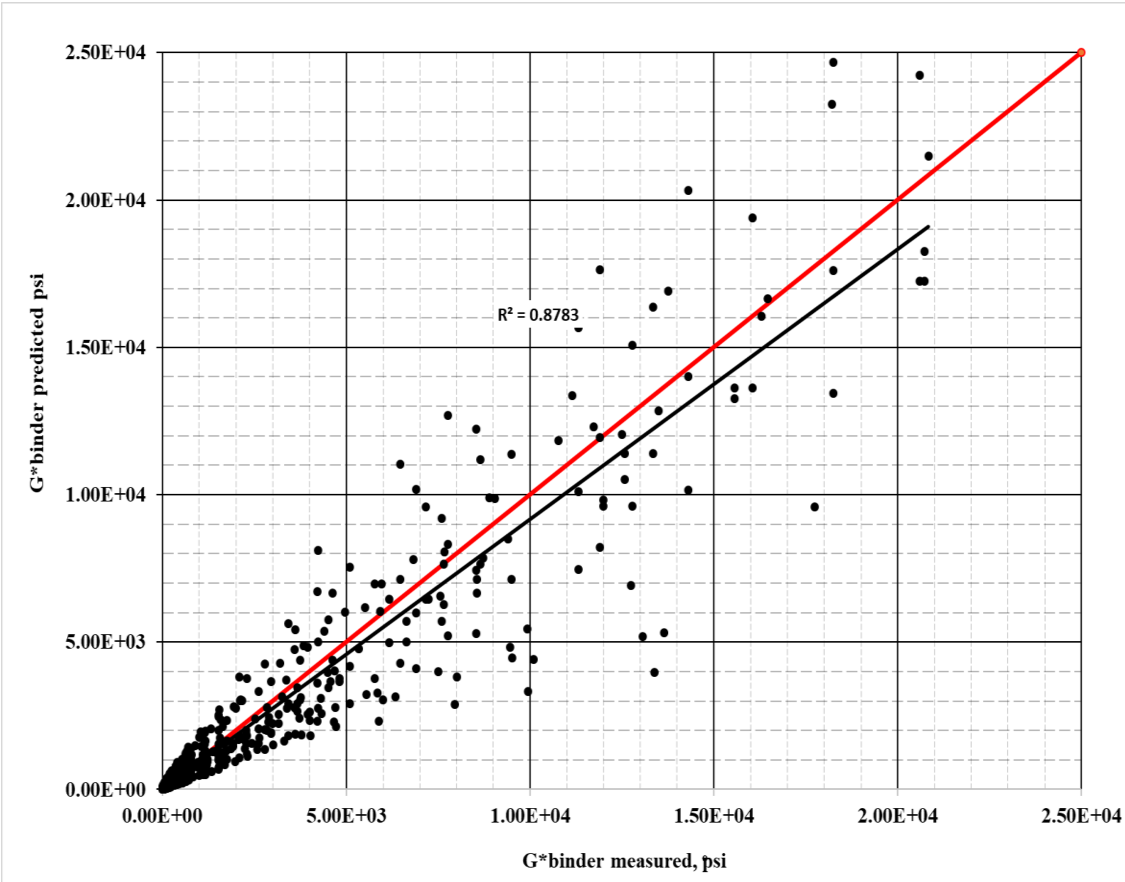

Figure 54: Experimental vs forward calculated modulus for verifying the backward model

Asphalt mixture shear modulus values were obtained experimentally using ASTM D7552 at 4 °C, 10 °C, 20 °C, 35 °C and frequencies of 25Hz, 10Hz, 5Hz, 5Hz, 1 Hz, 0.1Hz. Shear modulus values were used in conjunction with the calibrated modified Hirsch model to backward calculate asphalt binder modulus G* for 18 asphalt mixtures with different PG grades at different aging durations, HPTO, Recycled asphalt mixtures. Figure 54 shows the comparison of experimental vs forward calculated modulus results used to verify the backward model. Data showed good correlation for forward calculation represented by $R^2 = 87.80\%$.

7.4 Verification Backward Phase Angle Calculation Model

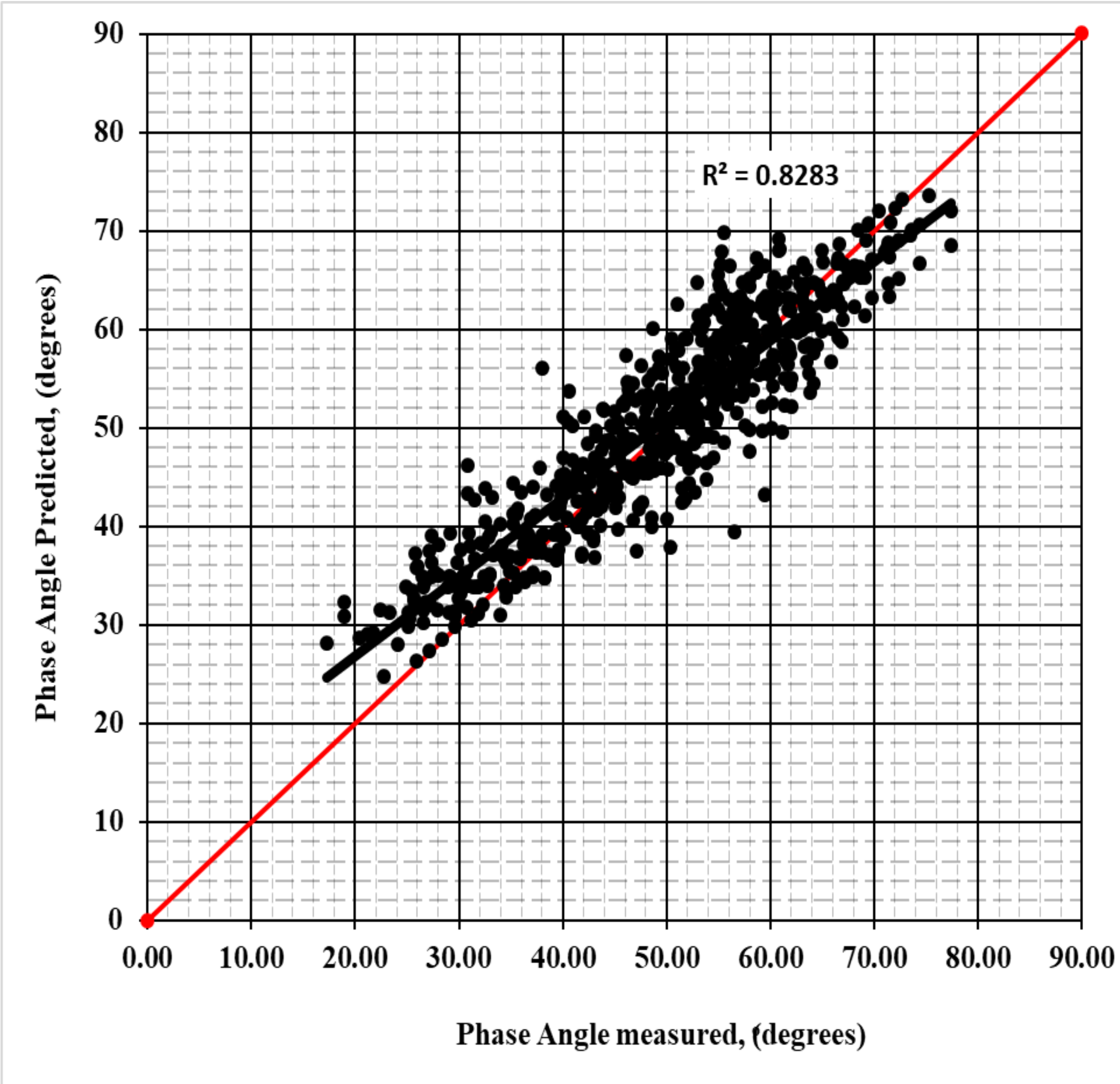

Figure 55: Backward predicted phase angle & measured phase angle for verifying mixes

Figure 55 shows a plot of the backward predicted phase angle and measured phase angle for verification mixes. The above comparison showed a relatively strong correlation with $R^2 = 82.83\%$.

Conclusions and recommendations

By conducting a thorough examination of various asphalt mixtures which exhibited a range of volumetric mixture properties by using standard practices as well as the lesser known sliver sample dynamic shear test, a model was developed that could estimate intrinsic properties to the asphalt mix by using the reduced size sliver samples. The proposed model was built from the basis of a Hirsch model and was validated through the repeated test of asphalt binder and asphalt mixture performance properties.

Throughout the process, sample preparation practices were honed and measurements were made utilizing two different models of similar equipment to evaluate the repeatability between units, which was found to be minimal or insignificant.

The following outcomes were driven by the results of the testing and the validation of the model:

Although the mixture types tested for this study have focused on primarily dense graded SuperPave mixes, the results showed strong correlations. The verification of the model succeeded in the goal to reduce the necessary sample size by using the sliver samples. Additional benefits of the small sample size include the ability to increase the number of samples tested to assure repeatability of results. The sliver test also supports the use of equipment that is regularly and easily accessible to many laboratories already with the addition of a simple fixture and an easy to build testing program for that equipment that uses similar parameters to those already understood in the discipline.

The predicted asphalt mixture modulus (forward calculation) obtained using the developed model showed acceptable correlation with the experimental asphalt mixture dynamic modulus E* obtained from laboratory samples (R^2=96.6%). The predicted asphalt binder dynamic modulus (backward calculation) obtained using the developed model showed good correlation with the experimental asphalt binder shear modulus G* obtained using laboratory prepared samples (R^2=93%).

As with any new testing protocol, the authors recommend additional testing and verification of similar mixture types as well as the testing of specialized mixtures in the future to determine the fit of the model compared to different aggregate gradations, alternative bituminous and non-bituminous binders, as well as the inclusion of additives such as RAP/RAS.

REFRENCES

[1] R. Texas Transportation, "Permeable Friction Courses Improve Safety on the Road," 1 09 2009. [Online]. Available: http://tti.tamu.edu/2009/09/01/out-of-harms-way/.

[2] r. t. The WASHTO, ""Part 2: Test data analysis and findings,"," Highway Research Board Special Report 22, 1955.

[3] W. N. Carey and P. E. Irick, ""The Pavement Serviceability-Performance Concept,"," in *Highway Research Board Bulletin 250*, 1960.

[4] D. H. Timm and J. M. McQueen, ""A Study of Manual vs Automated Pavement Condition Survey,"," Highway Research Center, Auburn. Alabama, 2004.

[5] T. W. Kennedy, F. L. Roberts and J. B. Rauhut, ""Distress and Related Materials for Premium Pavements,"," in *Transportation Reseaech Board*, 1979.

[6] J. Y. Welborn, ""State of the Art in Asphalt Pavement Specification,"," Federal Highway Administration, 1984.

[7] F. M. Hveem, E. Zube and J. Skog, "Proposed New Test Specification for Paving Grade Asphalts," in *Association of Asphalt Paving Technologists*, 1963.

[8] E. R. Brown, P. S. Kandhal and Z. Jingna, ""Performance Testing for Hot Mix Asphalt"," National Center For Asphalt Technology, Auburn, 2001.

[9] J. Sousa, J. Craus and C. Monismith, ""Summary Report On Permanant Deformation In Asphalt Concrete."," SHRP NAtional Research Council, Washington D.C., 1991.

[10] R. a. R. M. Leathy, ""Asphalt Mixes: Materials, Design and Characterization."," in *Proceedings of the Association of Asphalt Paving Technologists*, 1999.

[11] C. Campbell, ""The rocky Road of Mix Design"," in *Hot Mix Asphalt Technology*, Winter 1989.

[12] P. Kandhal and W. Koehler, ""Marshal Mix Design Method:Current Practices," 1985.

[13] "MIx Design Techniques-Part I," National Asphalt Pavement Association, April 1982.

[14] "Mix Design Methods for Asphalt Concrete and other Hot Mix Types," The Asphalt Institute, May 1984.

[15] "Civil Engineering Portal," 27 09 2015. [Online]. Available: http://www.engineeringcivil.com/what-is-marshall-mix-design-for-bituminous-materials.html.

[16] "Slide Share," 27 09 2015. [Online]. Available: http://www.slideshare.net/pokjak80/chapter3-road-pavement-10558620.

[17] ""Background of Superpave Asphalt Mixture Design and Analysis"," Federal Highway Administration, 1995.

[18] ""Superpave Asphalt Mixture Design: Illustrated Level I Lab Methods"," Federal Highway Administration, 1995.

[19] ""Superpave Level 1 Mix Design"," Asphalt Institute, Lexington, KY, 1995.

[20] R. L. Lytton, J. R. Uzan, D. R. Hiltunen and S. M. Stoffels, ""Development and Validation of Performance Prediction Models and Specifications for Asphalt Binder and Paving Mixes"," Strategic Highway Research Program, Washington DC: National Academy of Science, 1993.

[21] R. Cominsky, G. Huber, T. Kennedy and M. Anderson, ""The SuperPave Mix Design Manual for New Constructions and Overlays"," Strategic Highway Research Program, Washington, DC, 1994.

[22] E. T. Harriga, R. B. Leahy and J. S. and Youtcheff, ""The SuperPave Mix Design Manual Specification, Test Methods, and Practices"," Strategic Highway Research Group, Washington, DC, 1994.

[23] AI, "Reserach and Development of The Asphalt Institute's Thickness Design Manual (MS-1)," Asphalt Institute, 1982.

[24] E. C. Bingham, ""Fluidity and Plasticity,"," McGraw-Hill Book, New York, 1922.

[25] G. W. Scott Blair, ""A Survey of General and Applied Rheology,"," Sir Isaac Pitman & Sons, London, 1949.

[26] H. Markowitz, ""The Emerhence of Rheology,"," *Physics Today,* April 1968.

[27] R. B. Bird, R. C. Armstrong and O. Hassager, "Dynamics of Polymeric Liquids,", 2nd Ed. ed., vol. Vol. 1, New York: John wiley and Sons, 1987a.

[28] J. L. White, ""Principles of Polymer Engineering Rheology,"," J. Wiley & Sons, New York, 1990.

[29] R. I. Tanner and K. Walters, ""Rheology: an Historical Prespective,"," Elsevier, Amsterdam, 1998.

[30] D. Doraiswamy, "The Origins of Rheology: A Short Historical Excursion," Dupont iTechnologies, Eilmington, DE.

[31] Y. R. Kim, Ed., "Modeling of Asphalt Concrete, ASCE Press,, 2009.

[32] D. A. Anderson, D. W. Christensen, H. U. Bahia, R. Dongre, M. G. Sharma, C. E. Antle and J. Button, ""Binder Characterization and Evaluation,"," Stratigic Highway Research Program, Washington, DC, 1994.

[33] H. S. Pink, R. Merz and a. D. S. Bosniak, ""Asphalt Rheology: Experimental Determination of Dynamic Moduli at Low Temperature"," in *Proceedings of the Association of Asphalt Paving Technologists*, 1980.

[34] d. Bats and G. v. Gooswilligen, ""Practical Rheological Characterizationof Paving Grade Bitumes"," Shell Research, Amsterdam, 1995.

[35] S. Maccarone, ""Rheological Properties of Weathered Asphalts Extracted from Sprayed Seals Nearing Distress Conditions"," in *Proceedings of the Association of Asphalt Paving Technologists*, 1987.

[36] M. O. Marasteanu and D. A. Anderson, ""Improved Model for bitumen Rheological Caracterization"," in *Eurobitume Workshop on Performance Related Properties for Bitumenous Binders,*, Luxembourg, 1999.

[37] M. Zeng, H. U. Bahia, H. Zhai, M. Anderson and P. Turner, ""Rheological Modeling of Modified Asphalt Binder and Mixtures"," in *Journal of the Association of Asphalt Paving Technologists*, 2001.

[38] R. Dongre, ""The Development of Direct Tension Test Method to Characterize Failure Properties of Asphalt Cements,"," 1994.

[39] D. A. Anderson and T. W. Kennedy, ""Development of SHRP Binder Specification,"," in *Journal of the Asphalt Paving Technologists*, 1993.

[40] H. U. Bahia, H. Zhai and A. Rangel, ""Evaluation of Stability, Nature of Modifier, and Short Term Aging of Modified Binders Using New Tests: The lAST, The PAT, and The MRTFO,"," in *TRR38*, Washington D.C., 1998a.

[41] H. U. Bahia, H. Zhai and K. Bonnetti, ""Non Linear Viscoelastic and Fatigue Properties of Asphalt Binders,"," in *Journal of the Association of the Asphalt Paving Technologists*, 1999.

[42] FHWA, "LTPP Computed Parameter: Dynamic Modulus," Federal Highway Administration, Mclean, Virginia, 2011.

[43] R. C. Korzak, ""Utilizing the Canadian Long Term Pavement Performance (C-LTPP) Database for Asphalt Dynamic Modulus Prediction,"," University of Waterloo, Waterloo, Ontario, Canada, 2013.

[44] J. Bari, "Development of a New Revised Version of the Witczak E* Predictive Models for Hot Mix Asphalt Mixtures," Arizona State Ubinversity, Phoenix, AZ, 2005.

[45] J. Y. Welborn, "State of the Art in Asphalt Pavement Specification," Federal Highway Administration, 1984.

[46] M. Sakhaeifar, S. Underwood, R. Kim, J. Puccinelli and N. Jackson, "Development of Artificial Neural Network Predictive Models for Populating Dynamic Moduli of Long-term Pavement Performance Sections," in *Transportation Research Record*, 2010.

[47] J. Anderson, ""Introduction to Neural Networks,"," in *MIT Press*, Cambridge, MA, 1995.

[48] V. Yadama, "CE 537, Fall 2007," Civeil and Environmental Engineering, [Online]. Available: http://pas.ce.wsu.edu/CE537-1/Lectures/Rule%20of%20Mixtures.pdf.

[49] J. Christensen, T. Pellinen and R. F. Bonaquist, "Hirsch Model for Estimating the Modulus of Asphalt Concrete," in *Journal of the Association of Asphalt Paving Technologists*, 2003.

[50] C. Donald W. and B. Ramon F., "Design Guidance for Fatigue and Rut Resistance Mixtures," 2014.

[51] D. W. Christensen, ""Airfield Asphalt Pavement Technology Program Project 04-02: PG Binder Grade Selection for Airfield Pavevemnt"," Advanced Asphalt Technologies, 2008.

[52] R. M. Anderso, ""The asphalt binder handbook, MS-26."," (2011).

[53] D. I. Hanson, R. E. Boyer, K. Gayle and A. Nadkami, ""AAPTP Project 05-02: Fuel Resistant Seelers and Binders for HMA Airfield Pavements"," AMEC, 2009.

[54] G. Reinke, ""Report to NCAT-Rejuvenator Study - Study of Rejuvenator Type Of Mixture Stiffness"," Mathy Technology and Engineering Services, Inc,, May 2002.

[55] A. D7552, "Standard Test Method for Determining the Complex Shear Modulus (G*) of Bituminous Mixtures Using Dynamic Shear Rheometer", vol. Volume 04.03, West Conshohocken, PA, 2014.

[56] ". s. f. t. m. a. m. o. s. a. testing.", American Association of State Highway, and Transportation Officials., AASHTO, 2011.

[57] D. Zvirblis, ""Influence of High RAP on Binder Properties in Hot Mix Asphalt of North East"," Rutgers University -Graduate School- New Brunswick, 2014.

[58] A. International, "Standard Test Method for Determining the Complex Shear Modulus (G*) of Bituminous Mixtures Using Dynamic Shear Rheometer", vol. Volume 04.03, West Conshohocken, PA, 2014.

[59] D. W. J. Christense, P. Terhi and R. F. Bonaquist, ""Hirsch Model for Estimating the Modulus of Asphalt Concrete"," in *Asphalt Paving Technology 2003*, Lexington, Kentucky, 2003.

[60] C. S. C. and R. P. Canale, ""Numerical Methods for Engineers"," McGraw-Hill, Inc., New York, 1988.

APPENDICIES

APPENDIX A - Asphalt mixture properties

Sample Type	Sample ID	Wt in Air (grams)	Wt in Water (grams)	SSD Water (grams)	Bulk Specific	Max. Specific	Air Voids (%)	VMA (%)	VFA (%)	Effect. AC by Vol (%)
170	FPP 2017 EWR Axeon 6.1% 64-22 LTOA	6688.3	3842.0	6733.4	2.313	2.462	6.1	19.3	68.7	13.3
170	FPP 2017 EWR Axeon 6.1% 64-22 STOA	6655.1	3770.3	6686.3	2.282	2.462	7.3	20.4	64.2	13.1
170	FPP 2017 EWR Axeon 6.1% 76-22 LTOA	6682.5	3862.9	6759.2	2.309	2.462	6.2	19.5	68.1	13.3
170	FPP 2017 EWR Axeon 6.1% 76-22 STOA	6683.5	3823.9	6725.9	2.303	2.462	6.4	19.7	67.3	13.2
170	FPP 2017 EWR Axeon 6.5% 64-22 LTOA	6632.9	3783.3	6683.3	2.287	2.447	6.5	20.6	68.3	14.1
170	FPP 2017 EWR Axeon 6.5% 64-22 STOA	6661.9	3779.7	6692.7	2.292	2.447	6.3	20.4	69.0	14.1
170	FPP 2017 EWR Axeon 6.5% 76-22 LTOA	6636.7	3821.6	6714.6	2.296	2.447	6.2	20.3	69.5	14.1
170	FPP 2017 EWR Axeon 6.5% 76-22 STOA	6636.5	3779.1	6697.1	2.275	2.447	7.0	21.0	66.5	14.0
170	FPP 2017 EWR Axeon 6.9% 64-22 LTOA	6535.6	3707.5	6585.5	2.271	2.422	6.2	21.5	71.0	15.3
170	FPP 2017 EWR Axeon 6.9% 64-22 STOA	6531.5	3685.3	6588.4	2.251	2.422	7.1	22.2	68.1	15.1
170	FPP 2017 EWR Axeon 6.9% 76-22 LTOA	6539.6	3741.3	6624.0	2.271	2.422	6.2	21.5	70.9	15.3
170	FPP 2017 EWR Axeon 6.9% 76-22 STOA	6519.6	3693.7	6599.7	2.244	2.422	7.3	22.4	67.2	15.1
170	Stone Industries_125mm_SMA	7034.9	4242.1	7111.6	2.449	2.661	8.0	20.6	61.4	12.6
170	Stone Industries_Haledon_125mm_M64_R15	7084.7	4261.7	7164.5	2.439	2.659	8.3	19.7	58.0	11.4
170	Stone Industries_HPTO	6945.0	4023.4	6981.3	2.346	2.491	5.8	22.4	74.1	16.6
170	TilconMtHope_125mm_15RAP									
170	TilconOxford_HPTO	6728.4	3793.6	6736.8	2.284	2.435	6.2	20.9	70.4	14.7
170	TRI_KeasbeyPlant_125mm_M76_10RAP	7434.5	4531.2	7468.0	2.530	2.714	6.8	18.0	62.4	11.2
170	TRI_KeasbyPlant,125mm_M64_15RAP	7399.2	4483.3	7434.6	2.505	2.703	7.3	18.7	60.8	11.3

SIEVE NUMBER	OPENING (mm)	Stone Industries_125mm_SM	Stone Industries_Haledon	Stone Industries_HPTO	TilconOxford_HPTO	TRI_KeasbeyPlant_125mm_M76_10RAP	TRI_KeasbyPlant,125mm_M64_15RAP
		% Finer	% Finer	% Finer	% Finer	% Finer	% Finer
2.0"	50.00	100	100.00	100.00	100.00	100.00	100.00
1.5"	37.50	100.0	100.0	100.0	100.0	100.0	100.0
1.0"	25.00	100.0	100.0	100.0	100.0	100.0	100.0
3/4"	19.00	100.0	100.0	100.0	100.0	100.0	100.0
1/2"	12.50	89.6	93.8	100.0	99.8	97.5	96.1
3/8"	9.50	71.3	84.7	100.0	99.8	81.2	80.9
# 4	4.75	30.1	49.6	81.1	78.9	64.7	61.5
# 8	2.36	18.8	31.8	50.9	38.8	41.6	38.9
# 16	1.18	15.0	23.4	31.5	26.9	28.2	26.9
# 30	0.60	13.0	18.0	21.8	19.3	20.1	19.5
# 50	0.30	11.8	13.3	15.4	13.2	14.4	14.0
# 100	0.15	10.5	9.3	10.5	8.2	9.8	9.5
# 200	0.075	8.1	6.2	6.7	4.7	5.9	5.7

Stone Industries_125mm_SMA		
12.5SMA		
SIEVE NUMBER	**OPENING (mm)**	**% Finer**
2.0"	50.00	100.0
1.5"	37.50	100.0
1.0"	25.00	100.0
3/4"	19.00	100.0
1/2"	12.50	89.6
3/8"	9.50	71.3
# 4	4.75	30.1
# 8	2.36	18.8
# 16	1.18	15.0
# 30	0.60	13.0
# 50	0.30	11.8
# 100	0.15	10.5
# 200	0.075	8.1
Gravity Determination of -#8 (AASHTO T84)		
Gsb (g/cm^3)		2.865
Gssd (g/cm^3)		2.906
Gapp (g/cm^3)		2.988
ABS (%)		1.44
Gravity Determination of +#8 (AASHTO T85)		
Gsb (g/cm^3)		2.913
Gssd (g/cm^3)		2.948
Gapp (g/cm^3)		3.018
ABS (%)		1.20
Aggregate Blend Gsb		
Gsb (g/cm^3)		2.898
halt Content Determination - AASHTO T164 (Extracti		
Asphalt Content (%) - T164		5.980
Gravity Determination (Assumed from Gmm of Mix)		
Gmm (g/cm^3)		2.661
Gse (g/cm^3)		2.959

Stone Industries_Haledon_125mm_M64_R15		
12.5M64		
SIEVE NUMBER	**OPENING (mm)**	**% Finer**
2.0"	50.00	100.0
1.5"	37.50	100.0
1.0"	25.00	100.0
3/4"	19.00	100.0
1/2"	12.50	93.8
3/8"	9.50	84.7
# 4	4.75	49.6
# 8	2.36	31.8
# 16	1.18	23.4
# 30	0.60	18.0
# 50	0.30	13.3
# 100	0.15	9.3
# 200	0.075	6.2
Gravity Determination of -#8 (AASHTO T84)		
Gsb (g/cm3)		2.828
Gssd (g/cm3)		2.860
Gapp (g/cm3)		2.920
ABS (%)		1.11
Gravity Determination of +#8 (AASHTO T85)		
Gsb (g/cm3)		2.916
Gssd (g/cm3)		2.954
Gapp (g/cm3)		3.033
ABS (%)		1.33
Aggregate Blend Gsb		
Gsb (g/cm3)		2.888
halt Content Determination - AASHTO T164 (Extracti		
Asphalt Content (%) - T164		5.400
Gravity Determination (Assumed from Gmm of Mix)		
Gmm (g/cm3)		2.659
Gse (g/cm3)		2.923

Stone Industries_HPTO		
HPTO		
SIEVE NUMBER	**OPENING (mm)**	**% Finer**
2.0"	50.00	100.0
1.5"	37.50	100.0
1.0"	25.00	100.0
3/4"	19.00	100.0
1/2"	12.50	100.0
3/8"	9.50	100.0
# 4	4.75	81.1
# 8	2.36	50.9
# 16	1.18	31.5
# 30	0.60	21.8
# 50	0.30	15.4
# 100	0.15	10.5
# 200	0.075	6.7
Gravity Determination of -#8 (AASHTO T84)		
Gsb (g/cm3)		2.799
Gssd (g/cm3)		2.816
Gapp (g/cm3)		2.847
ABS (%)		0.60
Gravity Determination of +#8 (AASHTO T85)		
Gsb (g/cm3)		2.792
Gssd (g/cm3)		2.808
Gapp (g/cm3)		2.838
ABS (%)		0.58
Aggregate Blend Gsb		
Gsb (g/cm3)		2.797
phalt Content Determination - AASHTO T164 (Extractio		
Asphalt Content (%) - T164		7.04
Gravity Determination (Assumed from Gmm of Mix)		
Gmm (g/cm3)		2.491
Gse (g/cm3)		2.791

TilconOxford_HPTO		
HPTO		
SIEVE NUMBER	**OPENING (mm)**	**% Finer**
2.0"	50.00	100.0
1.5"	37.50	100.0
1.0"	25.00	100.0
3/4"	19.00	100.0
1/2"	12.50	99.8
3/8"	9.50	99.8
# 4	4.75	78.9
# 8	2.36	38.8
# 16	1.18	26.9
# 30	0.60	19.3
# 50	0.30	13.2
# 100	0.15	8.2
# 200	0.075	4.7
Gravity Determination of -#8 (AASHTO T84)		
Gsb (g/cm3)		2.690
Gssd (g/cm3)		2.698
Gapp (g/cm3)		2.713
ABS (%)		0.32
Gravity Determination of +#8 (AASHTO T85)		
Gsb (g/cm3)		2.664
Gssd (g/cm3)		2.676
Gapp (g/cm3)		2.696
ABS (%)		0.44
Aggregate Blend Gsb		
Gsb (g/cm3)		2.684
halt Content Determination - AASHTO T164 (Extracti		
Asphalt Content (%) - T164		7.040
Gravity Determination (Assumed from Gmm of Mix)		
Gmm (g/cm3)		2.435
Gse (g/cm3)		2.716

TRI_KeasbeyPlant_125mm_M76_10RAP		
12.5ME		
SIEVE NUMBER	**OPENING (mm)**	**% Finer**
2.0"	50.00	100.0
1.5"	37.50	100.0
1.0"	25.00	100.0
3/4"	19.00	100.0
1/2"	12.50	97.5
3/8"	9.50	81.2
# 4	4.75	64.7
# 8	2.36	41.6
# 16	1.18	28.2
# 30	0.60	20.1
# 50	0.30	14.4
# 100	0.15	9.8
# 200	0.075	5.9
Gravity Determination of -#8 (AASHTO T84)		
Gsb (g/cm3)		2.908
Gssd (g/cm3)		2.937
Gapp (g/cm3)		2.996
ABS (%)		1.01
Gravity Determination of +#8 (AASHTO T85)		
Gsb (g/cm3)		2.960
Gssd (g/cm3)		2.976
Gapp (g/cm3)		3.009
ABS (%)		0.54
Aggregate Blend Gsb		
Gsb (g/cm3)		2.926
halt Content Determination - AASHTO T164 (Extracti		
Asphalt Content (%) - T164		5.190
Gravity Determination (Assumed from Gmm of Mix)		
Gmm (g/cm3)		2.714
Gse (g/cm3)		2.981

TRI_KeasbyPlant,125mm_M64_15RAP		
12.5M64		
SIEVE NUMBER	**OPENING (mm)**	**% Finer**
2.0"	50.00	100.0
1.5"	37.50	100.0
1.0"	25.00	100.0
3/4"	19.00	100.0
1/2"	12.50	96.1
3/8"	9.50	80.9
# 4	4.75	61.5
# 8	2.36	38.9
# 16	1.18	26.9
# 30	0.60	19.5
# 50	0.30	14.0
# 100	0.15	9.5
# 200	0.075	5.7
Gravity Determination of -#8 (AASHTO T84)		
Gsb (g/cm3)		2.908
Gssd (g/cm3)		2.938
Gapp (g/cm3)		2.999
ABS (%)		1.05
Gravity Determination of +#8 (AASHTO T85)		
Gsb (g/cm3)		2.970
Gssd (g/cm3)		2.990
Gapp (g/cm3)		3.029
ABS (%)		0.65
Aggregate Blend Gsb		
Gsb (g/cm3)		2.932
halt Content Determination - AASHTO T164 (Extracti		
Asphalt Content (%) - T164		
Gravity Determination (Assumed from Gmm of Mix)		
Gmm (g/cm3)		2.704
Gse (g/cm3)		2.945

Newark Mix		
12.5M64/76		
SIEVE NUMBER	**OPENING (mm)**	**% Finer**
2.0"	50.00	100.0
1.5"	37.50	100.0
1.0"	25.00	100.0
3/4"	19.00	100.0
1/2"	12.50	91.5
3/8"	9.50	79.1
# 4	4.75	52.4
# 8	2.36	35.4
# 16	1.18	24.1
# 30	0.60	17.0
# 50	0.30	11.5
# 100	0.15	7.2
# 200	0.075	4.2
Gsb		2.69
Gsa		2.73

APPENDIX B - Model development forward modulus model family of curves

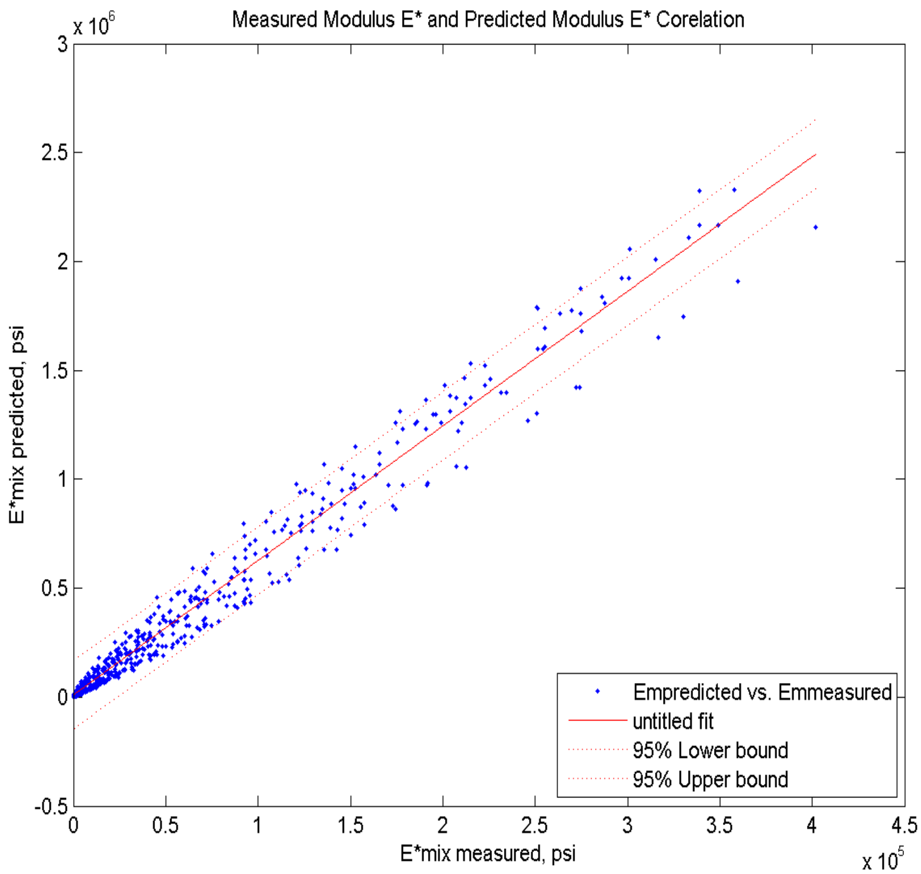

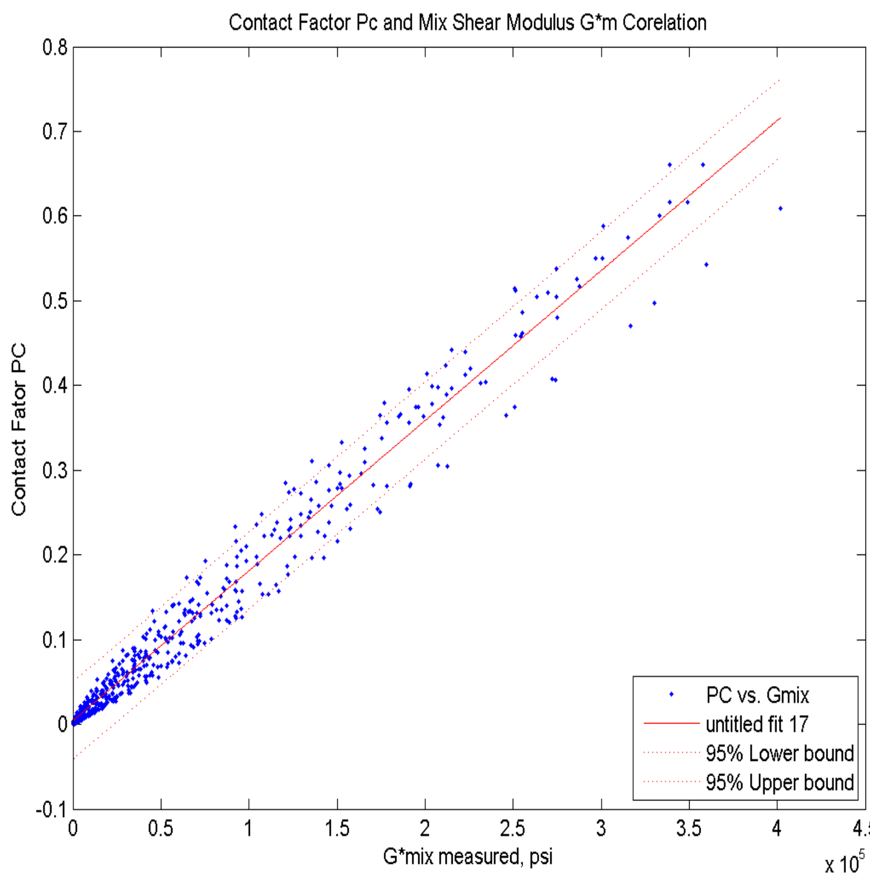

Contact Factor Pc and Mix Shear Modulus G*m Corelation
Contact Fator PC
G*mix measured, psi
x 10^5
0.8
0.7
0.6
0.5
0.4
0.3
0.2
0.1
0
-0.1
0
0.5
1
1.5
2
2.5
3
3.5
4
4.5
PC vs. Gmix
untitled fit 17
95% Lower bound
95% Upper bound

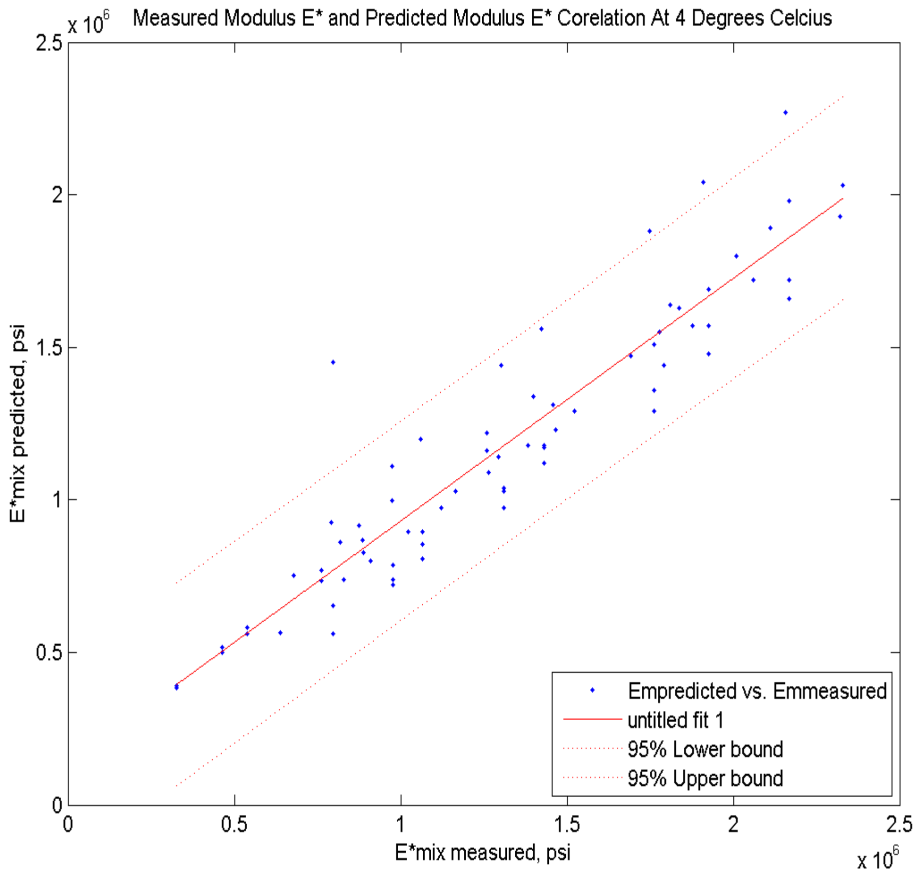

x 10^6
Measured Modulus E* and Predicted Modulus E* Corelation At 4 Degrees Celcius
E*mix predicted, psi
E*mix measured, psi
x 10^6
0
0.5
1
1.5
2
2.5
Empredicted vs. Emmeasured
untitled fit 1
95% Lower bound
95% Upper bound

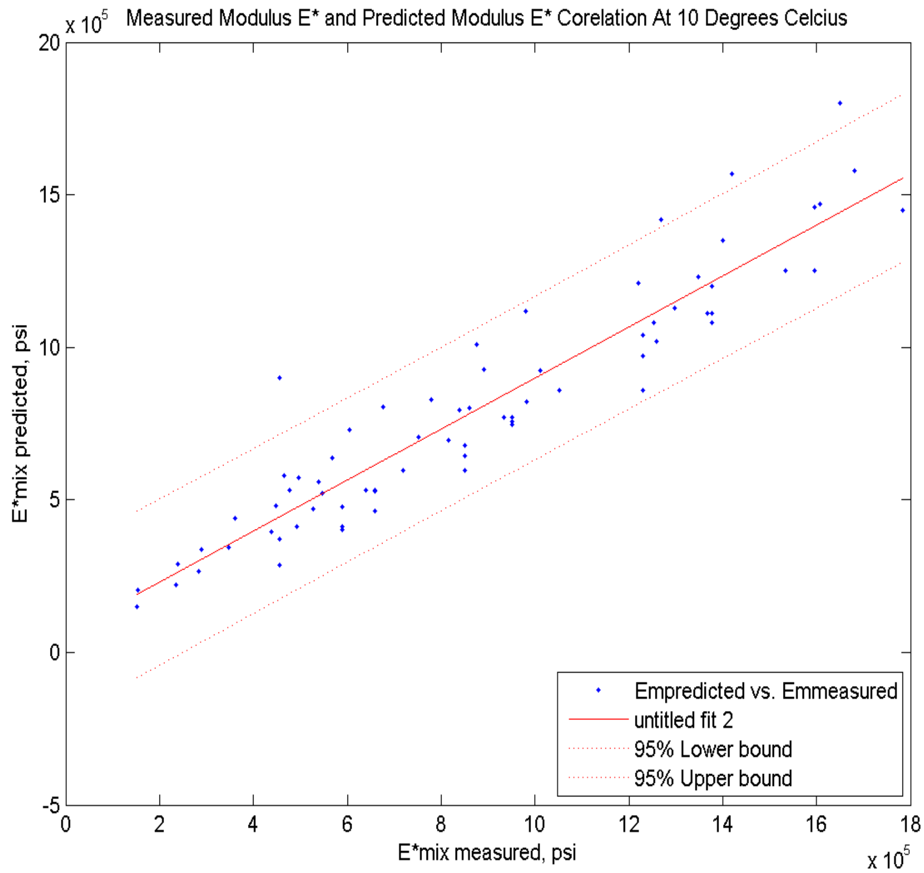
Measured Modulus E* and Predicted Modulus E* Corelation At 10 Degrees Celcius
x 10^5
E*mix predicted, psi
E*mix measured, psi
x 10^5
Empredicted vs. Emmeasured
untitled fit 2
95% Lower bound
95% Upper bound
20
15
10
5
0
-5
0
2
4
6
8
10
12
14
16
18

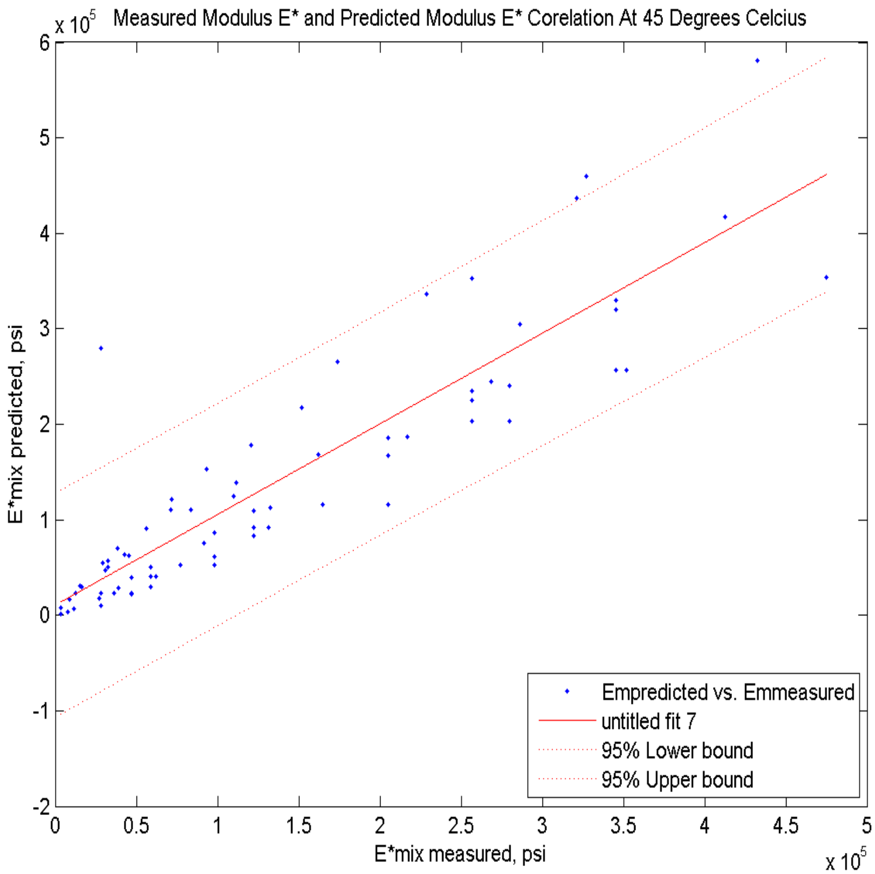
Measured Modulus E* and Predicted Modulus E* Corelation At 45 Degrees Celcius
x 10^5
E*mix predicted, psi
E*mix measured, psi
x 10^5
Empredicted vs. Emmeasured
untitled fit 7
95% Lower bound
95% Upper bound

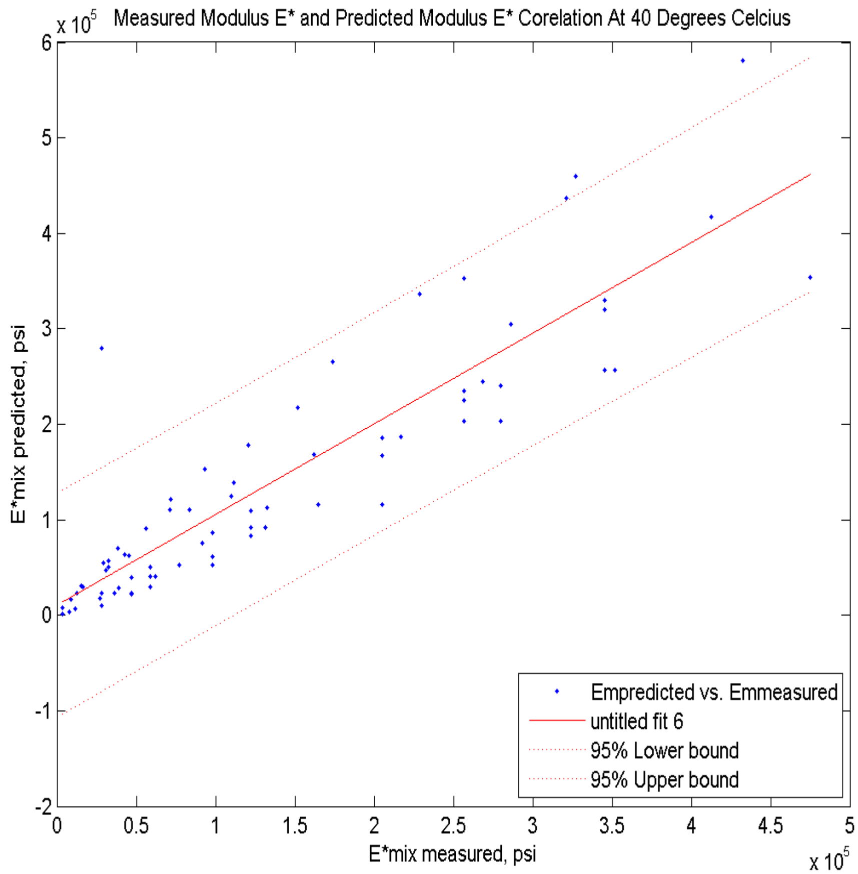
Measured Modulus E* and Predicted Modulus E* Corelation At 40 Degrees Celcius
x 10^5
E*mix predicted, psi
E*mix measured, psi
x 10^5
Empredicted vs. Emmeasured
untitled fit 6
95% Lower bound
95% Upper bound

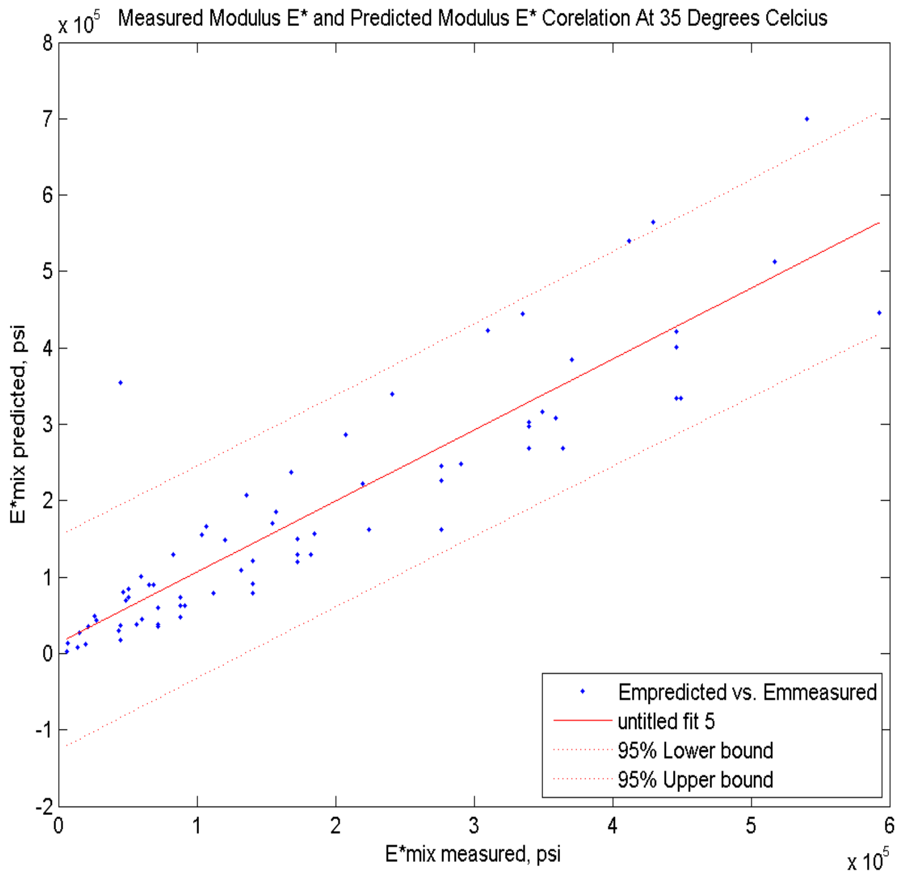
Measured Modulus E* and Predicted Modulus E* Corelation At 35 Degrees Celcius
x 10^5
8
7
6
5
4
3
2
1
0
-1
-2
E*mix predicted, psi
0
1
2
3
4
5
6
E*mix measured, psi
x 10^5
Empredicted vs. Emmeasured
untitled fit 5
95% Lower bound
95% Upper bound

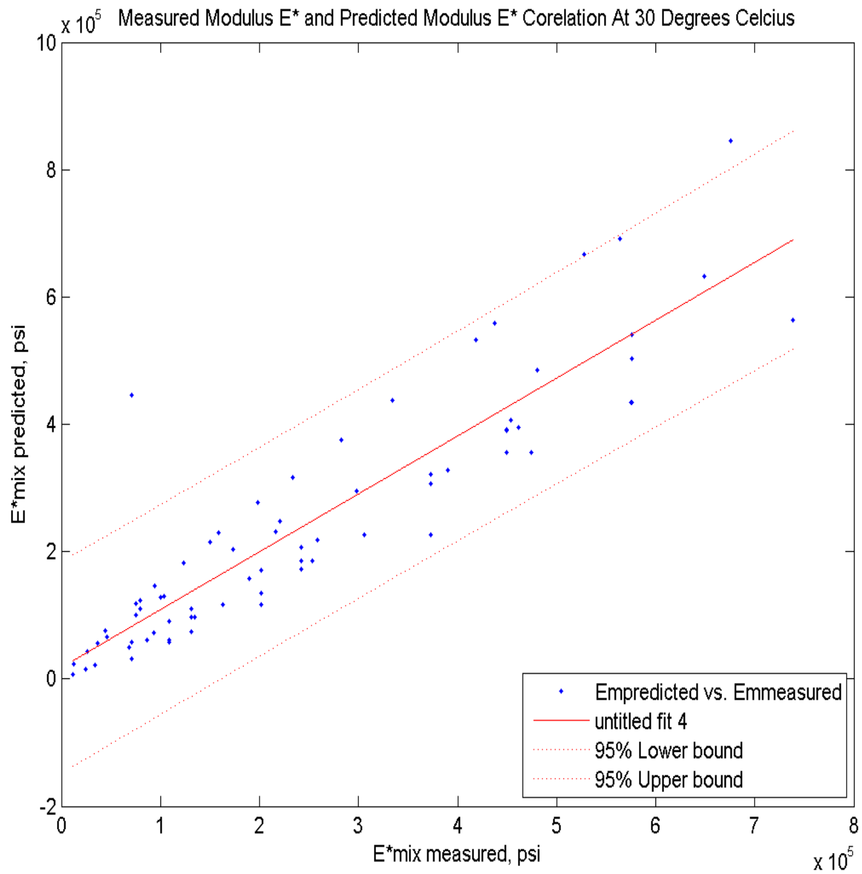
x 10^5
Measured Modulus E* and Predicted Modulus E* Corelation At 30 Degrees Celcius
10
8
6
4
2
0
-2
E*mix predicted, psi
0
1
2
3
4
5
6
7
8
E*mix measured, psi
x 10^5
Empredicted vs. Emmeasured
untitled fit 4
95% Lower bound
95% Upper bound

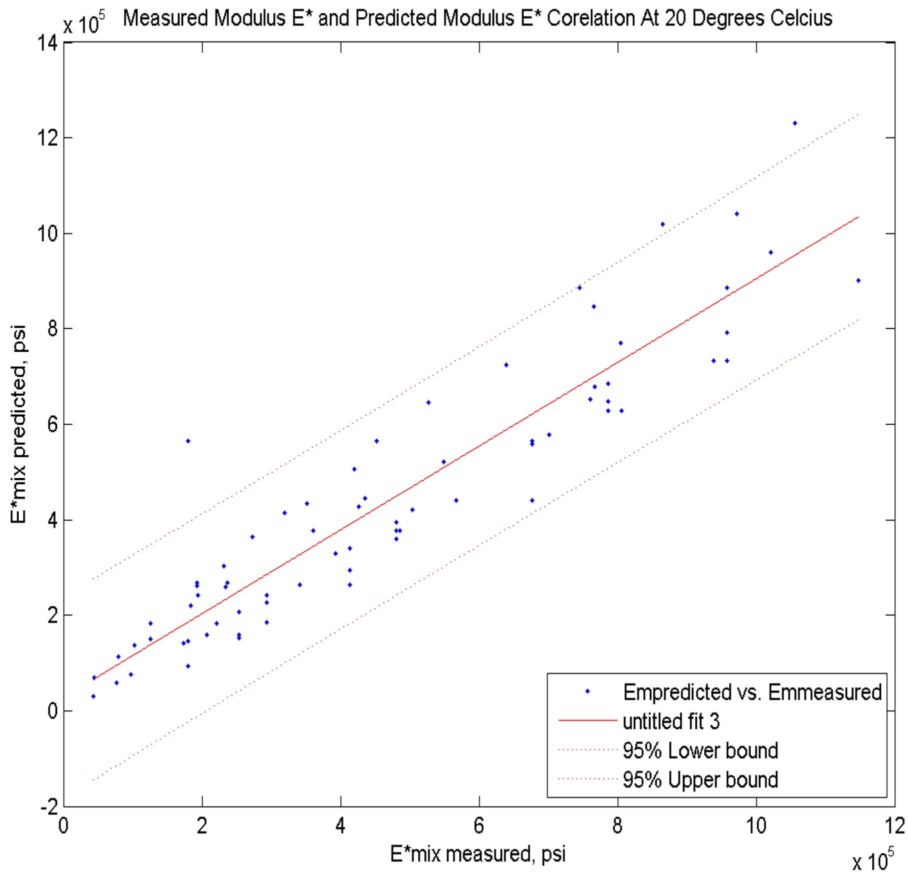
Measured Modulus E* and Predicted Modulus E* Corelation At 20 Degrees Celcius
x 10^5
14
12
10
8
6
4
2
0
-2
E*mix predicted, psi
0
2
4
6
8
10
12
E*mix measured, psi
x 10^5
Empredicted vs. Emmeasured
untitled fit 3
95% Lower bound
95% Upper bound

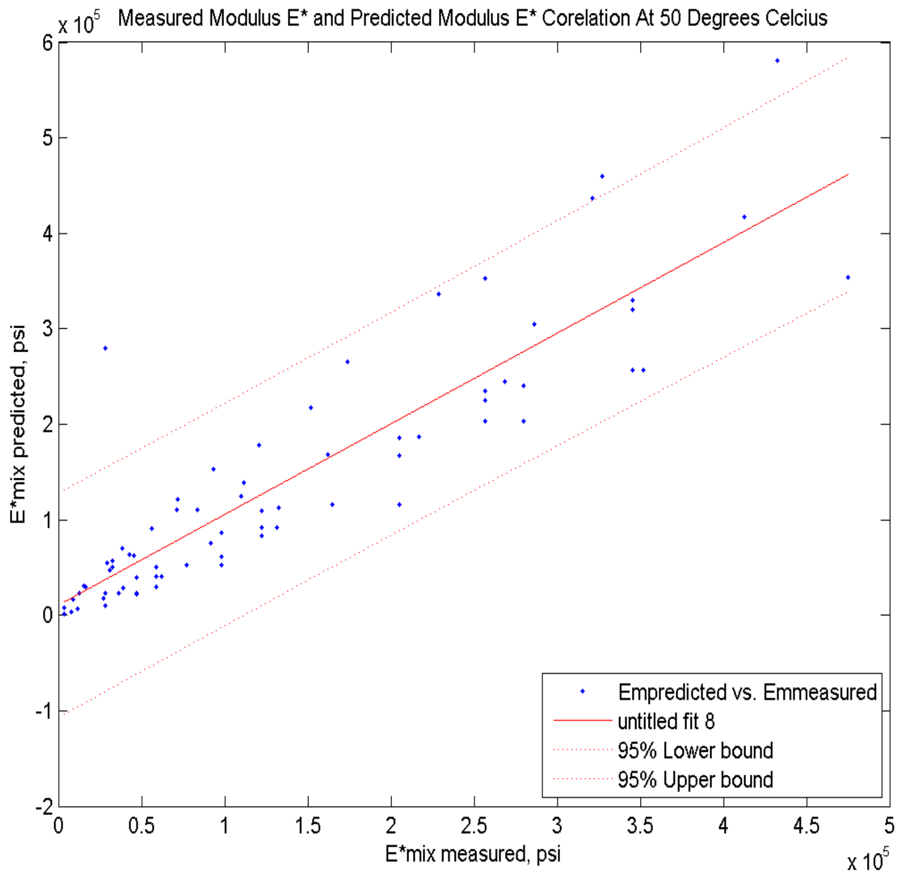
x 10^5 Measured Modulus E* and Predicted Modulus E* Corelation At 50 Degrees Celcius
E*mix predicted, psi
E*mix measured, psi
x 10^5
6
5
4
3
2
1
0
-1
-2
0
0.5
1
1.5
2
2.5
3
3.5
4
4.5
5
Empredicted vs. Emmeasured
untitled fit 8
95% Lower bound
95% Upper bound

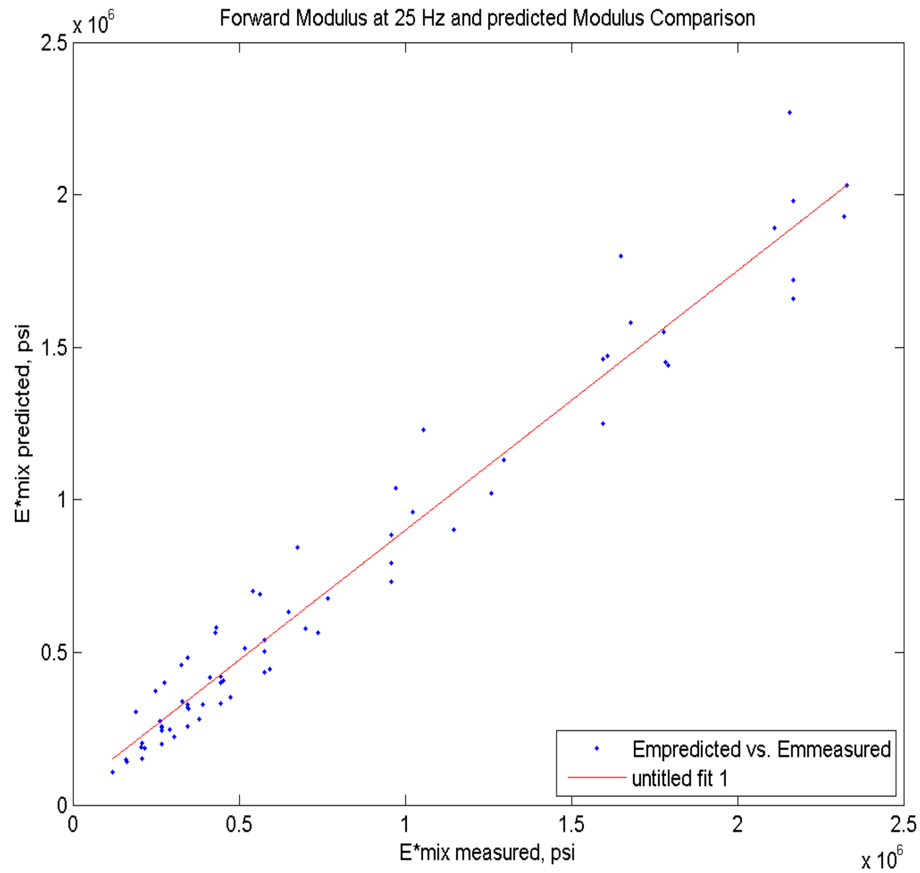

Forward Modulus at 25 Hz and predicted Modulus Comparison
x 10^6
2.5
2
1.5
1
0.5
0
E*mix predicted, psi
0
0.5
1
1.5
2
2.5
E*mix measured, psi
x 10^6
Empredicted vs. Emmeasured
untitled fit 1

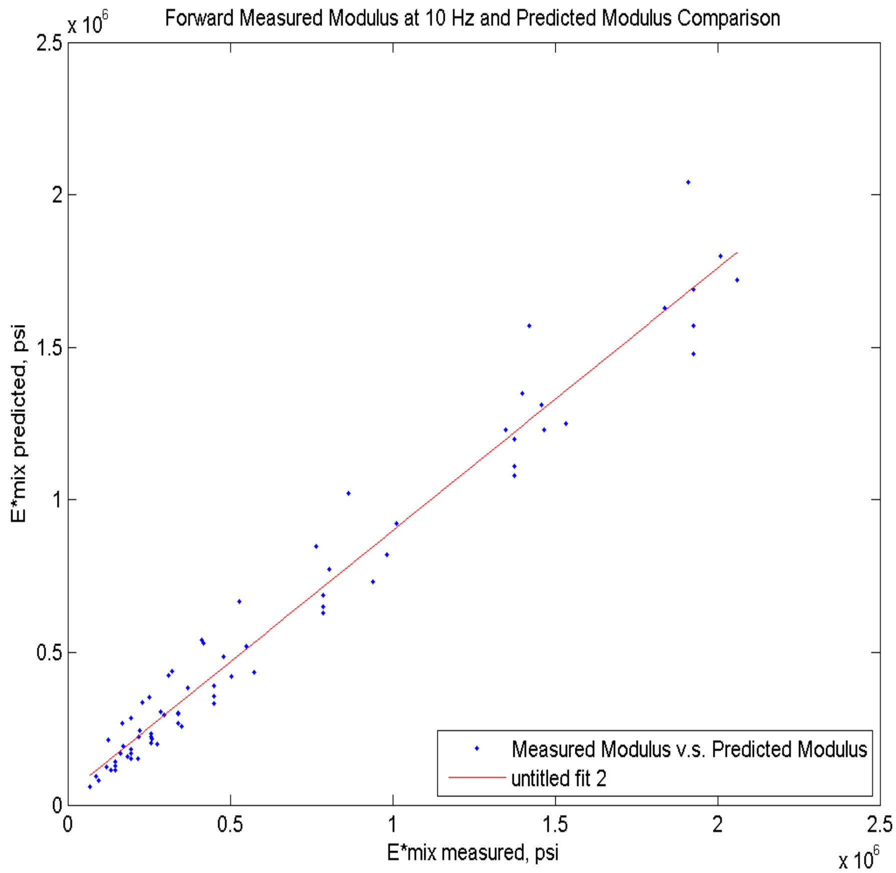

Forward Measured Modulus at 10 Hz and Predicted Modulus Comparison
x 10^6
2.5
2
1.5
1
0.5
0
E*mix predicted, psi
Measured Modulus v.s. Predicted Modulus
untitled fit 2
0
0.5
1
1.5
2
2.5
E*mix measured, psi
x 10^6

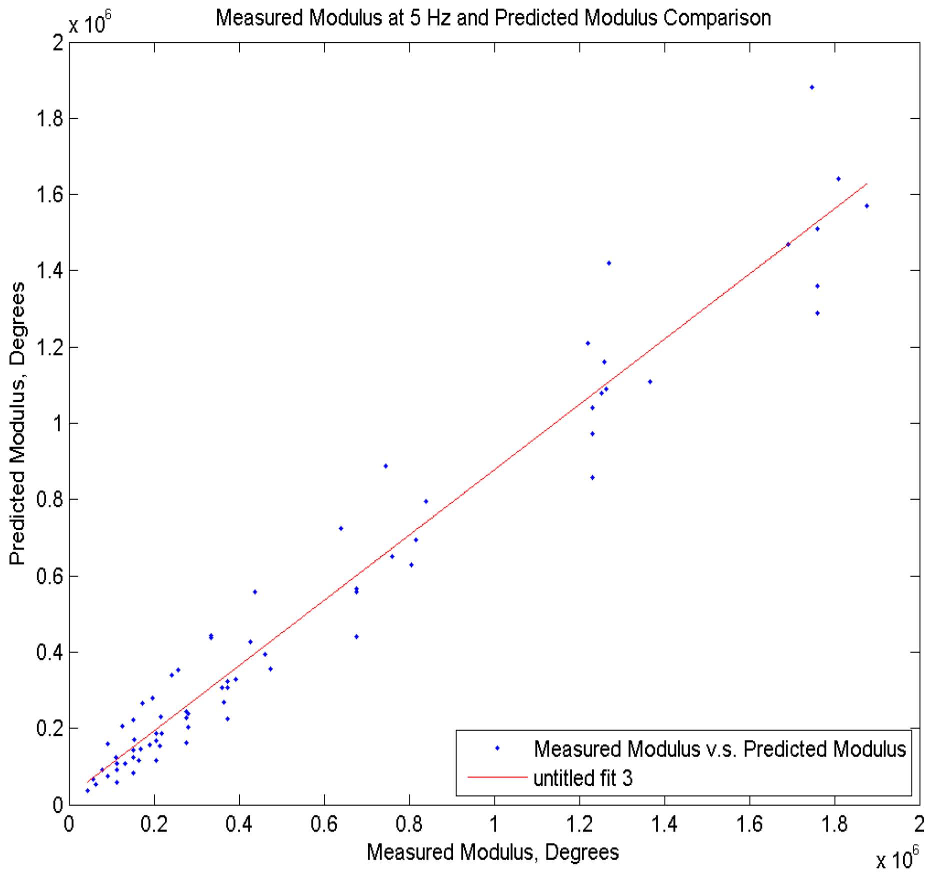
Measured Modulus at 5 Hz and Predicted Modulus Comparison
x 10^6
2
1.8
1.6
1.4
1.2
1
0.8
0.6
0.4
0.2
0
Predicted Modulus, Degrees
0
0.2
0.4
0.6
0.8
1
1.2
1.4
1.6
1.8
2
Measured Modulus, Degrees
x 10^6
Measured Modulus v.s. Predicted Modulus
untitled fit 3

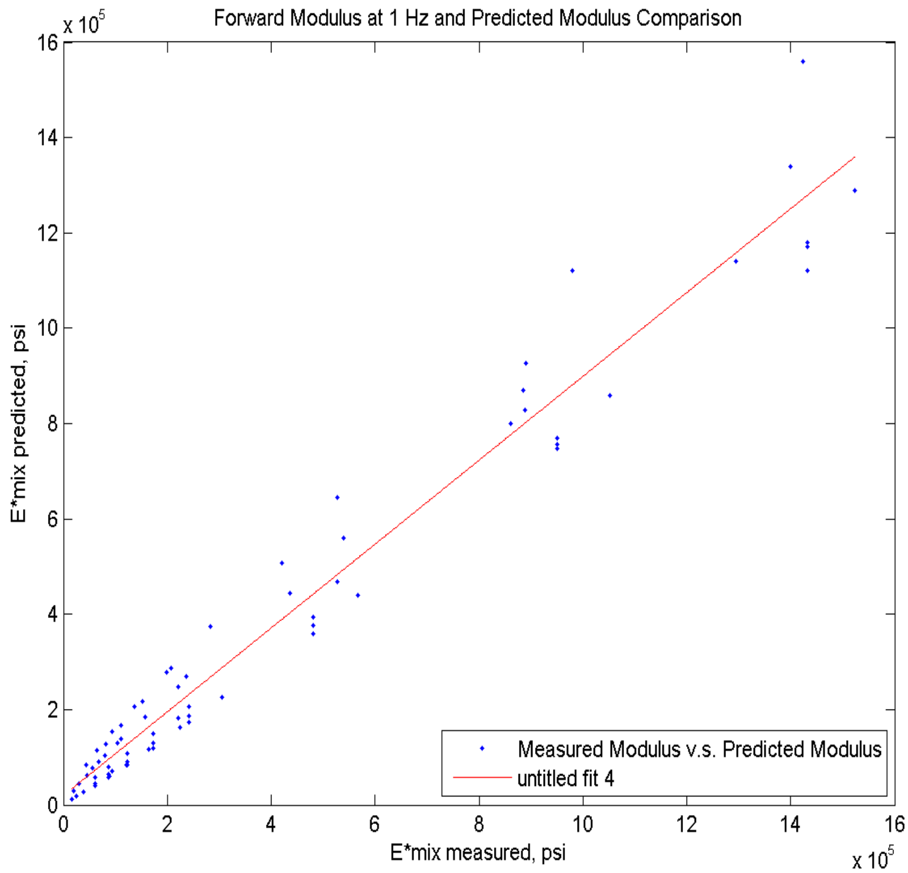

Forward Modulus at 1 Hz and Predicted Modulus Comparison
x 10^5
16
14
12
10
8
6
4
2
0
E*mix predicted, psi
0
2
4
6
8
10
12
14
16
E*mix measured, psi
x 10^5
Measured Modulus v.s. Predicted Modulus
untitled fit 4

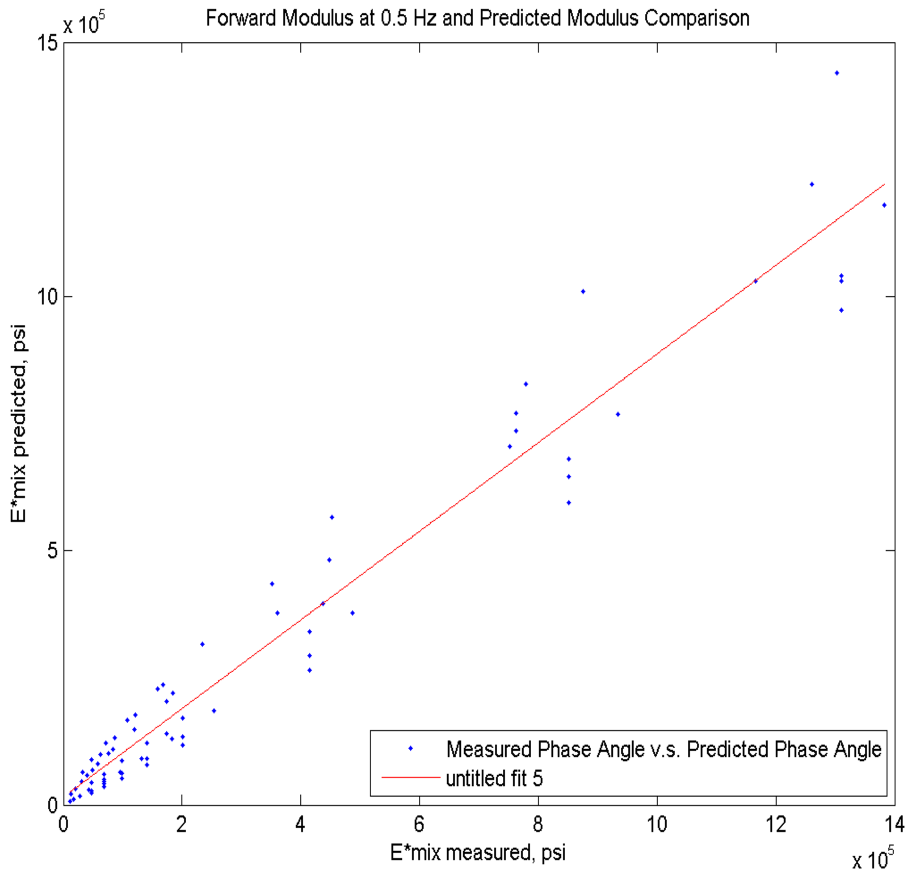
Forward Modulus at 0.5 Hz and Predicted Modulus Comparison
x 10^5
15
10
5
0
E*mix predicted, psi
0
2
4
6
8
10
12
14
E*mix measured, psi
x 10^5
Measured Phase Angle v.s. Predicted Phase Angle
untitled fit 5

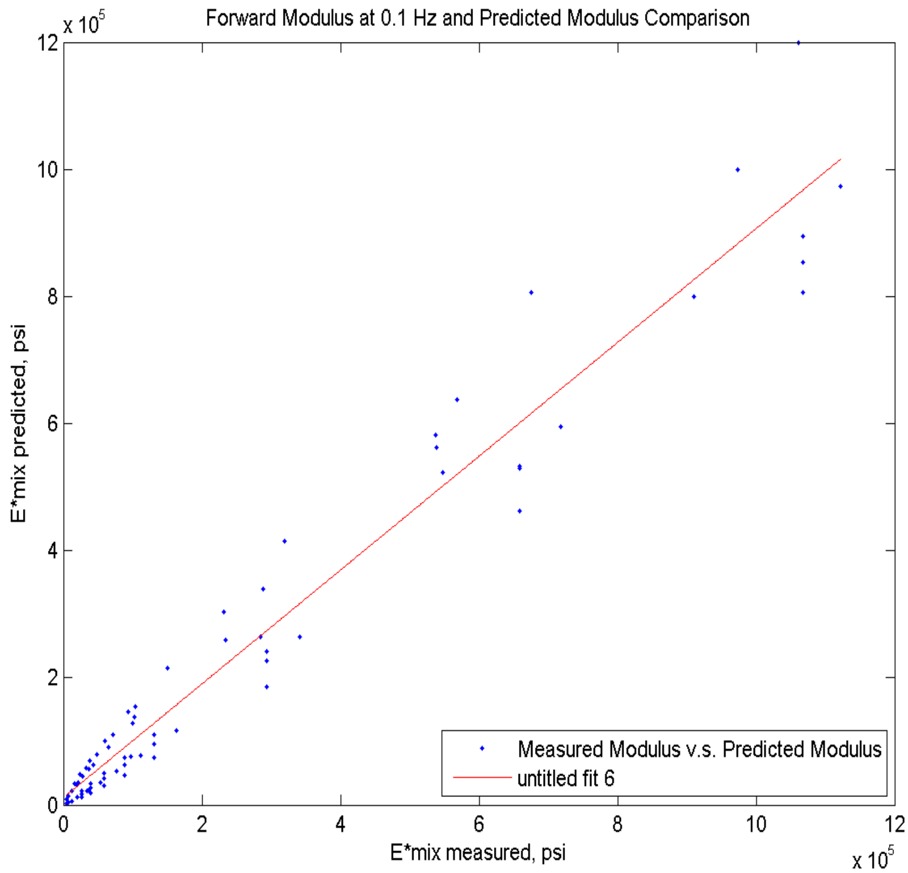
Forward Modulus at 0.1 Hz and Predicted Modulus Comparison
x 10^5
12
10
8
6
4
2
0
E*mix predicted, psi
0
2
4
6
8
10
12
E*mix measured, psi
x 10^5
Measured Modulus v.s. Predicted Modulus
untitled fit 6

APPENDIX C - Model development forward phase angle model family of curves

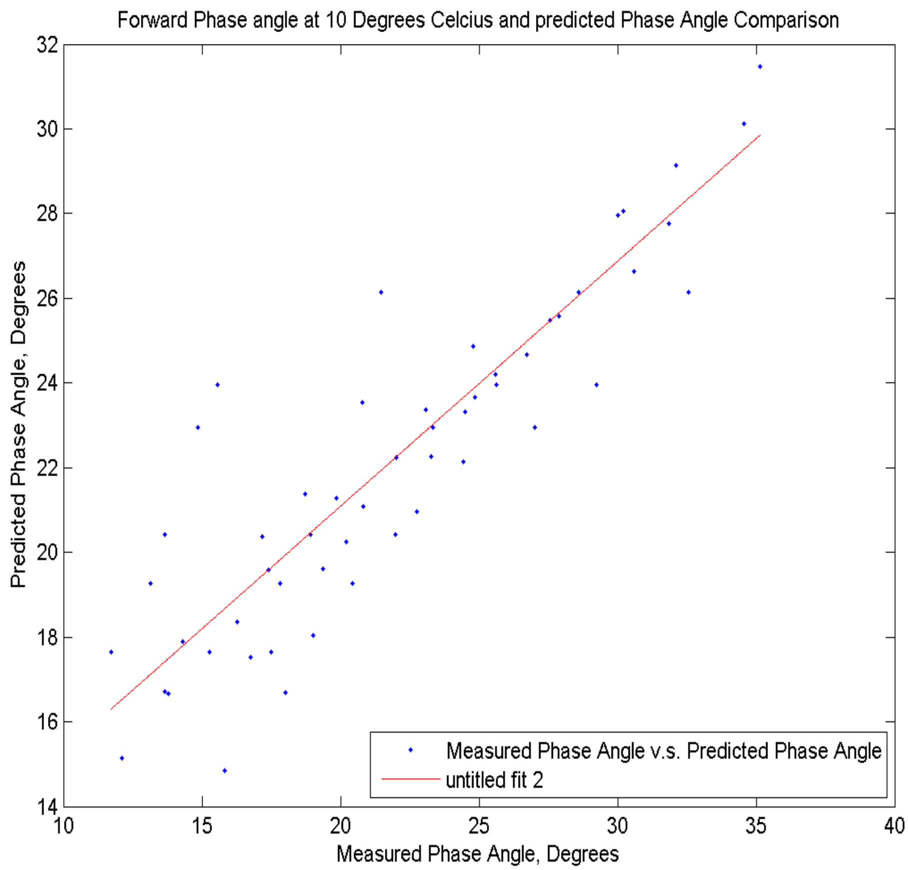

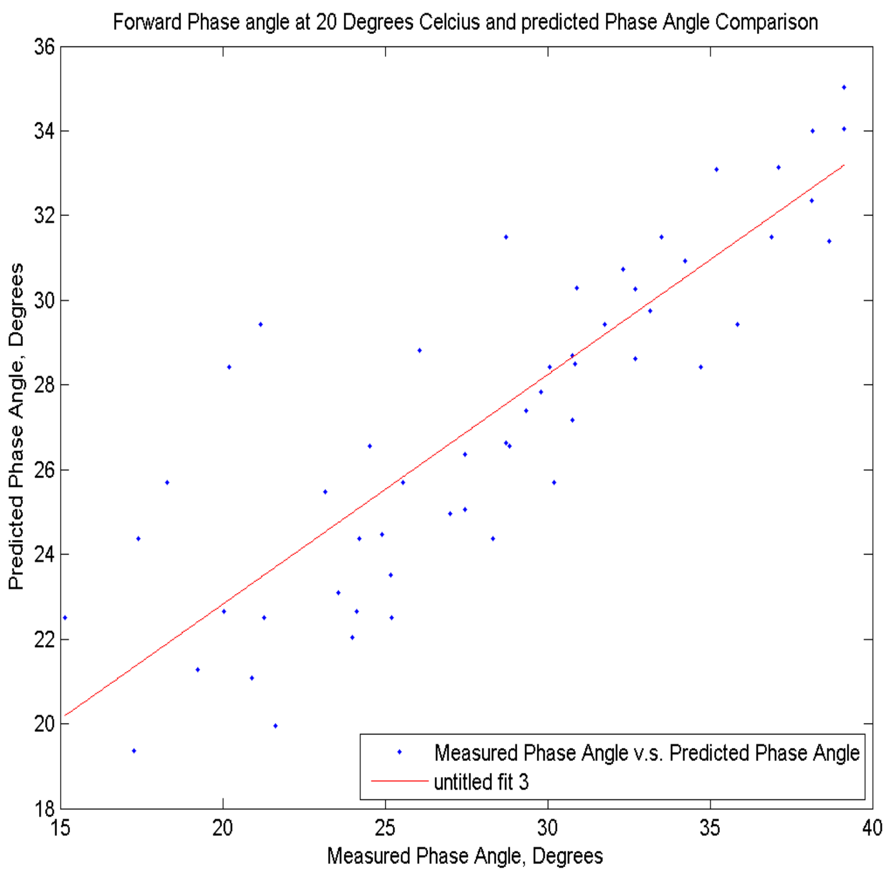
Forward Phase angle at 20 Degrees Celcius and predicted Phase Angle Comparison
Predicted Phase Angle, Degrees
Measured Phase Angle, Degrees
36
34
32
30
28
26
24
22
20
18
15
20
25
30
35
40
Measured Phase Angle v.s. Predicted Phase Angle
untitled fit 3

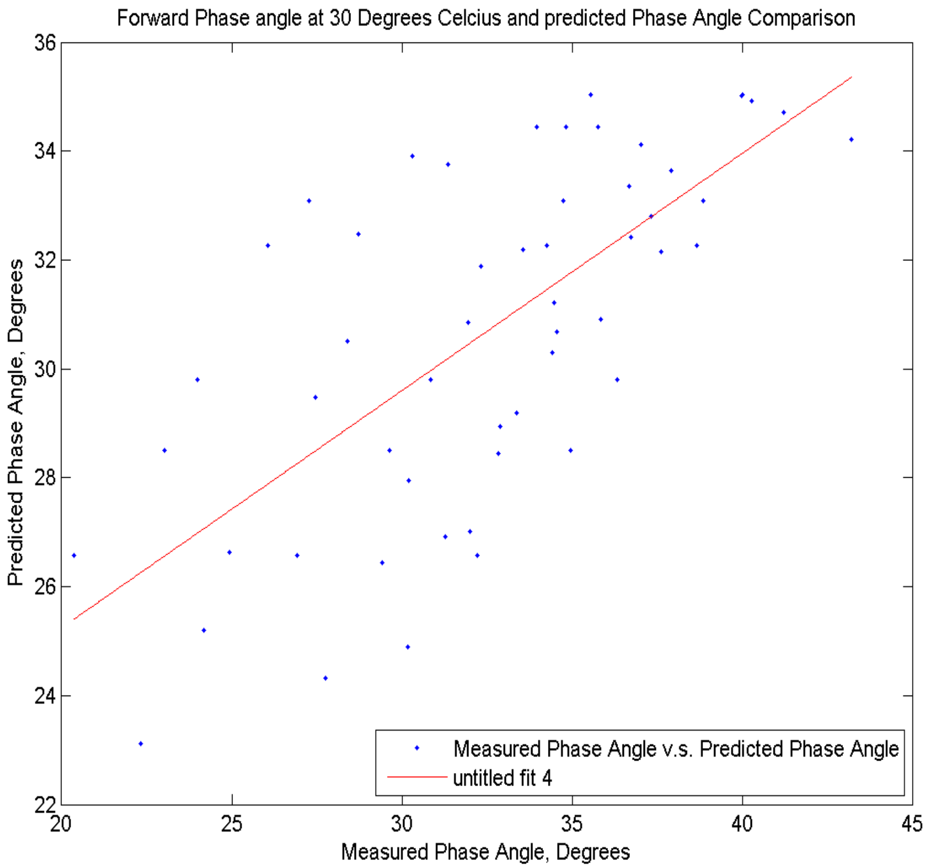
Forward Phase angle at 30 Degrees Celcius and predicted Phase Angle Comparison
Predicted Phase Angle, Degrees
Measured Phase Angle, Degrees
36
34
32
30
28
26
24
22
20
25
30
35
40
45
Measured Phase Angle v.s. Predicted Phase Angle
untitled fit 4

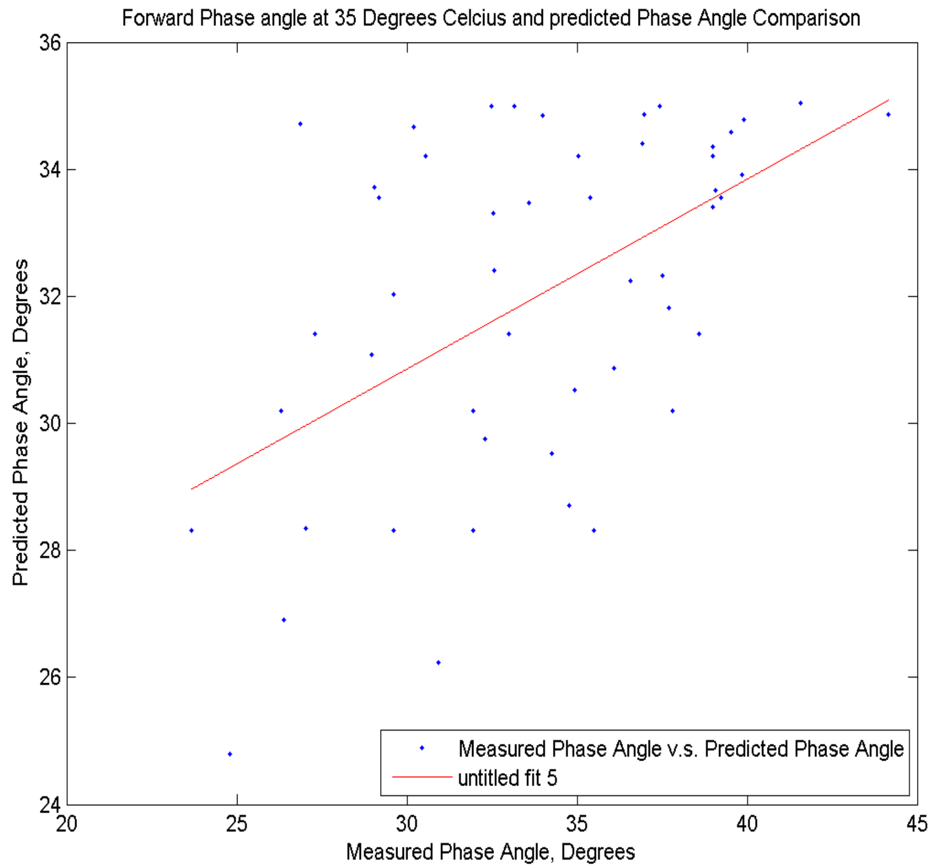
Forward Phase angle at 35 Degrees Celcius and predicted Phase Angle Comparison
Predicted Phase Angle, Degrees
Measured Phase Angle, Degrees
36
34
32
30
28
26
24
20
25
30
35
40
45
Measured Phase Angle v.s. Predicted Phase Angle
untitled fit 5

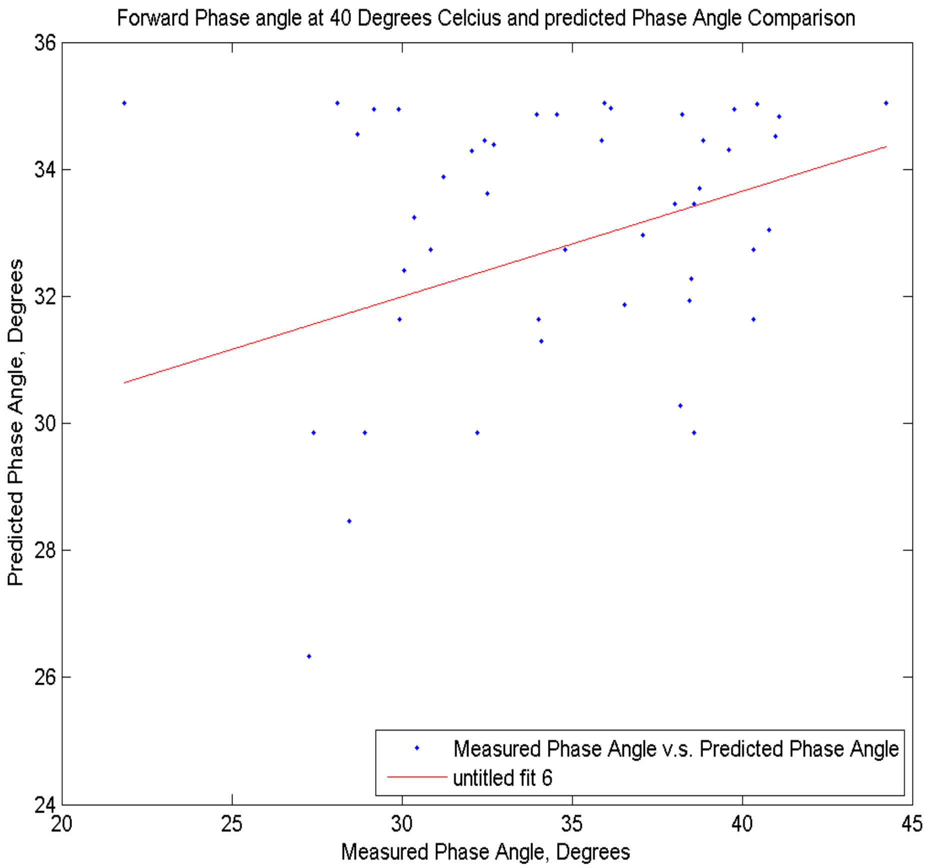
Forward Phase angle at 40 Degrees Celcius and predicted Phase Angle Comparison
Predicted Phase Angle, Degrees
Measured Phase Angle, Degrees
36
34
32
30
28
26
24
20
25
30
35
40
45
Measured Phase Angle v.s. Predicted Phase Angle
untitled fit 6

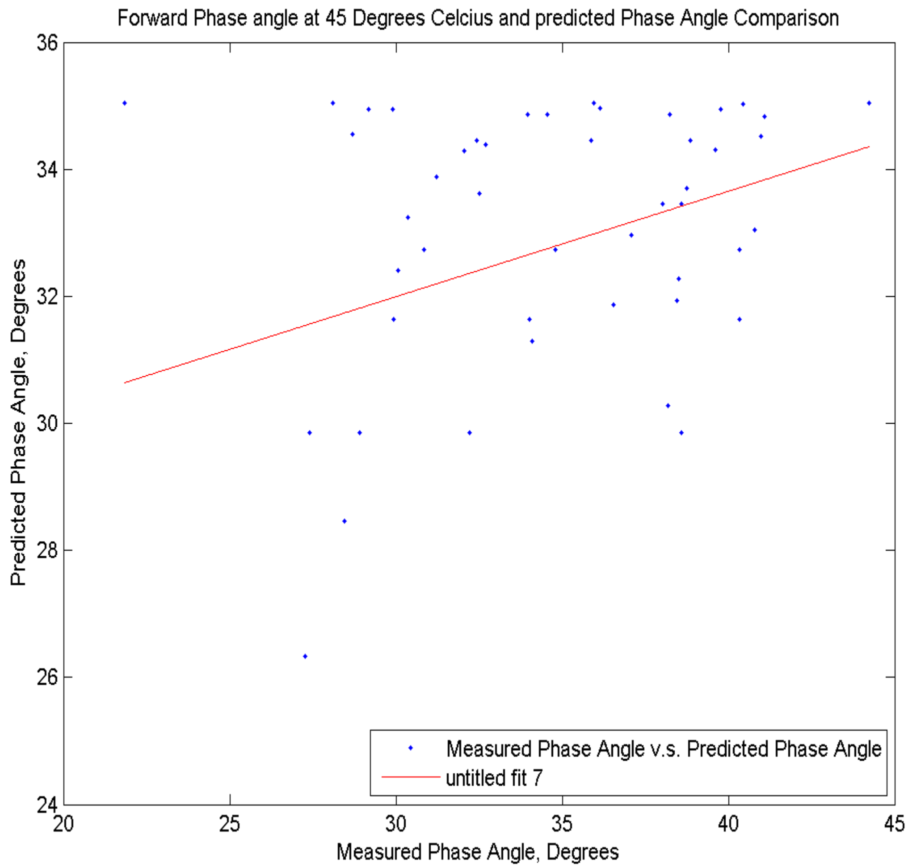
Forward Phase angle at 45 Degrees Celcius and predicted Phase Angle Comparison
Predicted Phase Angle, Degrees
Measured Phase Angle, Degrees
36
34
32
30
28
26
24
20
25
30
35
40
45
Measured Phase Angle v.s. Predicted Phase Angle
untitled fit 7

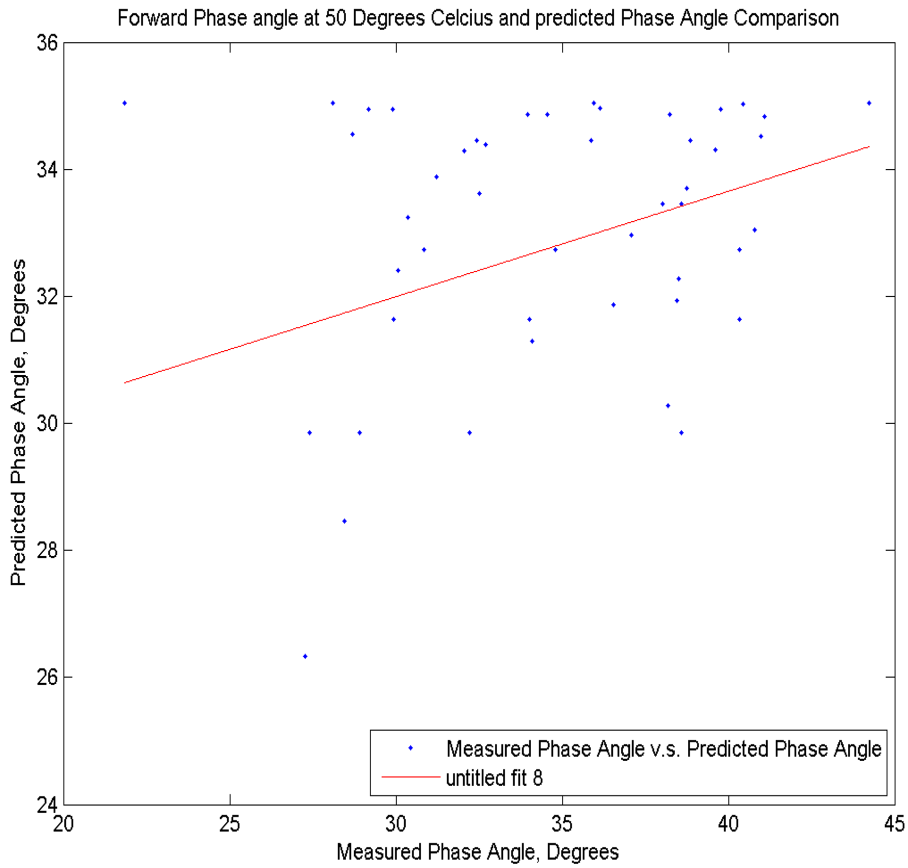
Forward Phase angle at 50 Degrees Celcius and predicted Phase Angle Comparison
Predicted Phase Angle, Degrees
Measured Phase Angle, Degrees
Measured Phase Angle v.s. Predicted Phase Angle
untitled fit 8
36
34
32
30
28
26
24
20
25
30
35
40
45

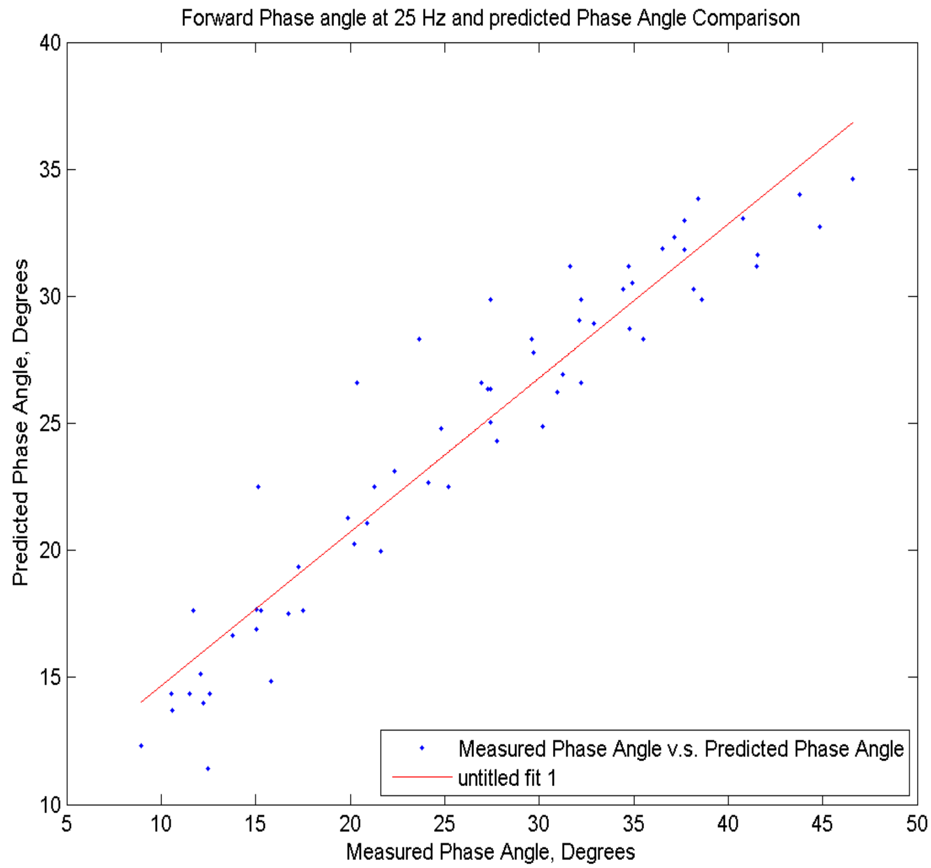
Forward Phase angle at 25 Hz and predicted Phase Angle Comparison
Predicted Phase Angle, Degrees
Measured Phase Angle, Degrees
Measured Phase Angle v.s. Predicted Phase Angle
untitled fit 1
40
35
30
25
20
15
10
5
10
15
20
25
30
35
40
45
50

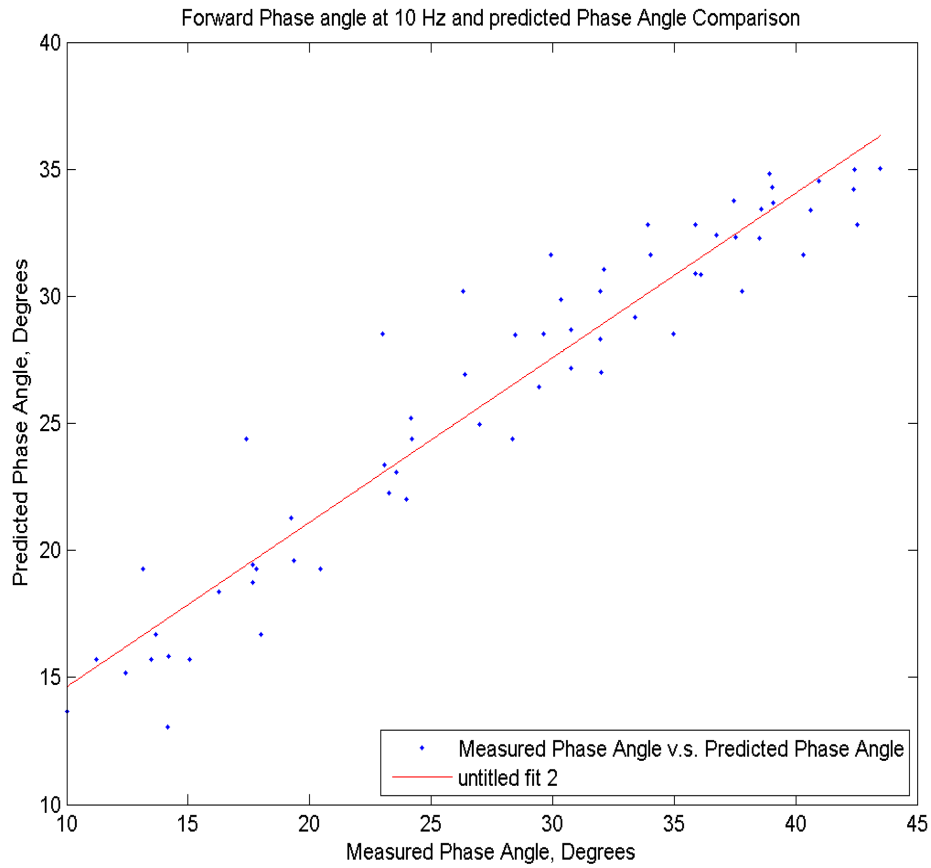
Forward Phase angle at 10 Hz and predicted Phase Angle Comparison
Predicted Phase Angle, Degrees
Measured Phase Angle, Degrees
Measured Phase Angle v.s. Predicted Phase Angle
untitled fit 2
10
15
20
25
30
35
40
45

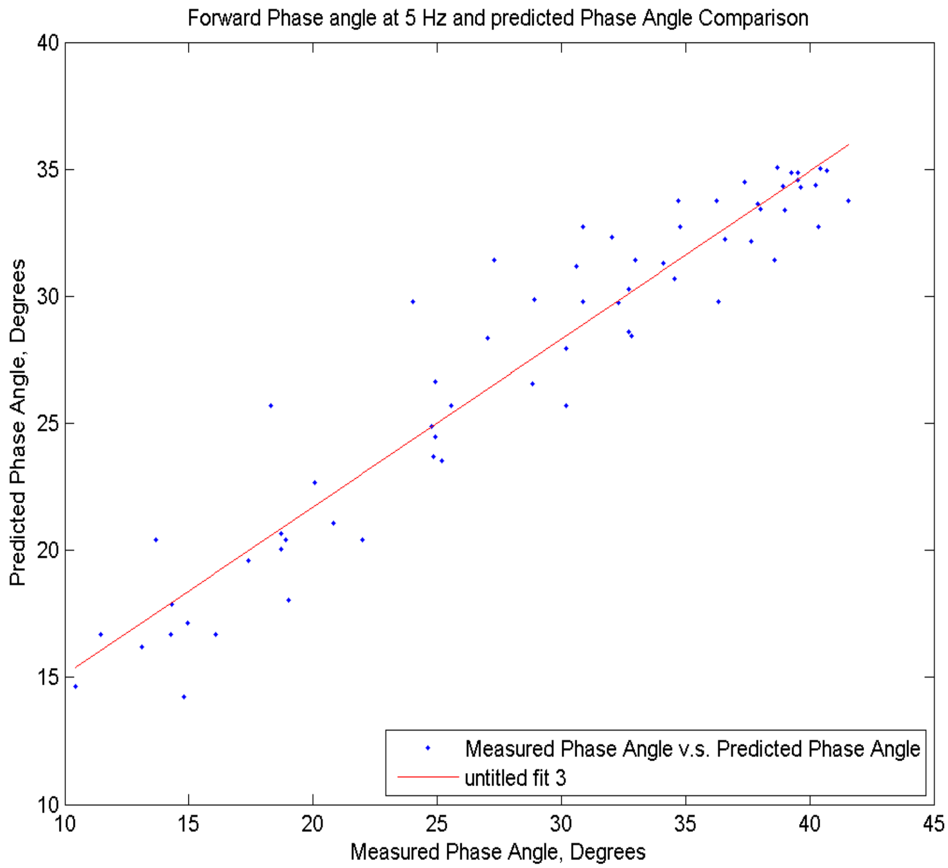
Forward Phase angle at 5 Hz and predicted Phase Angle Comparison
Predicted Phase Angle, Degrees
Measured Phase Angle, Degrees
Measured Phase Angle v.s. Predicted Phase Angle
untitled fit 3
10
15
20
25
30
35
40
45

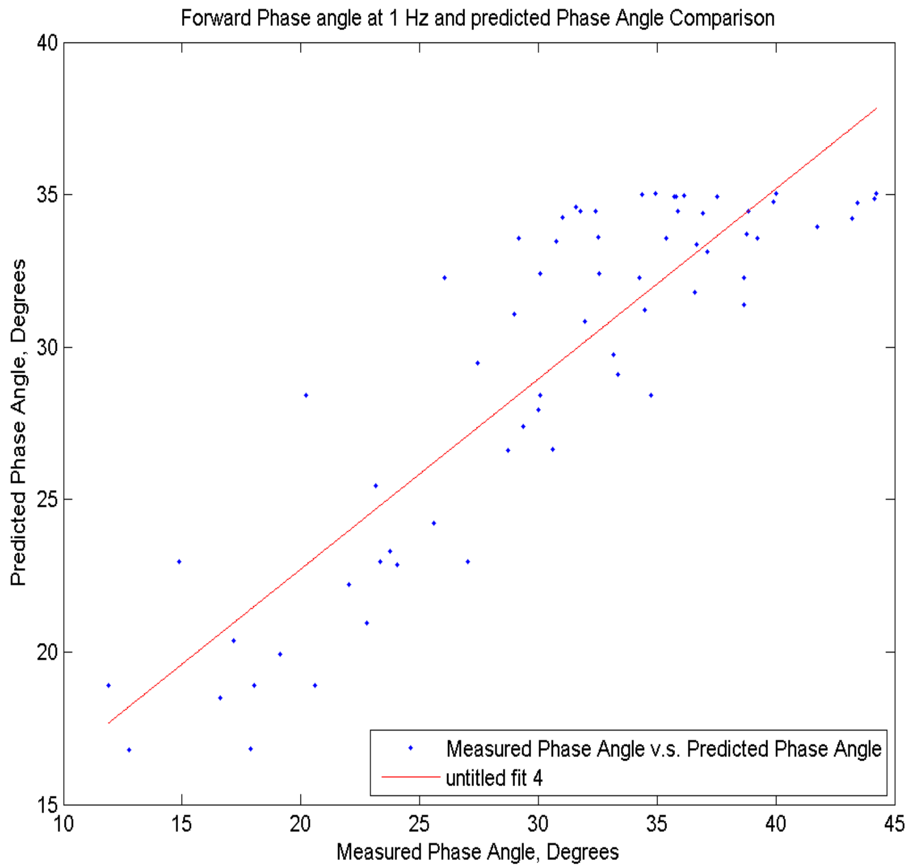

Forward Phase angle at 1 Hz and predicted Phase Angle Comparison
Predicted Phase Angle, Degrees
Measured Phase Angle, Degrees
Measured Phase Angle v.s. Predicted Phase Angle
untitled fit 4
40
35
30
25
20
15
10
15
20
25
30
35
40
45

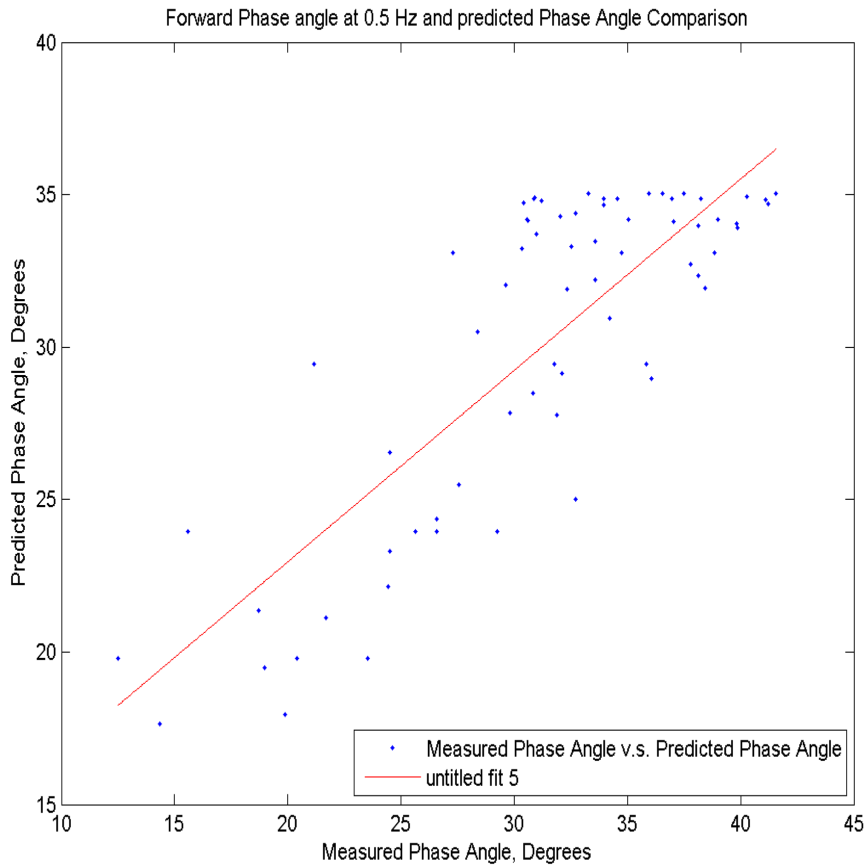
Forward Phase angle at 0.5 Hz and predicted Phase Angle Comparison
Predicted Phase Angle, Degrees
Measured Phase Angle, Degrees
Measured Phase Angle v.s. Predicted Phase Angle
untitled fit 5
40
35
30
25
20
15
10
15
20
25
30
35
40
45

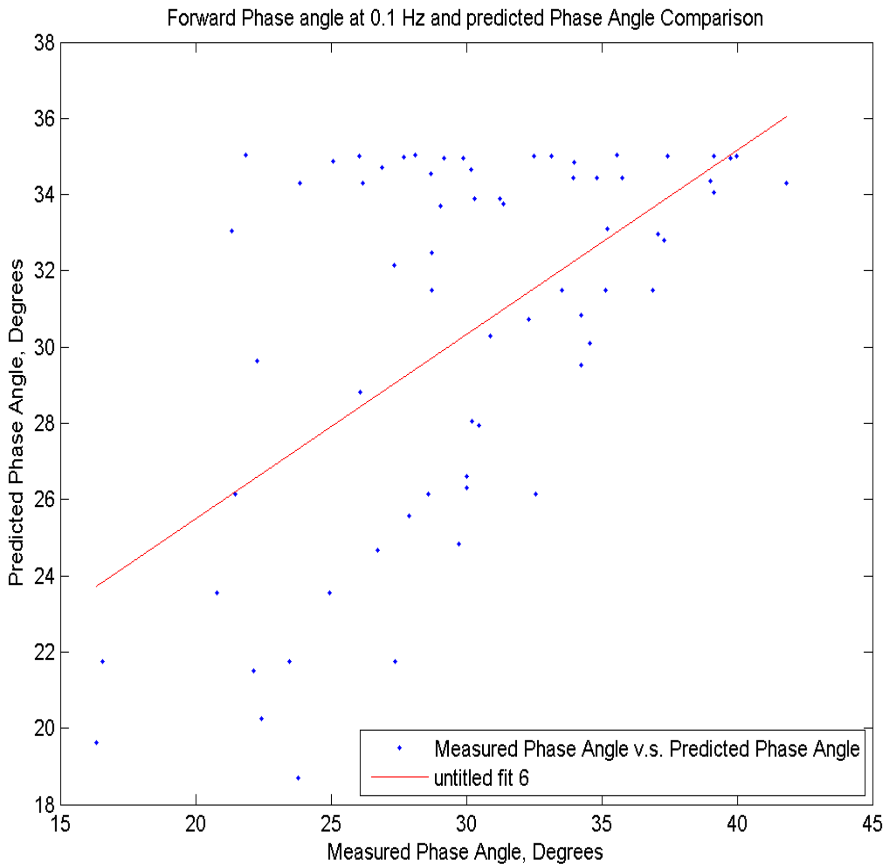
Forward Phase angle at 0.1 Hz and predicted Phase Angle Comparison
Predicted Phase Angle, Degrees
Measured Phase Angle, Degrees
Measured Phase Angle v.s. Predicted Phase Angle
untitled fit 6
38
36
34
32
30
28
26
24
22
20
18
15
20
25
30
35
40
45

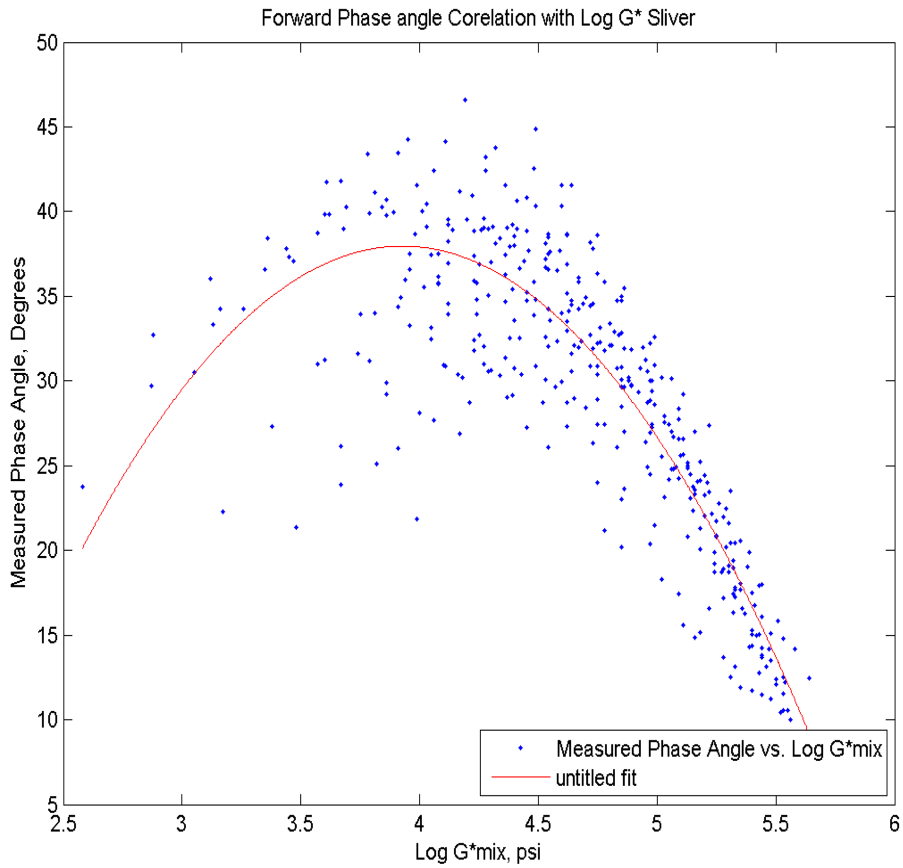
Forward Phase angle Corelation with Log G* Sliver
Measured Phase Angle, Degrees
Log G*mix, psi
Measured Phase Angle vs. Log G*mix
untitled fit
50
45
40
35
30
25
20
15
10
5
2.5
3
3.5
4
4.5
5
5.5
6

APPENDIX D - Model development backward asphalt binder shear modulus calculation family of curves

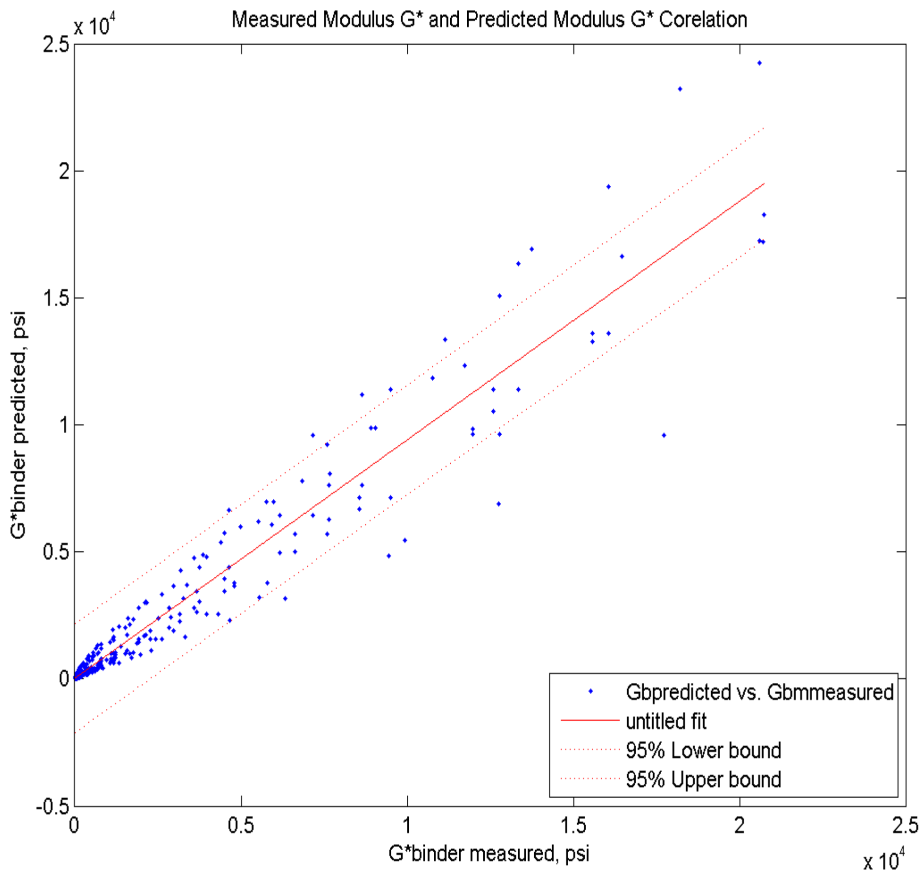

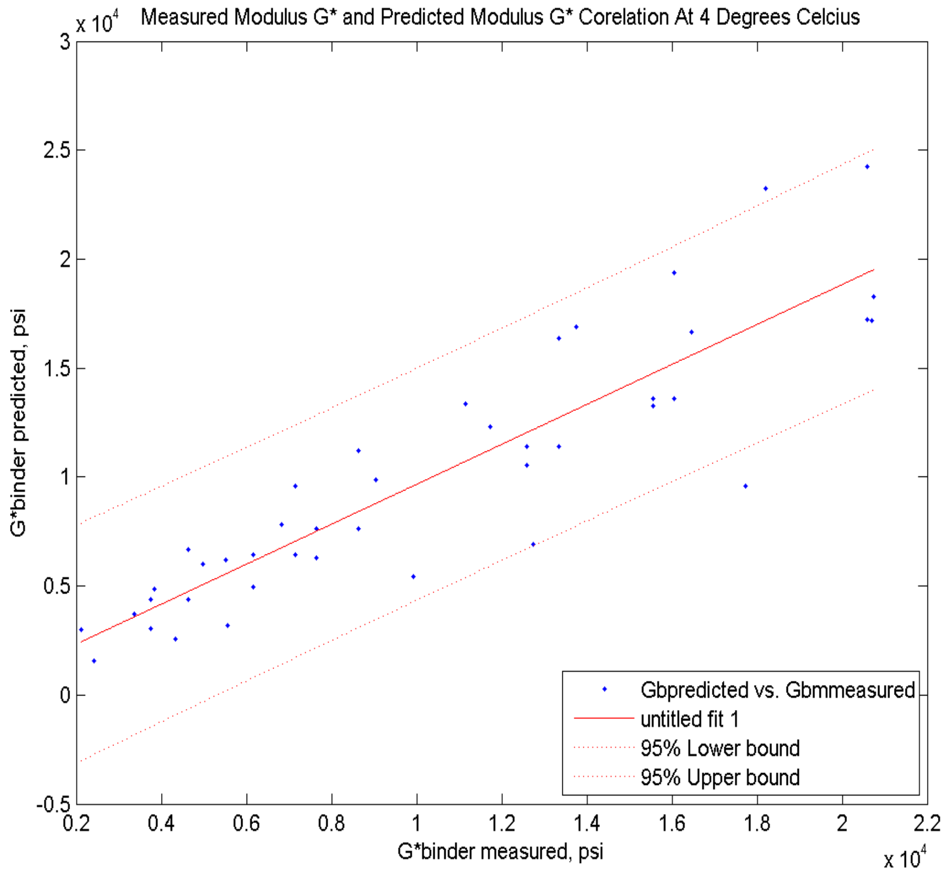

x 10^4
Measured Modulus G* and Predicted Modulus G* Corelation At 4 Degrees Celcius
3
2.5
2
1.5
1
0.5
0
-0.5
G*binder predicted, psi
0.2
0.4
0.6
0.8
1
1.2
1.4
1.6
1.8
2
2.2
G*binder measured, psi
x 10^4
Gbpredicted vs. Gbmmeasured
untitled fit 1
95% Lower bound
95% Upper bound

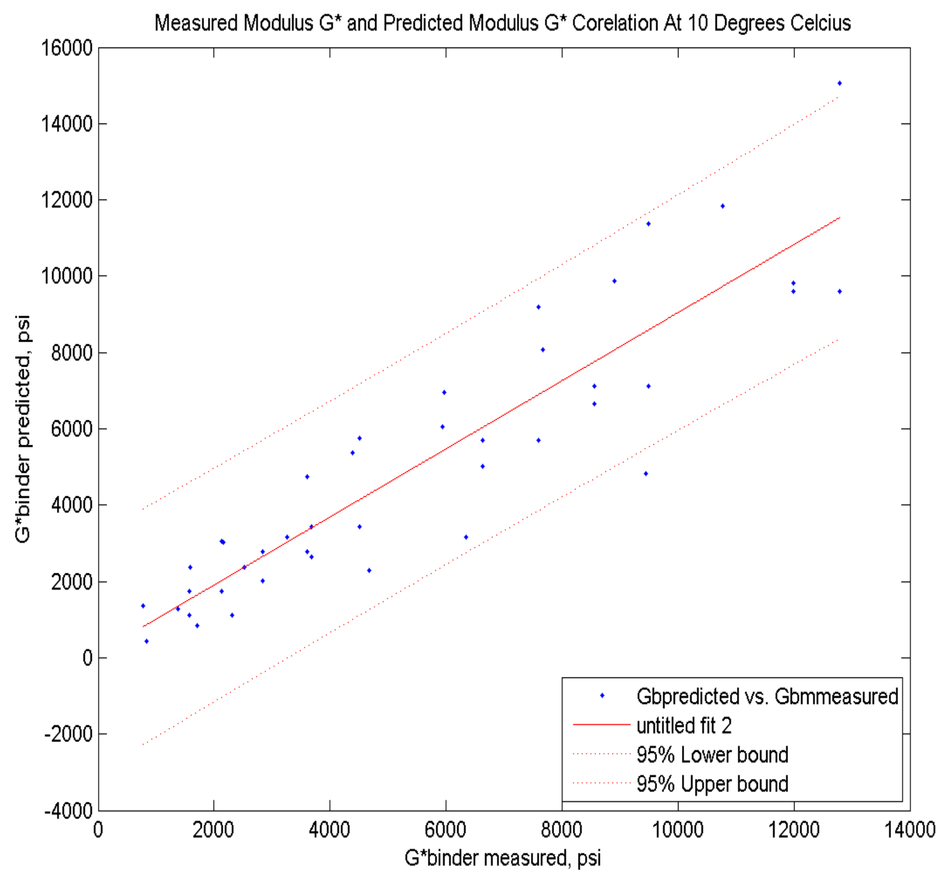
Measured Modulus G* and Predicted Modulus G* Corelation At 10 Degrees Celcius
16000
14000
12000
10000
8000
6000
4000
2000
0
-2000
-4000
G*binder predicted, psi
0
2000
4000
6000
8000
10000
12000
14000
G*binder measured, psi
Gbpredicted vs. Gbmmeasured
untitled fit 2
95% Lower bound
95% Upper bound

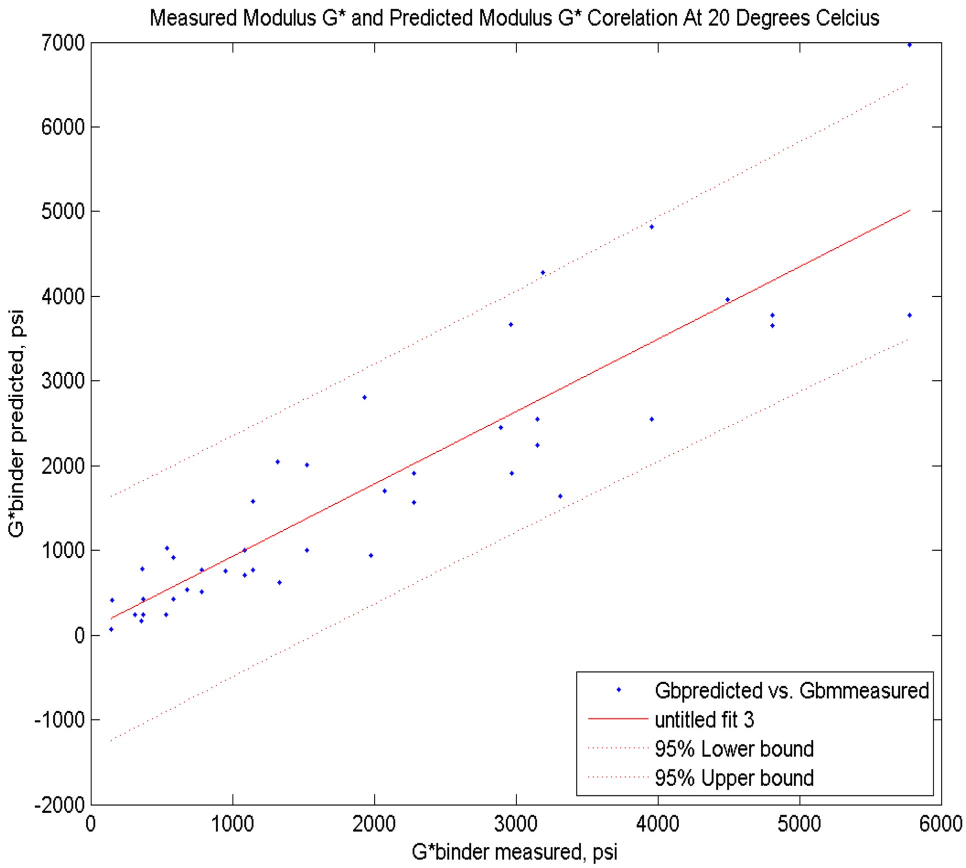

Measured Modulus G* and Predicted Modulus G* Corelation At 20 Degrees Celcius
7000
6000
5000
4000
3000
2000
1000
0
-1000
-2000
G*binder predicted, psi
0
1000
2000
3000
4000
5000
6000
G*binder measured, psi
Gbpredicted vs. Gbmmeasured
untitled fit 3
95% Lower bound
95% Upper bound

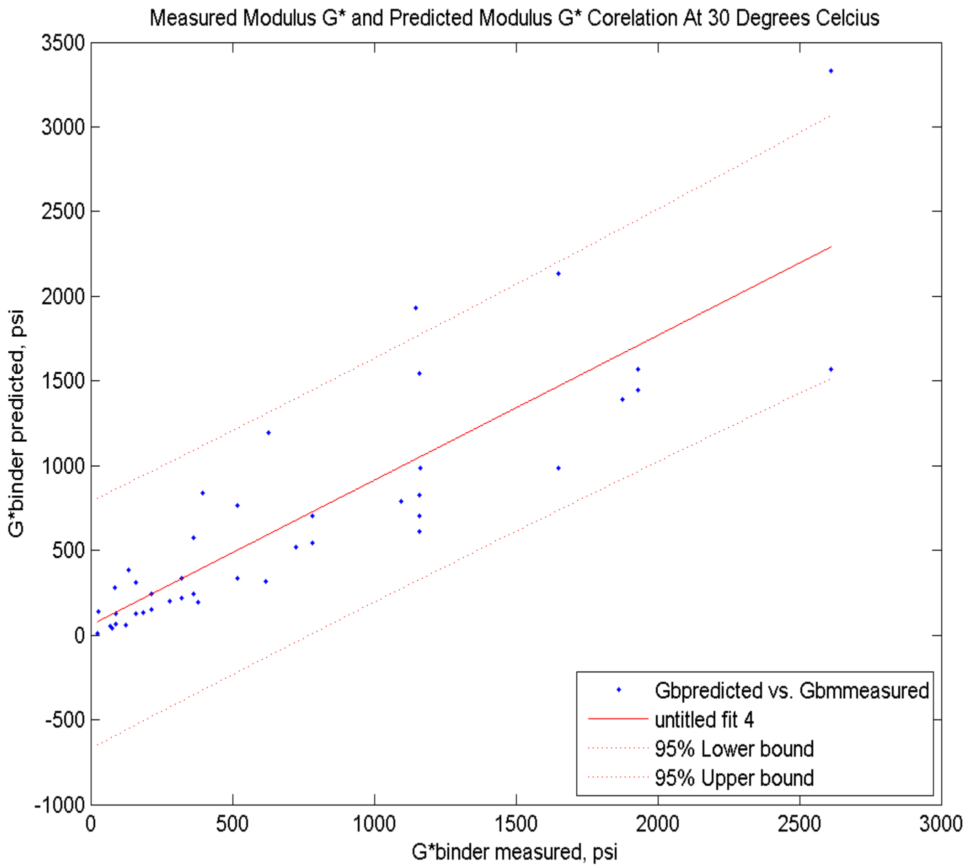

Measured Modulus G* and Predicted Modulus G* Corelation At 30 Degrees Celcius
G*binder predicted, psi
G*binder measured, psi
3500
3000
2500
2000
1500
1000
500
0
-500
-1000
0
500
1000
1500
2000
2500
3000
Gbpredicted vs. Gbmmeasured
untitled fit 4
95% Lower bound
95% Upper bound

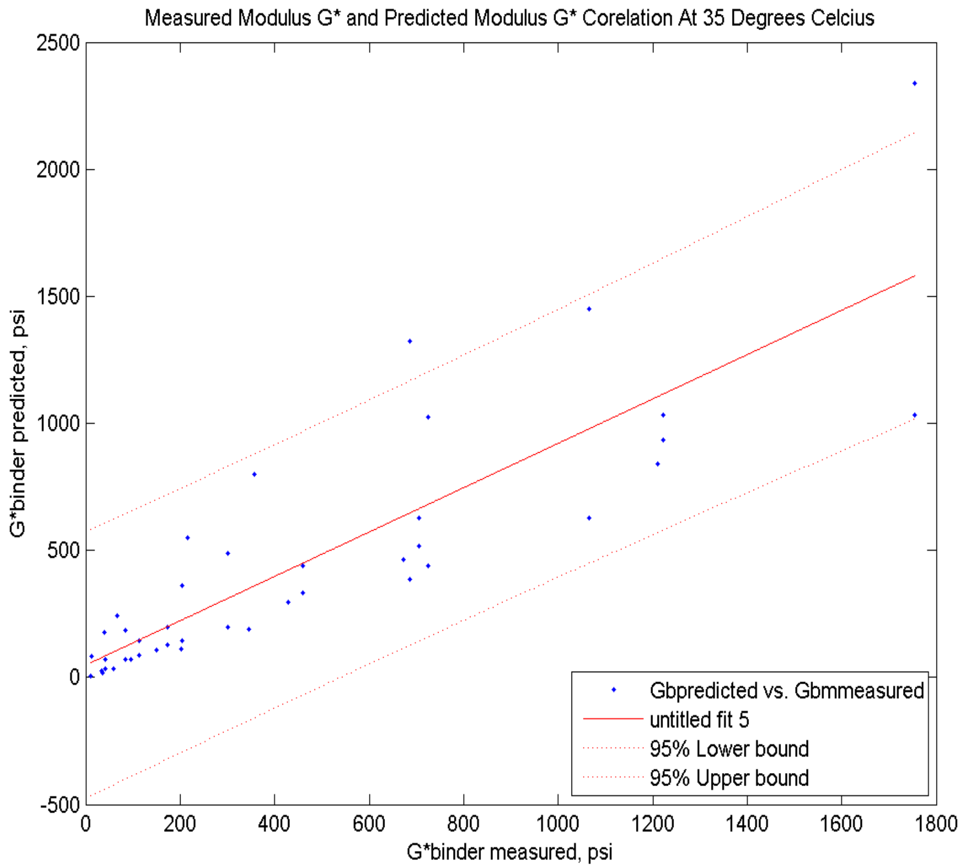
Measured Modulus G* and Predicted Modulus G* Corelation At 35 Degrees Celcius
G*binder predicted, psi
G*binder measured, psi
2500
2000
1500
1000
500
0
-500
0
200
400
600
800
1000
1200
1400
1600
1800
Gbpredicted vs. Gbmmeasured
untitled fit 5
95% Lower bound
95% Upper bound

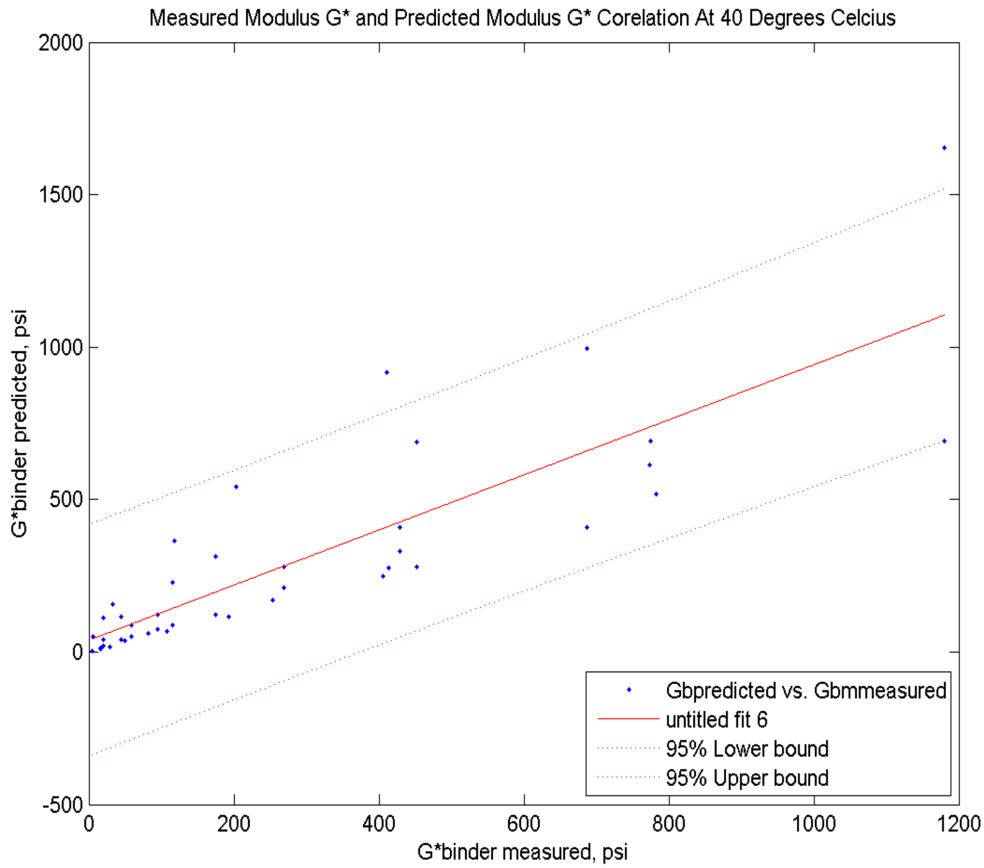
Measured Modulus G* and Predicted Modulus G* Corelation At 40 Degrees Celcius
2000
1500
1000
500
0
-500
G*binder predicted, psi
0
200
400
600
800
1000
1200
G*binder measured, psi
Gbpredicted vs. Gbmmeasured
untitled fit 6
95% Lower bound
95% Upper bound

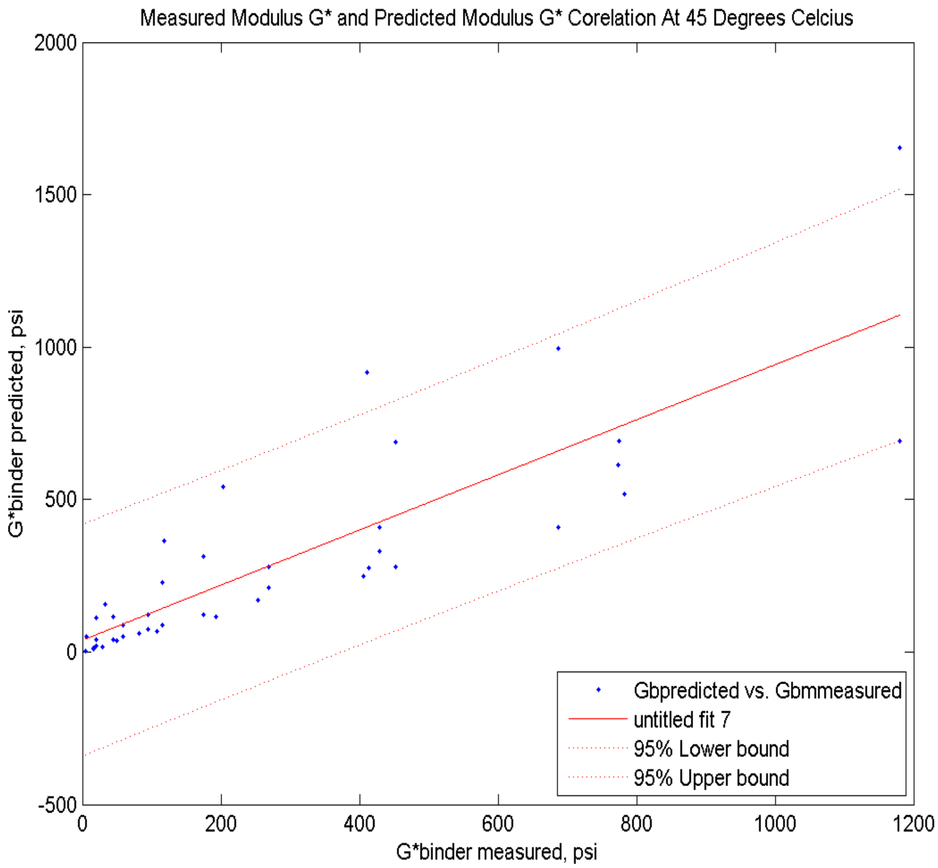

Measured Modulus G* and Predicted Modulus G* Corelation At 45 Degrees Celcius
G*binder predicted, psi
G*binder measured, psi
2000
1500
1000
500
0
-500
0
200
400
600
800
1000
1200
Gbpredicted vs. Gbmmeasured
untitled fit 7
95% Lower bound
95% Upper bound

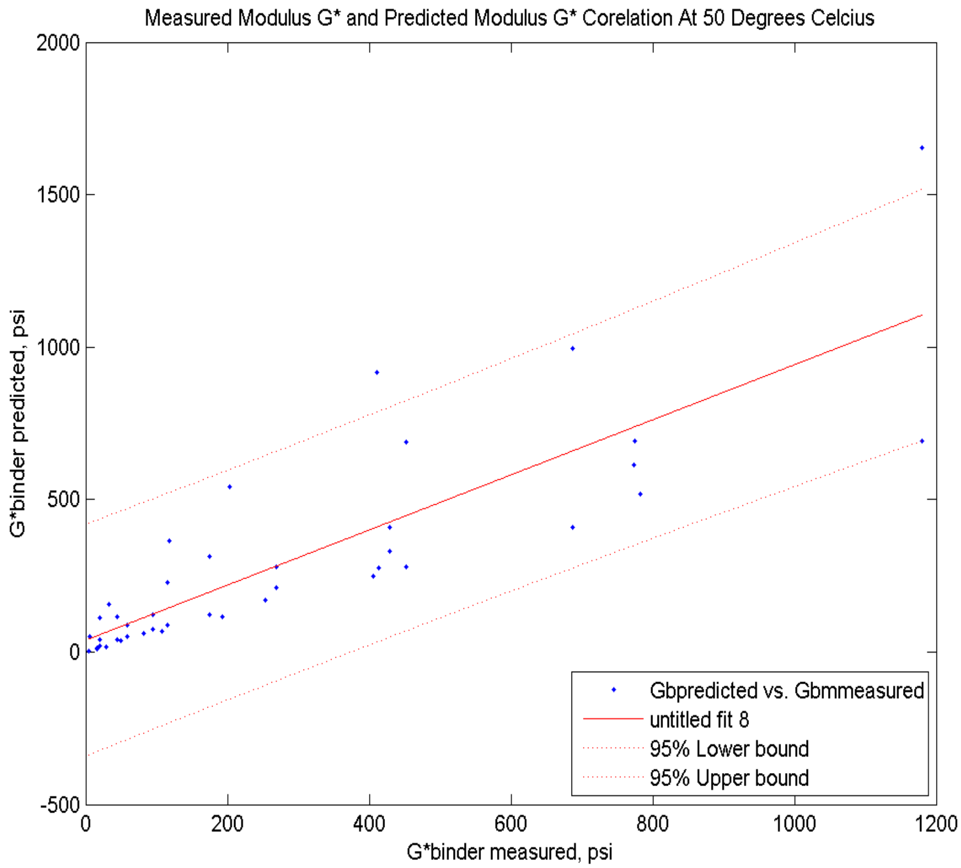

Measured Modulus G* and Predicted Modulus G* Corelation At 50 Degrees Celcius
G*binder predicted, psi
G*binder measured, psi
2000
1500
1000
500
0
-500
0
200
400
600
800
1000
1200
Gbpredicted vs. Gbmmeasured
untitled fit 8
95% Lower bound
95% Upper bound

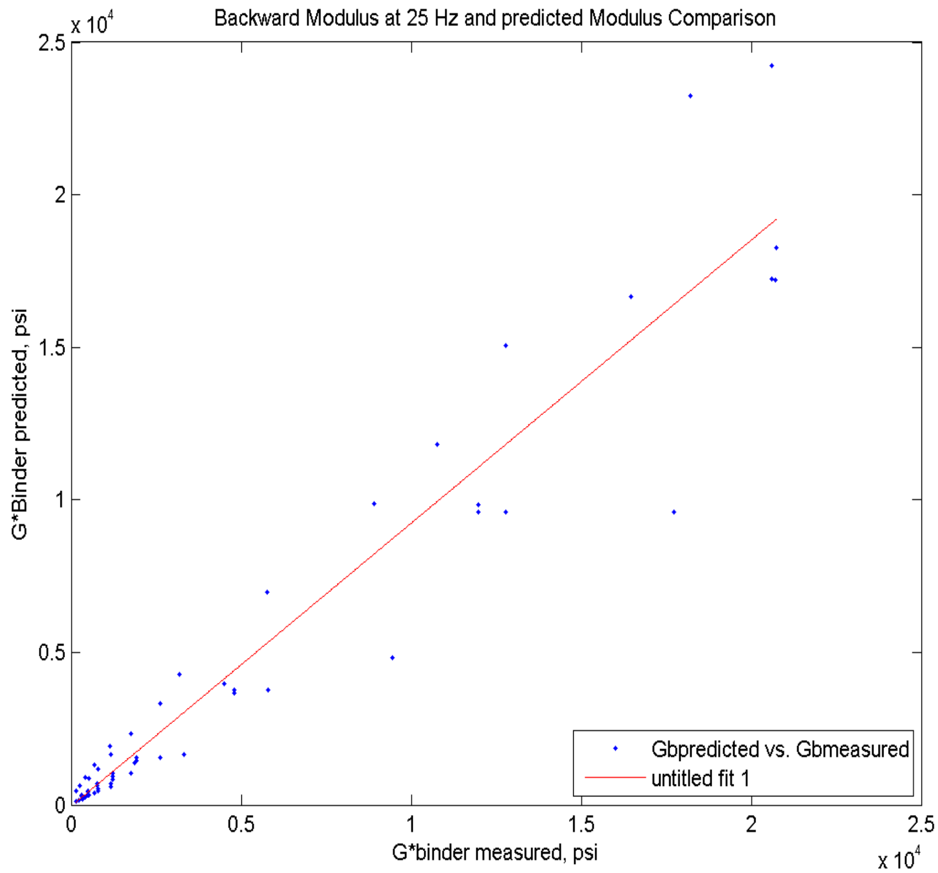
Backward Modulus at 25 Hz and predicted Modulus Comparison
x 10^4
2.5
2
1.5
1
0.5
0
G*Binder predicted, psi
0
0.5
1
1.5
2
2.5
x 10^4
G*binder measured, psi
Gbpredicted vs. Gbmeasured
untitled fit 1

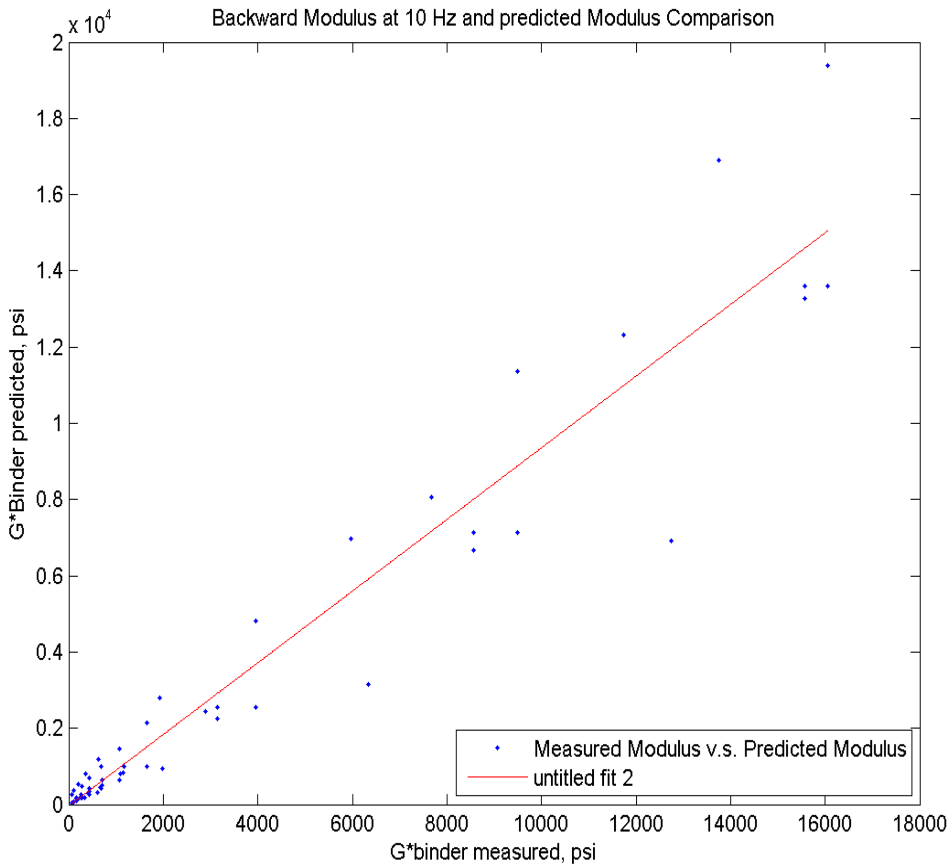
Backward Modulus at 10 Hz and predicted Modulus Comparison
x 10^4
2
1.8
1.6
1.4
1.2
1
0.8
0.6
0.4
0.2
0
G*Binder predicted, psi
0
2000
4000
6000
8000
10000
12000
14000
16000
18000
G*binder measured, psi
Measured Modulus v.s. Predicted Modulus
untitled fit 2

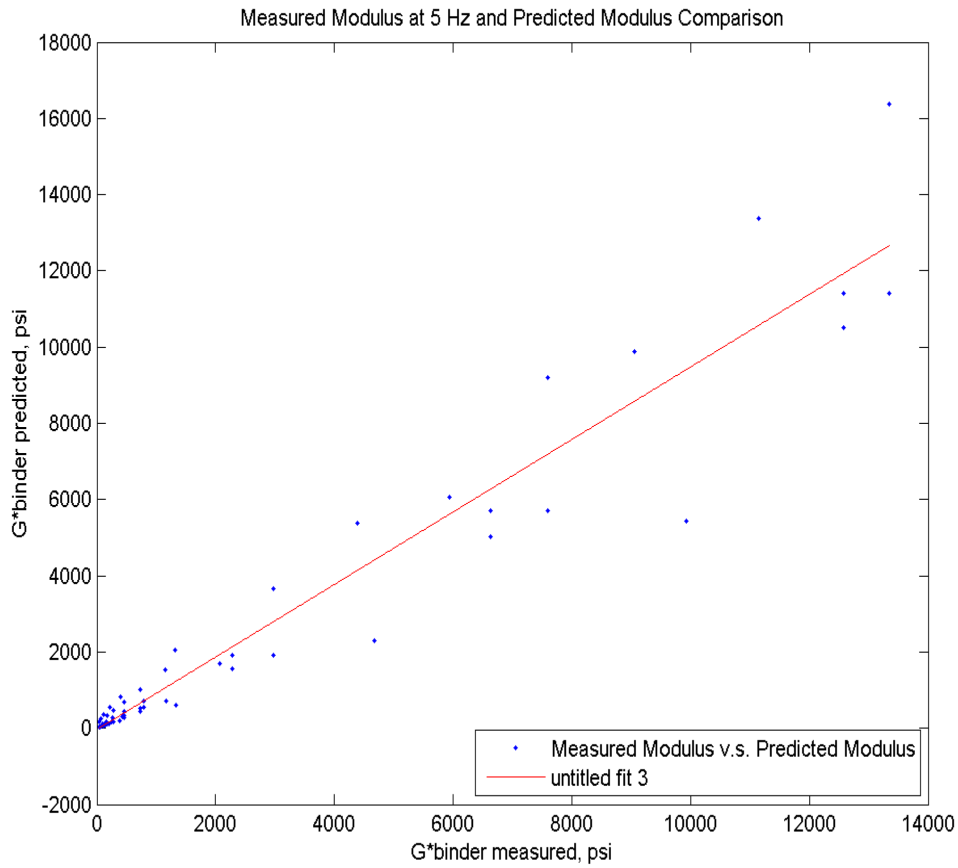
Measured Modulus at 5 Hz and Predicted Modulus Comparison
G*binder predicted, psi
G*binder measured, psi
18000
16000
14000
12000
10000
8000
6000
4000
2000
0
-2000
0
2000
4000
6000
8000
10000
12000
14000
Measured Modulus v.s. Predicted Modulus
untitled fit 3

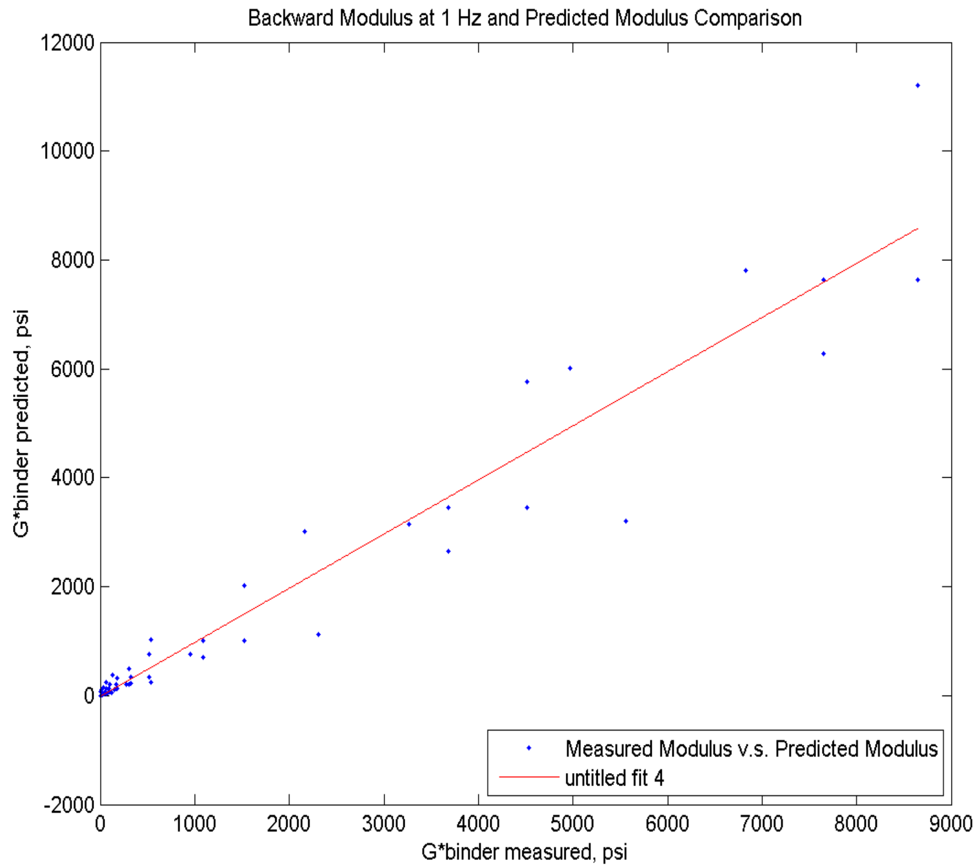
Backward Modulus at 1 Hz and Predicted Modulus Comparison
12000
10000
8000
6000
4000
2000
0
-2000
G*binder predicted, psi
0
1000
2000
3000
4000
5000
6000
7000
8000
9000
G*binder measured, psi
Measured Modulus v.s. Predicted Modulus
untitled fit 4

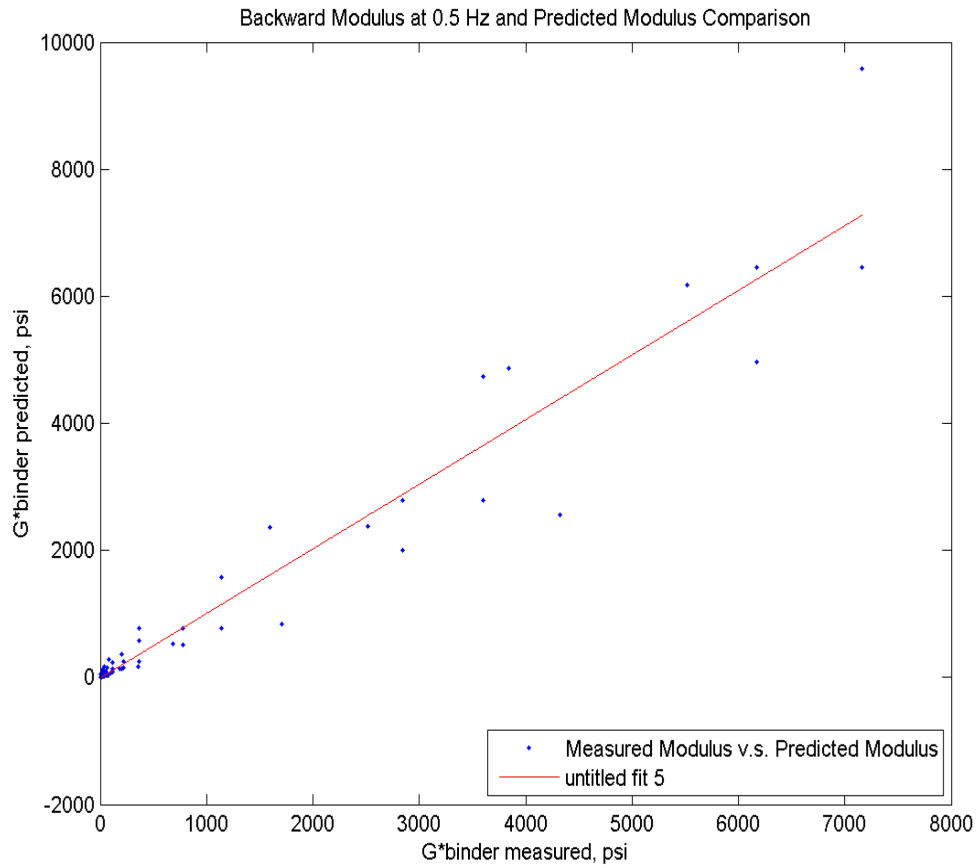

Backward Modulus at 0.5 Hz and Predicted Modulus Comparison
10000
8000
6000
4000
2000
0
-2000
0
1000
2000
3000
4000
5000
6000
7000
8000
G*binder predicted, psi
G*binder measured, psi
Measured Modulus v.s. Predicted Modulus
untitled fit 5

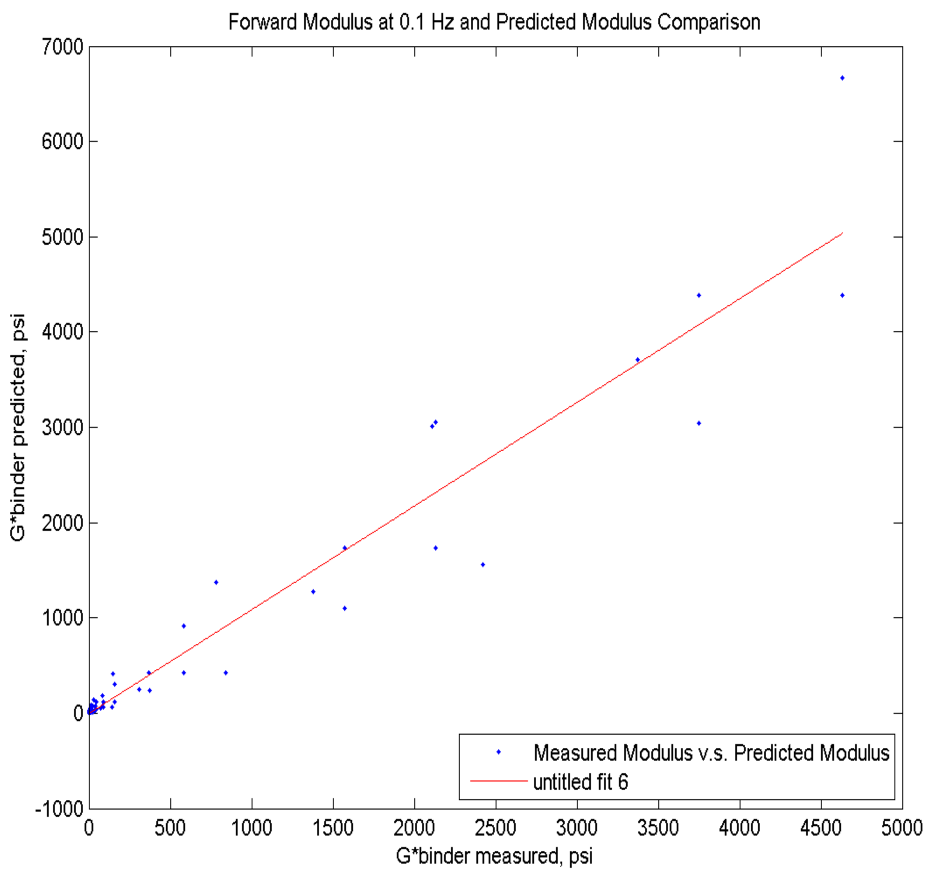

Forward Modulus at 0.1 Hz and Predicted Modulus Comparison
G*binder predicted, psi
G*binder measured, psi
7000
6000
5000
4000
3000
2000
1000
0
-1000
0
500
1000
1500
2000
2500
3000
3500
4000
4500
5000
Measured Modulus v.s. Predicted Modulus
untitled fit 6

APPENDIX E - Model development backward phase angle model family of curves

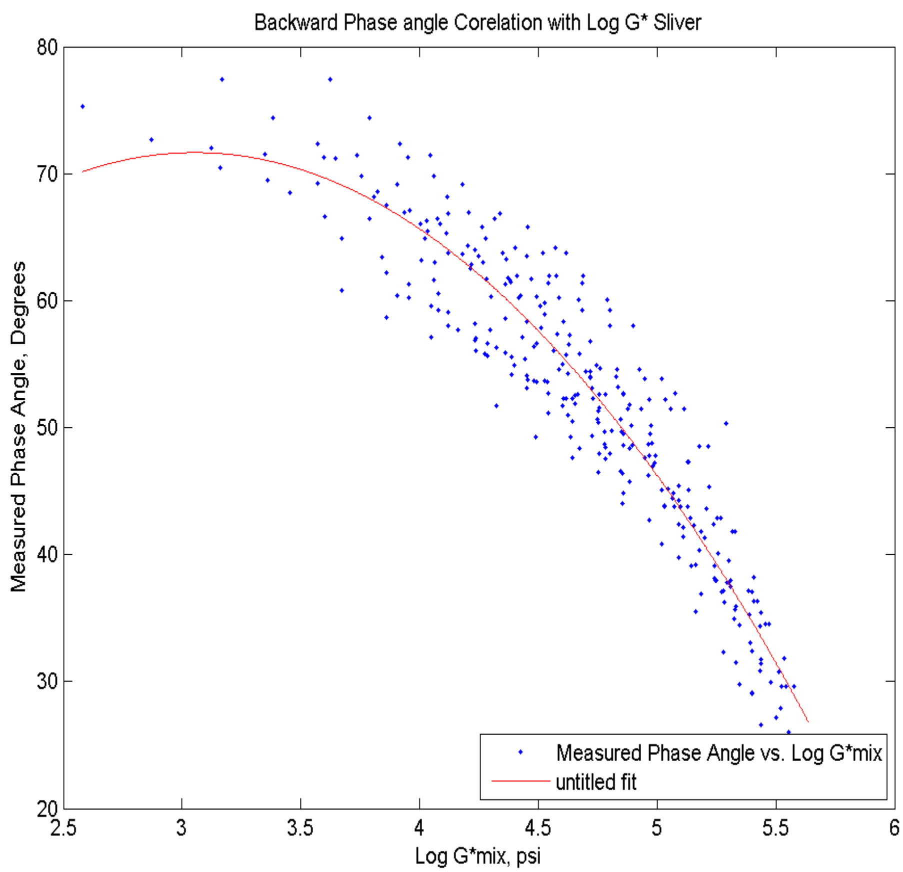

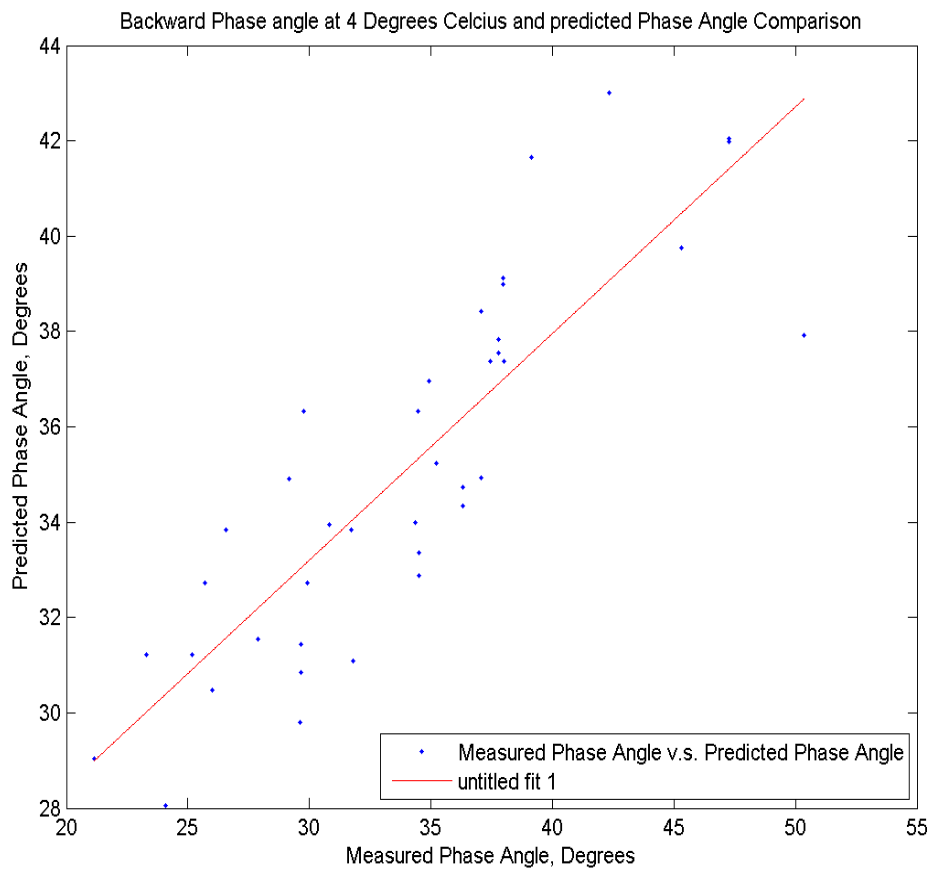
Backward Phase angle at 4 Degrees Celcius and predicted Phase Angle Comparison
Predicted Phase Angle, Degrees
Measured Phase Angle, Degrees
Measured Phase Angle v.s. Predicted Phase Angle
untitled fit 1
44
42
40
38
36
34
32
30
28
20
25
30
35
40
45
50
55

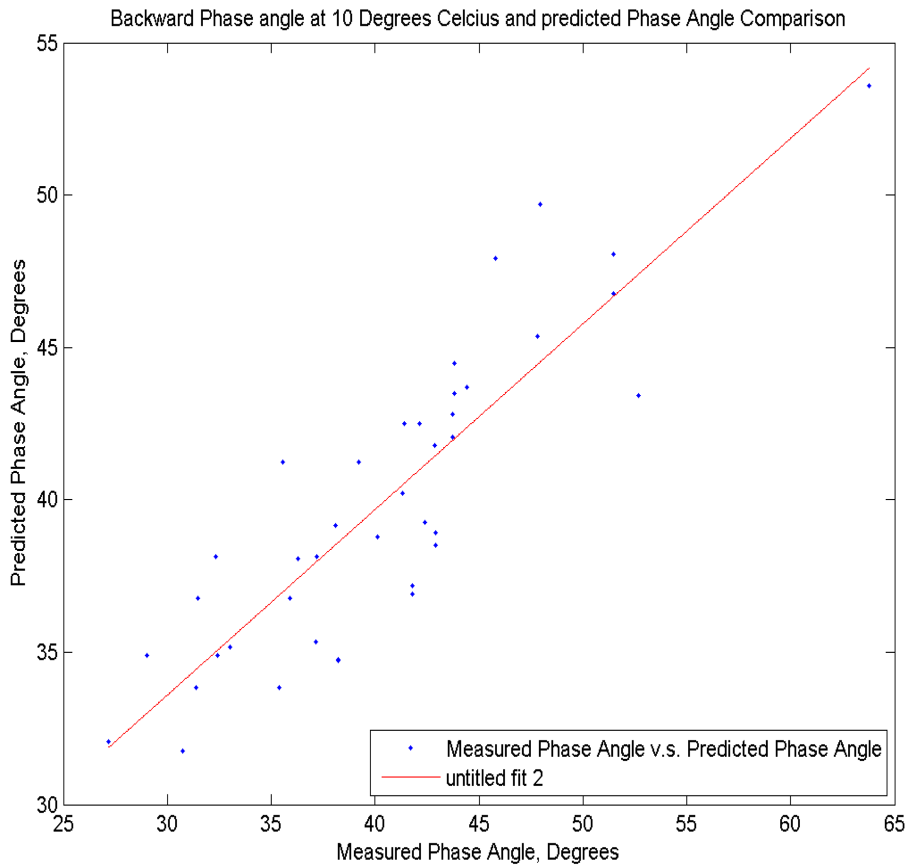
Backward Phase angle at 10 Degrees Celcius and predicted Phase Angle Comparison
Predicted Phase Angle, Degrees
Measured Phase Angle, Degrees
Measured Phase Angle v.s. Predicted Phase Angle
untitled fit 2
55
50
45
40
35
30
25
30
35
40
45
50
55
60
65

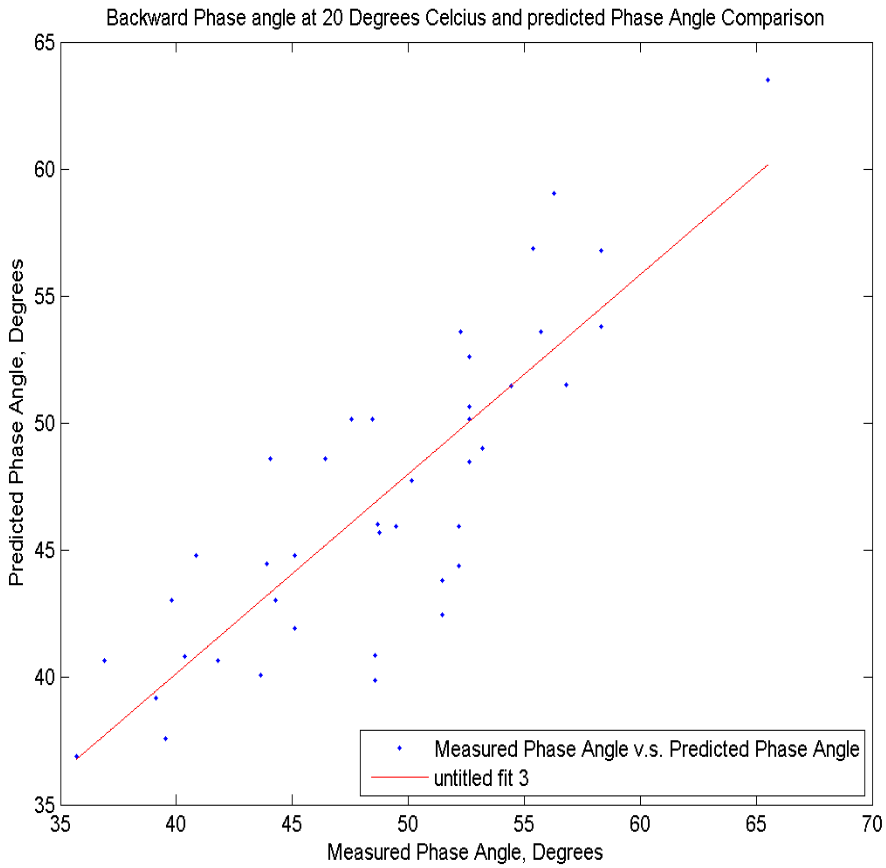
Backward Phase angle at 20 Degrees Celcius and predicted Phase Angle Comparison
Predicted Phase Angle, Degrees
Measured Phase Angle, Degrees
Measured Phase Angle v.s. Predicted Phase Angle
untitled fit 3
35
40
45
50
55
60
65
70

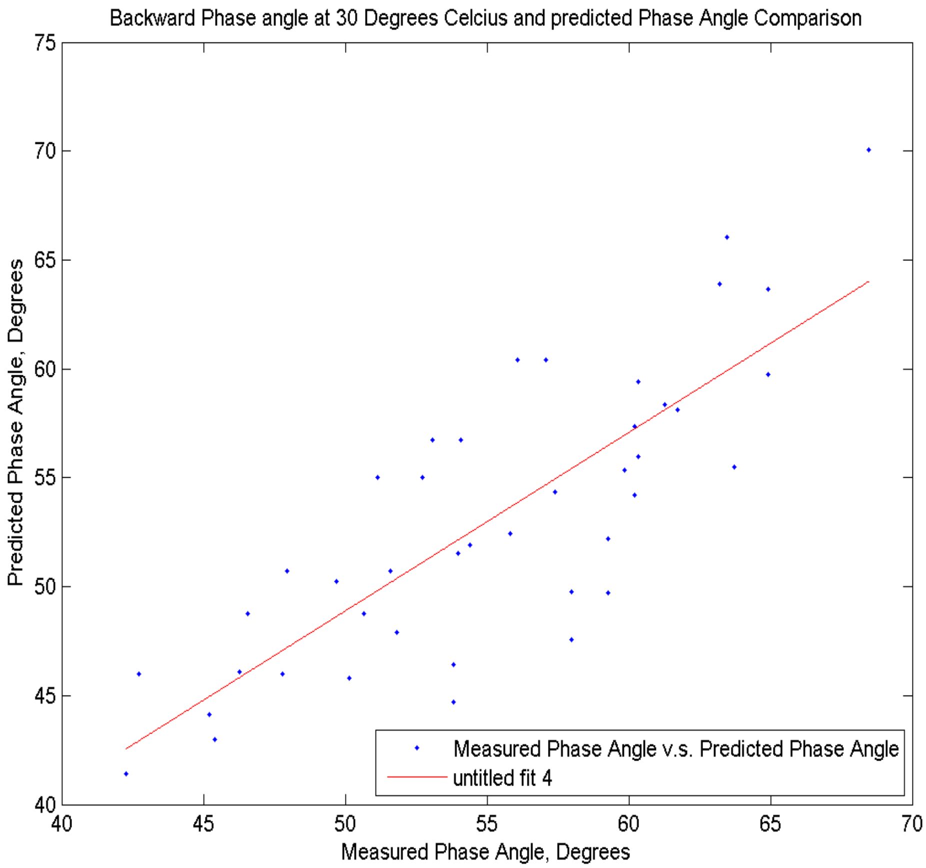

Backward Phase angle at 30 Degrees Celcius and predicted Phase Angle Comparison
Predicted Phase Angle, Degrees
Measured Phase Angle, Degrees
Measured Phase Angle v.s. Predicted Phase Angle
untitled fit 4
75
70
65
60
55
50
45
40
40
45
50
55
60
65
70

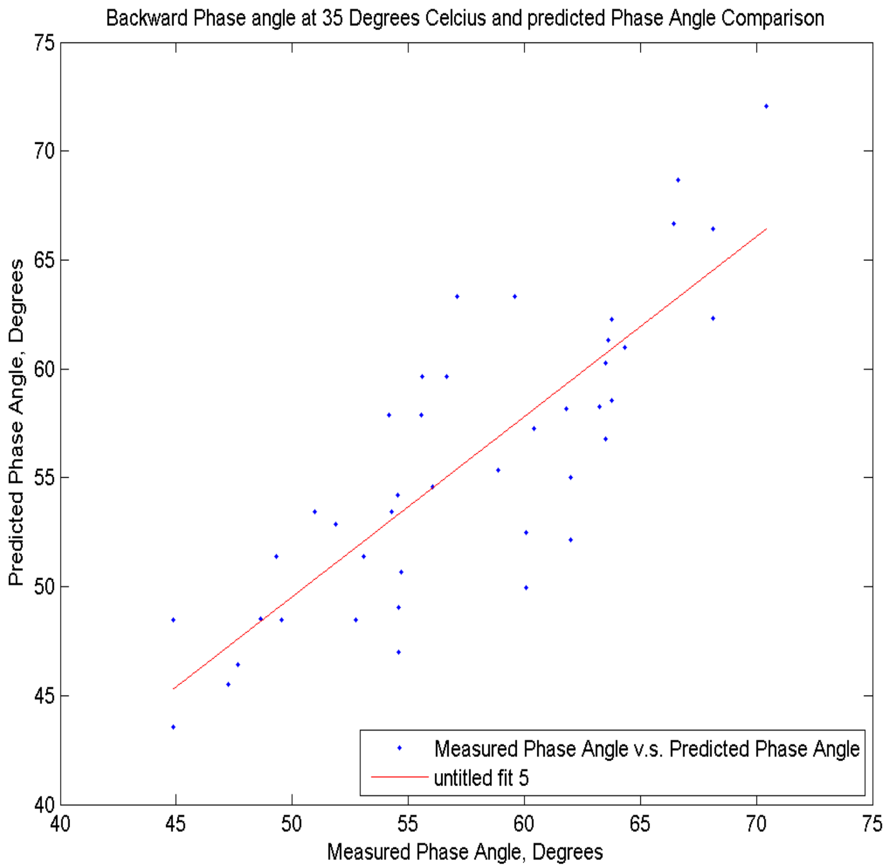
Backward Phase angle at 35 Degrees Celcius and predicted Phase Angle Comparison
Predicted Phase Angle, Degrees
Measured Phase Angle, Degrees
Measured Phase Angle v.s. Predicted Phase Angle
untitled fit 5
40
45
50
55
60
65
70
75

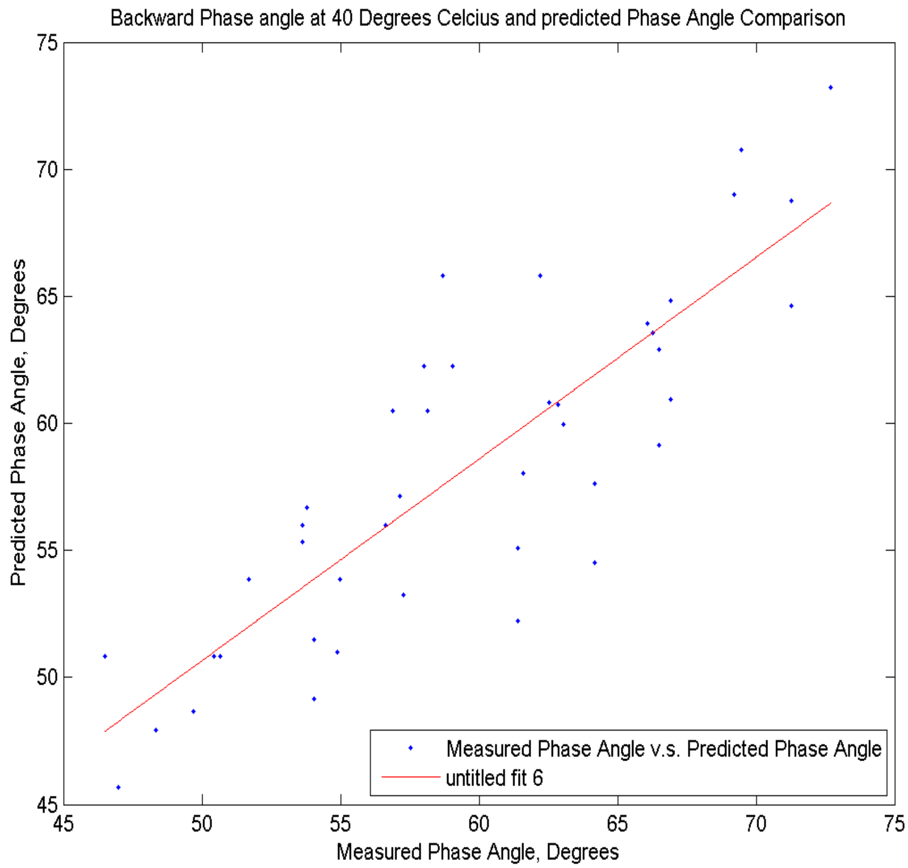
Backward Phase angle at 40 Degrees Celcius and predicted Phase Angle Comparison
Predicted Phase Angle, Degrees
Measured Phase Angle, Degrees
Measured Phase Angle v.s. Predicted Phase Angle
untitled fit 6
45
50
55
60
65
70
75

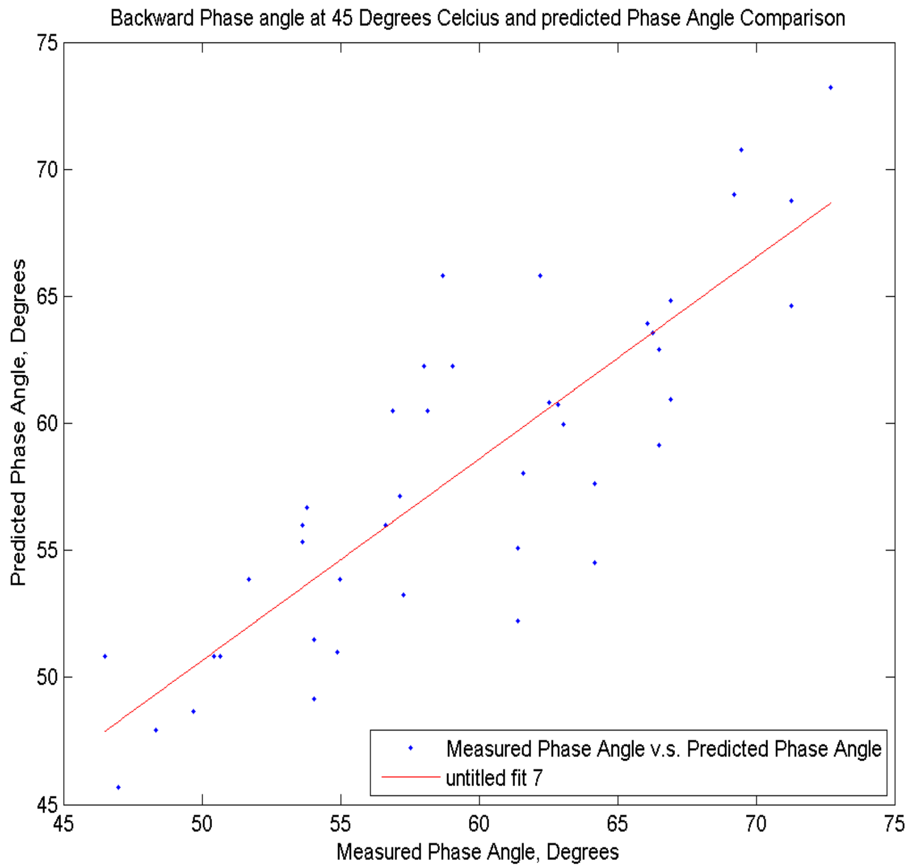
Backward Phase angle at 45 Degrees Celcius and predicted Phase Angle Comparison
Predicted Phase Angle, Degrees
Measured Phase Angle, Degrees
Measured Phase Angle v.s. Predicted Phase Angle
untitled fit 7
75
70
65
60
55
50
45
45
50
55
60
65
70
75

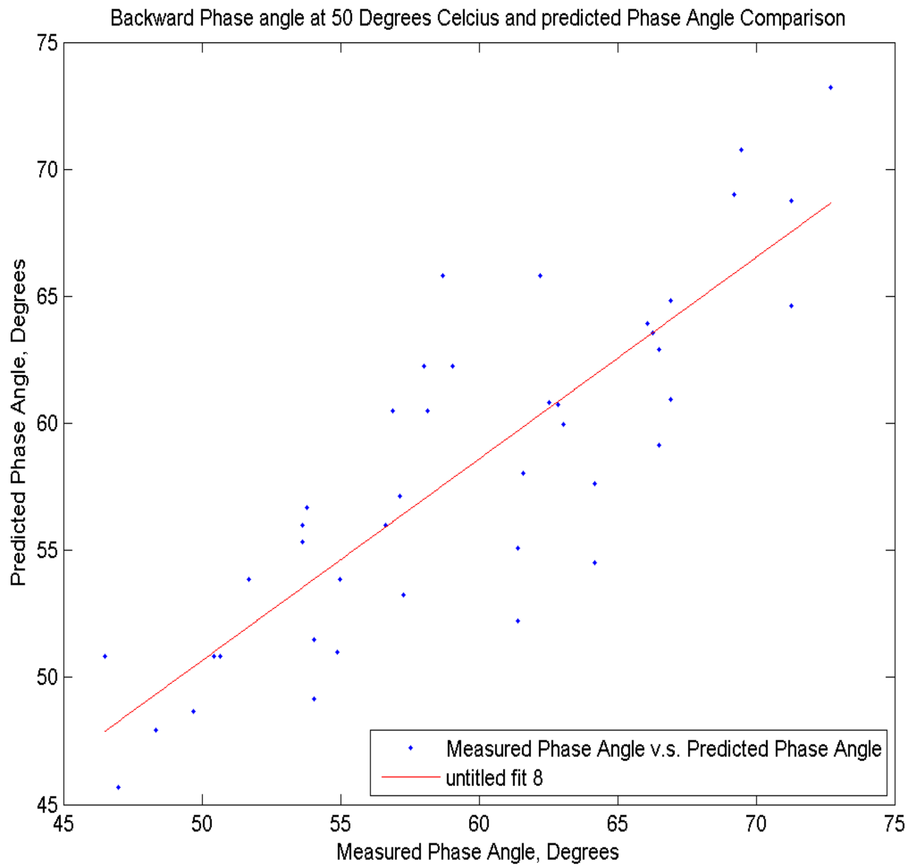
Backward Phase angle at 50 Degrees Celcius and predicted Phase Angle Comparison
Predicted Phase Angle, Degrees
Measured Phase Angle, Degrees
75
70
65
60
55
50
45
45
50
55
60
65
70
75
Measured Phase Angle v.s. Predicted Phase Angle
untitled fit 8

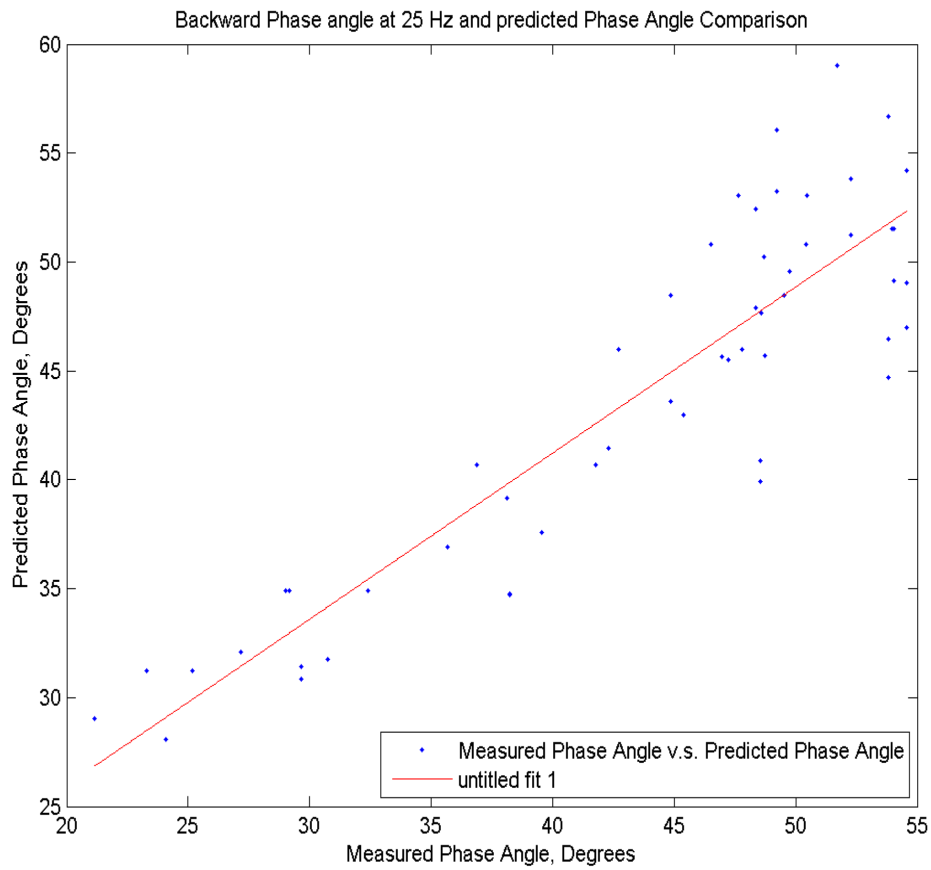
Backward Phase angle at 25 Hz and predicted Phase Angle Comparison
Predicted Phase Angle, Degrees
Measured Phase Angle, Degrees
Measured Phase Angle v.s. Predicted Phase Angle
untitled fit 1
60
55
50
45
40
35
30
25
20
25
30
35
40
45
50
55

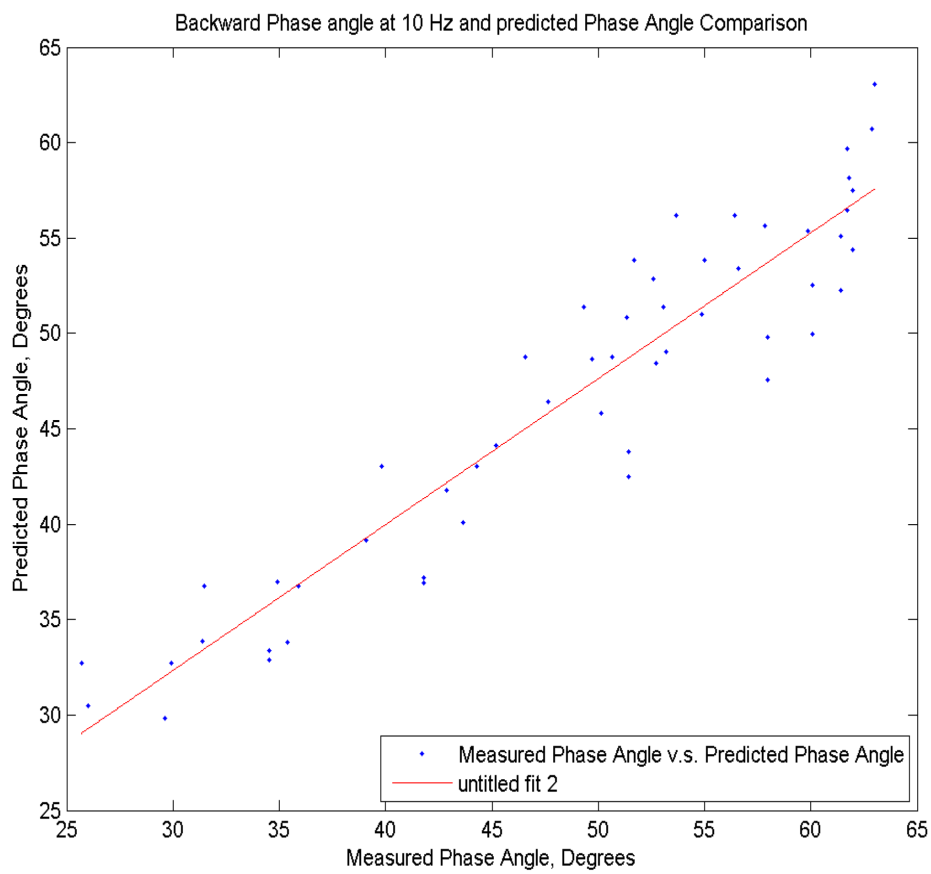
Backward Phase angle at 10 Hz and predicted Phase Angle Comparison
Predicted Phase Angle, Degrees
Measured Phase Angle, Degrees
Measured Phase Angle v.s. Predicted Phase Angle
untitled fit 2
65
60
55
50
45
40
35
30
25
25
30
35
40
45
50
55
60
65

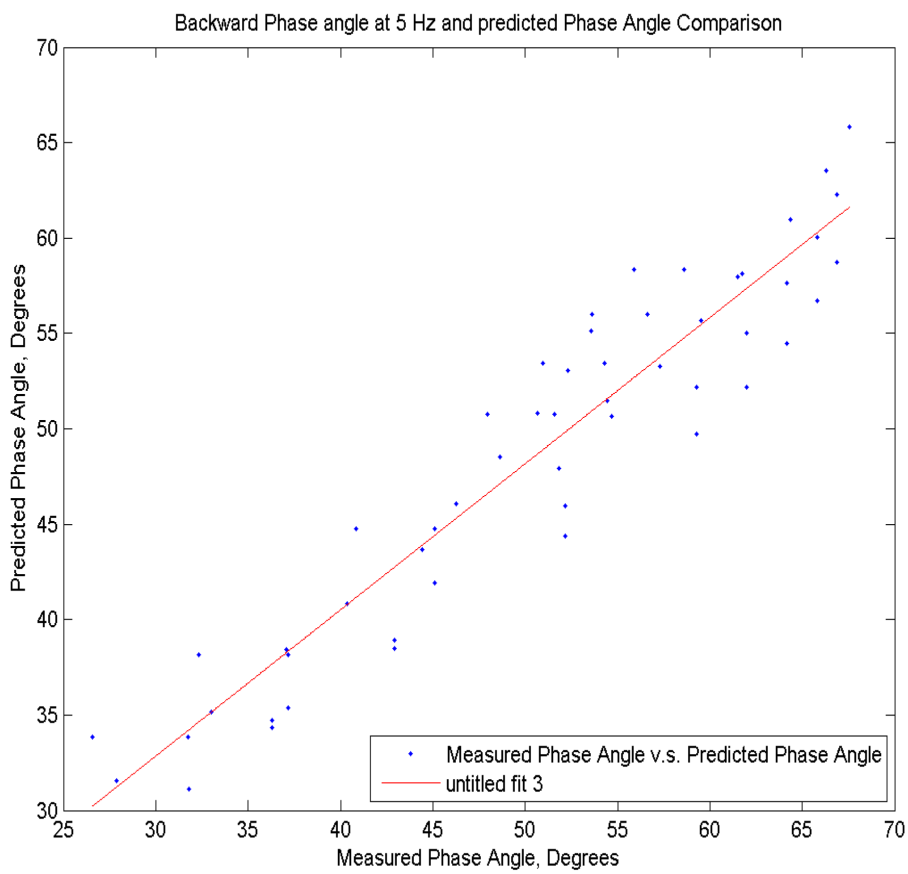
Backward Phase angle at 5 Hz and predicted Phase Angle Comparison
Predicted Phase Angle, Degrees
Measured Phase Angle, Degrees
Measured Phase Angle v.s. Predicted Phase Angle
untitled fit 3
70
65
60
55
50
45
40
35
30
25
30
35
40
45
50
55
60
65
70

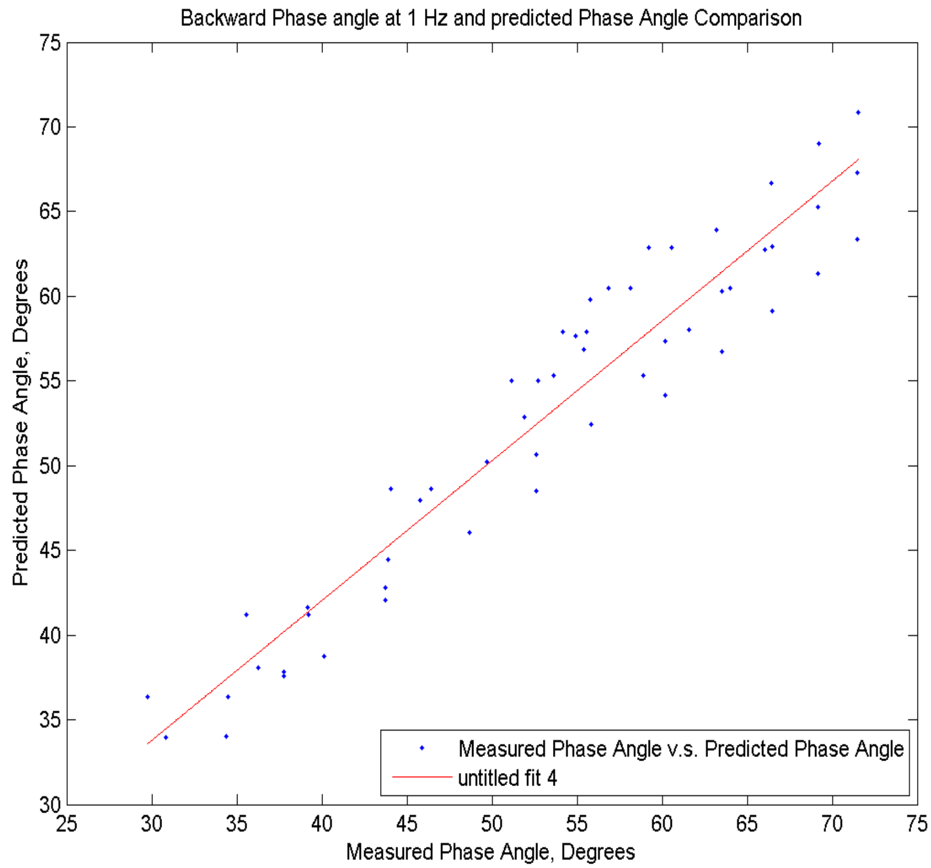

Backward Phase angle at 1 Hz and predicted Phase Angle Comparison
Predicted Phase Angle, Degrees
Measured Phase Angle, Degrees
75
70
65
60
55
50
45
40
35
30
25
Measured Phase Angle v.s. Predicted Phase Angle
untitled fit 4

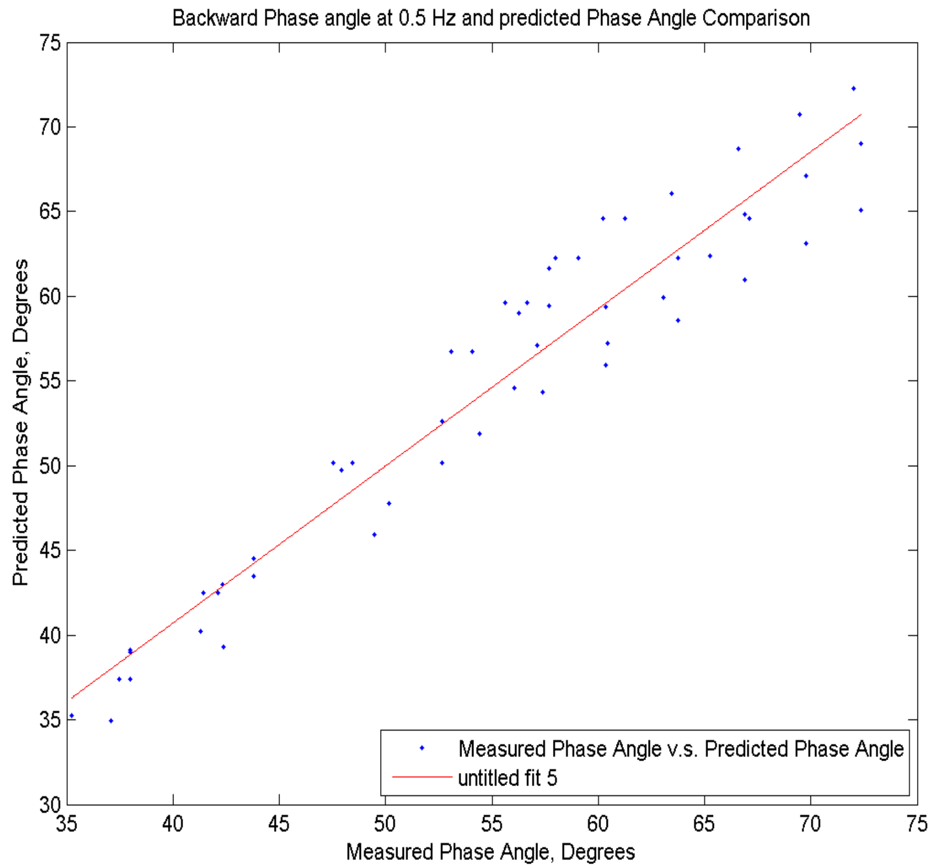
Backward Phase angle at 0.5 Hz and predicted Phase Angle Comparison
Predicted Phase Angle, Degrees
Measured Phase Angle, Degrees
Measured Phase Angle v.s. Predicted Phase Angle
untitled fit 5
30
35
40
45
50
55
60
65
70
75

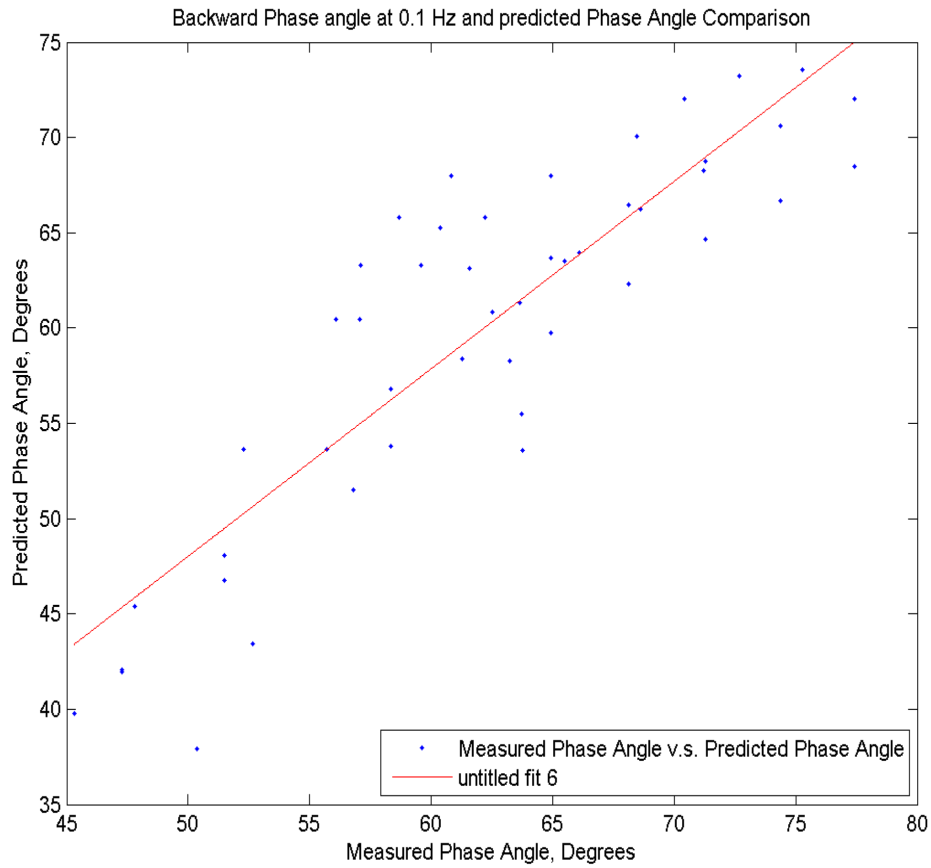
Backward Phase angle at 0.1 Hz and predicted Phase Angle Comparison
Predicted Phase Angle, Degrees
Measured Phase Angle, Degrees
Measured Phase Angle v.s. Predicted Phase Angle
untitled fit 6
75
70
65
60
55
50
45
40
35
45
50
55
60
65
70
75
80

APPENDIX F- Model verification forward modulus model family of curves

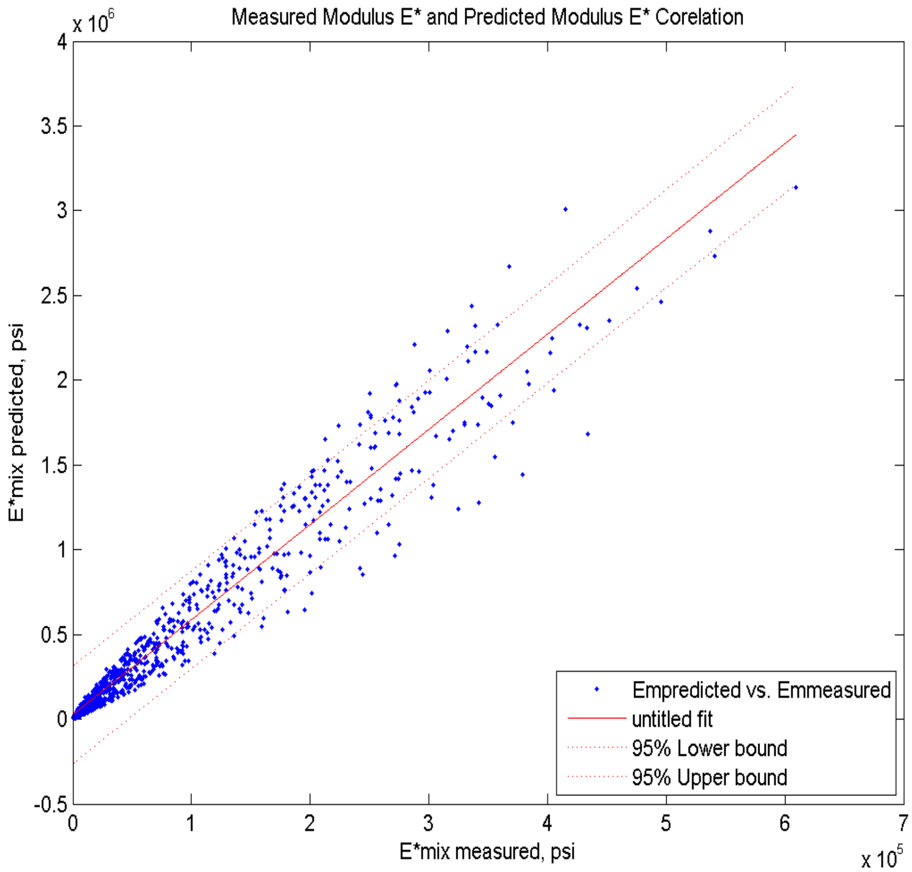

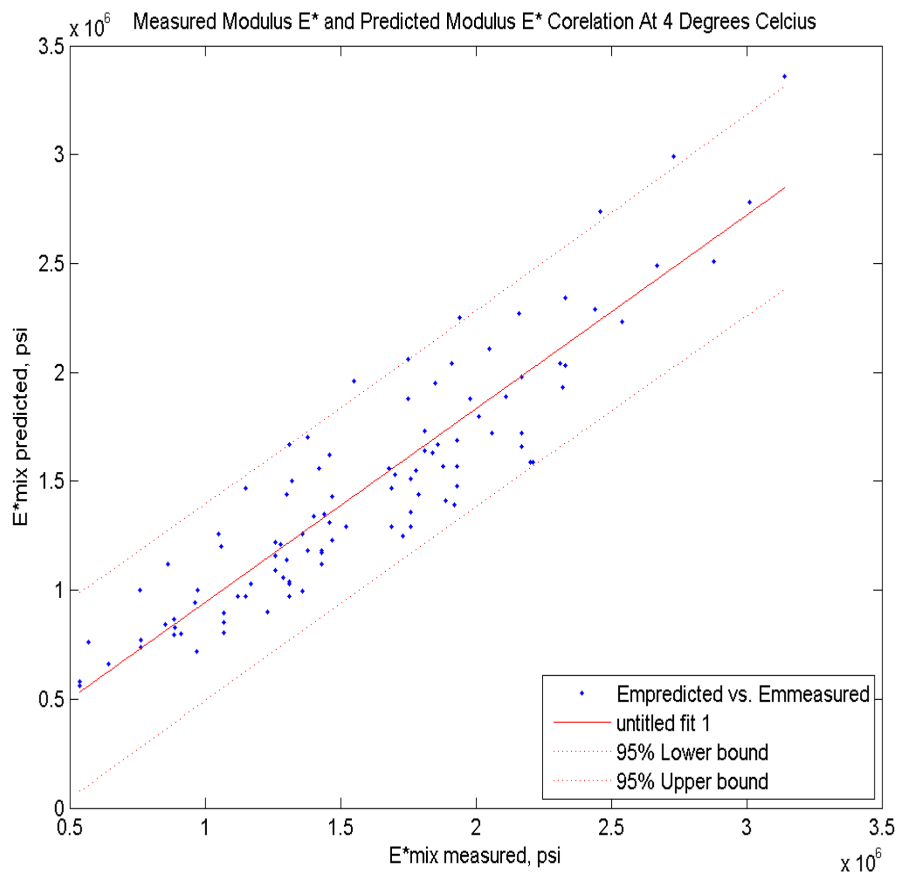

Measured Modulus E* and Predicted Modulus E* Corelation At 4 Degrees Celcius
x 10^6
3.5
3
2.5
2
1.5
1
0.5
0
E*mix predicted, psi
0.5
1
1.5
2
2.5
3
3.5
E*mix measured, psi
x 10^6
Empredicted vs. Emmeasured
untitled fit 1
95% Lower bound
95% Upper bound

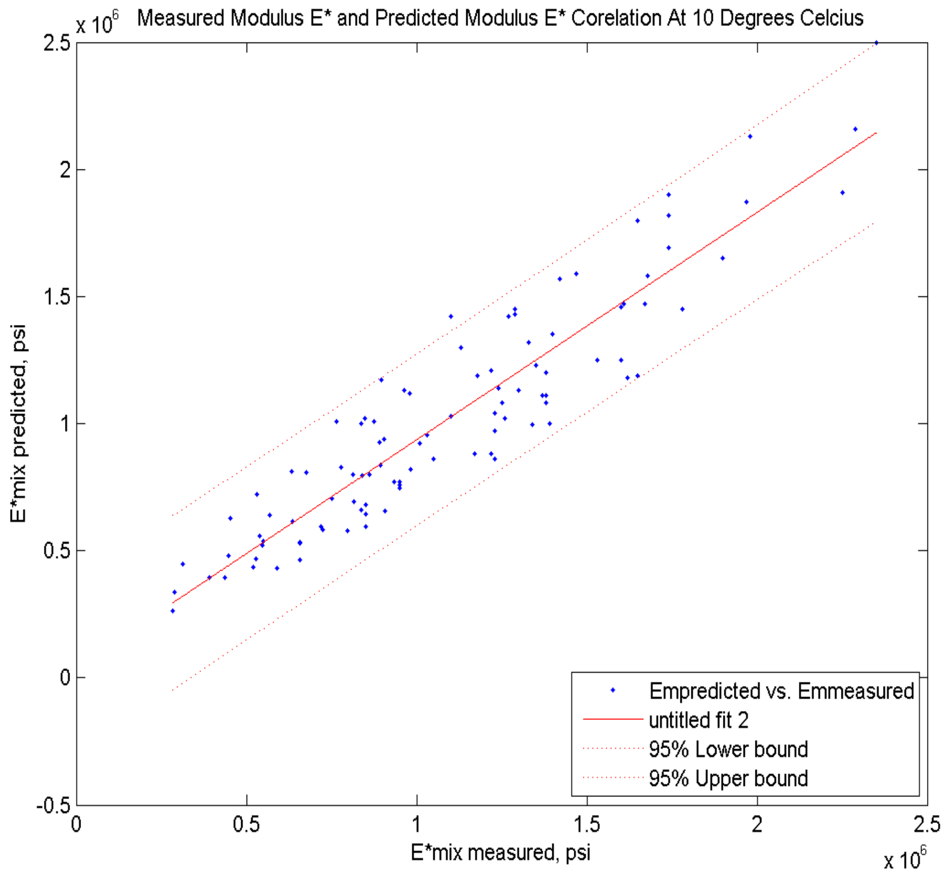
x 10^6 Measured Modulus E* and Predicted Modulus E* Corelation At 10 Degrees Celcius
2.5
2
1.5
1
0.5
0
-0.5
E*mix predicted, psi
0
0.5
1
1.5
2
2.5
E*mix measured, psi
x 10^6
Empredicted vs. Emmeasured
untitled fit 2
95% Lower bound
95% Upper bound

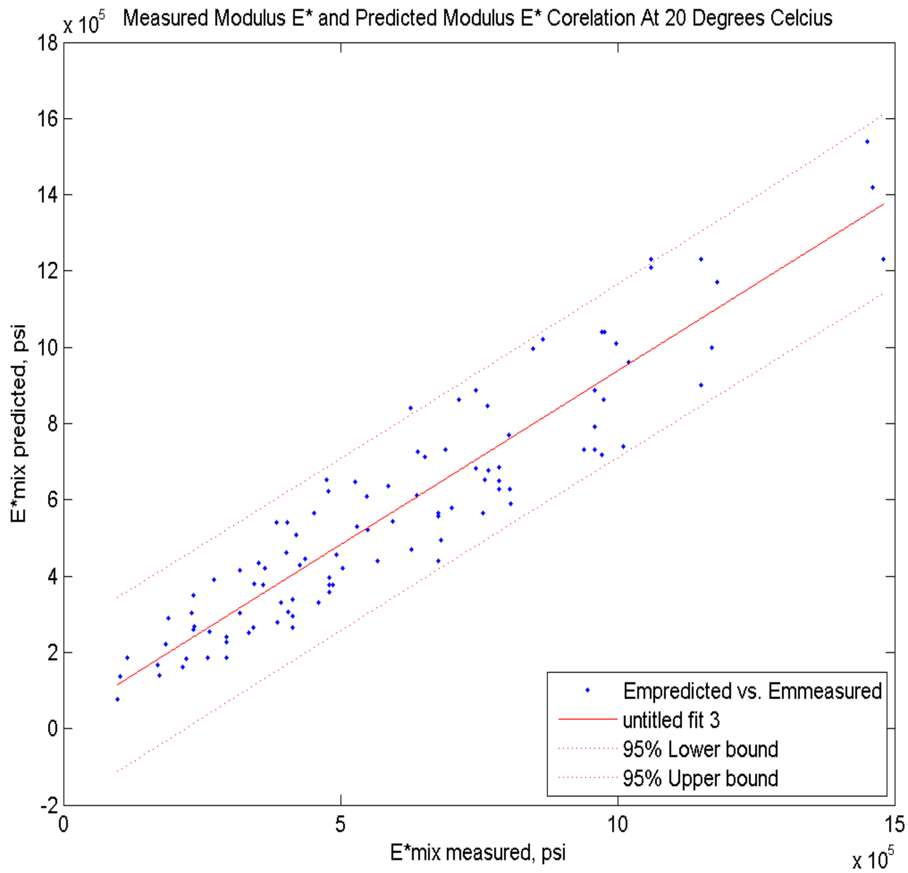
Measured Modulus E* and Predicted Modulus E* Corelation At 20 Degrees Celcius
x 10^5
18
16
14
12
10
8
6
4
2
0
-2
E*mix predicted, psi
0
5
10
15
E*mix measured, psi
x 10^5
Empredicted vs. Emmeasured
untitled fit 3
95% Lower bound
95% Upper bound

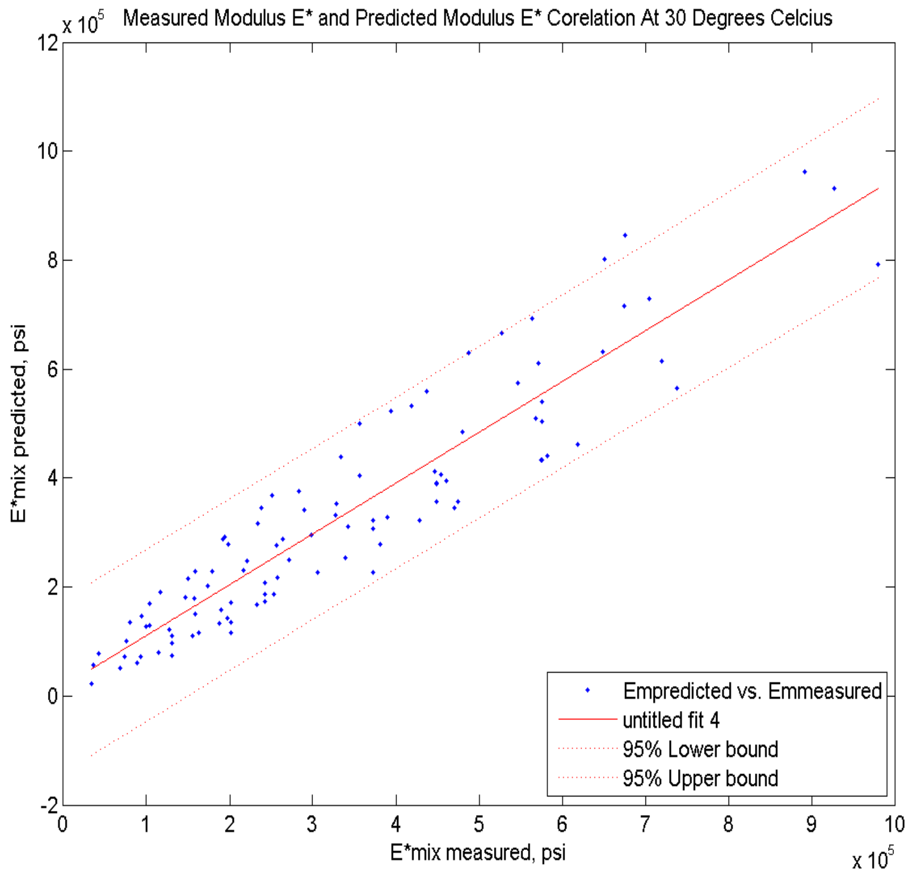

x 10^5
Measured Modulus E* and Predicted Modulus E* Corelation At 30 Degrees Celcius
12
10
8
6
4
2
0
-2
E*mix predicted, psi
0
1
2
3
4
5
6
7
8
9
10
E*mix measured, psi
x 10^5
Empredicted vs. Emmeasured
untitled fit 4
95% Lower bound
95% Upper bound

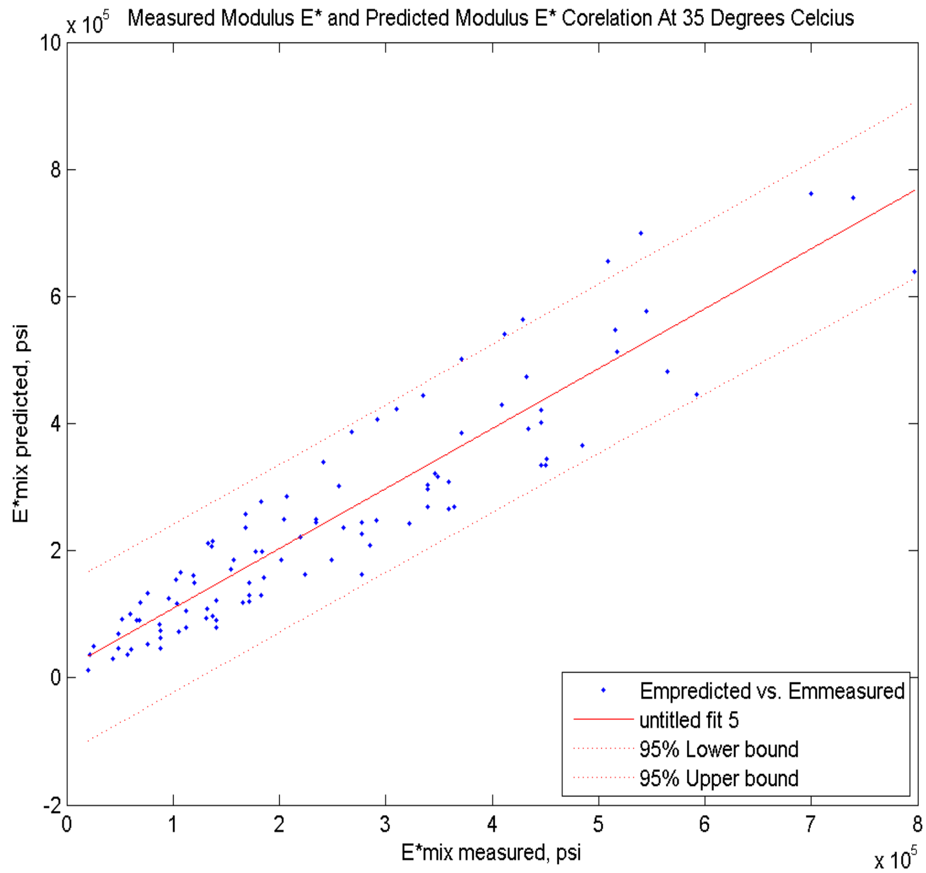

Measured Modulus E* and Predicted Modulus E* Corelation At 35 Degrees Celcius
x 10^5
10
8
6
4
2
0
-2
0
1
2
3
4
5
6
7
8
E*mix predicted, psi
E*mix measured, psi
x 10^5
Empredicted vs. Emmeasured
untitled fit 5
95% Lower bound
95% Upper bound

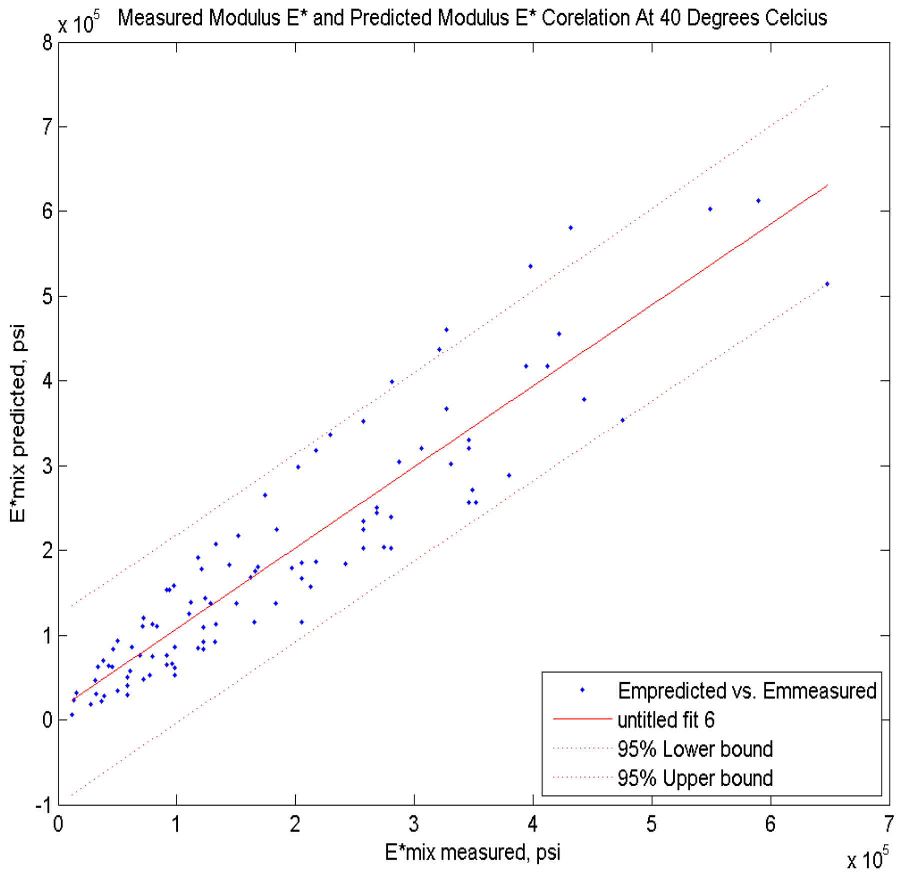
x 10^5
Measured Modulus E* and Predicted Modulus E* Corelation At 40 Degrees Celcius
E*mix predicted, psi
E*mix measured, psi
x 10^5
8
7
6
5
4
3
2
1
0
-1
0
1
2
3
4
5
6
7
Empredicted vs. Emmeasured
untitled fit 6
95% Lower bound
95% Upper bound

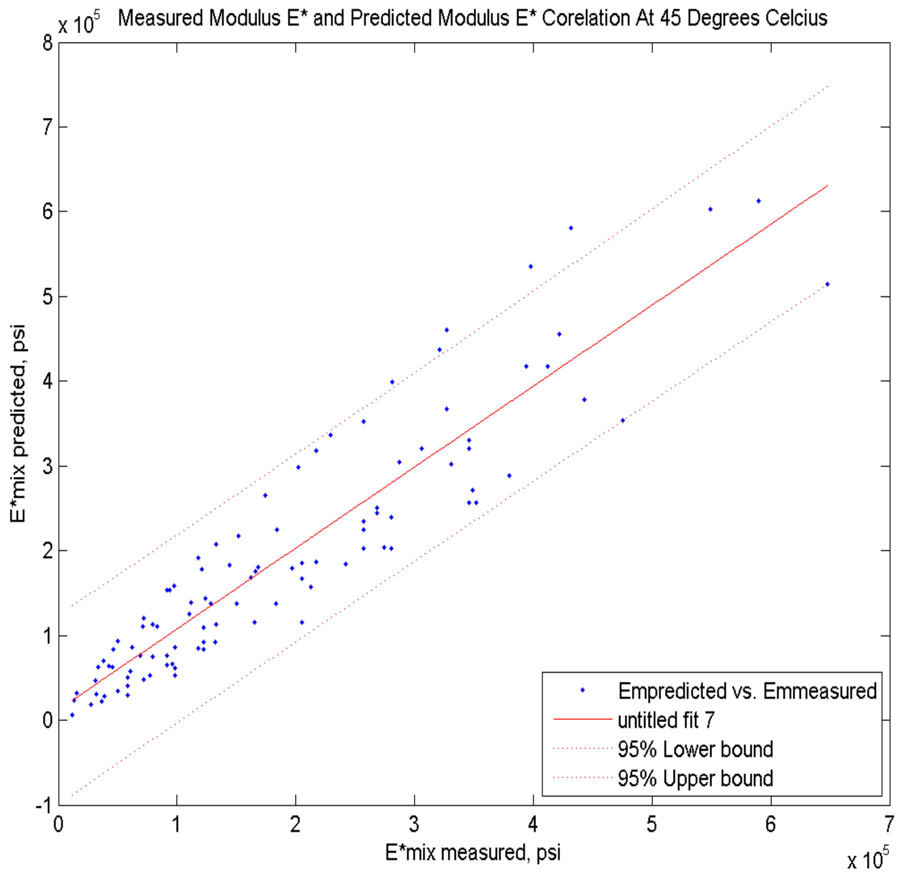

x 10^5 Measured Modulus E* and Predicted Modulus E* Corelation At 45 Degrees Celcius
E*mix predicted, psi
E*mix measured, psi
x 10^5
Empredicted vs. Emmeasured
untitled fit 7
95% Lower bound
95% Upper bound

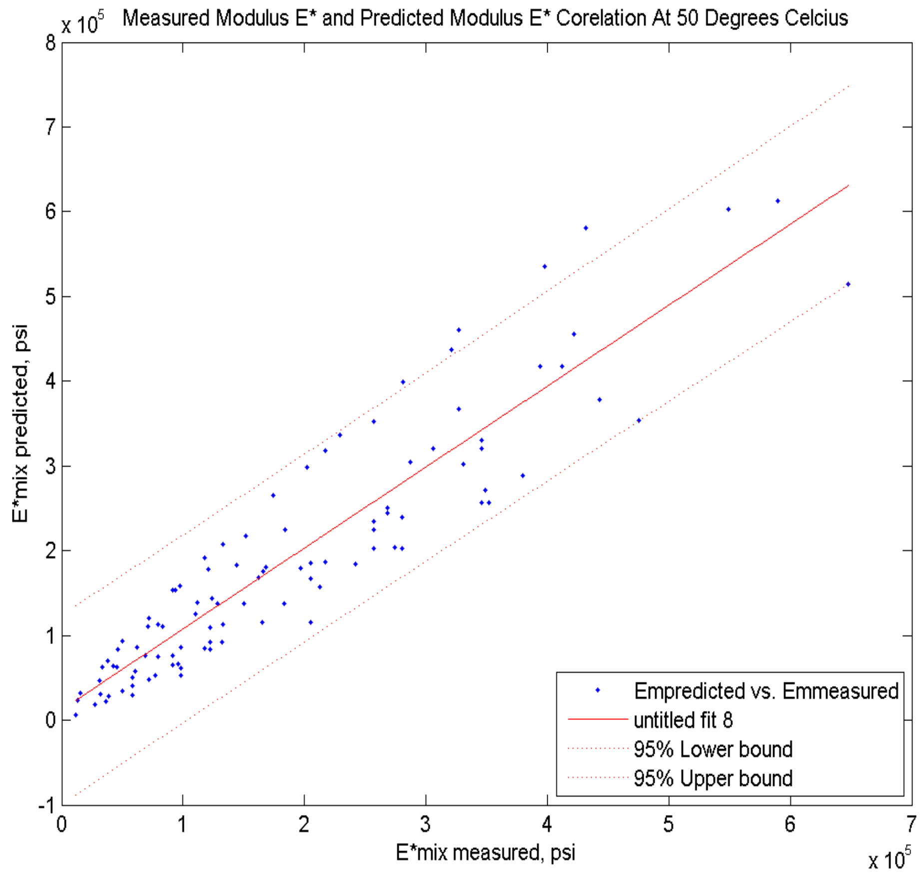

Measured Modulus E* and Predicted Modulus E* Corelation At 50 Degrees Celcius
x 10^5
E*mix predicted, psi
E*mix measured, psi
x 10^5
Empredicted vs. Emmeasured
untitled fit 8
95% Lower bound
95% Upper bound

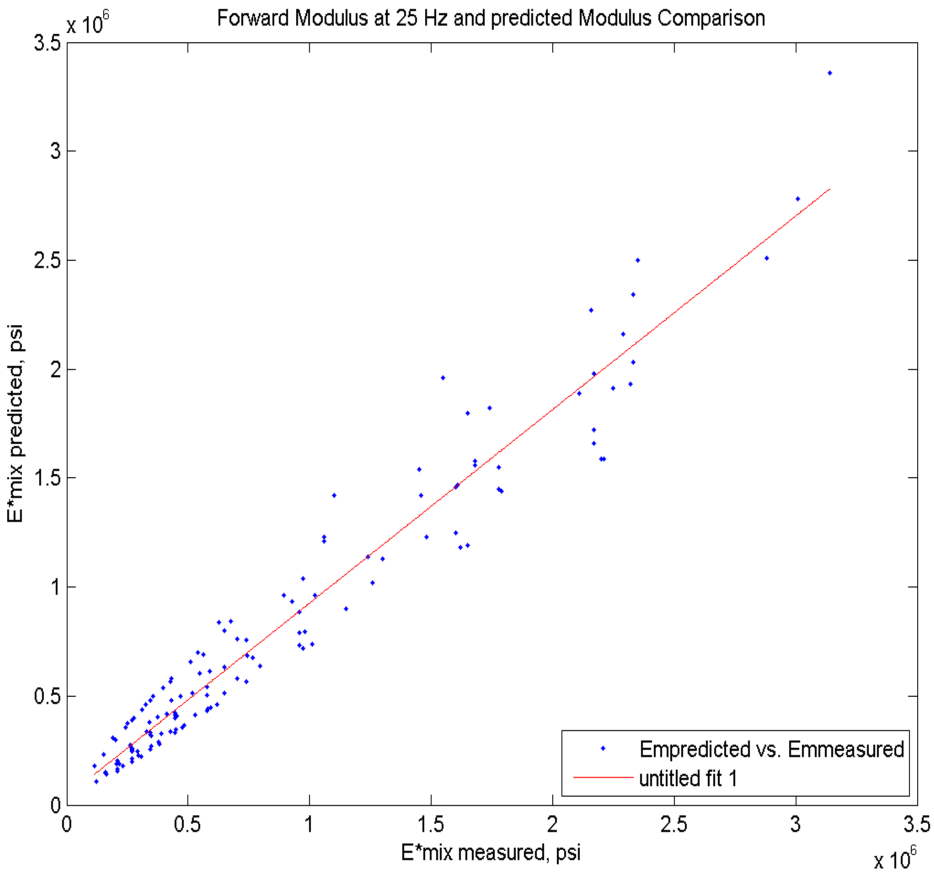

Forward Modulus at 25 Hz and predicted Modulus Comparison
x 10^6
3.5
3
2.5
2
1.5
1
0.5
0
E*mix predicted, psi
0
0.5
1
1.5
2
2.5
3
3.5
E*mix measured, psi
x 10^6
Empredicted vs. Emmeasured
untitled fit 1

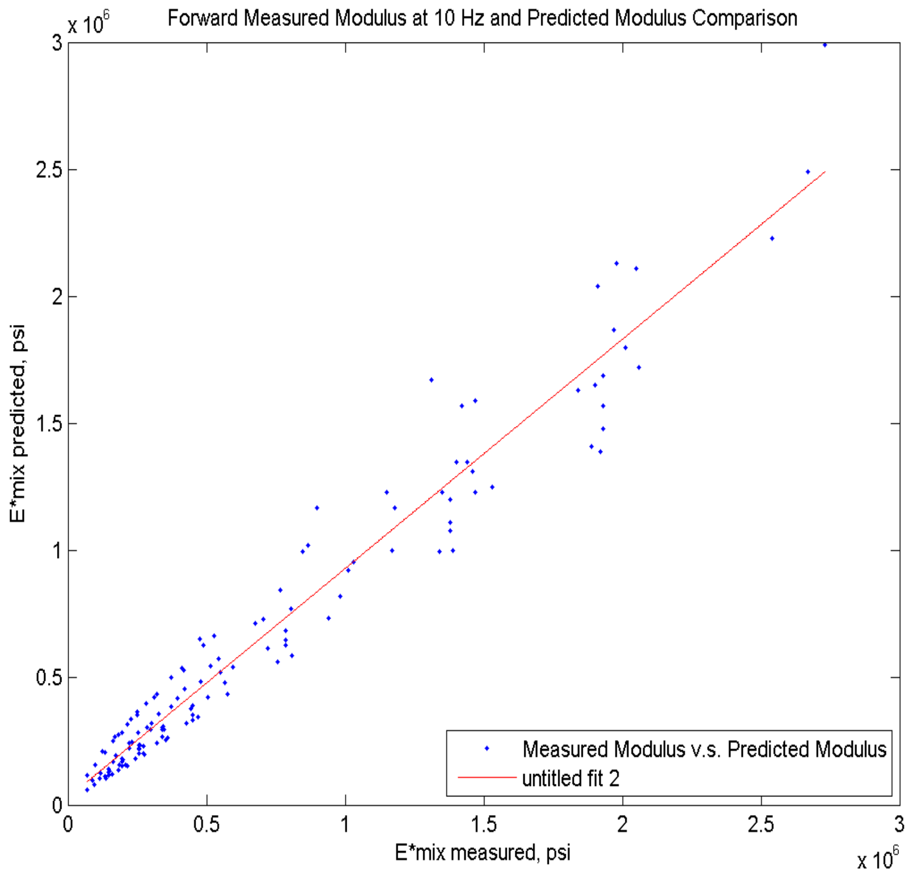
Forward Measured Modulus at 10 Hz and Predicted Modulus Comparison
x 10^6
3
2.5
2
1.5
1
0.5
0
E*mix predicted, psi
Measured Modulus v.s. Predicted Modulus
untitled fit 2
0
0.5
1
1.5
2
2.5
3
E*mix measured, psi
x 10^6

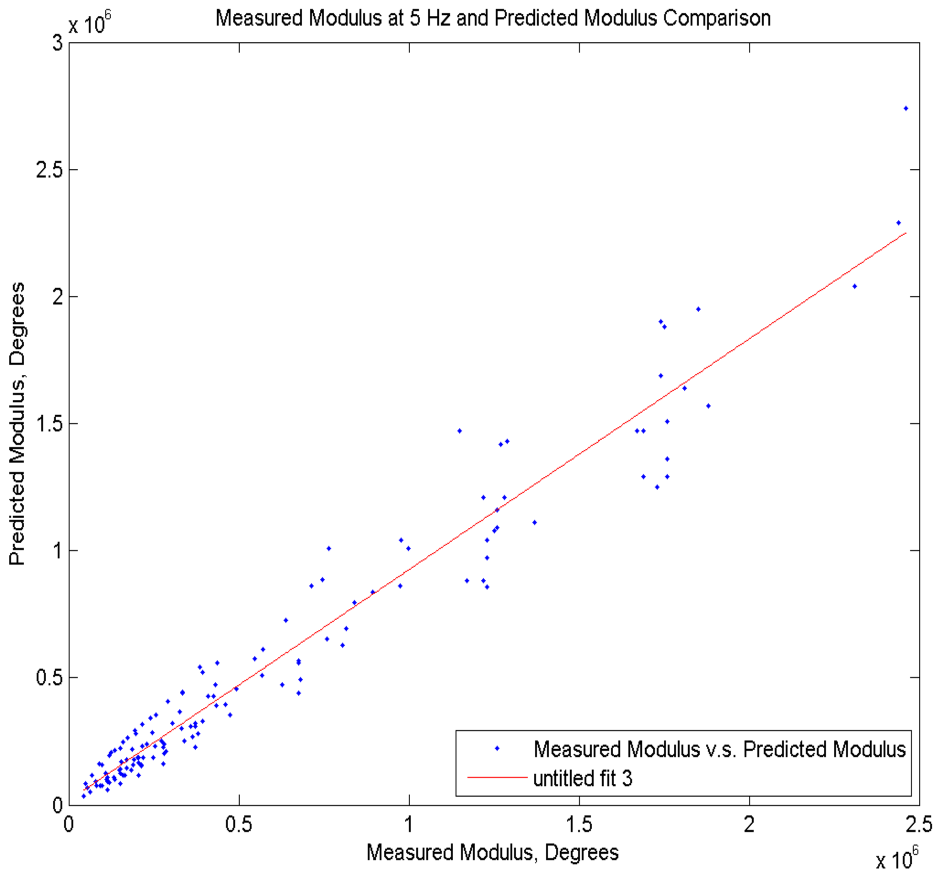
Measured Modulus at 5 Hz and Predicted Modulus Comparison
x 10^6
3
2.5
2
1.5
1
0.5
0
Predicted Modulus, Degrees
Measured Modulus v.s. Predicted Modulus
untitled fit 3
0
0.5
1
1.5
2
2.5
Measured Modulus, Degrees
x 10^6

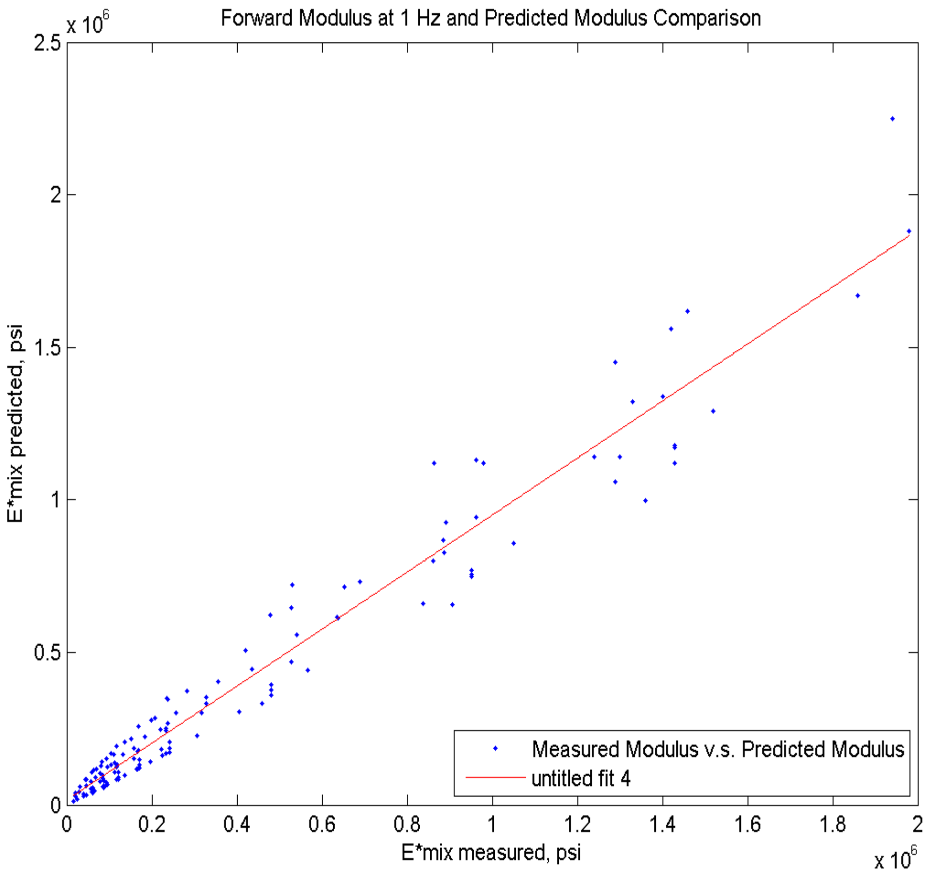
Forward Modulus at 1 Hz and Predicted Modulus Comparison
x 10^6
2.5
2
1.5
1
0.5
0
E*mix predicted, psi
0
0.2
0.4
0.6
0.8
1
1.2
1.4
1.6
1.8
2
E*mix measured, psi
x 10^6
Measured Modulus v.s. Predicted Modulus
untitled fit 4

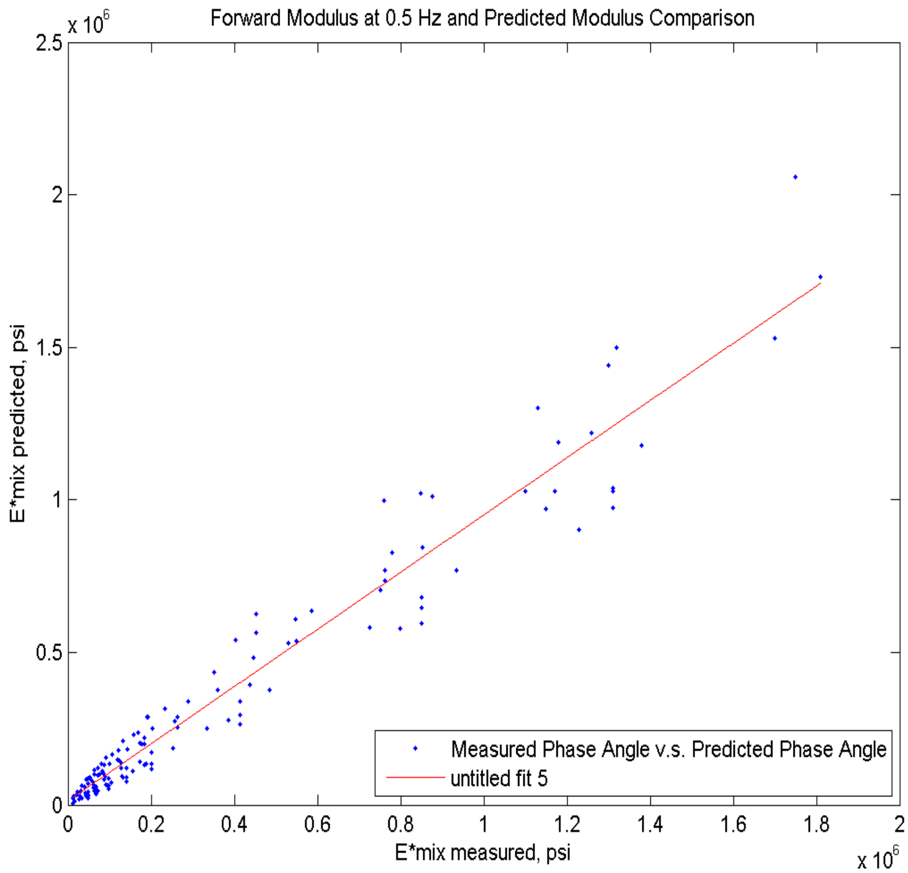
Forward Modulus at 0.5 Hz and Predicted Modulus Comparison
x 10^6
2.5
2
1.5
1
0.5
0
E*mix predicted, psi
0
0.2
0.4
0.6
0.8
1
1.2
1.4
1.6
1.8
2
E*mix measured, psi
x 10^6
Measured Phase Angle v.s. Predicted Phase Angle
untitled fit 5

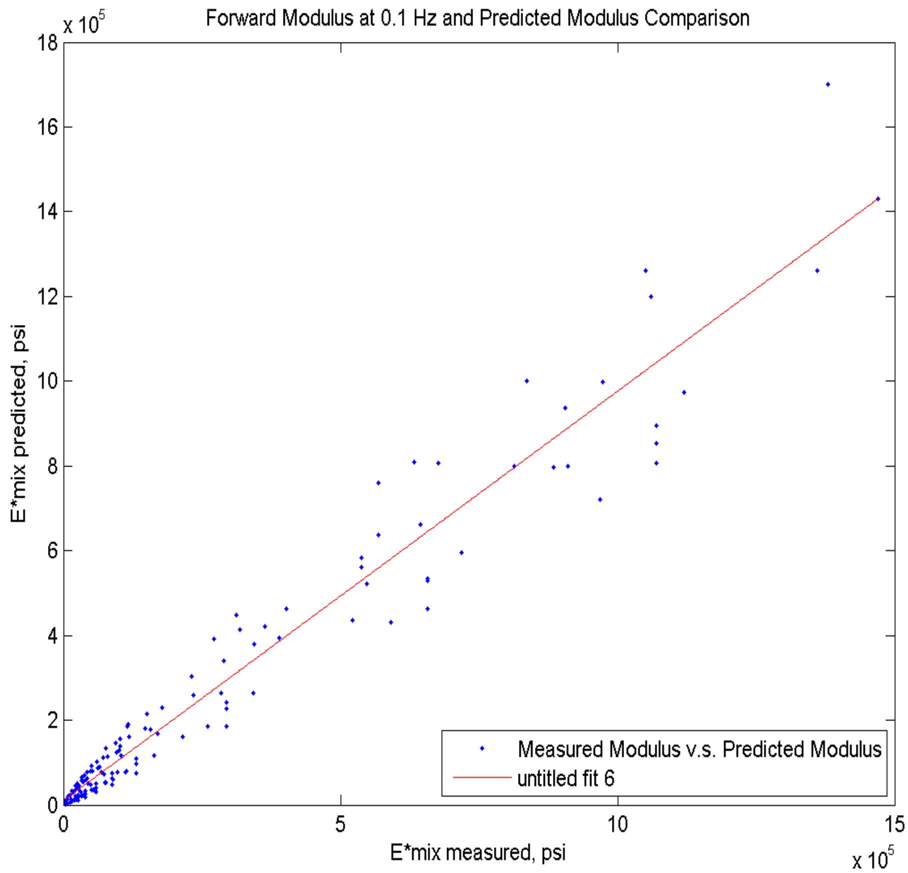

Forward Modulus at 0.1 Hz and Predicted Modulus Comparison
x 10^5
18
16
14
12
10
8
6
4
2
0
E*mix predicted, psi
0
5
10
15
E*mix measured, psi
x 10^5
Measured Modulus v.s. Predicted Modulus
untitled fit 6

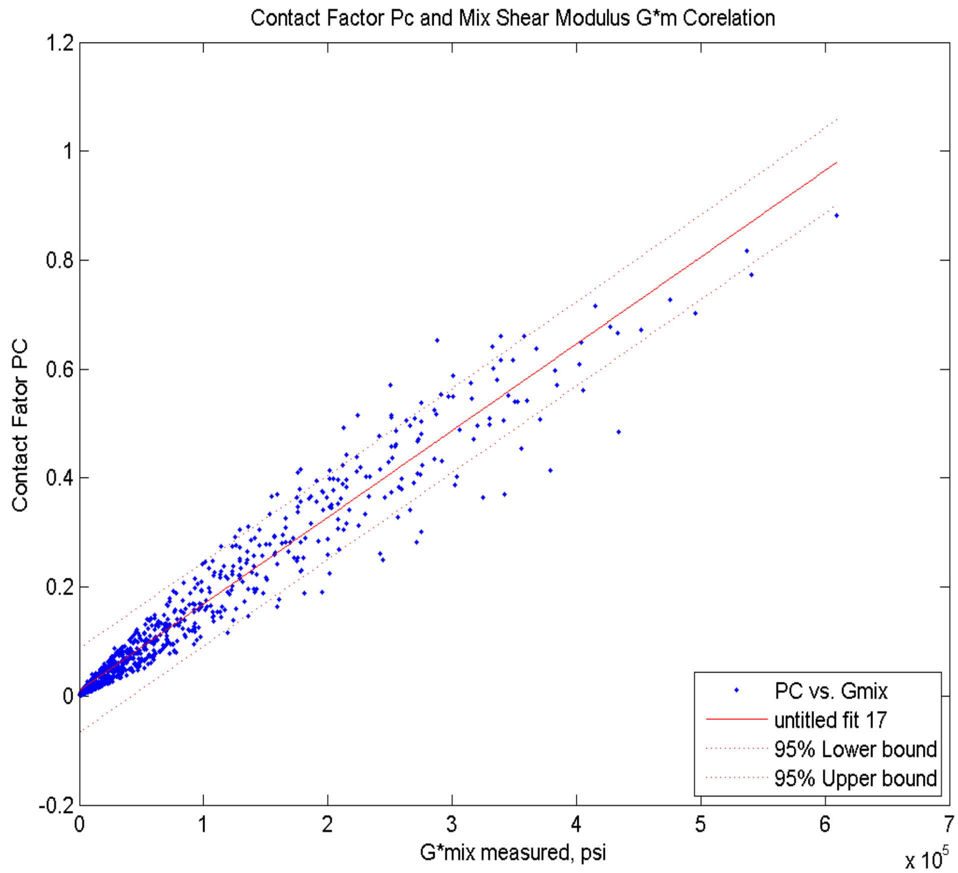
Contact Factor Pc and Mix Shear Modulus G*m Corelation
Contact Fator PC
G*mix measured, psi
x 10^5
PC vs. Gmix
untitled fit 17
95% Lower bound
95% Upper bound
1.2
1
0.8
0.6
0.4
0.2
0
-0.2
0
1
2
3
4
5
6
7

APPENDIX G - Model Verification Forward Phase Angle Model Family of Curves

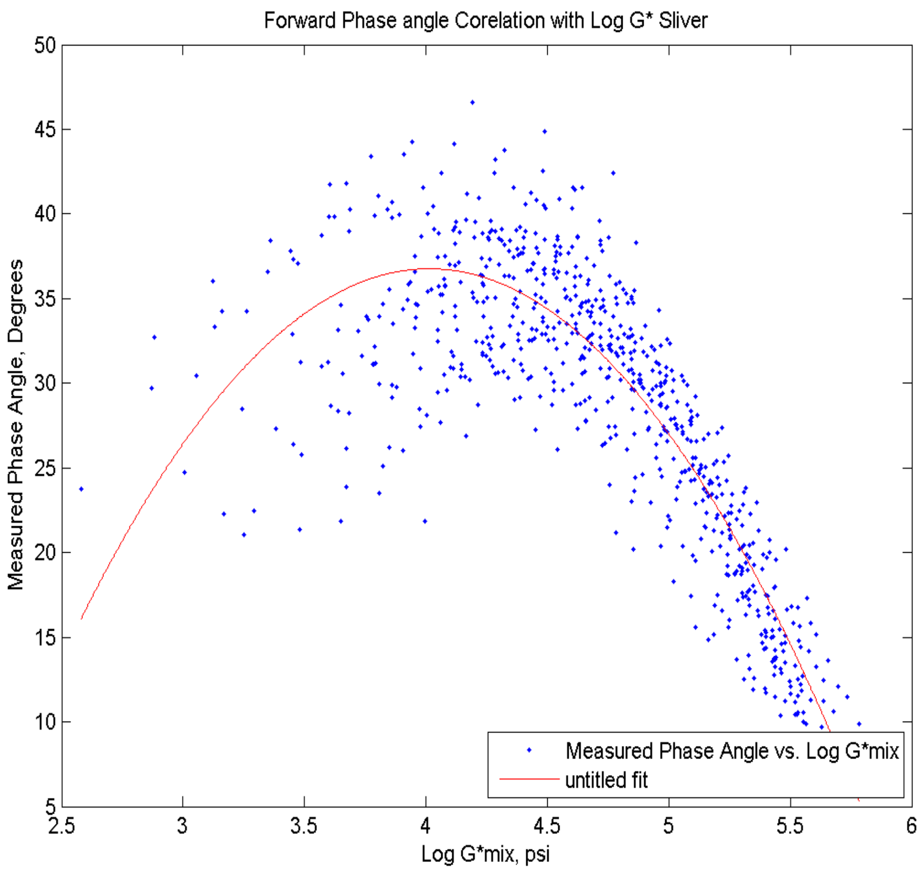

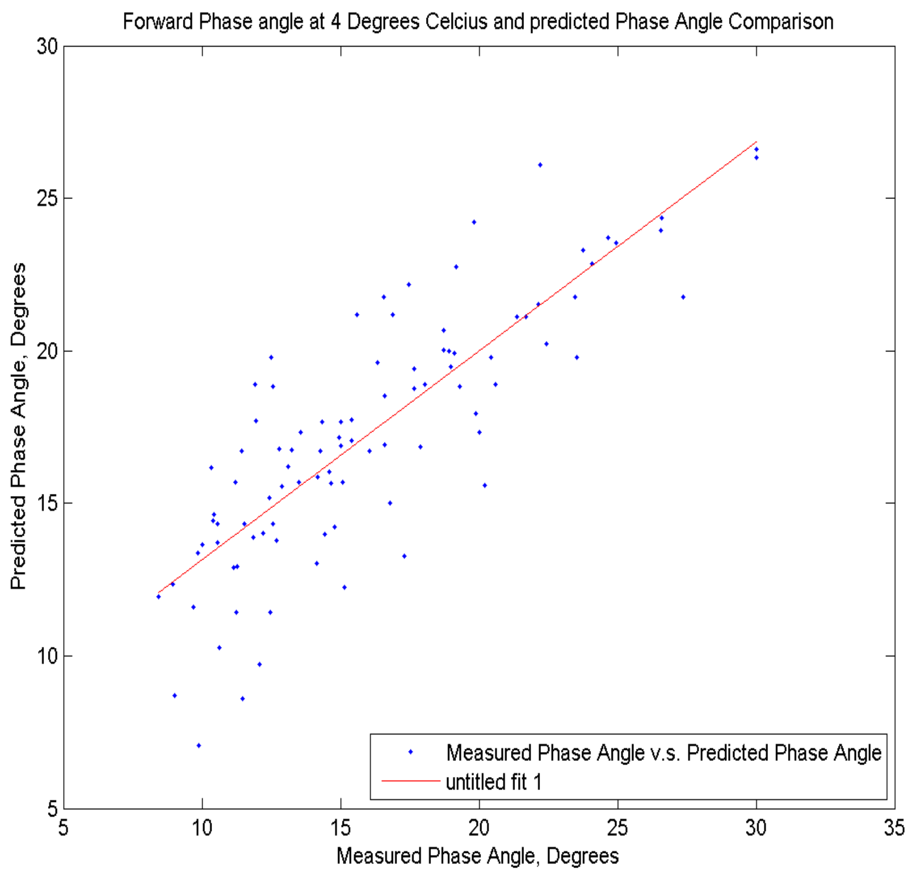
Forward Phase angle at 4 Degrees Celcius and predicted Phase Angle Comparison
Predicted Phase Angle, Degrees
Measured Phase Angle, Degrees
Measured Phase Angle v.s. Predicted Phase Angle
untitled fit 1
5
10
15
20
25
30
35

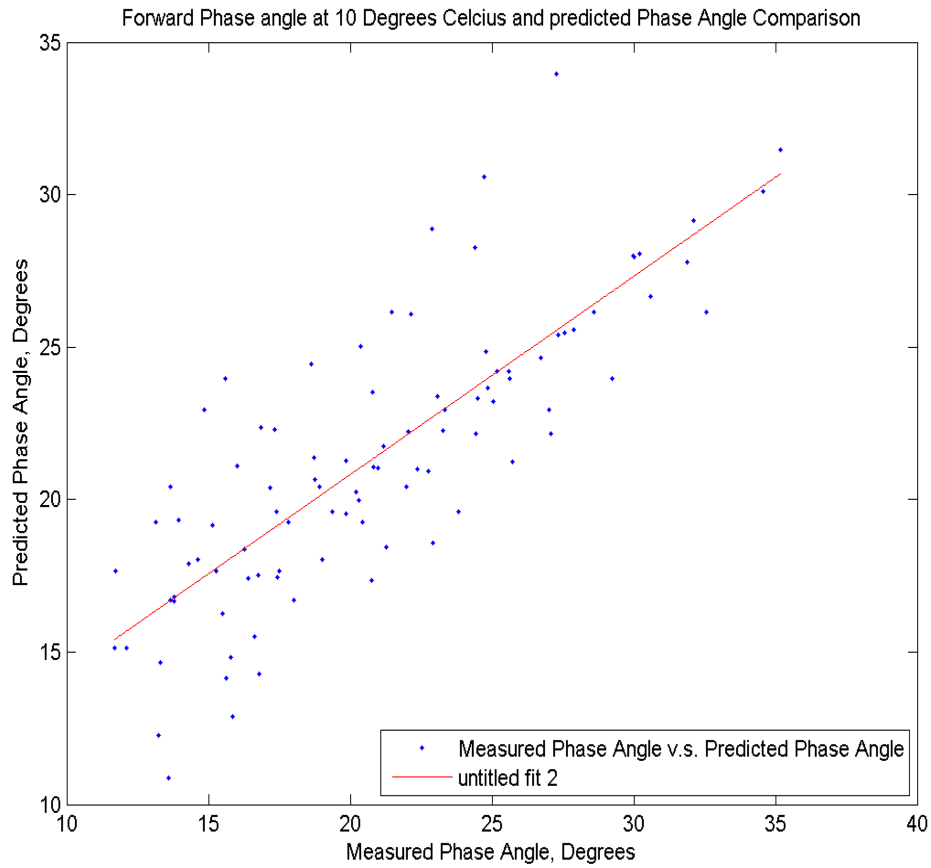
Forward Phase angle at 10 Degrees Celcius and predicted Phase Angle Comparison
Predicted Phase Angle, Degrees
Measured Phase Angle, Degrees
Measured Phase Angle v.s. Predicted Phase Angle
untitled fit 2
10
15
20
25
30
35
40

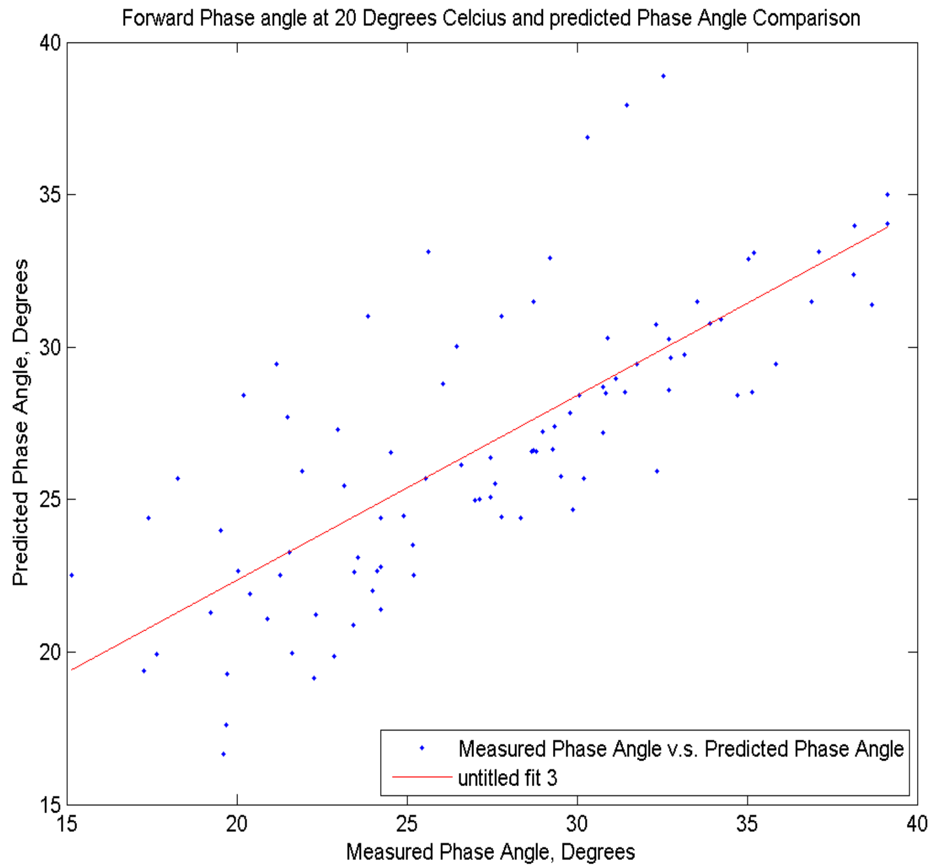
Forward Phase angle at 20 Degrees Celcius and predicted Phase Angle Comparison
Predicted Phase Angle, Degrees
Measured Phase Angle, Degrees
40
35
30
25
20
15
15
20
25
30
35
40
Measured Phase Angle v.s. Predicted Phase Angle
untitled fit 3

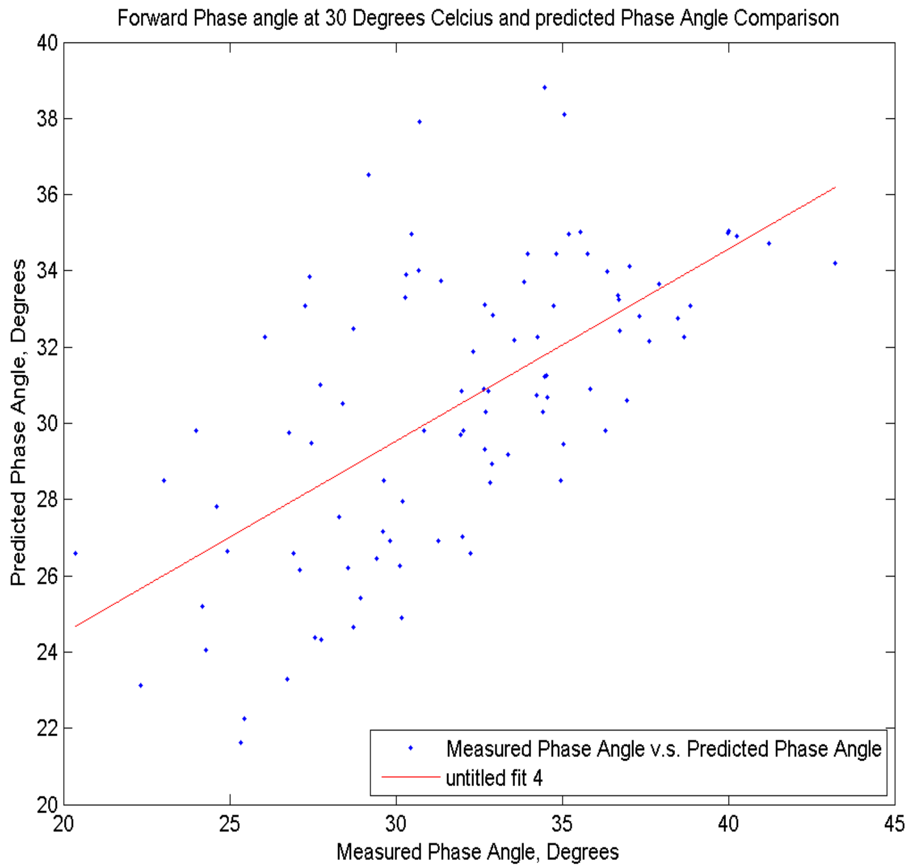
Forward Phase angle at 30 Degrees Celcius and predicted Phase Angle Comparison
Predicted Phase Angle, Degrees
Measured Phase Angle, Degrees
Measured Phase Angle v.s. Predicted Phase Angle
untitled fit 4
20
22
24
26
28
30
32
34
36
38
40
20
25
30
35
40
45

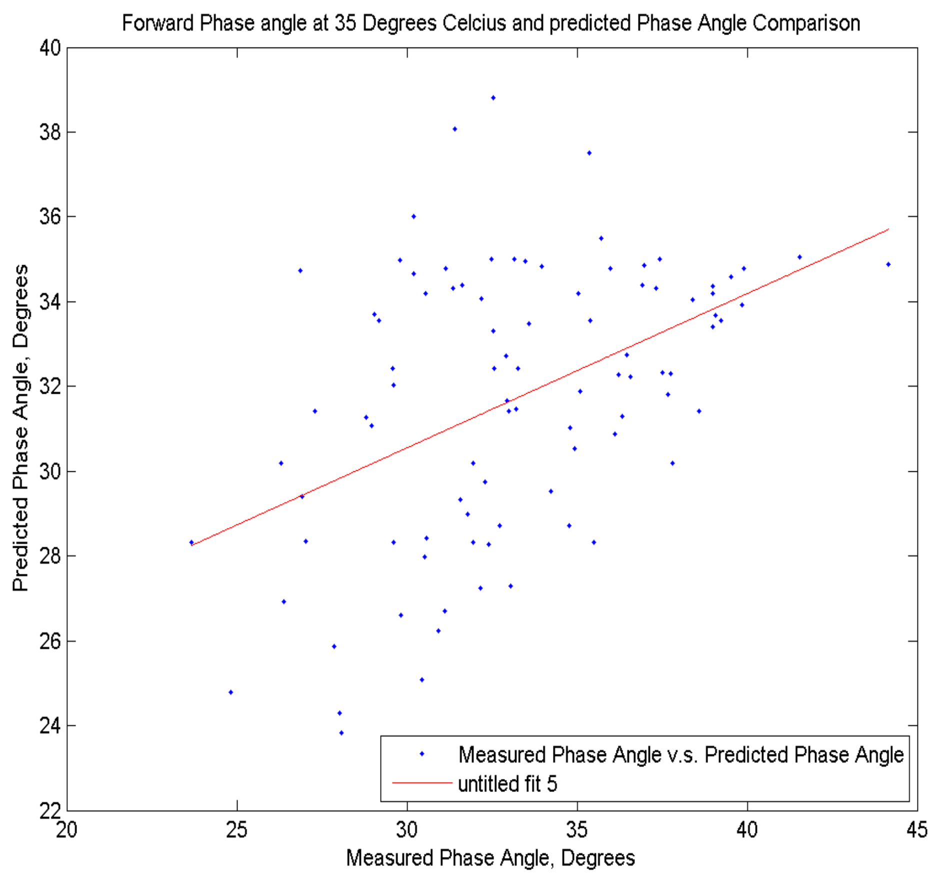

Forward Phase angle at 35 Degrees Celcius and predicted Phase Angle Comparison
Predicted Phase Angle, Degrees
Measured Phase Angle, Degrees
Measured Phase Angle v.s. Predicted Phase Angle
untitled fit 5
40
38
36
34
32
30
28
26
24
22
20
25
30
35
40
45

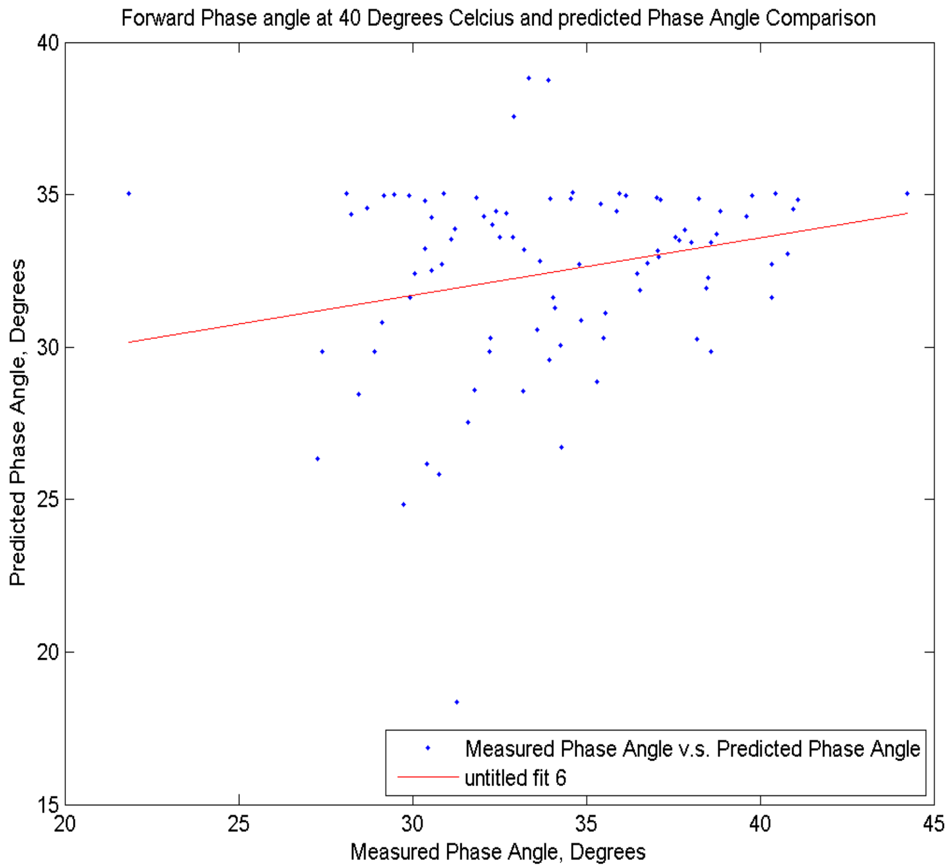
Forward Phase angle at 40 Degrees Celcius and predicted Phase Angle Comparison
Predicted Phase Angle, Degrees
Measured Phase Angle, Degrees
40
35
30
25
20
15
20
25
30
35
40
45
Measured Phase Angle v.s. Predicted Phase Angle
untitled fit 6

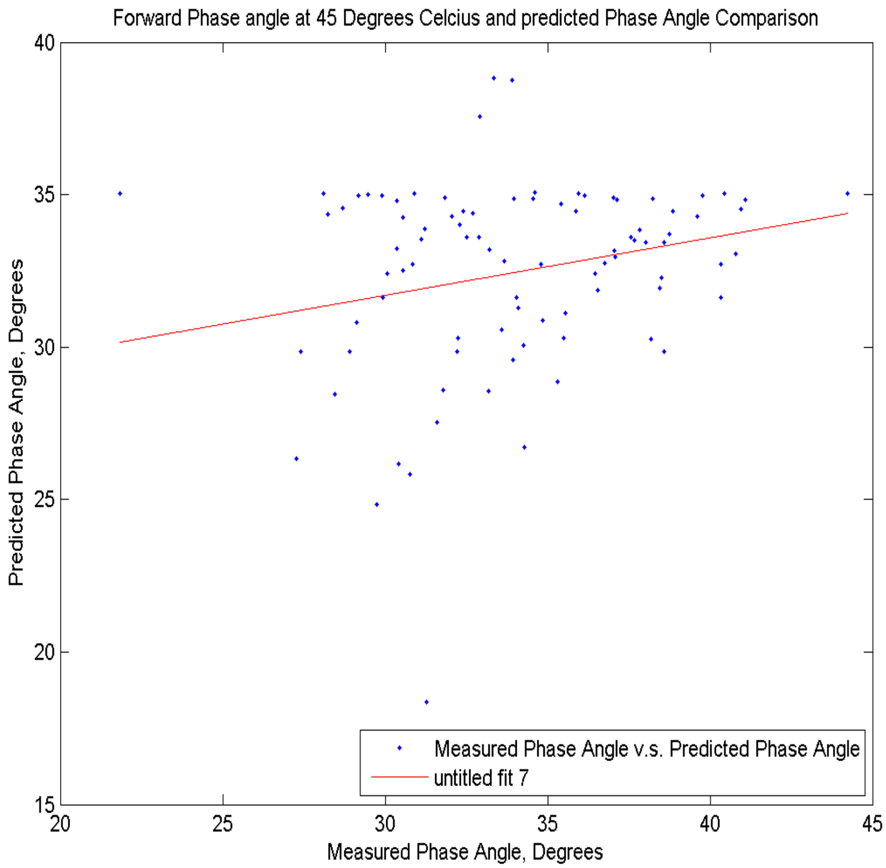
Forward Phase angle at 45 Degrees Celcius and predicted Phase Angle Comparison
Predicted Phase Angle, Degrees
Measured Phase Angle, Degrees
40
35
30
25
20
15
20
25
30
35
40
45
Measured Phase Angle v.s. Predicted Phase Angle
untitled fit 7

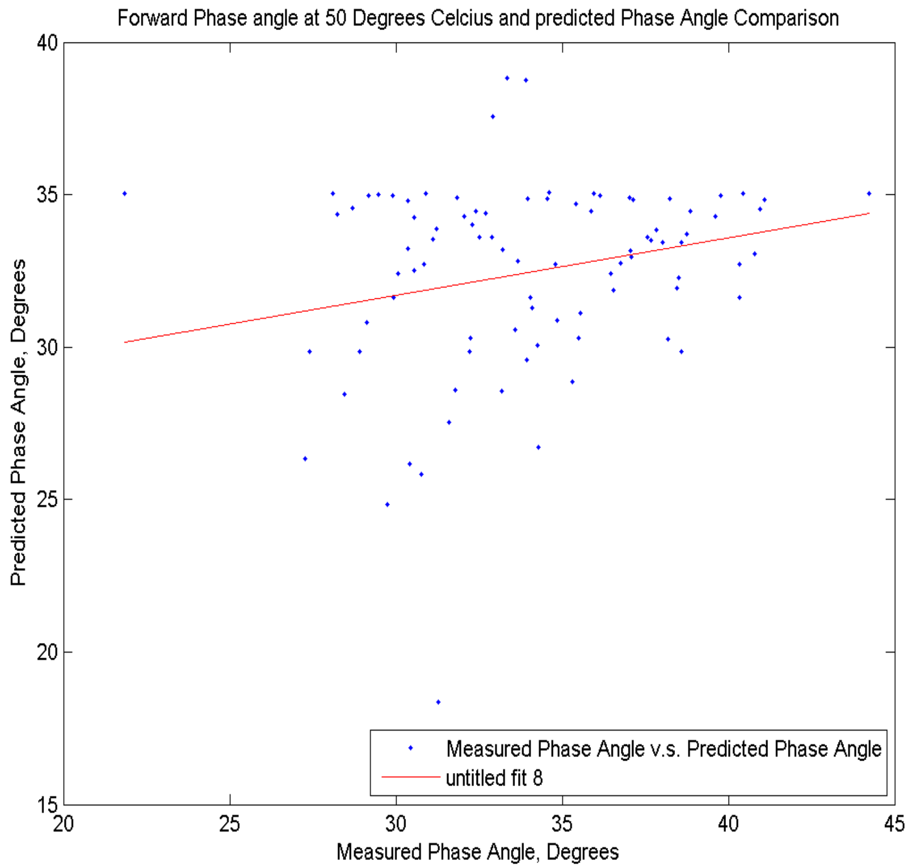
Forward Phase angle at 50 Degrees Celcius and predicted Phase Angle Comparison
Predicted Phase Angle, Degrees
Measured Phase Angle, Degrees
Measured Phase Angle v.s. Predicted Phase Angle
untitled fit 8
40
35
30
25
20
15
20
25
30
35
40
45

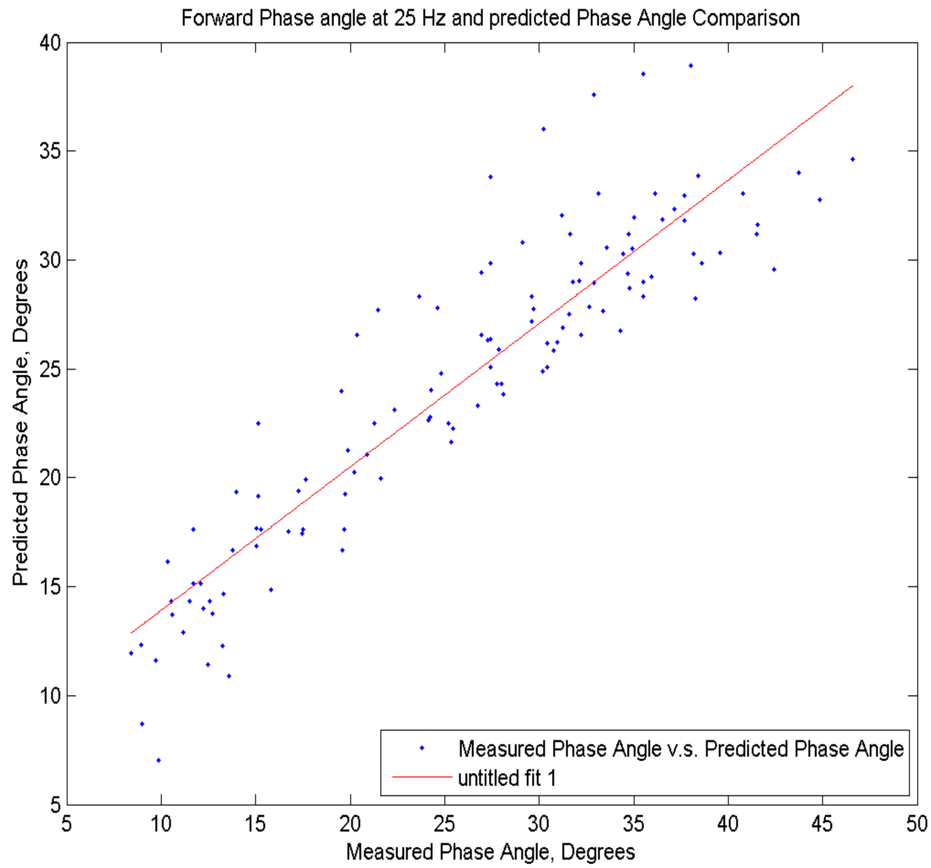
Forward Phase angle at 25 Hz and predicted Phase Angle Comparison
Predicted Phase Angle, Degrees
Measured Phase Angle, Degrees
Measured Phase Angle v.s. Predicted Phase Angle
untitled fit 1
40
35
30
25
20
15
10
5
5
10
15
20
25
30
35
40
45
50

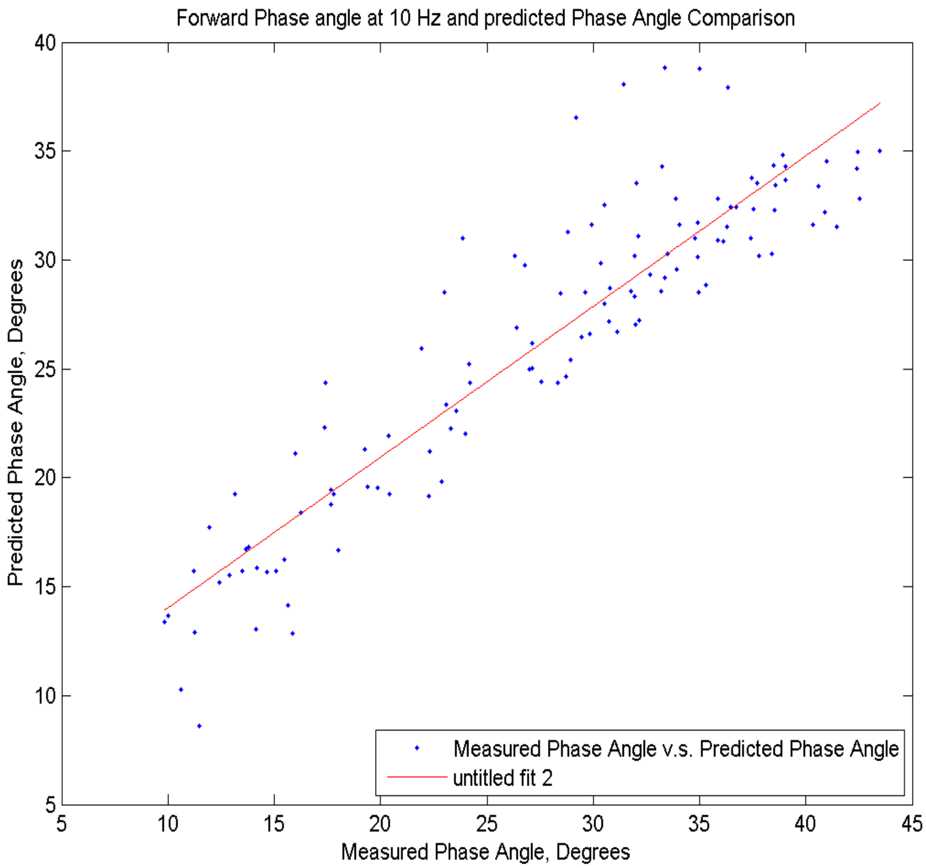

Forward Phase angle at 10 Hz and predicted Phase Angle Comparison
Predicted Phase Angle, Degrees
Measured Phase Angle, Degrees
Measured Phase Angle v.s. Predicted Phase Angle
untitled fit 2
5
10
15
20
25
30
35
40
45

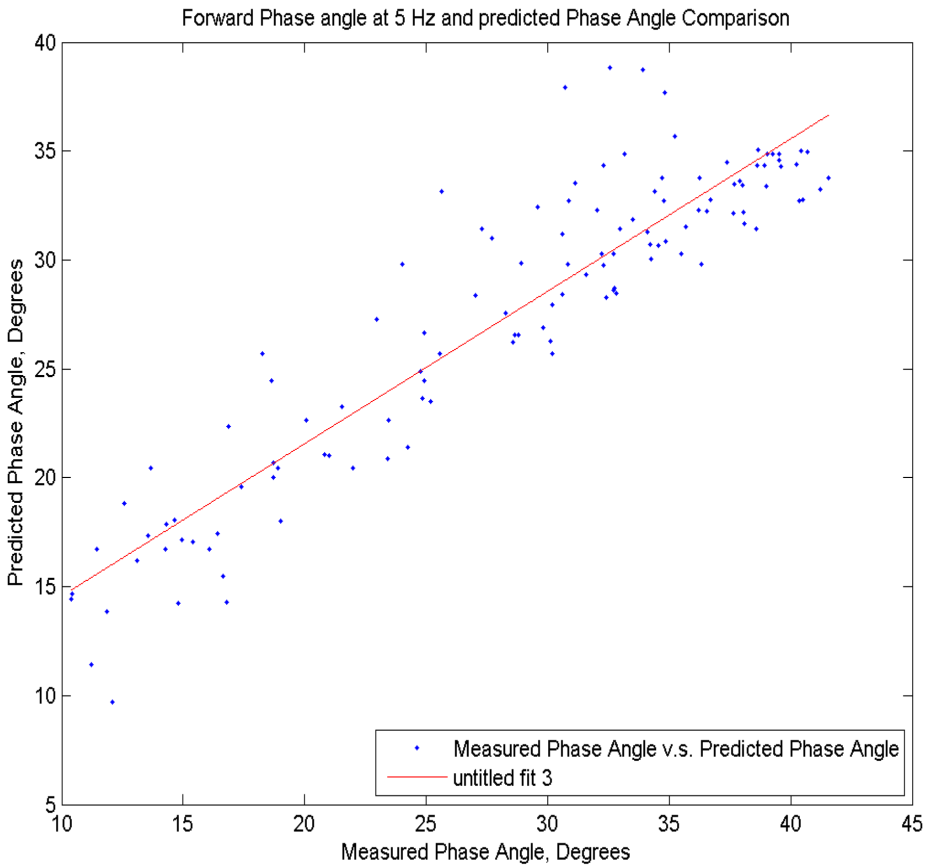

Forward Phase angle at 5 Hz and predicted Phase Angle Comparison
Predicted Phase Angle, Degrees
Measured Phase Angle, Degrees
40
35
30
25
20
15
10
5
10
15
20
25
30
35
40
45
Measured Phase Angle v.s. Predicted Phase Angle
untitled fit 3

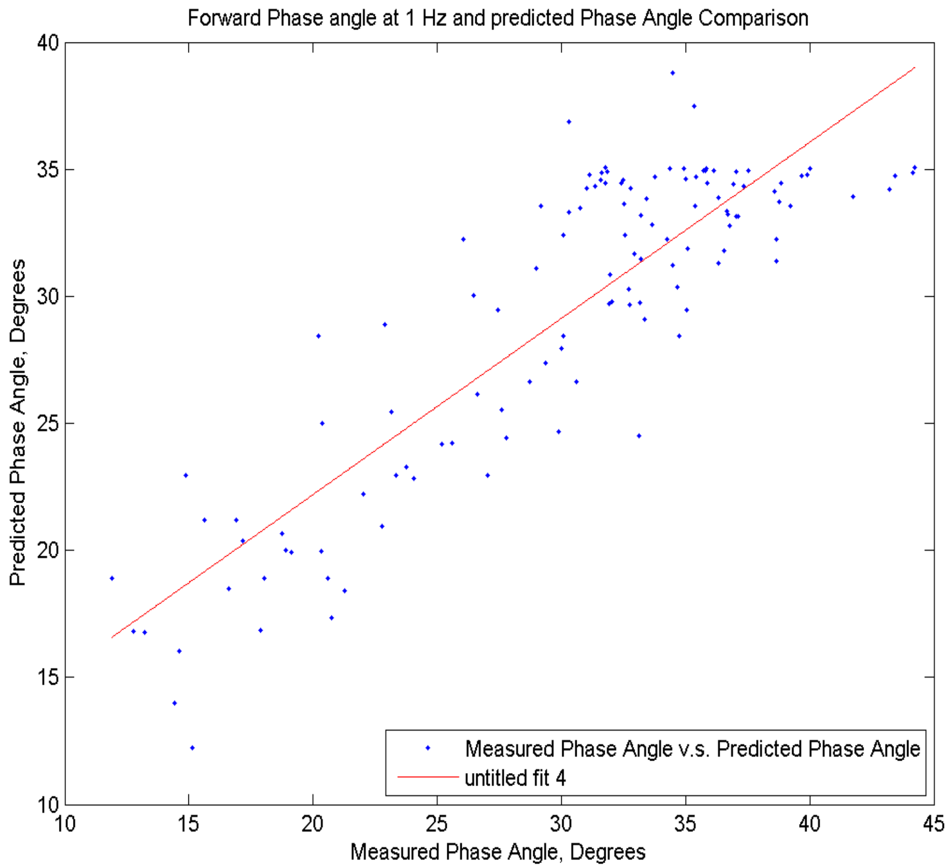
Forward Phase angle at 1 Hz and predicted Phase Angle Comparison
Predicted Phase Angle, Degrees
Measured Phase Angle, Degrees
Measured Phase Angle v.s. Predicted Phase Angle
untitled fit 4
10
15
20
25
30
35
40
45

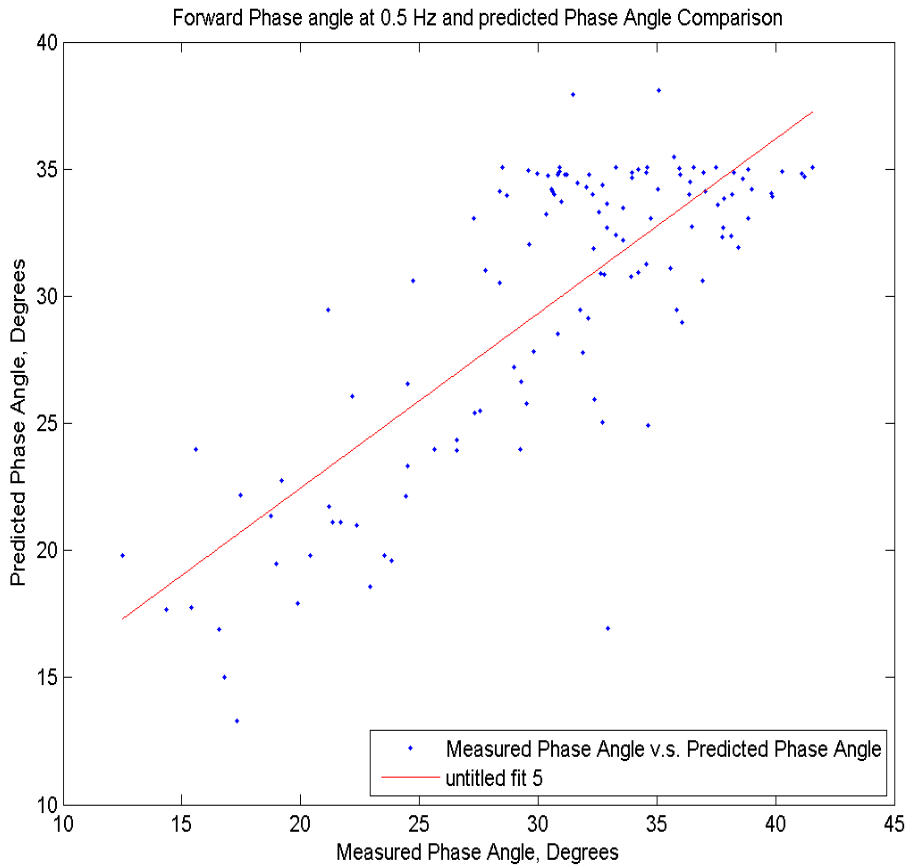

Forward Phase angle at 0.5 Hz and predicted Phase Angle Comparison
Predicted Phase Angle, Degrees
Measured Phase Angle, Degrees
Measured Phase Angle v.s. Predicted Phase Angle
untitled fit 5
10
15
20
25
30
35
40
45

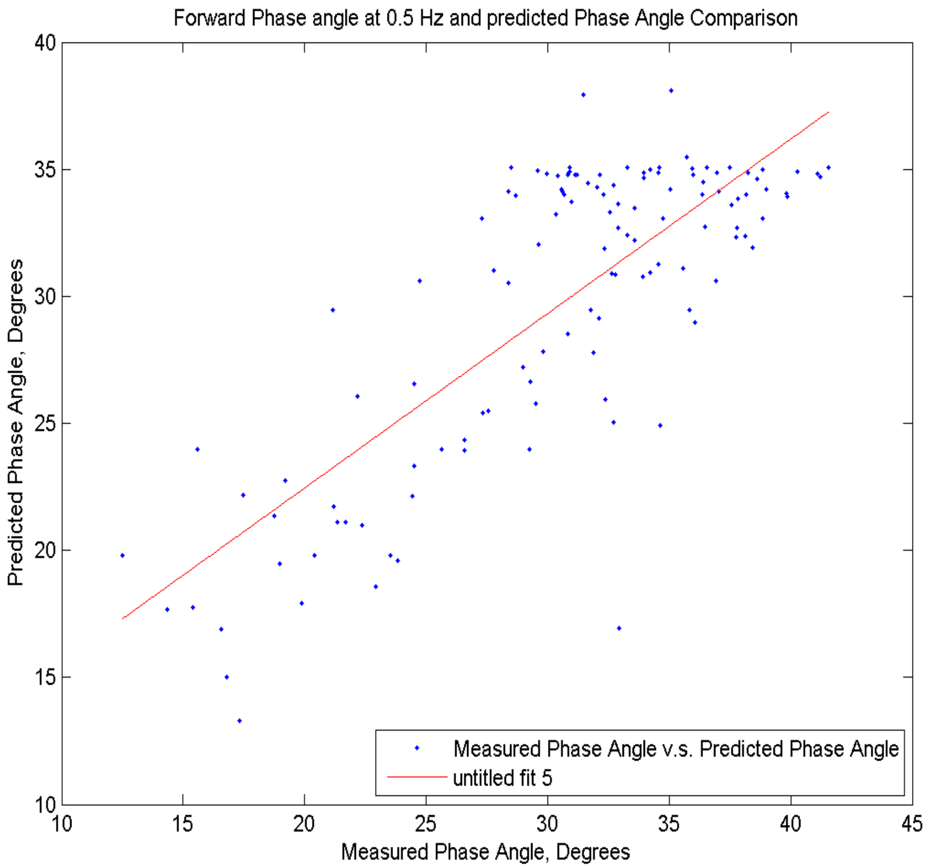
Forward Phase angle at 0.5 Hz and predicted Phase Angle Comparison
Predicted Phase Angle, Degrees
Measured Phase Angle, Degrees
Measured Phase Angle v.s. Predicted Phase Angle
untitled fit 5
10
15
20
25
30
35
40
45

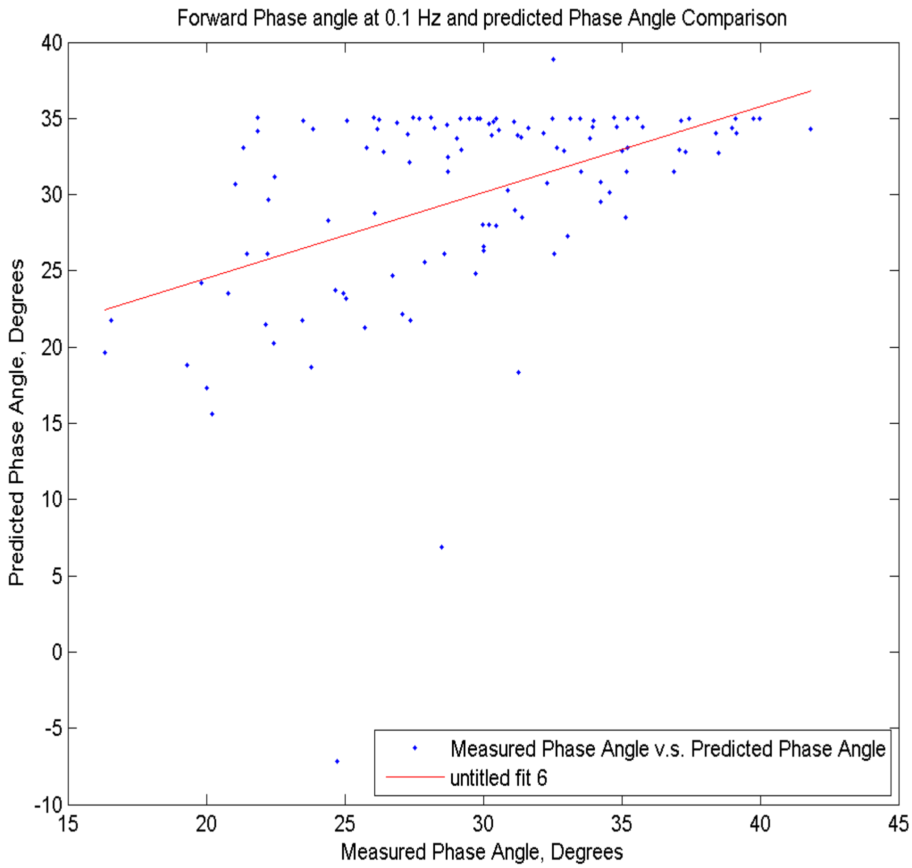

Forward Phase angle at 0.1 Hz and predicted Phase Angle Comparison
Predicted Phase Angle, Degrees
Measured Phase Angle, Degrees
Measured Phase Angle v.s. Predicted Phase Angle
untitled fit 6
40
35
30
25
20
15
10
5
0
-5
-10
15
20
25
30
35
40
45

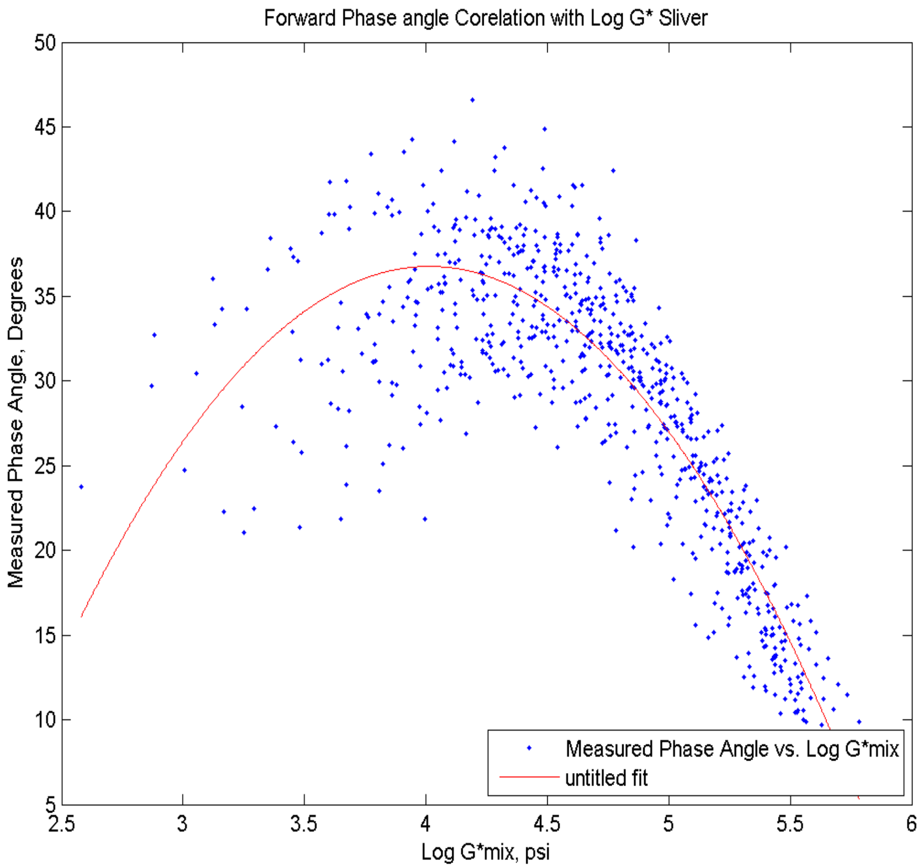
Forward Phase angle Corelation with Log G* Sliver
Measured Phase Angle, Degrees
Log G*mix, psi
Measured Phase Angle vs. Log G*mix
untitled fit
50
45
40
35
30
25
20
15
10
5
2.5
3
3.5
4
4.5
5
5.5
6

APPENDIX H - Model verification backward asphalt binder shear modulus calculation family of curves

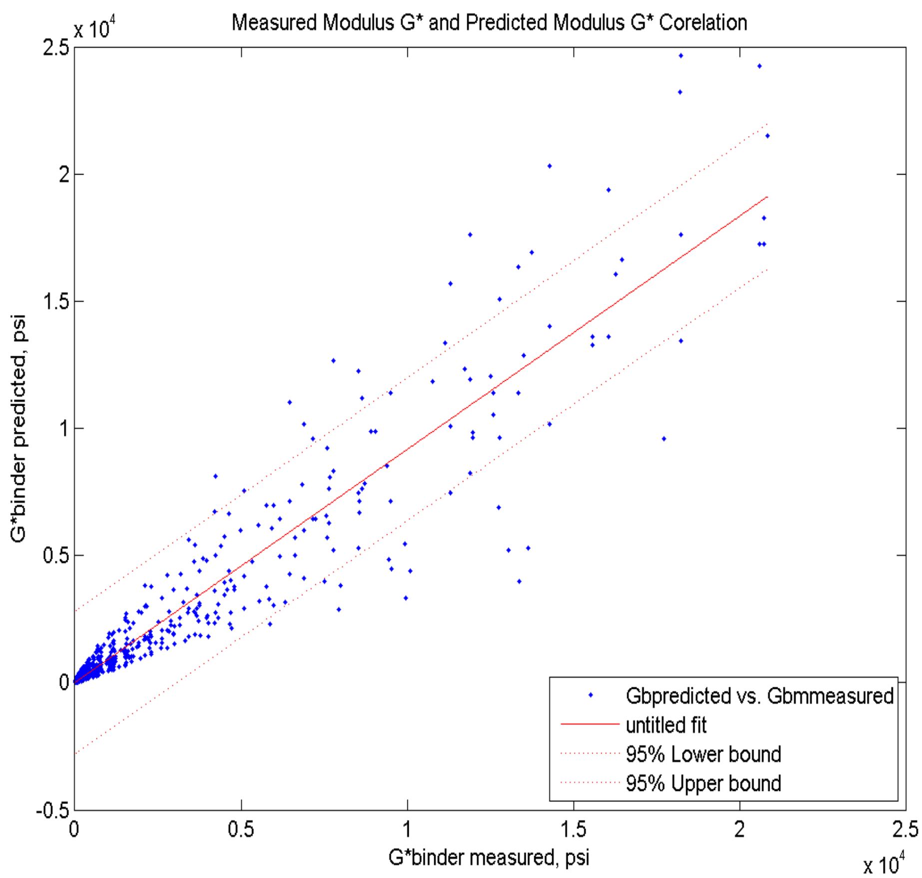

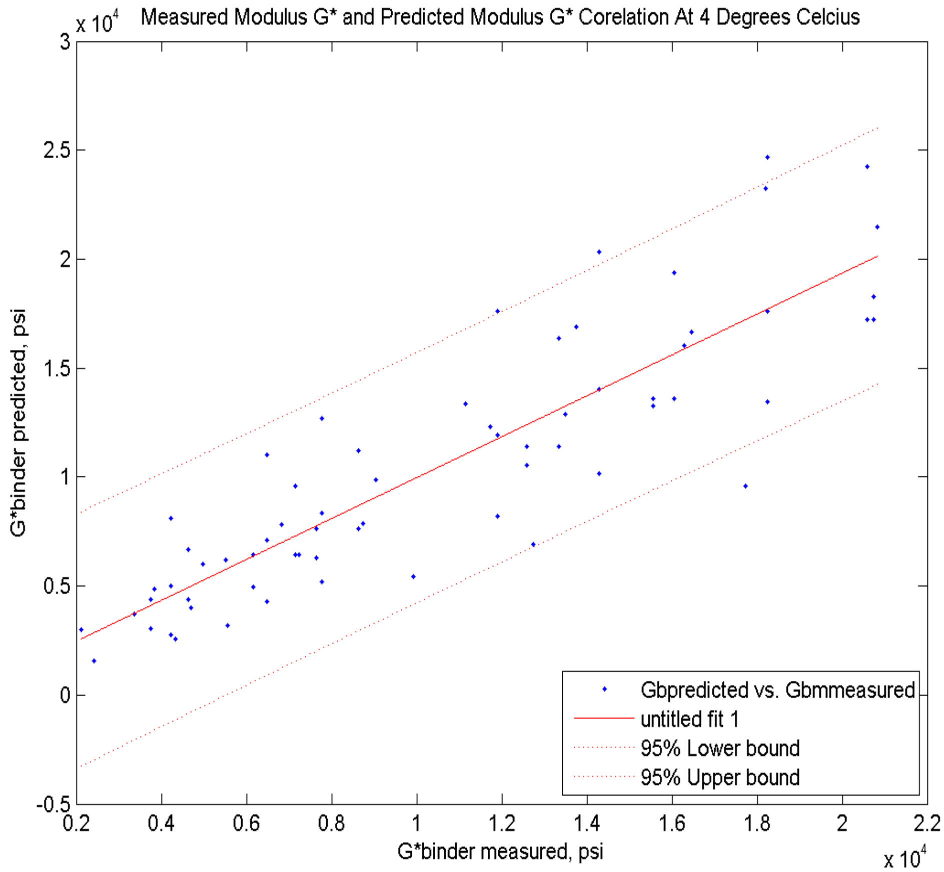

Measured Modulus G* and Predicted Modulus G* Corelation At 4 Degrees Celcius
x 10^4
3
2.5
2
1.5
1
0.5
0
-0.5
G*binder predicted, psi
0.2
0.4
0.6
0.8
1
1.2
1.4
1.6
1.8
2
2.2
G*binder measured, psi
x 10^4
Gbpredicted vs. Gbmmeasured
untitled fit 1
95% Lower bound
95% Upper bound

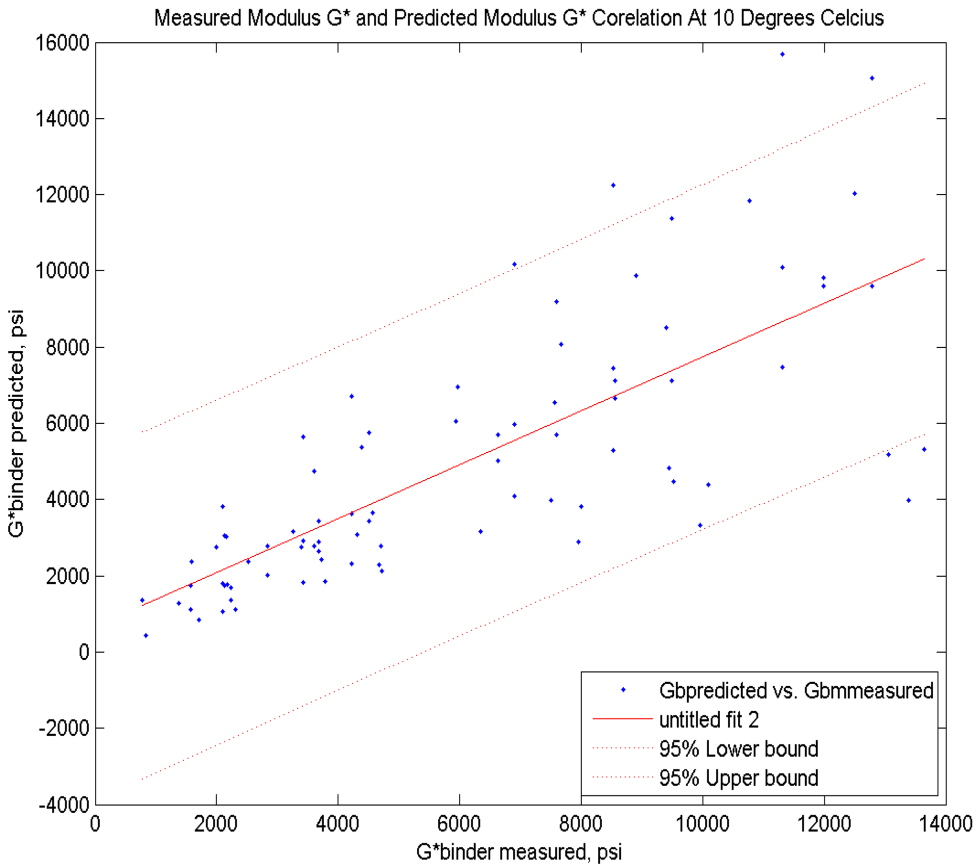

Measured Modulus G* and Predicted Modulus G* Corelation At 10 Degrees Celcius
G*binder predicted, psi
G*binder measured, psi
16000
14000
12000
10000
8000
6000
4000
2000
0
-2000
-4000
0
2000
4000
6000
8000
10000
12000
14000
Gbpredicted vs. Gbmmeasured
untitled fit 2
95% Lower bound
95% Upper bound

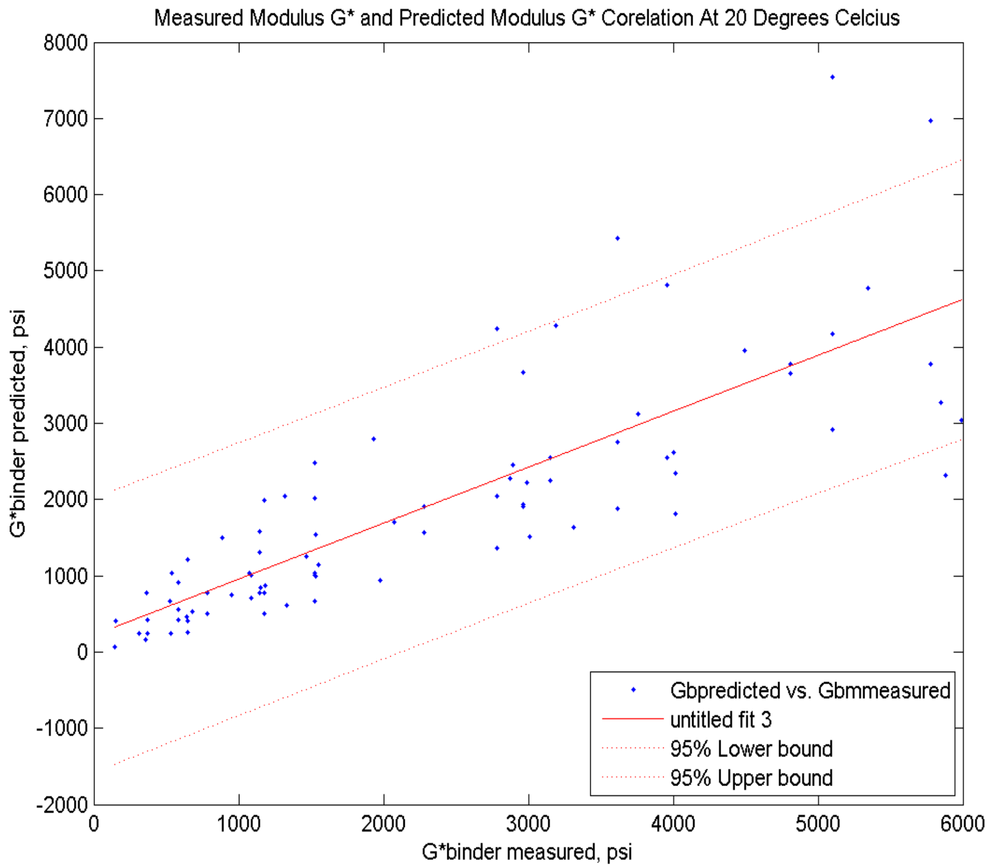

Measured Modulus G* and Predicted Modulus G* Corelation At 20 Degrees Celcius
G*binder predicted, psi
G*binder measured, psi
8000
7000
6000
5000
4000
3000
2000
1000
0
-1000
-2000
0
1000
2000
3000
4000
5000
6000
Gbpredicted vs. Gbmmeasured
untitled fit 3
95% Lower bound
95% Upper bound

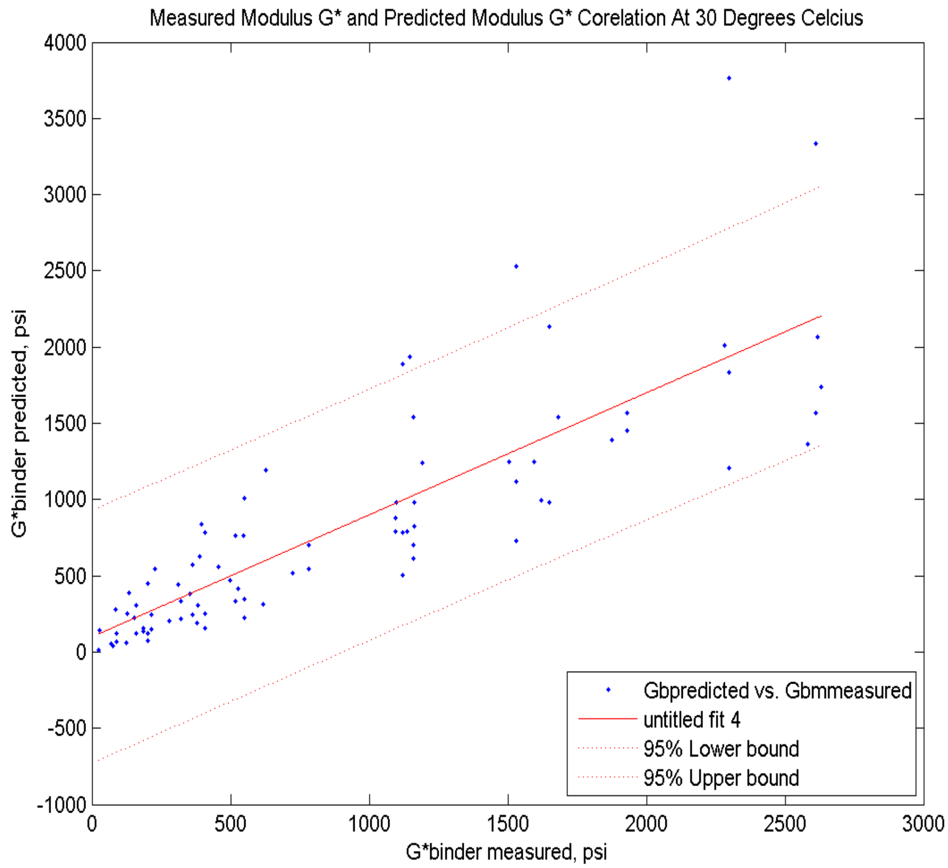
Measured Modulus G* and Predicted Modulus G* Corelation At 30 Degrees Celcius
G*binder predicted, psi
G*binder measured, psi
4000
3500
3000
2500
2000
1500
1000
500
0
-500
-1000
0
500
1000
1500
2000
2500
3000
Gbpredicted vs. Gbmmeasured
untitled fit 4
95% Lower bound
95% Upper bound

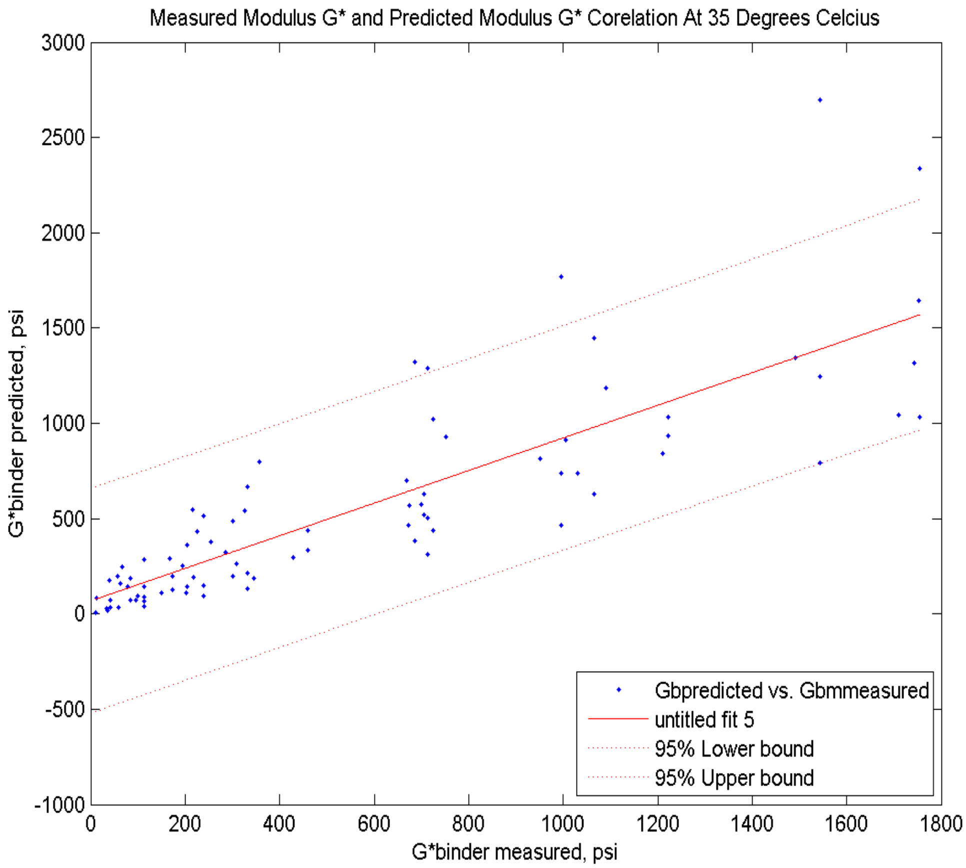

Measured Modulus G* and Predicted Modulus G* Corelation At 35 Degrees Celcius
G*binder predicted, psi
G*binder measured, psi
3000
2500
2000
1500
1000
500
0
-500
-1000
0
200
400
600
800
1000
1200
1400
1600
1800
Gbpredicted vs. Gbmmeasured
untitled fit 5
95% Lower bound
95% Upper bound

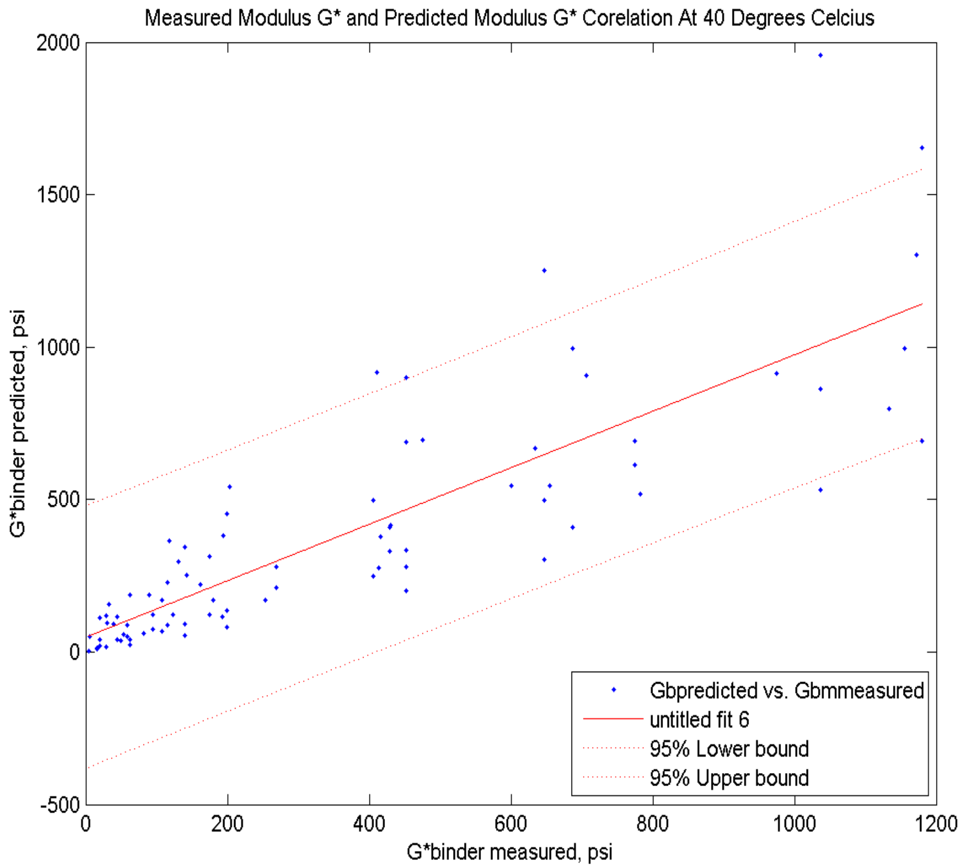

Measured Modulus G* and Predicted Modulus G* Corelation At 40 Degrees Celcius
G*binder predicted, psi
G*binder measured, psi
2000
1500
1000
500
0
-500
0
200
400
600
800
1000
1200
Gbpredicted vs. Gbmmeasured
untitled fit 6
95% Lower bound
95% Upper bound

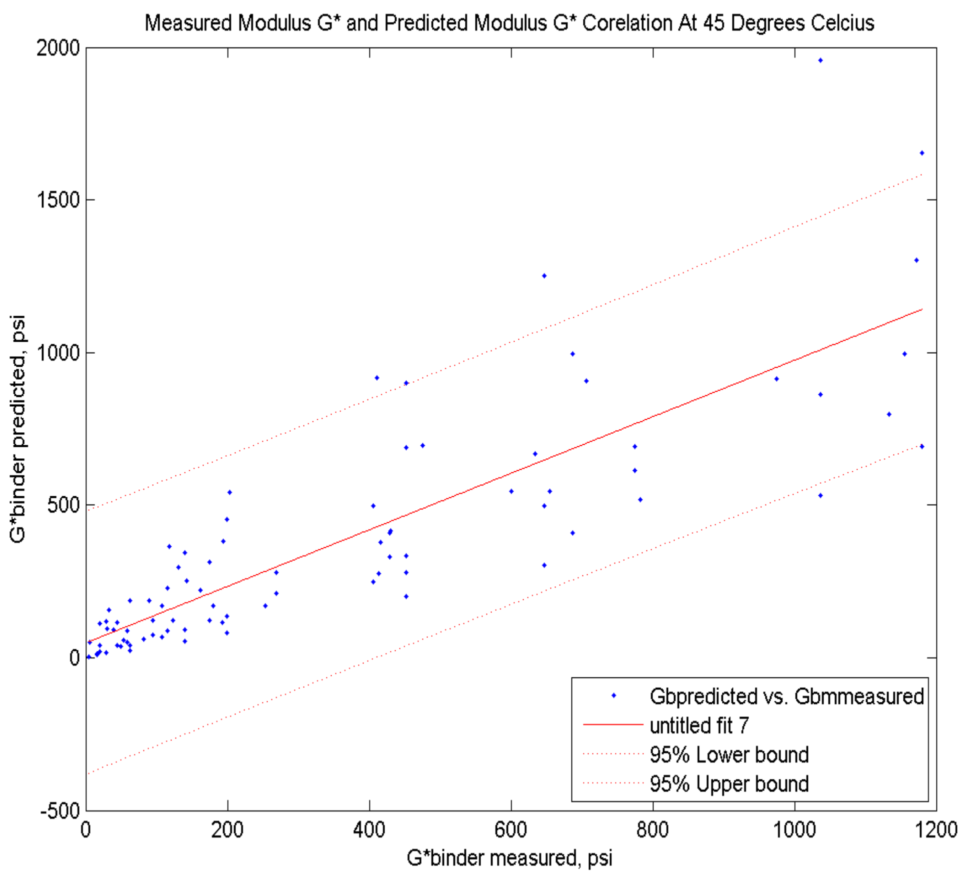

Measured Modulus G* and Predicted Modulus G* Corelation At 45 Degrees Celcius
G*binder predicted, psi
G*binder measured, psi
2000
1500
1000
500
0
-500
0
200
400
600
800
1000
1200
Gbpredicted vs. Gbmmeasured
untitled fit 7
95% Lower bound
95% Upper bound

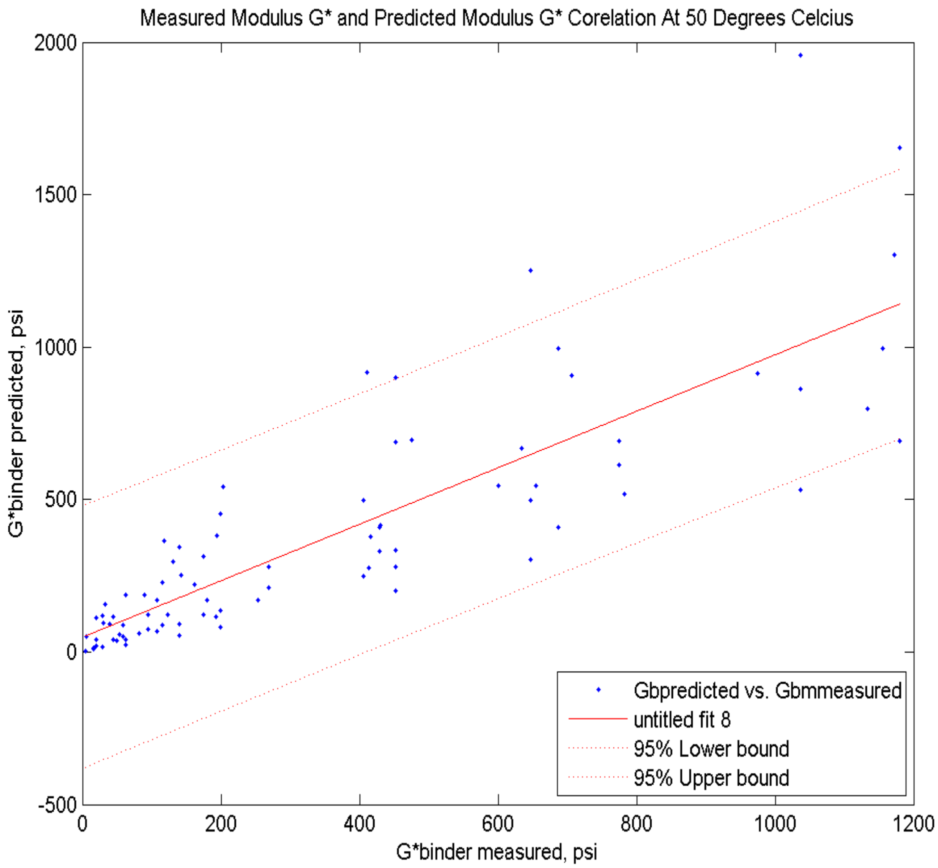
Measured Modulus G* and Predicted Modulus G* Corelation At 50 Degrees Celcius
2000
1500
1000
500
0
-500
0
200
400
600
800
1000
1200
G*binder predicted, psi
G*binder measured, psi
Gbpredicted vs. Gbmmeasured
untitled fit 8
95% Lower bound
95% Upper bound

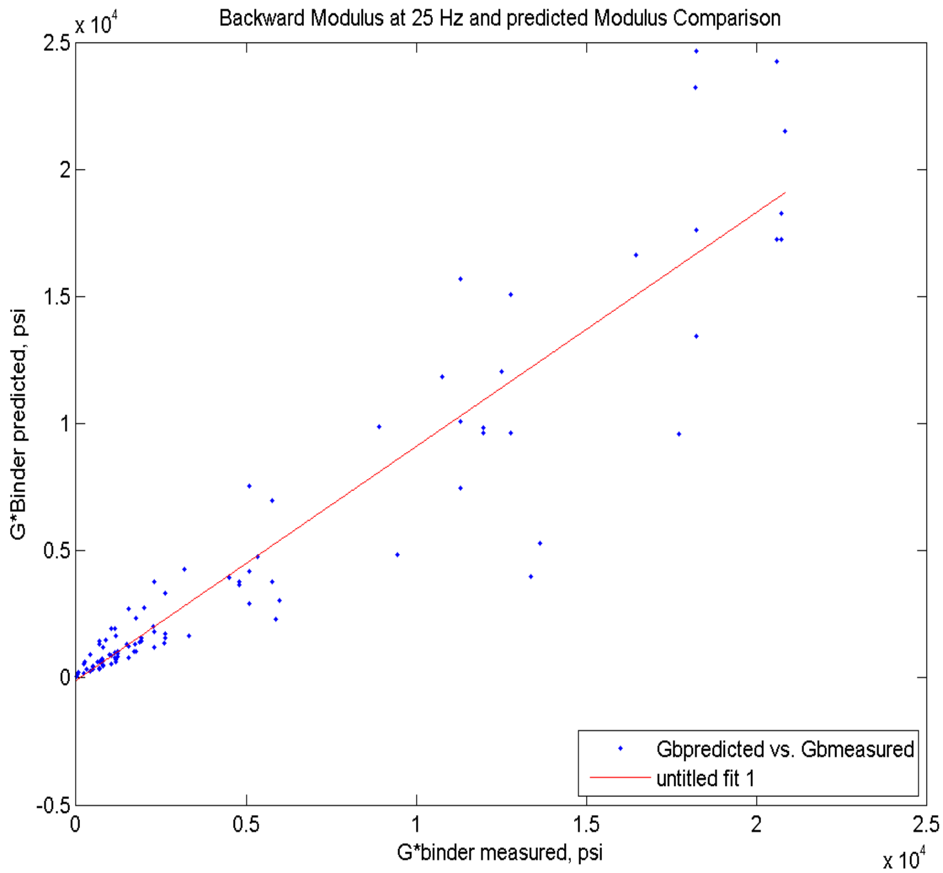
Backward Modulus at 25 Hz and predicted Modulus Comparison
x 10^4
2.5
2
1.5
1
0.5
0
-0.5
G*Binder predicted, psi
0
0.5
1
1.5
2
2.5
G*binder measured, psi
x 10^4
Gbpredicted vs. Gbmeasured
untitled fit 1

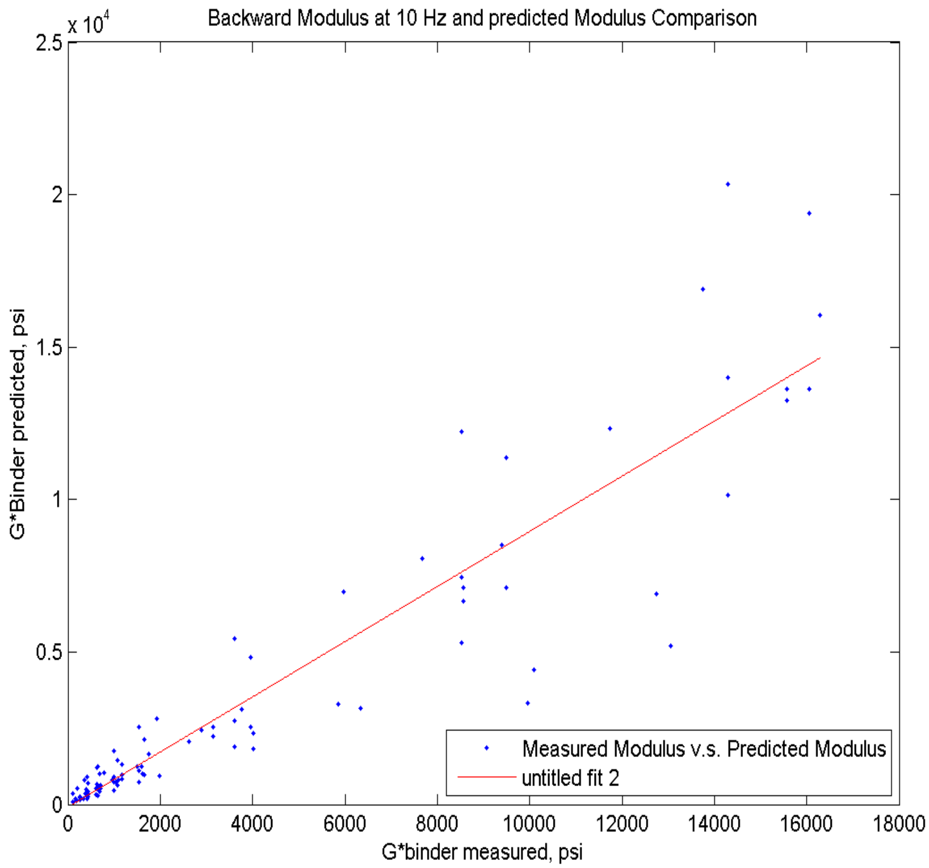
Backward Modulus at 10 Hz and predicted Modulus Comparison
x 10^4
2.5
2
1.5
1
0.5
0
G*Binder predicted, psi
0
2000
4000
6000
8000
10000
12000
14000
16000
18000
G*binder measured, psi
Measured Modulus v.s. Predicted Modulus
untitled fit 2

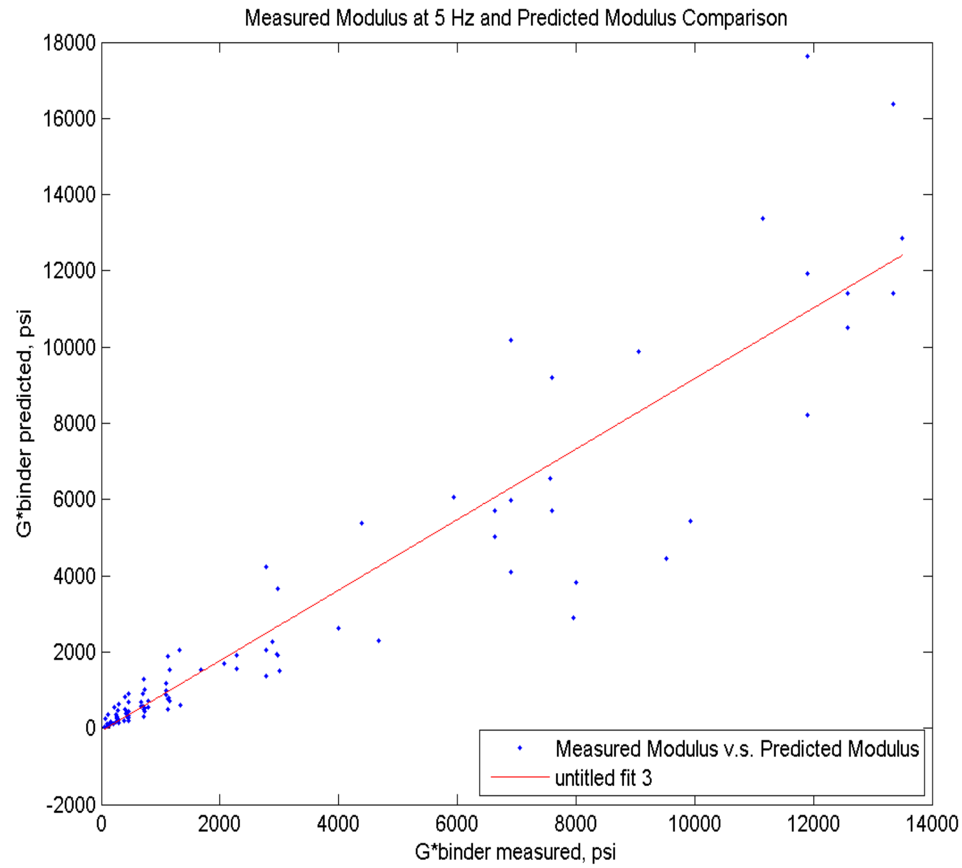
Measured Modulus at 5 Hz and Predicted Modulus Comparison
G*binder predicted, psi
G*binder measured, psi
18000
16000
14000
12000
10000
8000
6000
4000
2000
0
-2000
0
2000
4000
6000
8000
10000
12000
14000
Measured Modulus v.s. Predicted Modulus
untitled fit 3

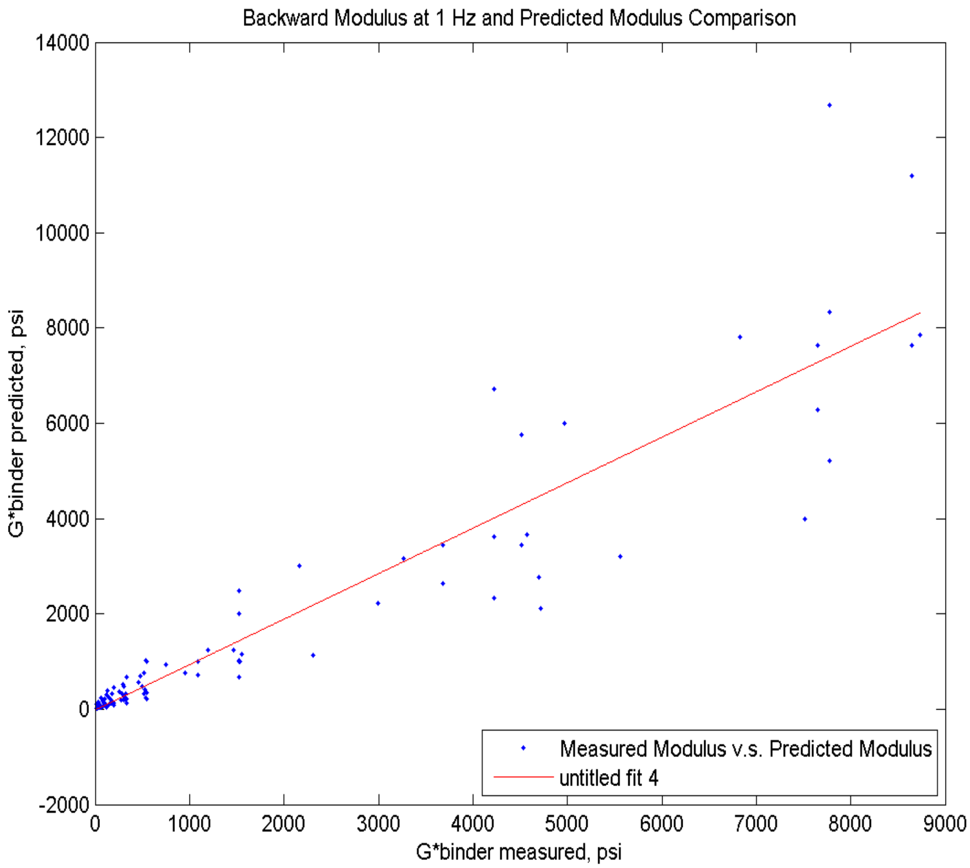

Backward Modulus at 1 Hz and Predicted Modulus Comparison
G*binder predicted, psi
G*binder measured, psi
14000
12000
10000
8000
6000
4000
2000
0
-2000
0
1000
2000
3000
4000
5000
6000
7000
8000
9000
Measured Modulus v.s. Predicted Modulus
untitled fit 4

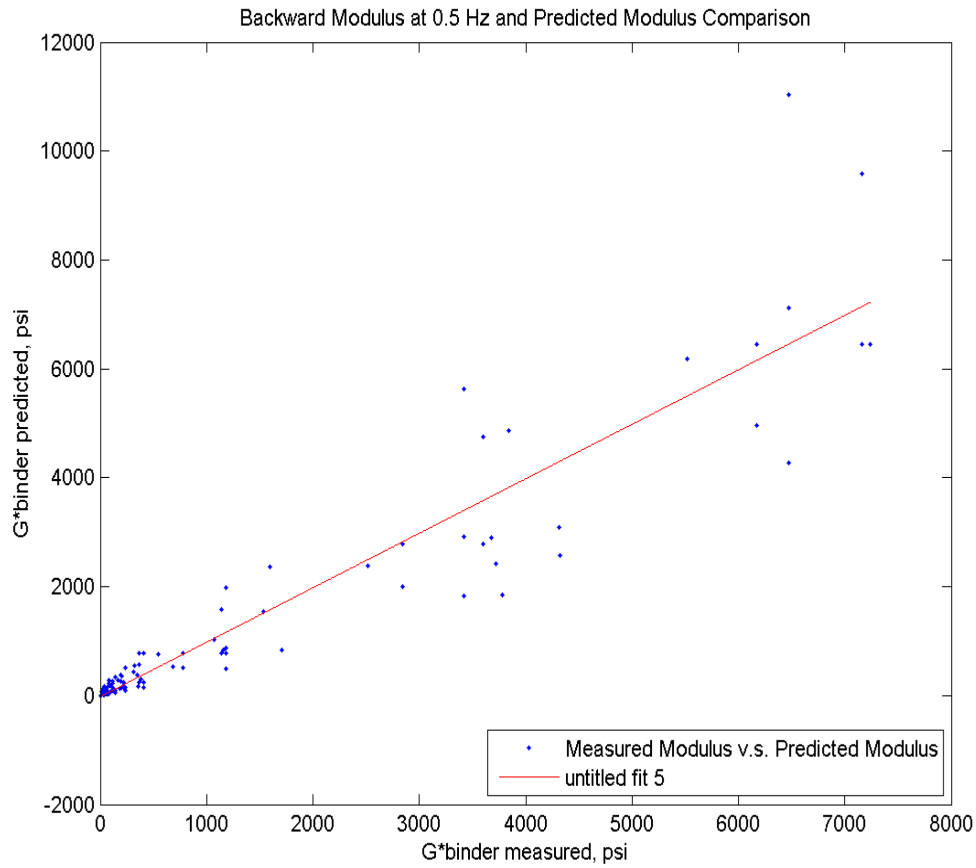
Backward Modulus at 0.5 Hz and Predicted Modulus Comparison
12000
10000
8000
6000
4000
2000
0
-2000
G*binder predicted, psi
0
1000
2000
3000
4000
5000
6000
7000
8000
G*binder measured, psi
Measured Modulus v.s. Predicted Modulus
untitled fit 5

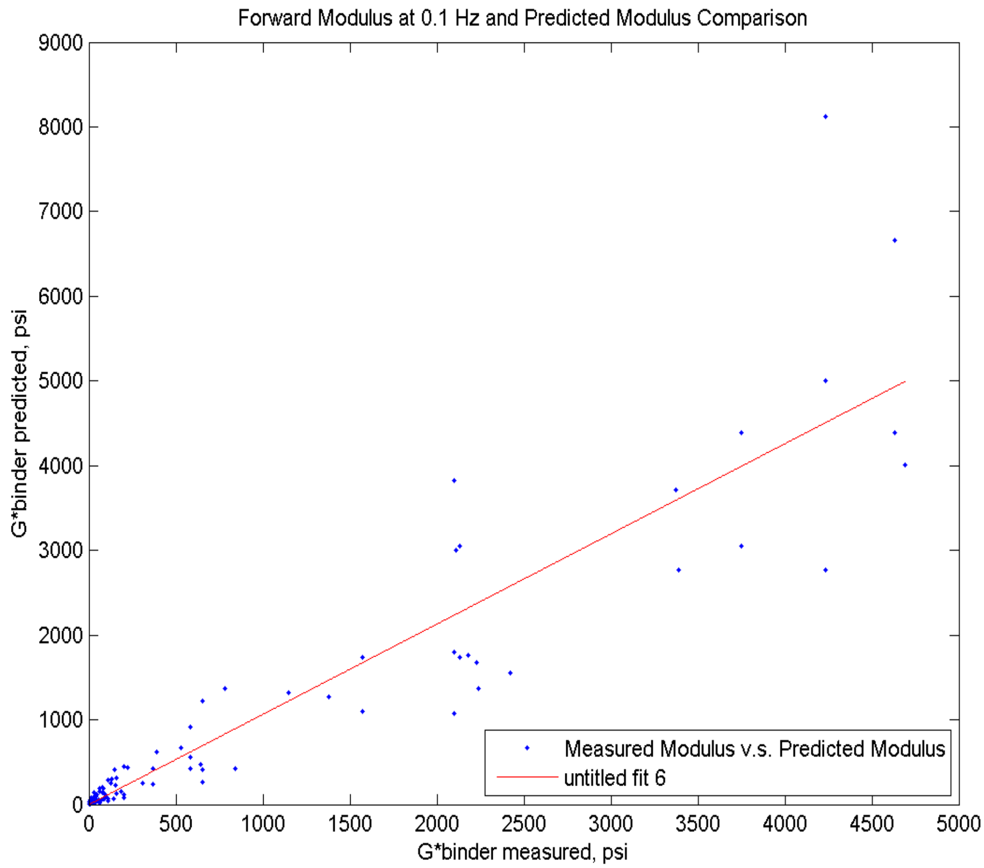
Forward Modulus at 0.1 Hz and Predicted Modulus Comparison
G*binder predicted, psi
G*binder measured, psi
0
1000
2000
3000
4000
5000
6000
7000
8000
9000
0
500
1000
1500
2000
2500
3000
3500
4000
4500
5000
Measured Modulus v.s. Predicted Modulus
untitled fit 6

APPENDIX I - Model verification backward phase angle model family of curves

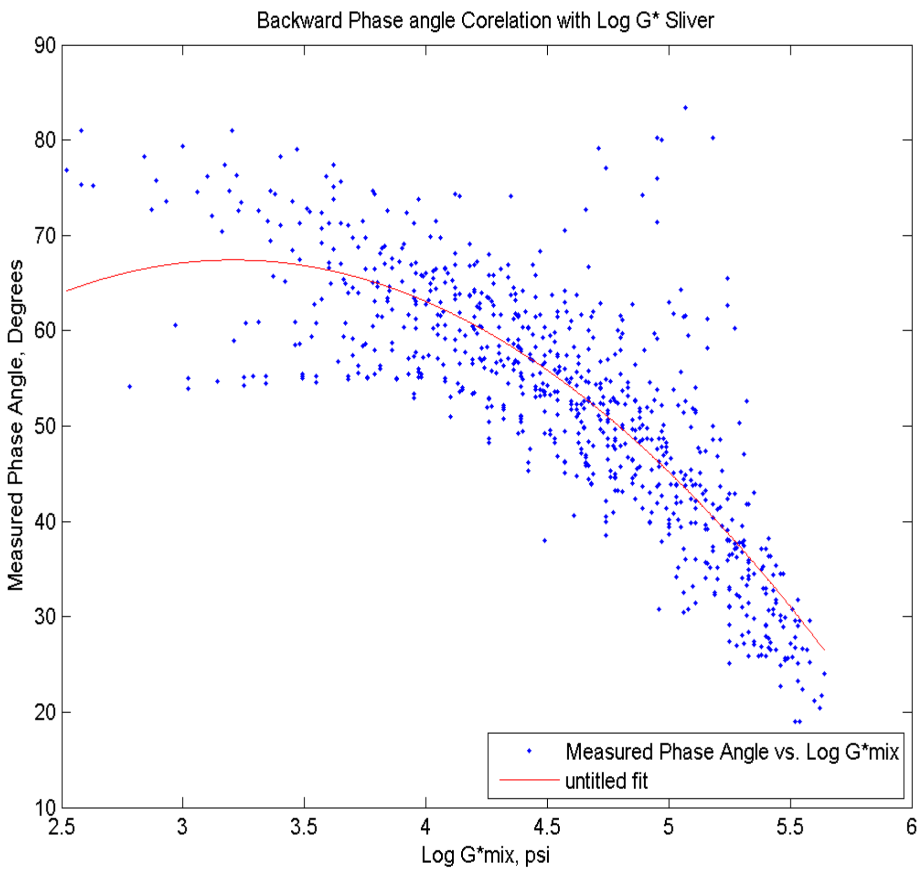

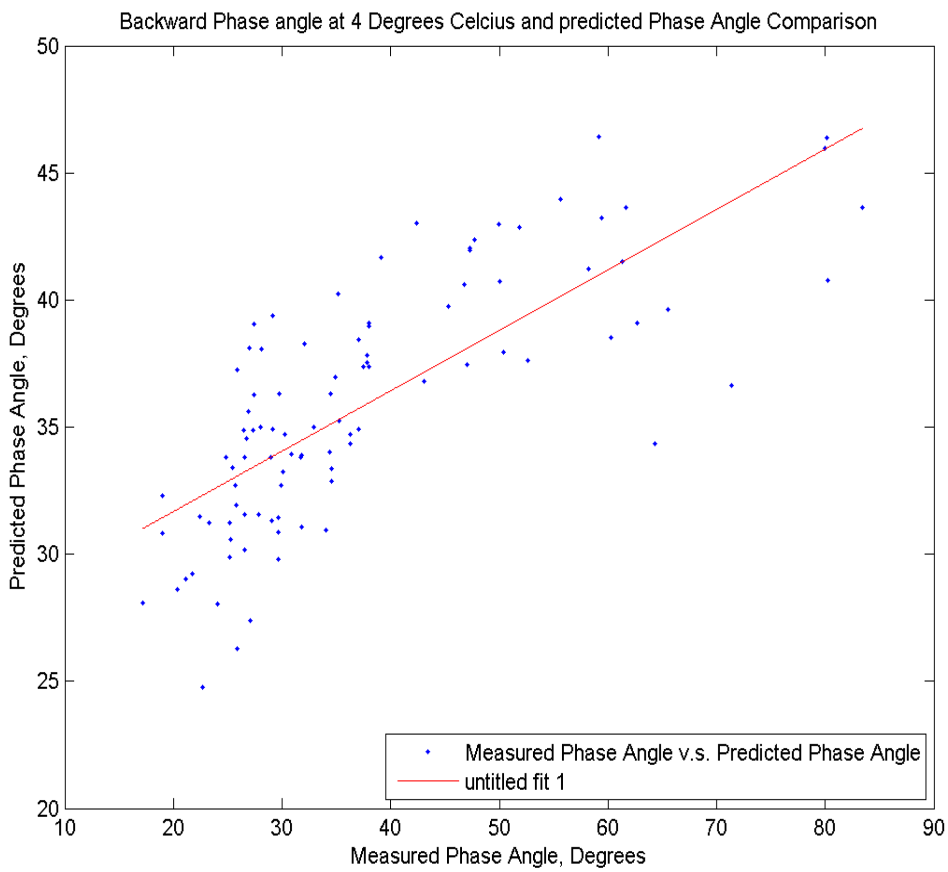
Backward Phase angle at 4 Degrees Celcius and predicted Phase Angle Comparison
Predicted Phase Angle, Degrees
Measured Phase Angle, Degrees
Measured Phase Angle v.s. Predicted Phase Angle
untitled fit 1
50
45
40
35
30
25
20
10
20
30
40
50
60
70
80
90

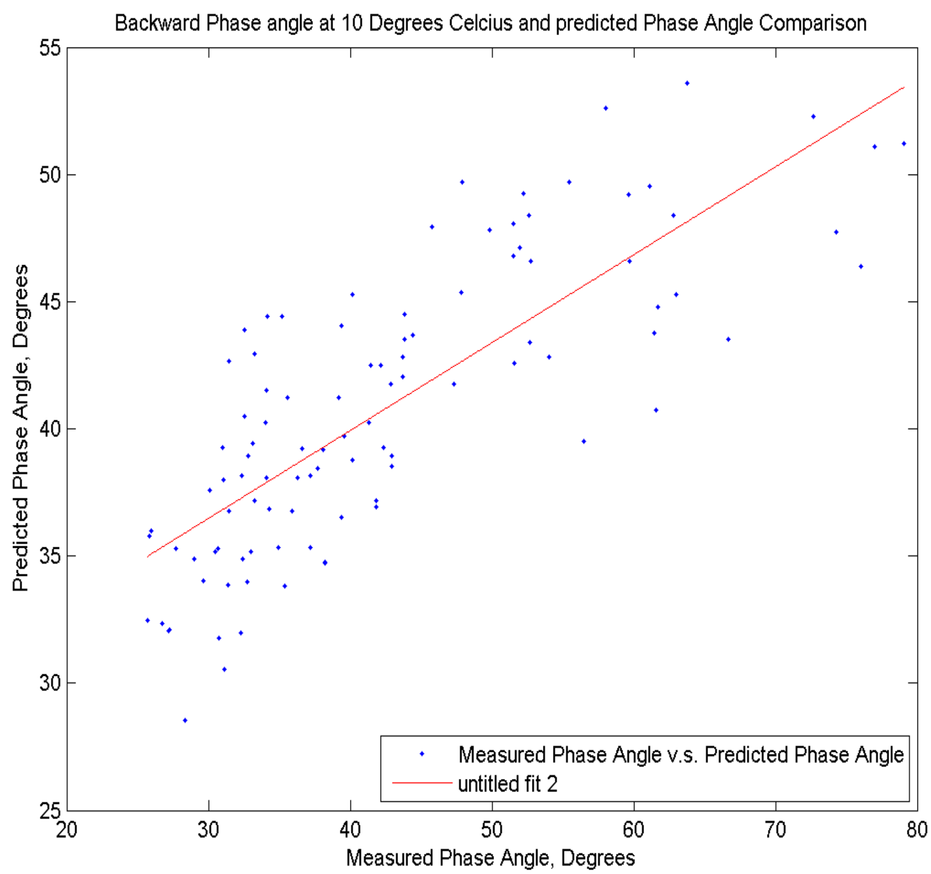
Backward Phase angle at 10 Degrees Celcius and predicted Phase Angle Comparison
Predicted Phase Angle, Degrees
Measured Phase Angle, Degrees
Measured Phase Angle v.s. Predicted Phase Angle
untitled fit 2
55
50
45
40
35
30
25
20
30
40
50
60
70
80

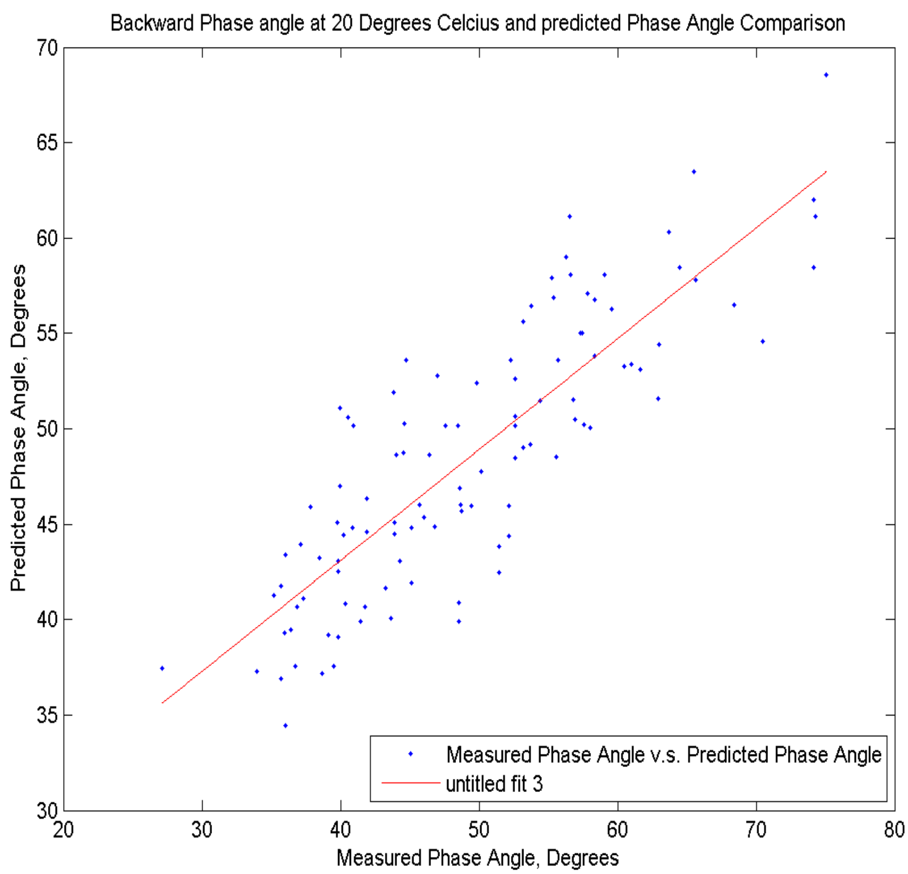
Backward Phase angle at 20 Degrees Celcius and predicted Phase Angle Comparison
Predicted Phase Angle, Degrees
Measured Phase Angle, Degrees
Measured Phase Angle v.s. Predicted Phase Angle
untitled fit 3
70
65
60
55
50
45
40
35
30
20
30
40
50
60
70
80

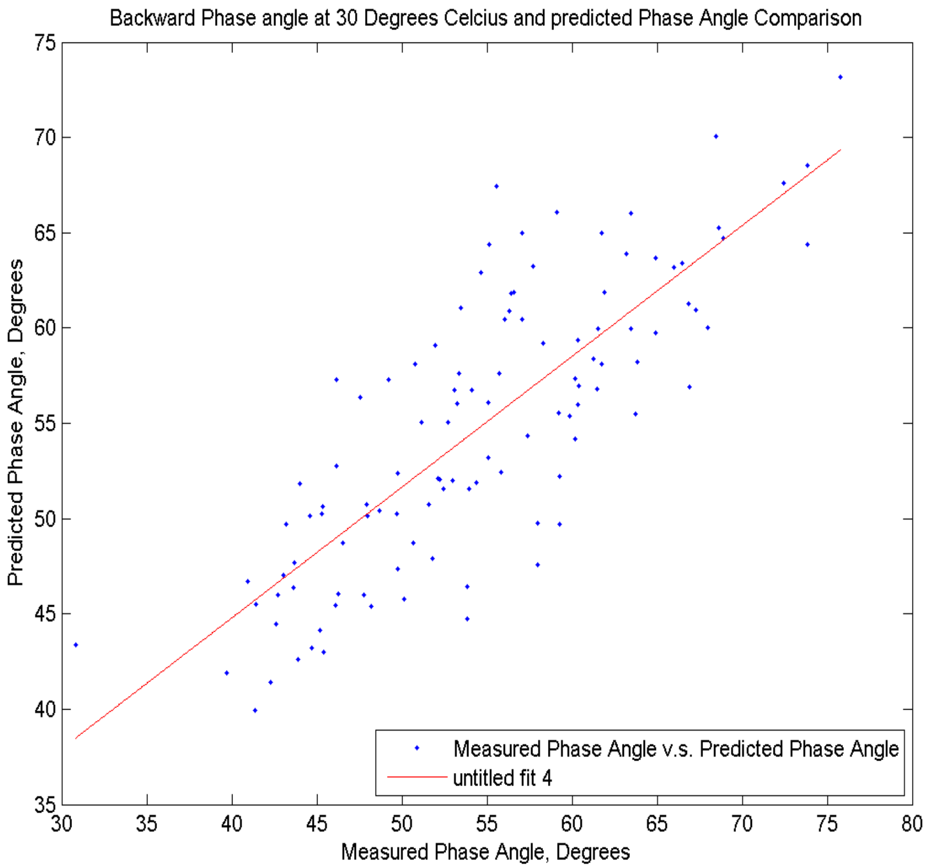

Backward Phase angle at 30 Degrees Celcius and predicted Phase Angle Comparison
Predicted Phase Angle, Degrees
Measured Phase Angle, Degrees
Measured Phase Angle v.s. Predicted Phase Angle
untitled fit 4
75
70
65
60
55
50
45
40
35
30
35
40
45
50
55
60
65
70
75
80

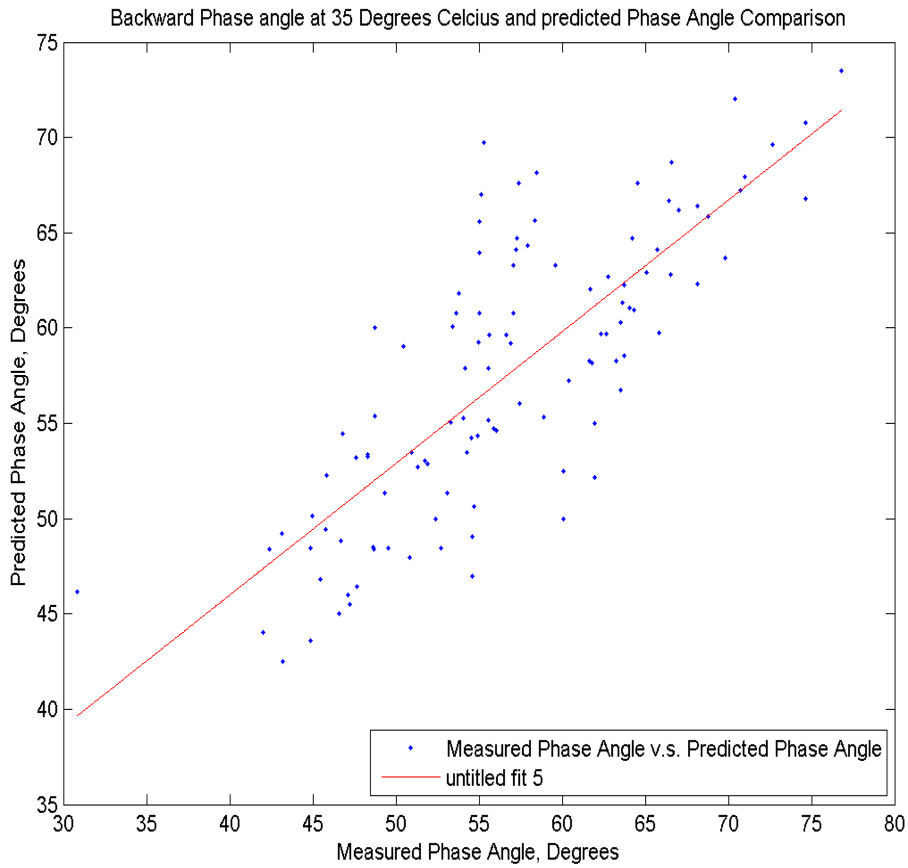
Backward Phase angle at 35 Degrees Celcius and predicted Phase Angle Comparison
Predicted Phase Angle, Degrees
Measured Phase Angle, Degrees
Measured Phase Angle v.s. Predicted Phase Angle
untitled fit 5
75
70
65
60
55
50
45
40
35
30
35
40
45
50
55
60
65
70
75
80

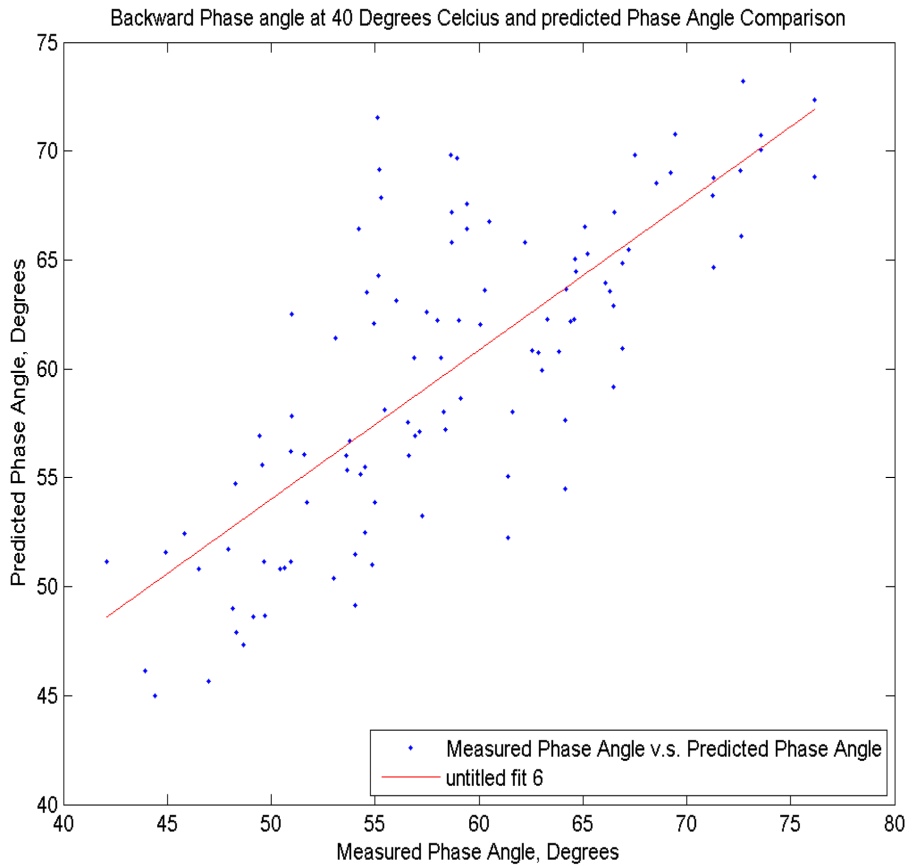
Backward Phase angle at 40 Degrees Celcius and predicted Phase Angle Comparison
Predicted Phase Angle, Degrees
Measured Phase Angle, Degrees
Measured Phase Angle v.s. Predicted Phase Angle
untitled fit 6
75
70
65
60
55
50
45
40
40
45
50
55
60
65
70
75
80

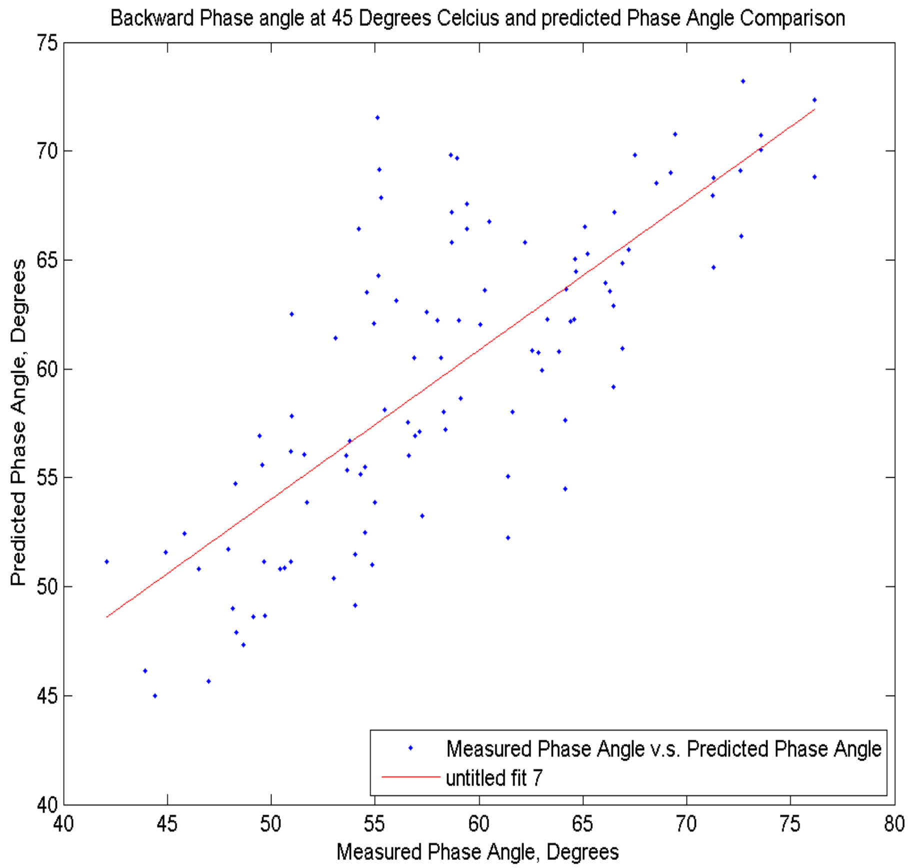

Backward Phase angle at 45 Degrees Celcius and predicted Phase Angle Comparison
Predicted Phase Angle, Degrees
Measured Phase Angle, Degrees
Measured Phase Angle v.s. Predicted Phase Angle
untitled fit 7
75
70
65
60
55
50
45
40
40
45
50
55
60
65
70
75
80

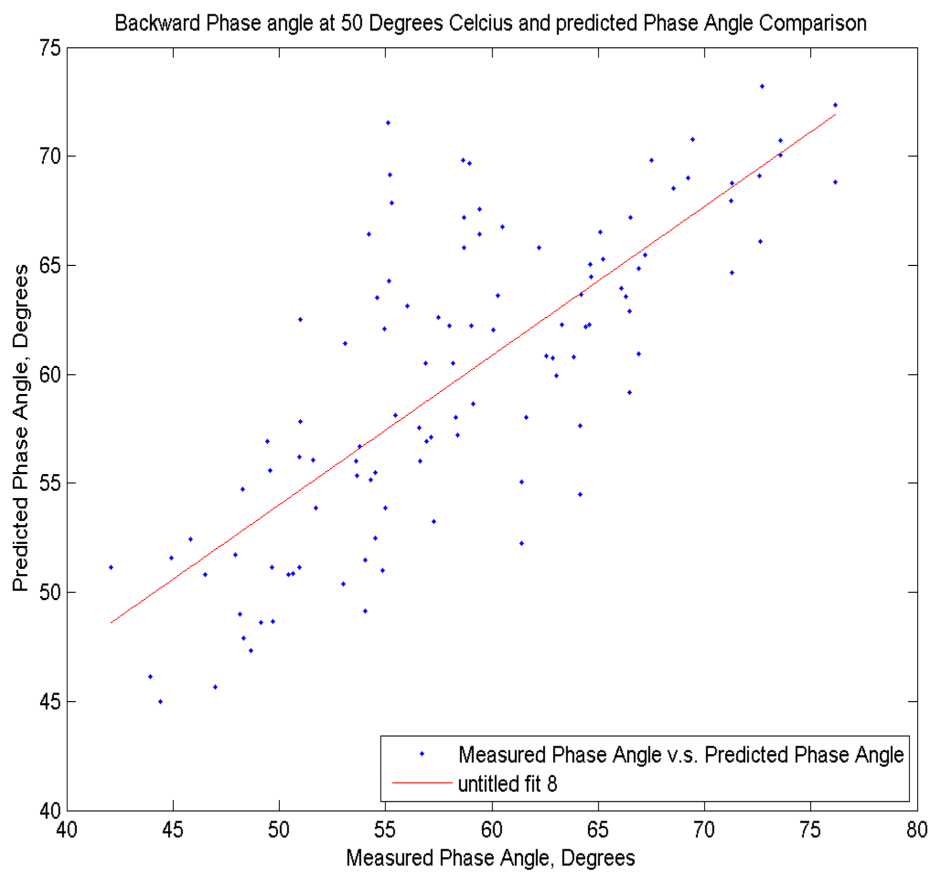
Backward Phase angle at 50 Degrees Celcius and predicted Phase Angle Comparison
Predicted Phase Angle, Degrees
Measured Phase Angle, Degrees
Measured Phase Angle v.s. Predicted Phase Angle
untitled fit 8
40
45
50
55
60
65
70
75
80

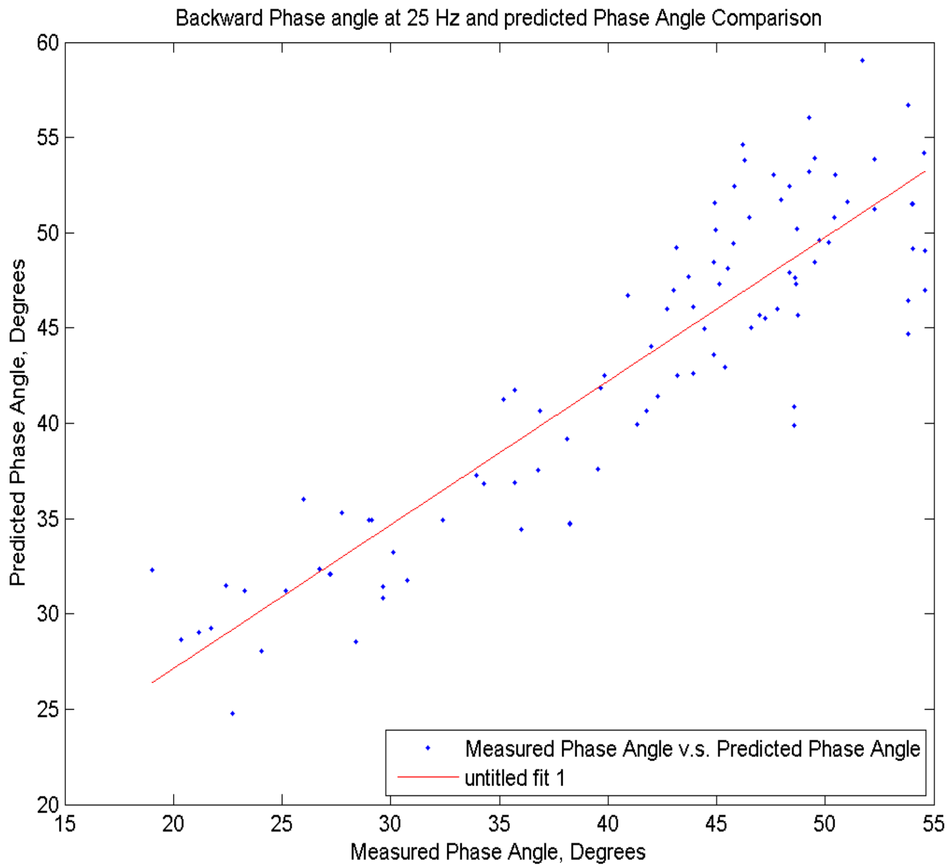

Backward Phase angle at 25 Hz and predicted Phase Angle Comparison
Predicted Phase Angle, Degrees
Measured Phase Angle, Degrees
Measured Phase Angle v.s. Predicted Phase Angle
untitled fit 1
60
55
50
45
40
35
30
25
20
15
20
25
30
35
40
45
50
55

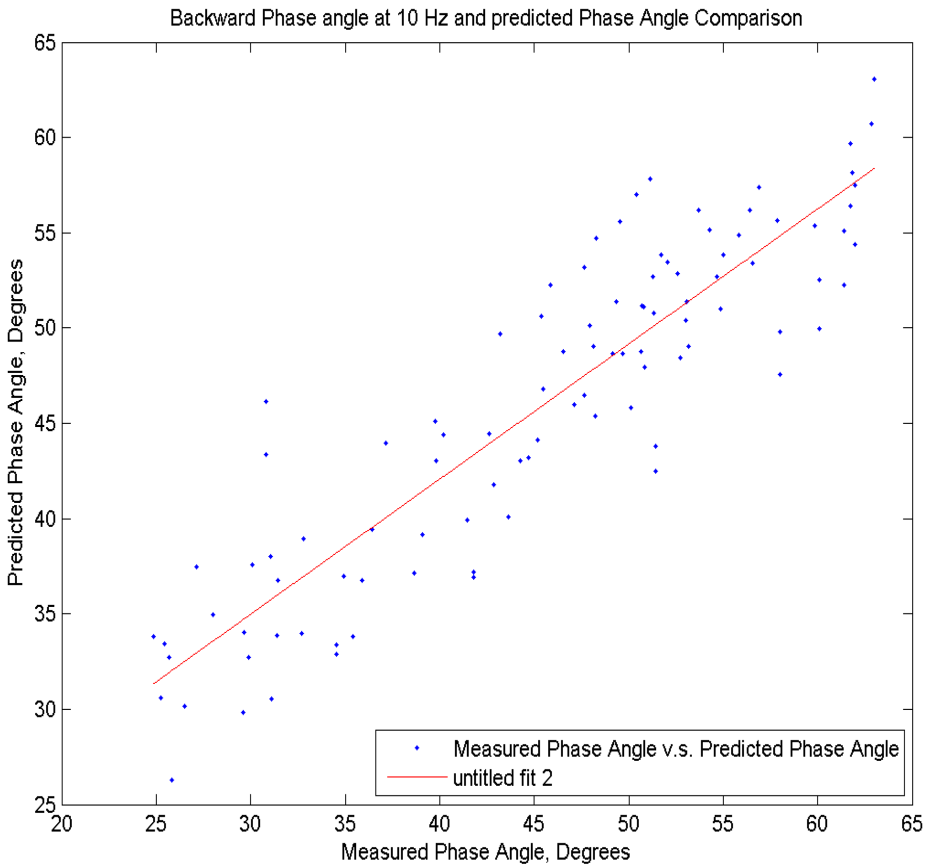

Backward Phase angle at 10 Hz and predicted Phase Angle Comparison
Predicted Phase Angle, Degrees
Measured Phase Angle, Degrees
Measured Phase Angle v.s. Predicted Phase Angle
untitled fit 2
65
60
55
50
45
40
35
30
25
20
25
30
35
40
45
50
55
60
65

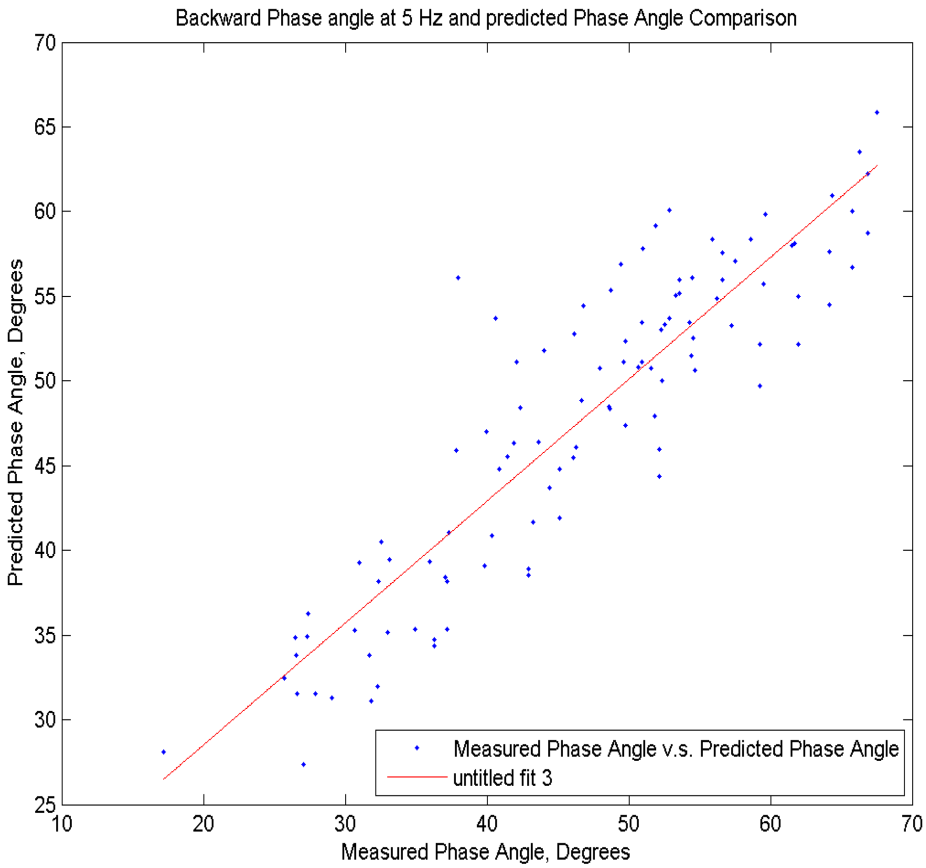
Backward Phase angle at 5 Hz and predicted Phase Angle Comparison
Predicted Phase Angle, Degrees
Measured Phase Angle, Degrees
Measured Phase Angle v.s. Predicted Phase Angle
untitled fit 3
70
65
60
55
50
45
40
35
30
25
10
20
30
40
50
60
70

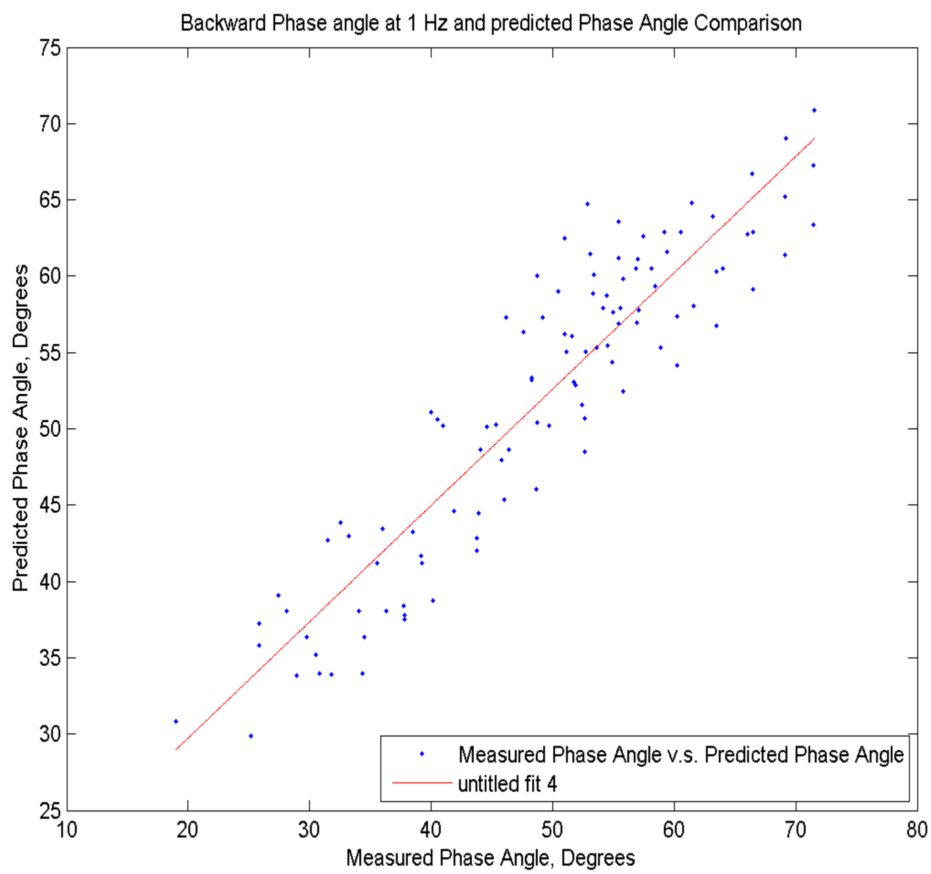
Backward Phase angle at 1 Hz and predicted Phase Angle Comparison
Predicted Phase Angle, Degrees
Measured Phase Angle, Degrees
Measured Phase Angle v.s. Predicted Phase Angle
untitled fit 4
75
70
65
60
55
50
45
40
35
30
25
10
20
30
40
50
60
70
80

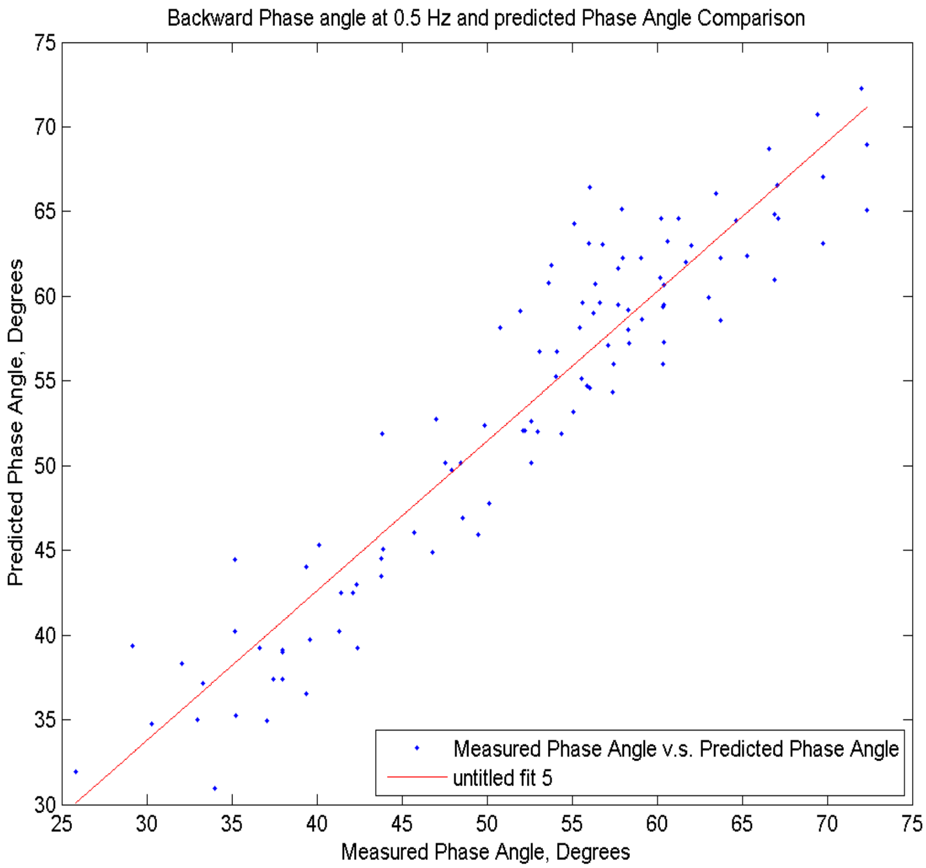

Backward Phase angle at 0.5 Hz and predicted Phase Angle Comparison
Predicted Phase Angle, Degrees
Measured Phase Angle, Degrees
Measured Phase Angle v.s. Predicted Phase Angle
untitled fit 5
75
70
65
60
55
50
45
40
35
30
25
30
35
40
45
50
55
60
65
70
75

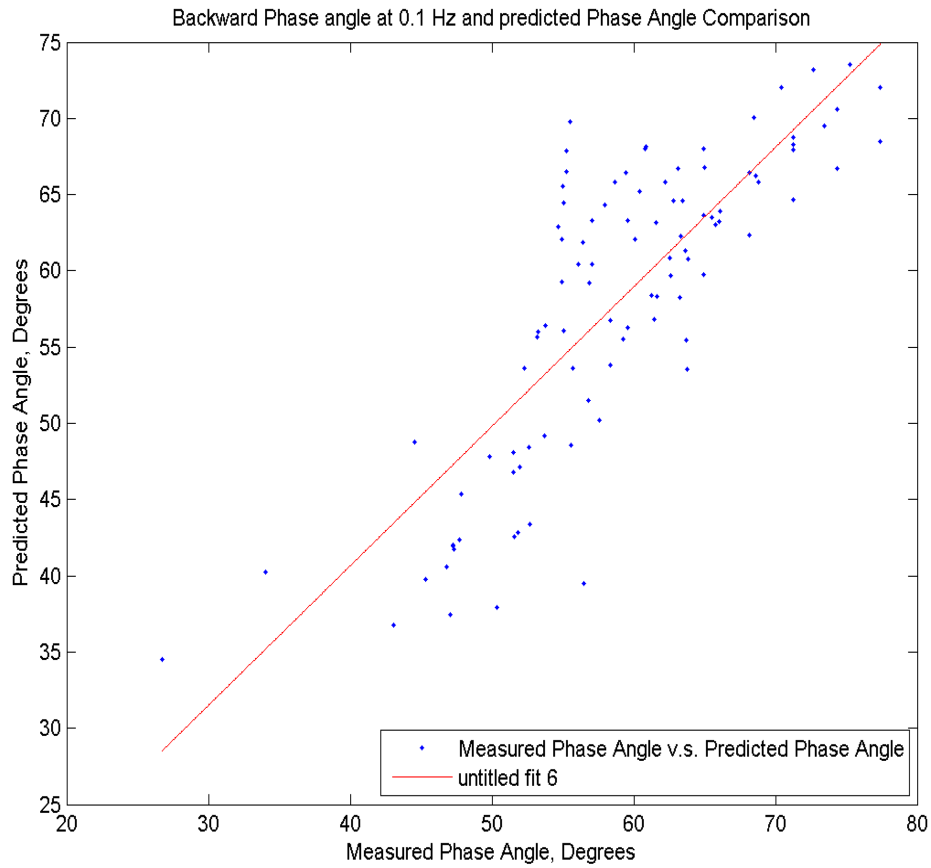

Backward Phase angle at 0.1 Hz and predicted Phase Angle Comparison
Predicted Phase Angle, Degrees
Measured Phase Angle, Degrees
Measured Phase Angle v.s. Predicted Phase Angle
untitled fit 6
75
70
65
60
55
50
45
40
35
30
25
20
30
40
50
60
70
80